

PART I

**3,4-DIAZABENZVALENE, THE AZOALKANE
PRECURSOR TO TETRAHEDRANE**

PART II

**MAGNETIC PROPERTIES
OF
POLARONIC POLYMERS**

Thesis by

David A. Kaisaki

In Partial Fulfillment of the Requirements
for the
Degree of Doctor of Philosophy

California Institute of Technology
Pasadena, California

1990

(Submitted May 10, 1990)

To Bridget

Acknowledgment

I would first like to thank my advisor, Dennis Dougherty, for his invaluable guidance throughout my graduate career. His understanding and support have helped to smooth the sometimes rocky road of graduate school.

Many thanks also goes to the Dougherty group members past and present for their friendship and unselfish assistance. I feel privileged to have been able to work (and play) with the people in this group. Special thanks goes to Gary Snyder, Frank Coms, and Rakesh Jain for their help and advice on biradical matters. I would also like to thank Wonghil Chang for performing the 4 K magnetization measurements that appear in this thesis. Thanks also goes to Rich Barrans and Dennis Dougherty, who wrote the Brillouin fitting program.

I would also like to thank the people outside of the Dougherty group who have been a source of help and support. Special thanks goes to Bob Grubbs and his group, especially Tim Swager, Lynda Johnson, Mike Rock, and Chris Gorman for their help and experience in the polymer and metathesis areas. I would also like to thank Jim Hanson for his assistance with the FT-IR Displex instrument. I would especially like to acknowledge the help of Chris Reed, Robert Orotz, and Carol Koch at the University of Southern California for their invaluable assistance with the SQUID.

Many thanks goes to the people who helped with the writing of this thesis, especially Dave Shultz, Lynda Johnson, Pat Kearney, Rich Barrans, Frank Coms, Alison McCurdy, Leslie Jimenez, Laura Mizoue, and Brad White. I would also like to thank Susan A. Kaisaki and Debbie

Chester for typing this thesis.

Finally, I would like to thank Mom and Dad and my sisters for their love and support. I would also like to thank Adel Naylor and Judy and Don Nollar for their support, especially during the past nine months.

Abstract

The synthesis and reactivity of 3,4-diazabenzvalene (**9**) are described. This strained diazene thermally decomposes to yield cyclobutadiene dimer with a unimolecular rate at constant -60°C of $5.24 \times 10^{-4} \text{ sec}^{-1}$. This corresponds to a half-life for **9** of 22 min. at -60°C . The high thermal reactivity of **9** is postulated to be due to a six-electron, concerted $\sigma_{2s} + \sigma_{2a} + \sigma_{2a}$ N_2 extrusion mechanism as opposed to the one-bond diazenyl biradical mechanism observed in the similar molecule, **48**. Low temperature (-100 to -150°C) ^1H NMR spectroscopy of -196°C photolysis products of **9** in a variety of solvents showed the formation of cyclobutadiene dimer and pyridazine. Attempts at the 10 K FT-IR matrix isolation photolysis studies on **9** failed due to our inability to sublime the cooled, unstable diazene onto the matrix window. No evidence of tetrahedrane formation upon photolysis or thermolysis at any temperature was observed.

The magnetic behavior of AsF_5 - and I_2 -doped poly(*meta*-phenyleneoctatetraene) (PMPOT) derivatives is also investigated. A synthetic scheme for O-alkyl substituted PMPOT derivatives is developed using the Wittig reaction as the polymerization method. O-alkyl substitution provides an increase in solubility and degree of polymerization relative to the unsubstituted, intractable, parent polymer PMPOT. The O-octadecyl-substituted PMPOT derivative, PMPOT-18, is completely soluble in chloroform or toluene and has a degree of polymerization of 22.

Oxidative doping of PMPOT-18 and PMPOT-6 (O-hexyl-substituted) with AsF_5 or I_2 produces small concentrations (0.2-4 spins/100 monomers) of polarons (partially delocalized radical cations). Fitting the Brillouin function to the magnetization behavior of these polaronic materials

provides a method of obtaining the spin state without the need of an estimate of the concentration of polarons present. A spin state of $S = 2.2$ for AsF_5 -doped PMOT-18 was found at 1.95 K, while I_2 -doped PMPOT-6 and PMPOT-18 fit to a Brillouin function with $S = 1.2 - 1.3$. This is consistent with a net ferromagnetic coupling between 2-4 polarons. Temperature-dependent magnetic susceptibility measurements indicate the presence of both antiferro- and ferromagnetic interactions at temperatures below *ca.* 50 K. This is interpreted in terms of a model in which doping produces clusters of polarons that interact ferromagnetically. There is also a weaker, antiferromagnetic interaction between clusters that is apparent at low temperatures.

Table of Contents

| | |
|--|-----------|
| Acknowledgment | iii |
| Abstract | v |
| List of Figures | x |
| List of Tables | xiii |
| List of Schemes | xiv |
| PART I 3,4-DIAZABENZVALENE, THE AZOALKANE PRECURSOR TO | |
| TETRAHEDRANE | 1 |
| Chapter 1 - 3,4-Diazabenzvalene, The Azoalkane Precursor To | |
| Tetrahedrane | 2 |
| Introduction | 3 |
| Theoretical Studies | 7 |
| Experimental Studies | 18 |
| Synthesis, Results and Discussion | 28 |
| Thermal Reactivity | 35 |
| Photochemical Reactivity | 38 |
| Matrix Isolation Studies | 41 |
| Conclusion | 42 |
| Experimental | 43 |
| References | 50 |
| PART II MAGNETIC PROPERTIES OF POLARONIC POLYMERS | 55 |
| Chapter 2 - Design of Molecular Magnetic Materials | 56 |
| Hund's Rule | 59 |

| | |
|---|------------|
| McConnell Spin-Exchange Model | 66 |
| Charge Transfer Model | 69 |
| Topological Coupling Model | 70 |
| Polaronic Ferromagnetism | 75 |
| References | 81 |
| Chapter 3 - Magnetism | 85 |
| Introduction | 86 |
| Magnetic Definitions | 86 |
| Magnetic Substances | 90 |
| Magnetic Characterization | 98 |
| Curie Law | 100 |
| Effective Magnetic Moment | 105 |
| Curie Behavior -- A Closer Look | 109 |
| Brillouin Treatment | 119 |
| References | 133 |
| Chapter 4 - Magnetic Properties of Doped Poly(<i>meta</i>-phenylene- | |
| octatetraene) Derivatives | 135 |
| General Considerations | 136 |
| Synthesis and Characterization | 140 |
| PMPOT | 146 |
| PMPOT-6 | 152 |
| PMPOT-18 | 160 |
| Other Polymers | 166 |
| Spin Concentration | 166 |
| PMPOT-6 | 167 |

| | |
|--|-----|
| PMPOT-18 | 170 |
| Doped PMPOT Spin States | 175 |
| PMPOT-6 | 175 |
| PMPOT-18 | 187 |
| Magnetization References | 201 |
| Discussion | 204 |
| PMPOT Structure | 206 |
| Polaron Densities | 207 |
| Is one-dimensional coupling ferromagnetic? | 215 |
| Ferromagnetism - PMPOT and impurities | 228 |
| Conclusion | 231 |
| Experimentals | 233 |
| References | 246 |

List of Figures

| | | |
|-------------|---|------------|
| 1-1 | Cyclic diazene reactivity | 6 |
| 1-2 | C ₄ H ₄ MINDO/3 potential energy surface | 14 |
| 1-3 | Reactivity of 12a | 17 |
| 1-4 | One-bond cleavage mechanism | 37 |
| 1-5 | Thermochemistry of diazabenzvalene | 39 |
| 2-1 | Singlet state preference of two p-orbitals | 61 |
| 2-2 | H ₂ potential energy system | 62 |
| 2-3 | Orthogonal p-orbitals | 64 |
| 2-4 | Diphenylcarbene cyclophanes | 68 |
| 2-5 | An approach to ferromagnetic polymers | 77 |
| 3-1 | Types of magnetic behavior | 87 |
| 3-2 | Magnetic dipole in field | 89 |
| 3-3 | Diamagnetism and paramagnetism | 91 |
| 3-4 | General spin interactions | 93 |
| 3-5 | Curie-Weiss law | 102 |
| 3-6 | Effective magnetic moment as a function of temperature | 108 |
| 3-7 | Curie-Weiss behavior of charge transfer salts | 110 |
| 3-8 | Effective magnetic moment behavior of charge transfer salts | 111 |
| 3-9 | Energy levels of an $S = \frac{5}{2}$ system in a magnetic field | 113 |
| 3-10 | Energy levels of an $S = \frac{1}{2}$ system in a magnetic field | 114 |
| 3-11 | Brillouin function | 123 |
| 3-12 | Cr ³⁺ , Fe ³⁺ , and Gd ³⁺ magnetization behavior | 125 |

| | | |
|------|---|-----|
| 4-1 | Step-growth polymerization | 144 |
| 4-2 | PMPOT work-up | 155 |
| 4-3 | PMPOT-6 GPC | 157 |
| 4-4 | IR spectrum of PMPOT-6 | 159 |
| 4-5 | IR spectrum of PMPOT-18 | 163 |
| 4-6 | ^1H NMR spectrum of PMPOT-18 | 165 |
| 4-7 | I_2 -doped PMPOT-6 spin concentration | 168 |
| 4-8 | Vacuum I_2 -doped PMPOT-6 spin concentration | 169 |
| 4-9 | AsF_5 -doped PMPOT-6 spin concentration | 171 |
| 4-10 | Vacuum I_2 -doped PMPOT-18 spin concentration | 172 |
| 4-11 | AsF_5 -doped PMPOT-18 spin concentration | 174 |
| 4-12 | Plot of χ_e vs. $1/T$ for AsF_5 -doped PMPOT-18 | 176 |
| 4-13 | AsF_5 -doped PMPOT-18 Curie behavior | 178 |
| 4-14 | μ_{eff}' of AsF_5 -doped PMPOT-6 | 180 |
| 4-15 | Magnetization behavior of AsF_5 -doped PMPOT-6 | 181 |
| 4-16 | AsF_5 -doped PMPOT-6 Brillouin fit | 183 |
| 4-17 | I_2 -doped PMPOT-6 Brillouin fit | 185 |
| 4-18 | I_2 -doped PMPOT-6 Brillouin fit (CCl_4) | 186 |
| 4-19 | I_2 -doped PMPOT-18 Brillouin fit | 188 |
| 4-20 | I_2 -doped PMPOT-18 Brillouin fit (CCl_4) | 189 |
| 4-21 | μ_{eff}' of I_2 -doped PMPOT-18 | 191 |
| 4-22 | AsF_5 -doped PMPOT-18 Brillouin fit | 193 |
| 4-23 | Magnetization of AsF_5 -doped PMPOT-18 | 195 |
| 4-24 | AsF_5 -doped PMPOT-18 Brillouin fit | 196 |
| 4-25 | Heavily AsF_5 -doped PMPOT-18 Brillouin fit | 197 |
| 4-26 | Curie-Weiss plot of AsF_5 -doped PMPOT-18 | 199 |
| 4-27 | μ_{eff}' of AsF_5 -doped PMPOT-18 | 200 |

| | | |
|-------------|---|------------|
| 4-28 | Doped PMPOT-18 Brillouin fit at 2 and 4 K | 202 |
| 4-29 | Brillouin fit of AsF ₅ -doped PPPV | 203 |
| 4-30 | Brillouin fit of I ₂ -doped PPPOT | 205 |
| 4-31 | <i>Meta</i> coupling of polarons | 211 |
| 4-32 | Typical spin concentration behavior in doped polymers | 213 |
| 4-33 | Brillouin fit of Cr(acac) ₃ | 220 |
| 4-34 | μ_{eff} behavior of Cr(acac) ₃ | 221 |
| 4-35 | Polaron cluster model | 223 |
| 4-36 | 1,3,5-trimethylenebenzene-linked PMPOT network | 227 |
| 4-37 | Fe magnetization behavior | 230 |

List of Tables

| | | |
|------------|---------------------------------------|-----|
| 1-1 | Strain energies | 5 |
| 1-2 | ^1H NMR data for 45 | 31 |
| 1-3 | Azoalkane UV absorptions | 34 |
| 3-1 | Magnetic susceptibilities | 99 |
| 3-2 | Effective magnetic moments | 106 |
| 4-1 | Elemental analysis of polymers | 149 |
| 4-2 | DP of PMPOT-6 | 158 |
| 4-3 | DP of PMPOT derivatives | 161 |
| 4-4 | Doped PMPOT-6 spin states | 187 |
| 4-5 | Spin concentrations of doped polymers | 209 |
| 4-6 | Spin states of doped polymers | 216 |
| 4-7 | Biradical singlet-triplet gaps | 225 |

List of Schemes

| | | |
|------------|-------------------------------------|-----|
| 1-1 | Precursor activation energies | 15 |
| 1-2 | Synthesis of 42 | 29 |
| 1-3 | Synthesis of 45 | 30 |
| 1-4 | ^1H NMR photolysis studies | 40 |
| 2-1 | Polaron formation | 79 |
| 4-1 | Polaronic polymer design | 138 |
| 4-2 | Wittig polymerization | 141 |
| 4-3 | PMPOT synthesis | 147 |
| 4-4 | Bis-phosphonium salt synthesis | 154 |

PART I

**3,4-DIAZABENZVALENE, THE AZOALKANE PRECURSOR
TO TETRAHEDRANE**

Chapter 1

3,4-Diazabenzvalene, The Azoalkane Precursor To Tetrahedrane

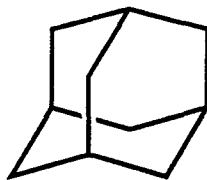
Introduction

The study of strained molecules^{1,7} has long been a fascination of chemists. In the late 19th century, Baeyer² postulated a strain theory in which the geometry of an unstrained carbon molecule had bond angles of approximately tetrahedral values (109.5°). Any large deviation from this value would induce strain and cause an overall destabilization of the molecule. Since that time, organic chemists have pursued the synthesis of highly strained organic compounds with a variety of procedures to gain a better understanding of the effects of strain on molecular thermodynamic stability and reactivity. The obvious method to build in strain is the use of a cyclic or polycyclic framework of C-C bonds. The most simple monocyclic ring systems, cyclopropane and cyclobutane, have long been known to be stable, although they are significantly destabilized in comparison to their acyclic analogs.

Three-dimensionally strained polycyclic ring systems have been the subject of many an organic chemist's fantasy, and in fact many of the simple polycyclic ring systems have been isolated under various conditions. For instance, the first derivative of bicyclo[1.1.0] butane was reported in 1959, and the parent compound (1) was synthesized in 1963.¹ Adamantane¹



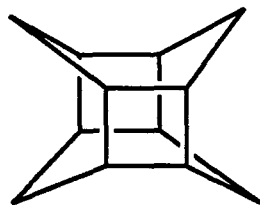
1



2



3



4



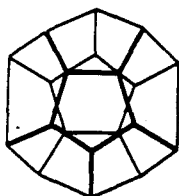
5

(2), prismane¹ (3), tetraasterane¹ (4), and more recently [1.1.1]propellane³ (5) have proven to be synthetically accessible.

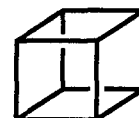
Due to their novelty and high symmetry, great attention has been paid to the series of polycyclic rings whose frameworks form a regular, three-dimensional, solid polyhedron. Of the five Platonic polyhedra – tetrahedron, hexahedron, dodecahedron, octahedron, and icosahedron – only the first three are thought to constitute possible organic structures.⁴



6



8





7

Of these three only hexahedron (7)¹ (commonly known as cubane) and dodecahedrane (8)⁵ have been reported to be isolable species. Tetrahedrane (6) has continued to elude experimentalists over the past 50 years,⁶ though not from a lack of effort.

Tetrahedrane is of chemical interest not only due to symmetry and its aesthetic qualities, but from other viewpoints as well. Tetrahedrane should exhibit the effects of extreme angle strain since it should have the most deviated bond angles and subsequently the highest strain energy per carbon atom of any polyhedron. Table 1-1⁷ compares the estimated strain energy of tetrahedrane with several other cyclic hydrocarbons. The study of isolated tetrahedrane could yield a vast amount of information regarding the reactivity of presumably stable molecules.

Table 1-1. Hydrocarbon Strain Energies

| | Strain Energy (kcal/mol) |
|---|-----------------------------|
| 5 | 68 |
|  | 27.5 |
|  | 26.5 |
| 6 | 140.0 |

The physical properties of tetrahedrane may also serve as a valuable comparison between theory and experiment. The simplicity and high symmetry of the molecule allow state-of-the-art *ab initio* and semi-empirical calculations to be performed without exacting a prohibitive amount of computation time. These predictions of stability, physical

properties, and reactivity may be compared to experimental reality, allowing the usefulness of such predictions to be gauged.

Cyclic 1,2 diazenes (azoalkanes) have been shown to be of great value in the synthesis of reactive and strained molecules.⁸ Extrusion of N₂, either by thermal or photochemical means, produces a biradical which can then undergo C-C bond formation to form the closed ring (Figure 1-1). A variety of such structures have been prepared, but the tricyclic compound, 3,4-diazatricyclo[3.1.0.0^{2,6}]hex-3-ene (**9**, 3,4-diazabenzvalene), had yet to be described at the outset of this work.

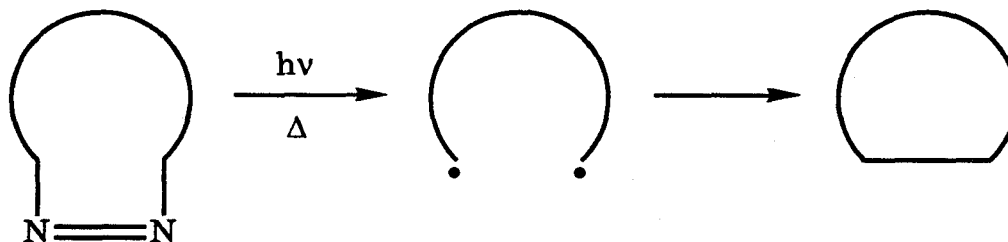


Figure 1-1. Cyclic diazene reactivity.

This molecule is of considerable interest, both in relation to its own inherent strain energy (ca. 77 kcal/mol, the amount estimated for benzvalene⁹) and reactivity, and as a potential precursor to tetrahedrane.

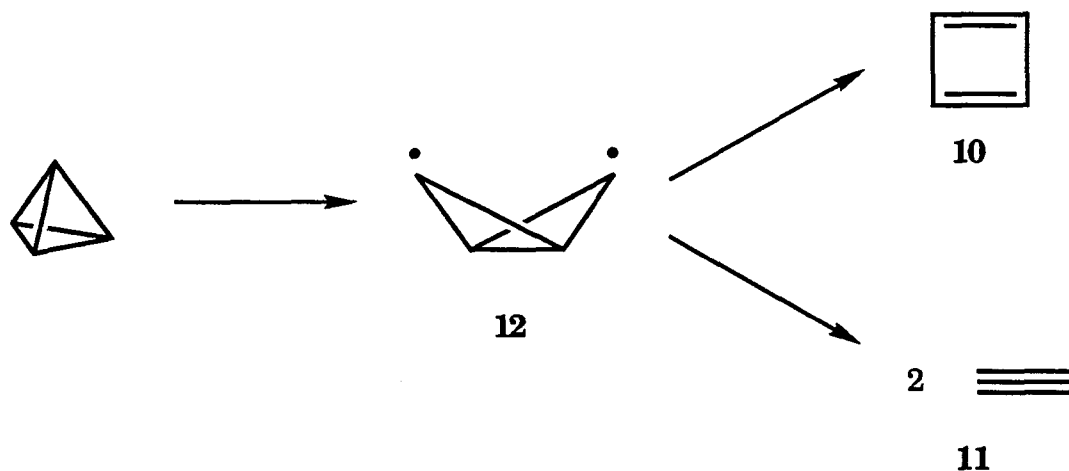


9

The present work is concerned with the synthesis, characterization, and study of 3,4-diazabenzvalene. Initially, there were two main goals for this study. First, the actual synthesis of 3,4-diazabenzvalene was an issue. It was not clear at the onset of this work that this strained structure could even be synthesized, much less isolated and manipulated. The second goal was to use this molecule as a precursor for the synthesis of tetrahedrane. This involved low temperature isolation techniques using ^1H NMR spectroscopy and matrix isolation methods with FT-IR spectroscopy. Of these two techniques, only the low temperature ^1H NMR method proved to be useful in determining the decomposition products of 3,4-diazabenzvalene.

Theoretical Studies

The C_4H_4 potential energy surface has been studied in part by several *ab initio* methods¹⁰ and to a greater extent by semi-empirical methods.^{16,17} Due to its inherent high symmetry, which makes such calculations much less time consuming, the stability and reactivity of tetrahedrane has been investigated quite closely. Most studies have concentrated on the conversion of tetrahedrane to cyclobutadiene (10) or two acetylene molecules (11). Woodward and Hoffman have stated¹⁸ that the direct concerted thermal conversion of tetrahedrane to 10 or 11 is symmetry forbidden.



However, the process of homolytic cleavage of a single tetrahedrane C–C bond followed by a second cleavage is not governed by symmetry arguments due to loss of concert. Therefore, single bond rupture to form the bicyclobutyl biradical (12) has been favored as the preliminary step in the decomposition of tetrahedrane.^{13,17}

The first study which theoretically established that tetrahedrane lies in a local minimum was done by Schulman and Venanzi¹¹ (earlier studies^{10a-c} had established that tetrahedrane was significantly destabilized compared to cyclobutadiene (CBD), but absolute stability was not addressed). Using a 4-31G basis set with the SCF method, an equilibrium geometry was obtained with C–C and C–H bond lengths of 1.482 and 1.054 Å, respectively. The heat of formation of tetrahedrane was calculated to be between 129 and 127 kcal/mol, with an overall strain energy of 21-23 kcal/mol per C–C bond.¹⁹ The photoelectron spectrum, as well as approximate IR and Raman frequencies, were also calculated.

The hybridization of the bonds in tetrahedrane was also estimated using an INDO calculation. The p character of the C–C bonds was 83% ($sp^{4.99}$) with the C–H bonds having 45% s character ($sp^{1.21}$). The C–C p character is estimated to be greater²⁰ than that of cyclopropane ($sp^{4.16}$) and the bicyclobutane side bond ($sp^{2.65}$). However, it is estimated to be less than that of the bicyclobutane bridgehead bond (94% p). The s character in the C–H bonds was calculated to be greater than that of the bridgehead C–H bond of bicyclobutane ($sp^{1.58}$) or cyclopropene²¹ ($sp^{1.31}$). However, it is smaller than acetylene (sp^1). These values resulted in a prediction for the nuclear spin-spin coupling constants J_{13CH} and J_{13C13C} of 240 Hz and 7.1 Hz, respectively. The J_{13CH} value is lower than that of acetylene²² (249 Hz) and slightly lower than the value for tricyclo[2.1.0.0^{2,5}]pentane-3-one²³ (247 Hz). However, it is greater than those found for cyclopropene (220 Hz) and the bridgehead CH of benzvalene⁹ (205.2 Hz). These high coupling constants reflect the increasing ring strain and large s character of the C–H bond.

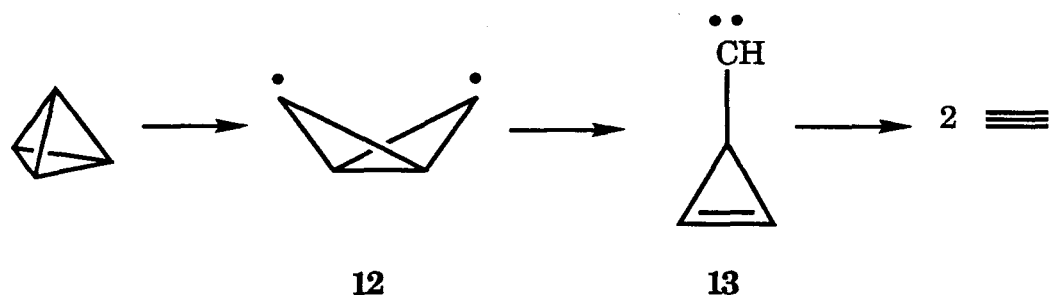
Homolytic cleavage of a C–C bond in tetrahedrane to form the biradical **12** was estimated to require an activation energy of *ca.* 18 kcal/mol. The stability of this biradical was not addressed, nor was its corresponding conversion to CBD.

Subsequent theoretical studies have addressed the question of the relative energy of tetrahedrane and its possible decomposition products. It is of great value to know the most energetically favorable decomposition route of tetrahedrane, since many experimental studies have used product analysis to justify or eliminate the formation of tetrahedral intermediates. While it may be assumed that the highly strained tetrahedrane must have decomposition products which are lower in energy, intuition alone cannot determine which pathway is the most favorable. The results of some of

these studies have indicated the possibility of forming tetrahedrane from intermediates along the tetrahedrane decomposition pathway which have a large barrier to further decomposition when compared to reformation of tetrahedrane.

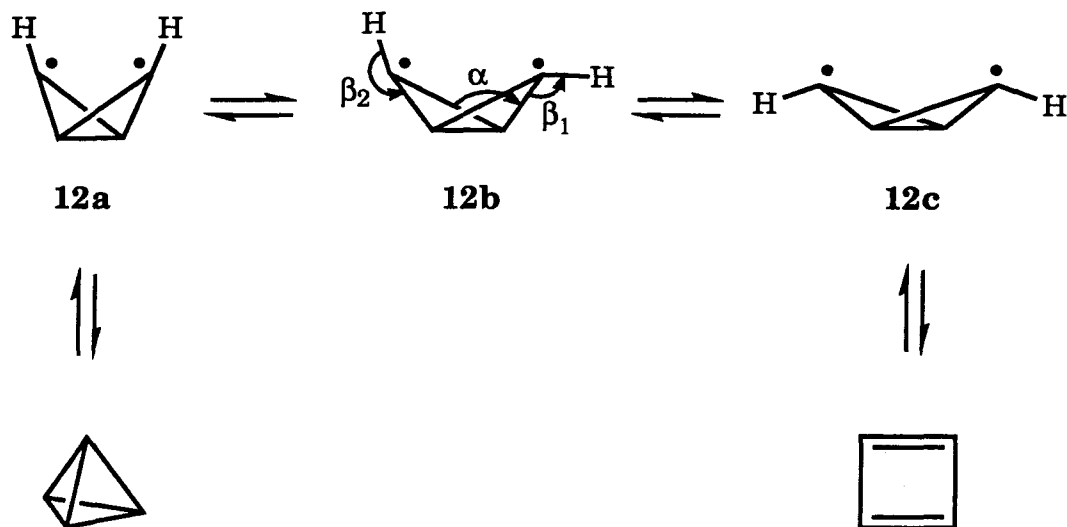
While Schulman and Venanzi's study was the first and, in certain aspects, the most comprehensive study of the characteristics of tetrahedrane, it is by no means the most state of the art study. The 4-31G basis set used fails to adequately describe the contribution of polarization, which in small rings is particularly important.²⁴ Electron correlation was also neglected, which may lead to inflated calculated energies. Subsequent *ab initio* studies have included the use of d-functions and electron correlation. More recent calculated heats of formation for tetrahedrane and CBD using a 6-31G* basis set with RMP2¹⁴ are 132.3 and 103.7 kcal/mol, respectively. Geometry optimization was performed using 6-31G*-SCF calculations. This estimates the overall heat of reaction from tetrahedrane to CBD to be 28.6 kcal/mol exothermic. Another recent calculation using 6-31G*-MP2¹⁵ for both geometry optimization and relative energy calculations estimated the heat of reaction to be only 23 kcal/mol (no absolute heats of formation were calculated).

The symmetry forbidden conversion of tetrahedrane to acetylene has been studied by both *ab initio* and semi-empirical methods. Kollmar,¹³ using a DZ + D basis set and electron correlation (CEPA), has concluded that the heat of formation of cyclobutadiene is a few kcal/mol lower than acetylene. Dewar's MINDO/3¹⁷ calculations found that the acetylene molecules are *ca.* 11 kcal/mol higher in energy than CBD. In both studies tetrahedrane was assumed to pass through the 3-cyclopropenyl carbene (13) intermediate via the biradical 12.



Dewar found an activation energy of 24 kcal/mol for the conversion of tetrahedrane to **13** and 23.3 kcal/mol for the conversion of **13** to acetylene. Both activation barriers are more than double the calculated MINDO/3 activation barrier for tetrahedrane to CBD. Kollmar found that the carbene was 34.7 kcal/mol higher in energy than tetrahedrane and was at least 5-10 kcal/mol greater than the activation energy for the conversion of tetrahedrane to CBD. He did not attempt to calculate the energy barrier from tetrahedrane to **13** or **13** to acetylene.

The conversion of tetrahedrane to CBD has been intensively studied in several of the aforementioned articles. In Kollmar's calculation, the reaction coordinate is a C-C bond stretching motion which passes through three different conformers of the bicyclobutyl biradical (**12a,b,c**). The asymmetric nature of the transition state between **12a** and **12c** (*i.e.*, **12b**) is due to an avoided orbital crossing. The effect of the C-C bond stretch is to gradually increase the dihedral angle α from **12a** to **12c** with **12b** representing the transition state.



A local minimum for **12a** was found with geometries of $\alpha = 106^\circ$, $\beta_1 = 230^\circ$, $\beta_2 = 230^\circ$. This biradical had an energy 5.5 kcal/mol higher than tetrahedrane with an activation energy of 2 kcal/mol for its conversion to tetrahedrane. The lowest energy transition state for **12b** had a geometry of $\alpha = 122^\circ$, $\beta_1 \approx 140^\circ$, $\beta_2 \approx 230^\circ$. The energy of **12b** was found to be *ca.* 25 kcal/mol above tetrahedrane (**12b** is not a stable, local minimum, but the transition state for the minimum energy reaction path between **12a** and **12c**). The conformer **12c** has its HOMO antisymmetric with respect to the C_2 axis which is parallel to the C-C bond stretch (the HOMO of **12a** is symmetric). Geometry optimization of **12c** led to a local minimum with $\alpha = 146^\circ$. The energy of this conformer is 7.6 kcal/mol lower than tetrahedrane. The activation energy was not stated for the conversion of **12c** to CBD (but is probably < 2 kcal/mol). The conclusion was that the rearrangement of tetrahedrane to CBD passed through the transition state **12b** which exacted an activation energy of at least 25 kcal/mol.

The most comprehensive analysis of the C_4H_4 potential energy surface was done by Dewar using the MINDO/3 method.¹⁷ Shown in

Figure 1-2 is the potential energy surface for a variety of C_4H_4 isomers and the activation energies required for their interconversion. Included are tetrahedrane and acetylene, as previously discussed.

Dewar's MINDO/3 study also examined the biradicals **12a** and **12c**. Similar to Kollmar's results, **12a** and **12c** were found to lie in local minima. Geometry-optimized **12a** was found to lie 9.5 kcal/mol above tetrahedrane with a barrier to tetrahedrane of *ca.* 1.2 kcal/mol. The conformer **12c** was found to be 27 kcal/mol below tetrahedrane. An activation barrier of 1-2 kcal/mol was calculated for the conversion of **12a** to **12c** with an overall activation energy of 11 kcal/mol for the conversion of tetrahedrane to CBD (the activation energy for **12c** to CBD was 0.5 kcal/mol). Dewar did not publish data concerning the geometries of **12a** or **12c**. However, in terms of activation energy, the reactions of **12a** to form tetrahedrane or CBD are virtually isoenergetic.

This semiempirical study gives an indication of the activation energies required to form tetrahedrane from several reactive precursors. Scheme 1-1 shows the activation energies for three potential precursors for tetrahedrane. The bicyclobutane carbene **14** has the largest barrier towards formation of tetrahedrane. The methylenecyclopropene carbene **13** has a smaller barrier (11 kcal/mol). Unfortunately, there exists another decay pathway to methylenecyclopropane which has a significantly smaller activation energy (4 kcal/mol).¹⁷

As discussed, the bicyclobutyl biradical **12** has the lowest barrier to formation of tetrahedrane. However, there does exist the alternate pathway of cyclobutadiene formation which is equienergetic to tetrahedrane formation in terms of activation energy (Figure 1-3).¹⁷ The

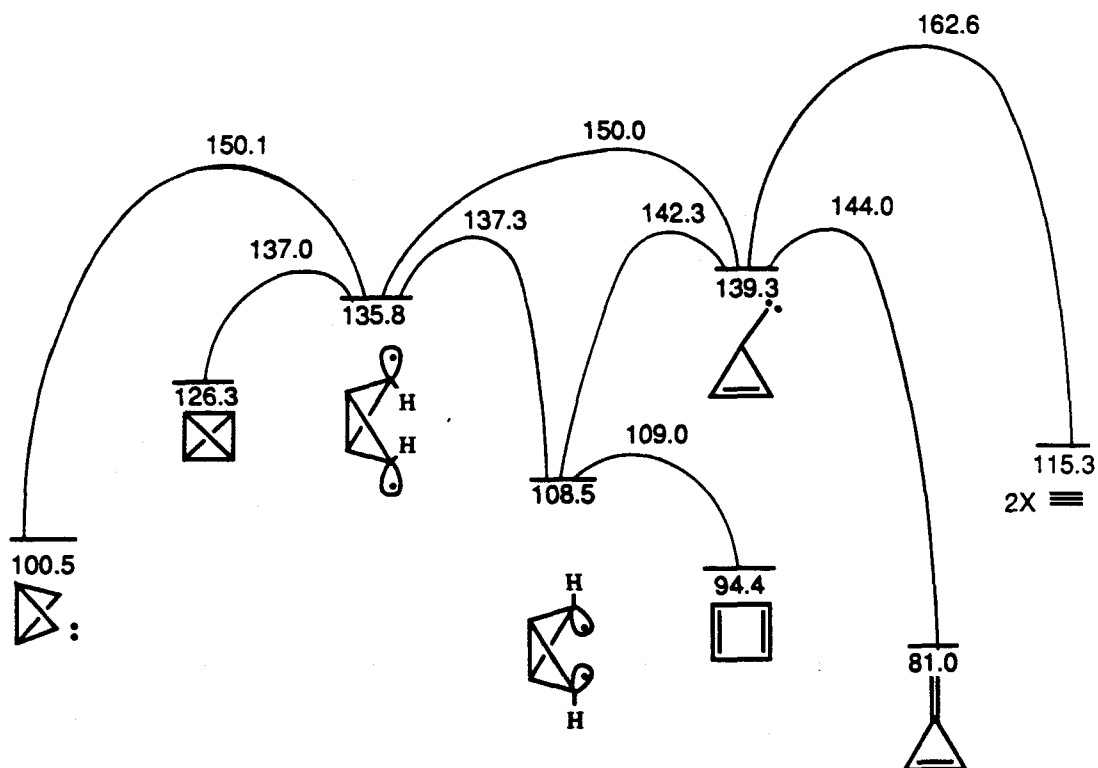
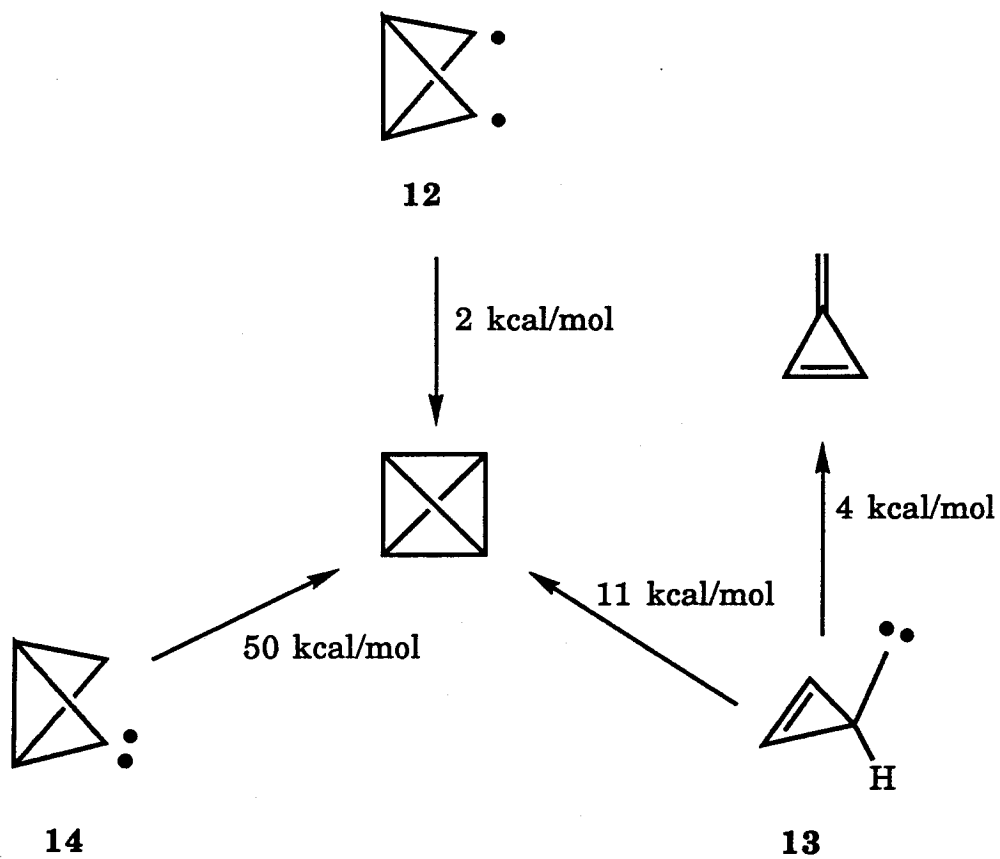


Figure 1-2. Potential energy surface (MINDO/3) for C_4H_4 isomers, including tetrahedrane and cyclobutadiene.¹⁷ Energies are in kcal/mol.

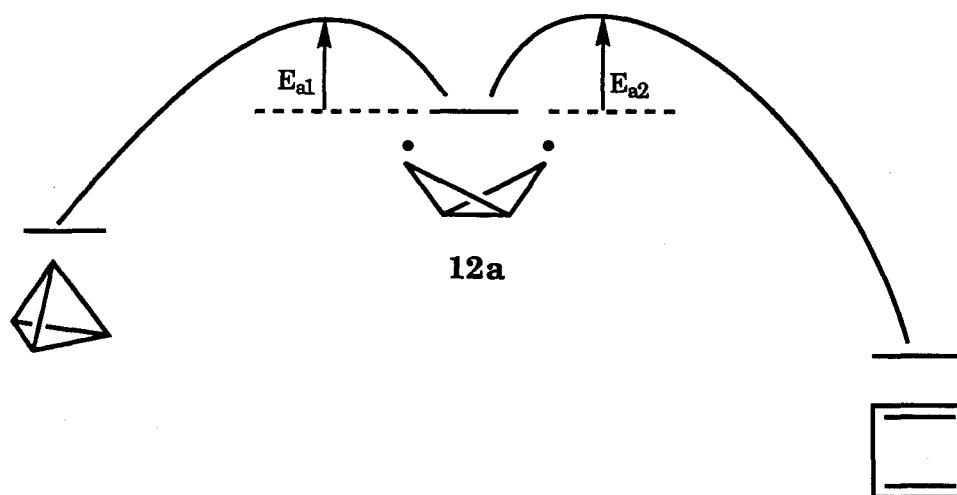
Scheme 1-1. Activation energies (MINDO/3) for the conversion to tetrahedrane for several potential precursors.¹⁷



ab initio results of Kollmar¹⁵ gives a higher barrier towards formation of cyclobutadiene relative to tetrahedrane (17 kcal/mol difference).

If the decay barriers for the biradical are equivalent, then the geometry of the biradical which is formed on the reaction coordinate may determine the success or failure of the biradical precursor in terms of forming tetrahedrane. In Figure 1-3, points on the reaction coordinate to the left of **12a** correspond to biradical geometries close to tetrahedrane, while points to the right of **12a** correspond to CBD-like geometries. If the biradical is born on the reaction coordinate close to tetrahedrane, then it is more likely that the reaction will continue in that direction since the barrier at that point in the reaction coordinate to tetrahedrane formation is smaller than conversion to cyclobutadiene. On the other hand, if the biradical is formed on the reaction coordinate close to cyclobutadiene, then the barrier to tetrahedrane formation is larger than cyclobutadiene conversion. Hence, the likelihood of observation of tetrahedrane would be remote.

Due to the high estimated strain energy (~ 130 kcal/mol) of tetrahedrane,⁷ the species may only be stable at cryogenic temperatures.¹ Assignment of structure will undoubtedly depend on low temperature spectroscopic studies of the compound in a matrix. The approximate IR and Raman frequencies of tetrahedrane were calculated by Schulman and Venanzi using the 4-31G basis set.¹¹ More recently Hess and Schaad¹⁵ calculated the vibrational frequencies of tetrahedrane and perdeuterotetrahedrane using a much more extensive basis set and electron correlation (6-31G*-SCF and MP2). The relative IR intensities were also obtained using 6-31G*-SCF calculations. Tetrahedrane was



| | Dewar ^a | Kollmar ^b |
|----------|--------------------|----------------------|
| | (kcal/mol) | |
| E_{a1} | 2 | 2 |
| E_{a2} | 2 | 19 |

^a MINDO/3, ref. 17. ^b *Ab initio*, ref. 13.

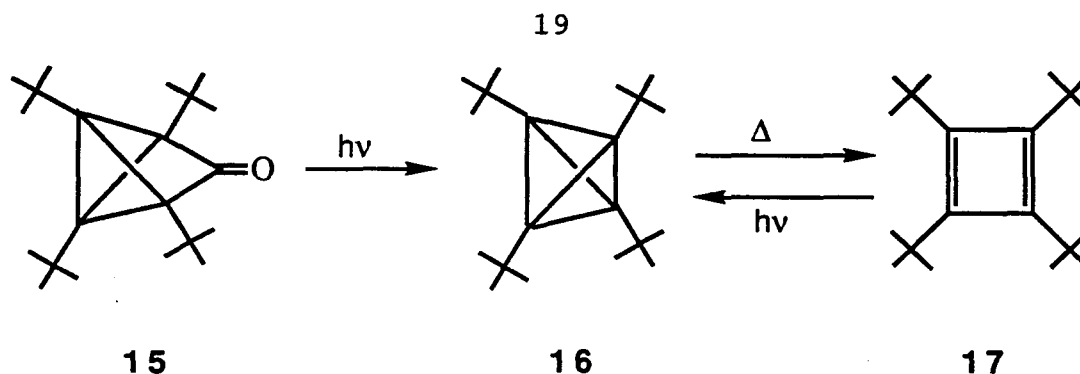
Figure 1-3. Activation energies for decay of 12a to tetrahedrane or cyclobutadiene.

calculated to have an IR spectrum consisting of a strong absorption at 895 cm^{-1} and two weak absorptions at 1291 and 3513 cm^{-1} .

The results of these theoretical studies indicate that tetrahdrane is a stable, isolable species. Kollmar's data implies that the bicyclobutane biradical with a dihedral angle α less than 122° is energetically favored to close to form tetrahdrane. The biradical appears to have the lowest activation barrier of possible C_4H_4 precursors towards generation of tetrahdrane.

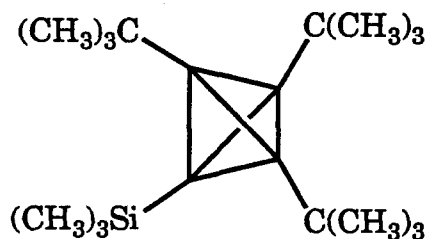
Experimental Studies

The pursuit of tetrahdrane has not only been a fertile ground for theorists, but experimentalists as well. The first claim of a tetrahdrane derivative was in 1920.²⁵ However, 40 years later it was discovered only to be a proposal for the synthesis, since reproduction of the reported method²⁶ failed to yield the product. The first isolated and unequivocally identified tetrahdrane derivative was tetra-*tert*-butyltetrahdrane²⁷ (**16**). Irradiation of **15** at 254 nm gave **16** which could be isolated as air-stable crystals with a melting point of 135°C . Upon heating to 135°C , **16** rearranged to the corresponding CBD (**17**). This process was found to be reversible upon photolysis of **17**. Crystal structure analysis²⁸ confirmed the structure of **16**, which had C-C bond lengths in the tetrahedral framework of 1.485 Å with dihedral angles between the sides of the tetrahdrane of 70.5° , as expected from symmetry.



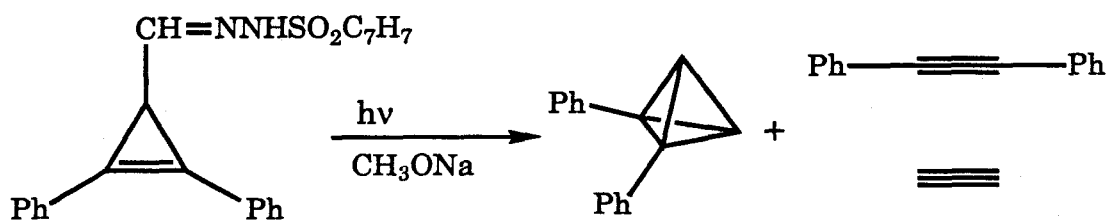
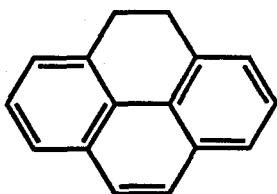
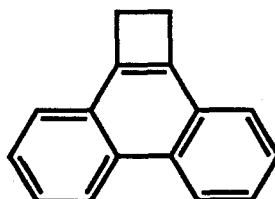
The ^{13}C spin-spin coupling constants²⁹ in the ring framework were found to be $J_{\text{C}_R\text{-C}_R} = 9.2$ Hz (cyclopropane = 12.4 Hz), and the hybridization of the bonds in the ring was calculated to be $\text{sp}^{5.20}$. The hybridization of the bonds connecting the *t*-butyl groups to the ring system was *ca.* $\text{sp}^{1.04}$. The stability of **16** was attributed to the effect of steric repulsion of the *t*-butyl groups. Any cleavage of a C–C bond in the ring will cause the *t*-butyl groups on the ring to approach one another as the framework forms a cyclobutadienyl geometry. The tetrahedral structure, however, allows maximal distance between the *t*-butyl groups.

Recently, Maier reported⁵⁸ the synthesis of a second tetrahedrane derivative, **18**. Similiar to **16**, **18** is formed upon photolysis of the cyclobutadiene. This highly strained molecule is stable up to 180°C!

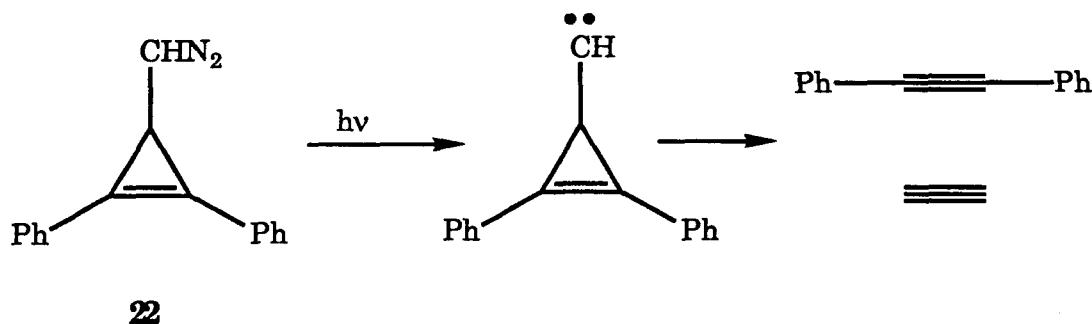


18

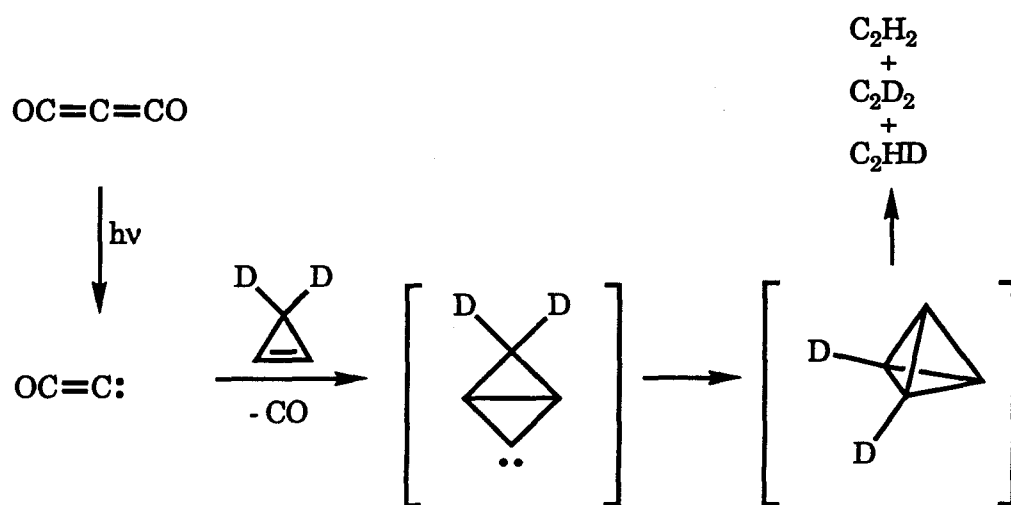
A claim for the synthesis of diphenyltetrahedrane from irradiation of **19** in the presence of sodium methoxide with a Hg lamp appeared in the literature in 1965.³⁰ Irradiation of the tosylhydrazone gave acetylene, diphenyl acetylene, and an unknown compound which was assigned to be diphenyltetrahedrane on the basis of mass, UV, and NMR spectroscopy. However, the authors later retracted their claim³¹ and assigned the unknown compound to be either **20** or **21**.

**19****20****21**

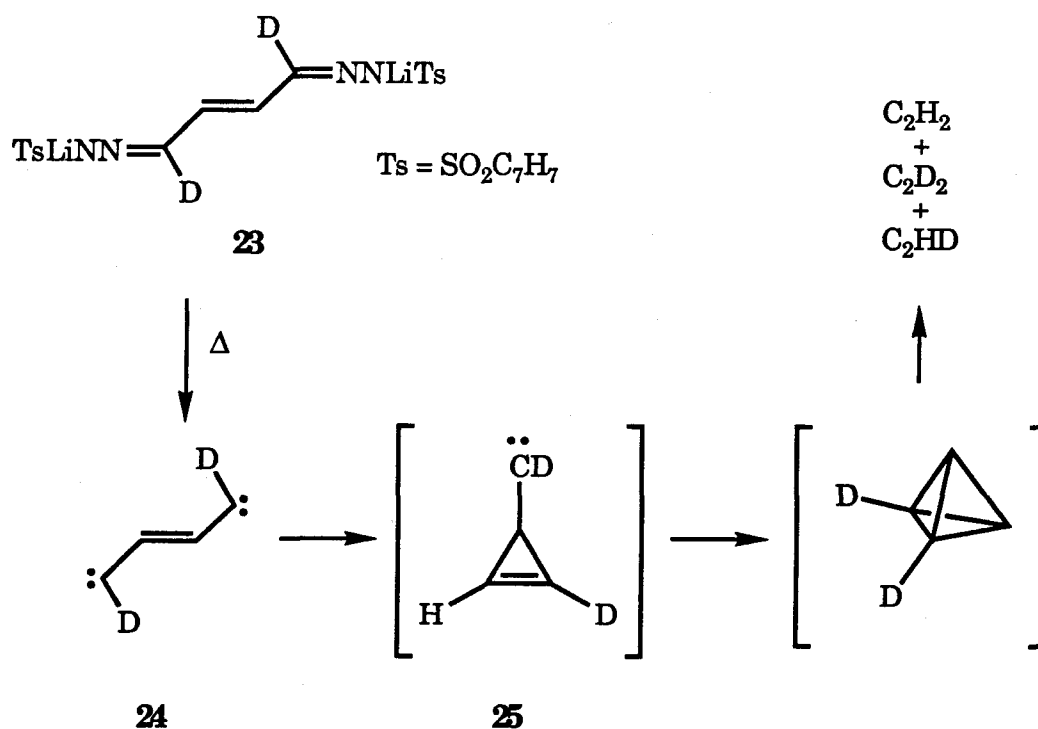
The role of a carbene intermediate in the previous example was further investigated using a diazo precursor^{32,33} (**22**). This extremely reactive molecule was photolyzed at -78°C to form a carbene which decomposed to give acetylene and diphenylacetylene. No tetrahedrane or CBD derivatives were detected.



Subsequently, the use of carbenes as precursors to tetrahedrane continued to generate much interest. The carbene generated by the photolysis of carbon suboxide in the presence of specifically deuterated cyclopropene³⁴ yielded labeled acetylenes and vinylacetylene. Mass spectroscopic analysis of the acetylene fragments showed the ratio of CHCH:CDCH:CD₂D to be approximately 1:4:1 when corrected for the presence of unlabeled cyclopropene in the reaction. This ratio was taken to be evidence for a tetrahedral intermediate. However, the reaction of carbon suboxide and 1,2-dimethylcyclopropene did not yield any acetylenic products.³⁵

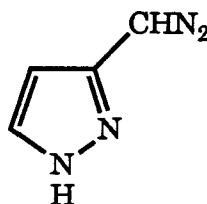


Another experiment which utilized deuterium labeling to find evidence for the intermediacy of tetrahedrane was performed using **23**. When heated, this should have formed the dicarbene **24**, which upon cyclization would have formed the carbene intermediate **25**. Product analysis showed the formation of C_2H_2 and C_2D_2 as well as $CHCD$. It was hypothesized that a tetrahedral intermediate was formed which would account for the appearance of C_2D_2 and C_2H_2 . A problem with this scheme (which the authors fail to address) is that the amount of C_2H_2 formed is four times that of C_2D_2 in the actual experiment. Ergodically speaking, they should have been equal.

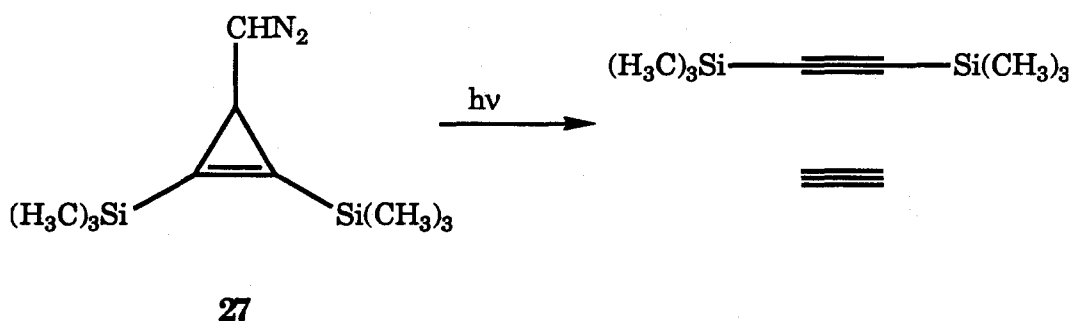


Later attempts by Maier to reproduce these results failed.^{6b} Maier found that pyrolysis of the precursor did not yield any observable acetylene

products. Instead, the only identifiable product was 3-pyrazolyldiazomethane (**26**). It was concluded that **26** was also an intermediate in the aforementioned study.

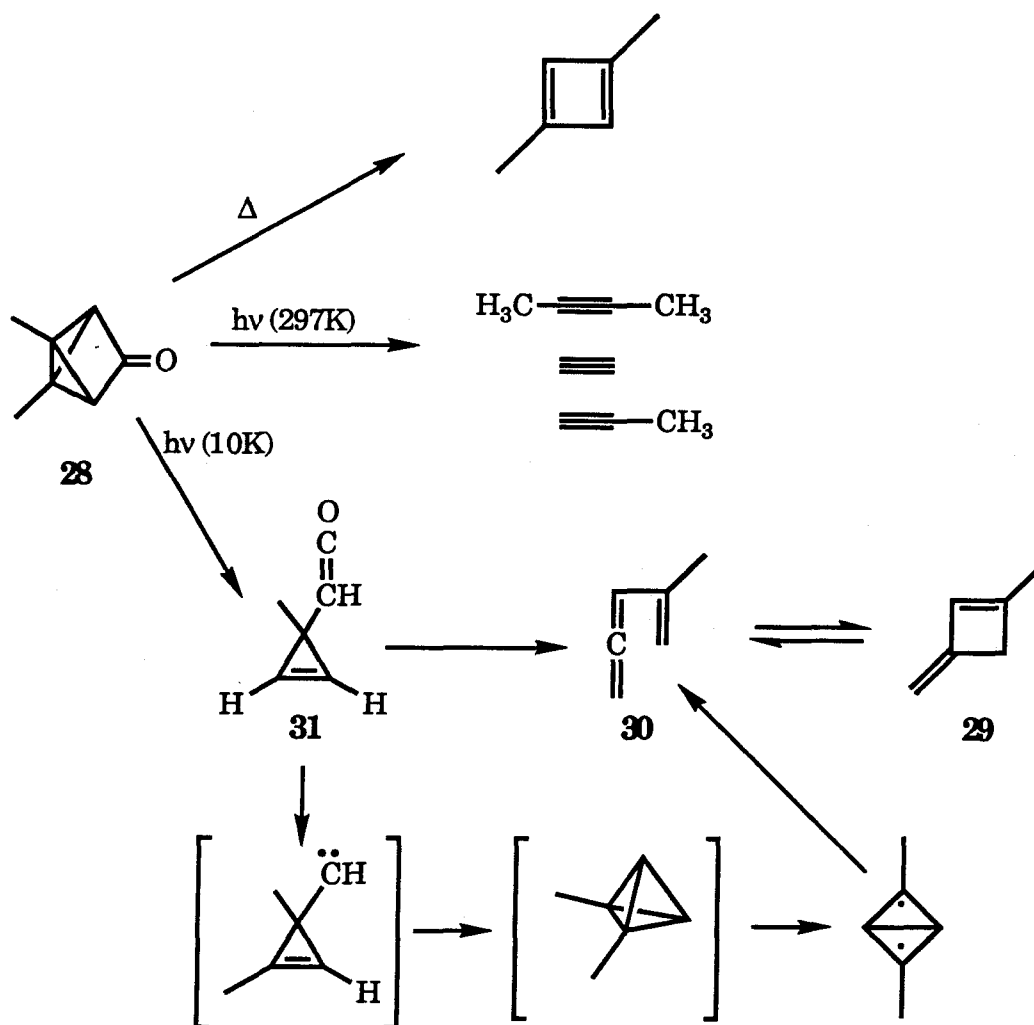
**26**

A di-(trimethylsilyl)-substituted cyclopropenylcarbene was formed from the diazo precursor **27** in an attempt by Maier³⁷ to form the substituted tetrahedrane. Photolysis in an Ar matrix at 10 K gave acetylene and the disubstituted acetylene. No evidence for a tetrahedral intermediate was seen.



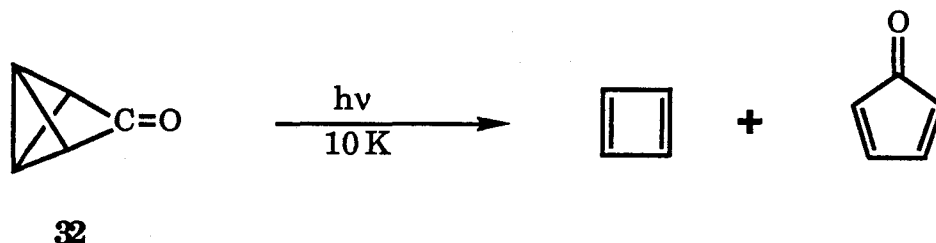
Biradicals have also been used as possible precursors to tetrahedranes. The dimethyltricyclopentanone molecule **28** has been extensively studied using thermal and photochemical activation.^{38,39} Thermolysis of **28** yielded CBD products.³⁹ Photolysis of **28** at room temperature gave 2% acetylene, 6% propyne, and 2% butyne, which was

taken as evidence of a tetrahedral intermediate. Matrix photolytic excitation³⁹ of **28** at 10 K gave a methylenecyclobutene (**29**) and a vinylallene (**30**). The postulated intermediate for the matrix reaction was not the biradical, but instead the cyclopropene derivative **31**. It is possible that **31** may have decarbonylated to form a carbene, which in turn could have formed the observed products via a tetrahedral intermediate.

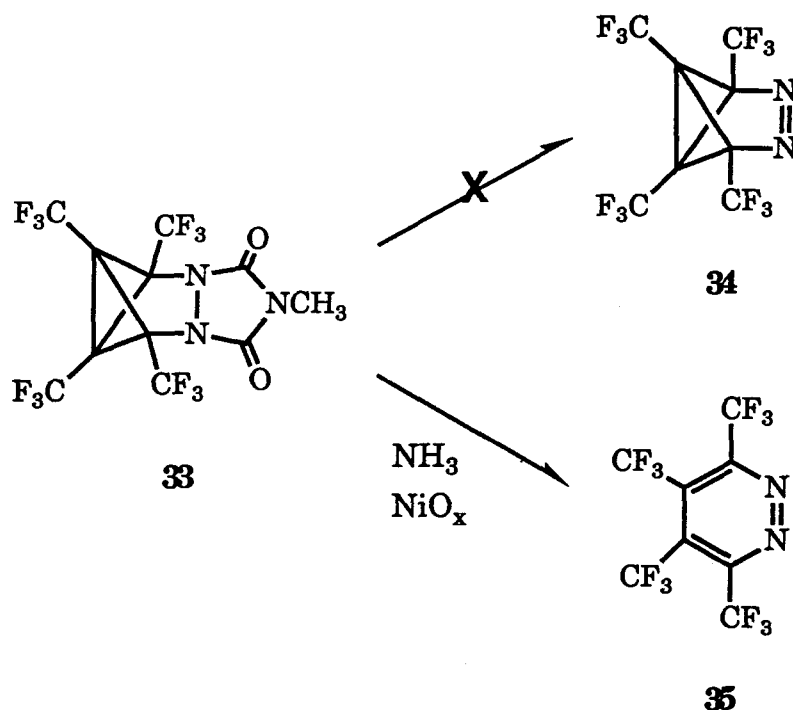


Similar experiments with the diphenyl ketone³³ gave CBD products upon photolysis at room temperature. Matrix photolysis at 10 K gave cyclopentadienone products. While these CBD products may have been formed via tetrahedrane, no direct spectroscopic observation was ever made. Tetra-methyl-substituted diketones⁴⁰ were also photolytically decomposed under matrix isolation conditions with no direct evidence of a tetrahedrane derivative.

The parent ketone, **32**, was synthesized by Maier²⁰ and photolyzed under matrix isolation conditions. Irradiation at 10 K with 240 nm light in an argon matrix gave CBD, cyclopentadienone, and acetylene (formed from secondary photolysis of CBD). No indication of tetrahedrane was seen in the FT-IR spectrum.

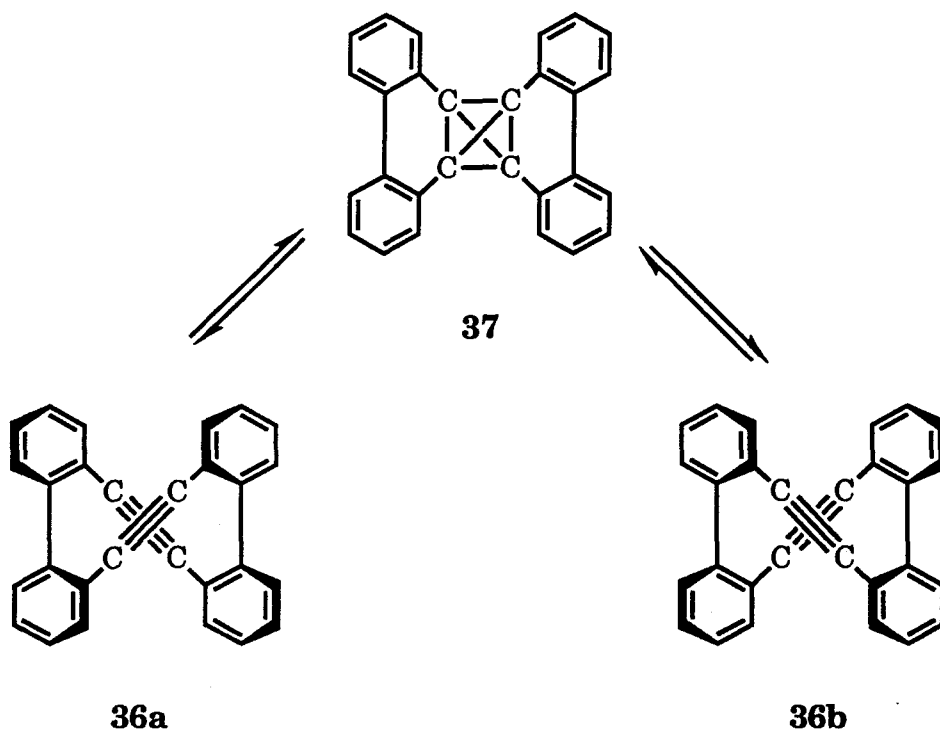


The only documented attempt to form an azo precursor to a tetrahedrane derivative was the attempted synthesis of **34**.⁴¹



When the urazole adduct **33** was reacted with NH_3 and oxidized with nickel peroxide, only the pyridazine derivative **35** was formed. Attempted hydrolysis of **33** with KOH failed. No cyclic azo compound was ever detected. The perfluoromethyl groups on the bridgeheads may have had a destabilizing effect upon **34**.

A novel route for the formation of a tetrahedrane derivative is the cycloaddition of two acetylene molecules. The acetylene-linked tetraphenyl compound **36** has been synthesized by Staab et al.⁴² If the two enantiomers (**36a** and **36b**) could have been separated, photolysis of one form would have given a racemic mixture assuming the tetrahedrane intermediate **37** was formed. Unfortunately, separation of **36a** and **36b** was not possible.



In view of the theoretical studies by Dewar and Kollmar, the use of carbenes as precursors to tetrahedrane is suspect. The aforementioned labeling studies all interpreted formation of acetylenic products as evidence for a tetrahedral intermediate, yet theory predicts the formation of CBD to be more favorable than formation of acetylene in the decomposition reaction of tetrahedrane. However, in no carbene experiment was CBD ever observed. In fact, only in studies involving ketone precursors were CBD products detected. The theoretical treatments outlined above suggests that of all the viable precursors, the biradical **12** (which is a logical product of the photolysis of **9**), has the greatest potential of forming tetrahedrane.

Synthesis, Results and Discussion

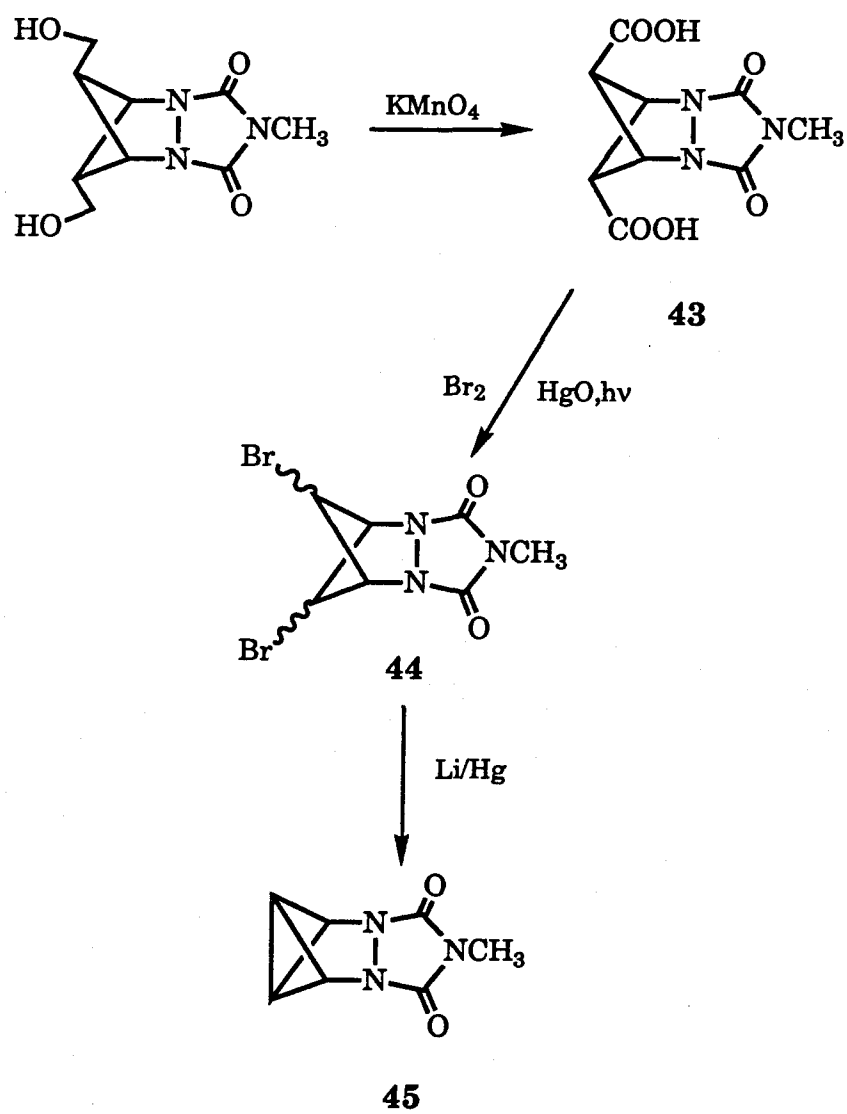
As previously mentioned, the method of choice for generating biradical **12** is through the azo precursor **9**. Our synthetic scheme for the synthesis of this molecule begins with the dihydroxymethyl MTAD adduct **42**.

This diol was synthesized using the reactions in Scheme 1-2 which were developed in these laboratories.⁴³ The synthesis of **42** begins with benzvalene (**38**),⁹ which is readily available in moderate quantities. Ozonolysis and reduction of benzvalene with lithium aluminum hydride afforded the *endo, endo* diol **39** in 55% yield. Protection of **39** with *t*-butyldimethylsilyl chloride gave **40** in near quantitative yield. Photolytic addition of 4-methyltriazolinedione across the strained bond of **40** afforded exclusively *endo, endo* substituted adduct **41** in 22% yield. Deprotection of the MTAD adduct with tetrabutylammonium fluoride gave diol **42** in 90% yield. The overall yield from benzvalene to **42** was 8.4%.

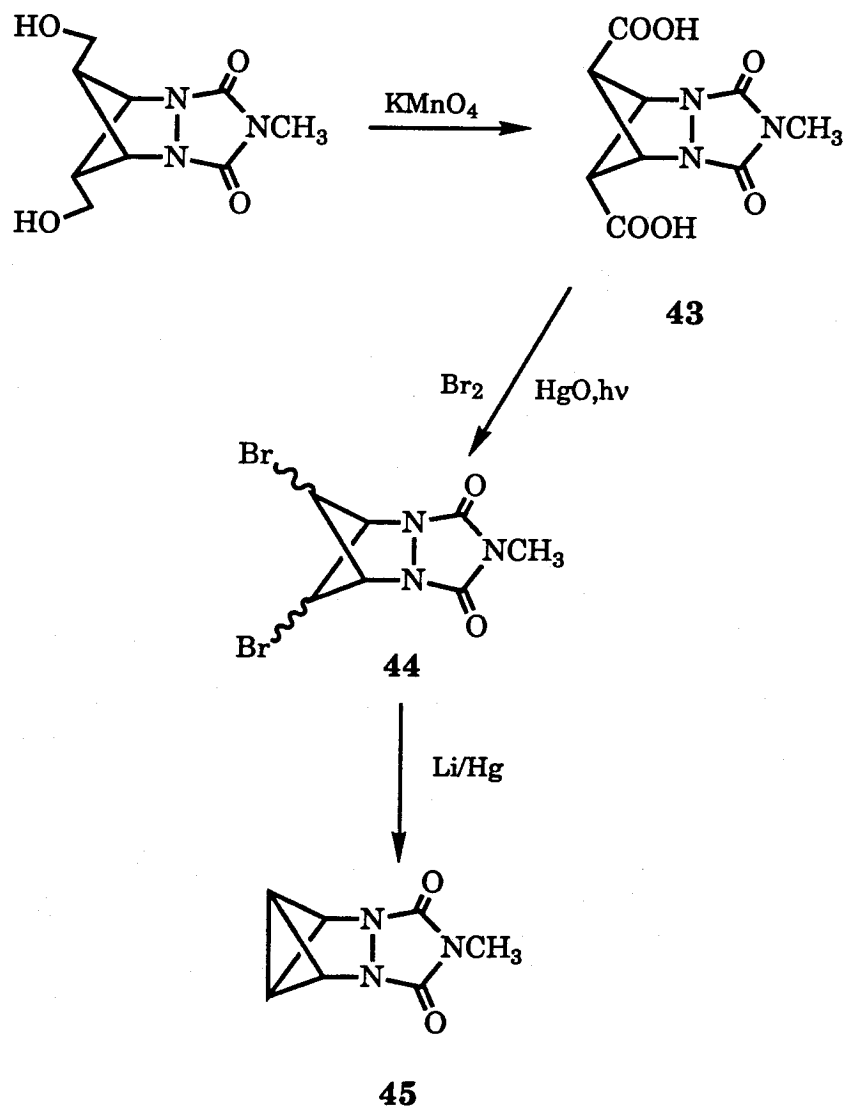
The urazole adduct **45** was synthesized from the diol according to Scheme 1-3. The diacid, **43**, was formed in 55% yield by oxidation with potassium permanganate in water. This was followed by a modified Hunsdiecker reaction.⁴⁴ Refluxing **43** in the presence of bromine and mercuric oxide with magnesium sulfate in methylene chloride while irradiating with a 67 watt incandescent light bulb afforded a mixture of three isomers of the dibromide **44** in 44% yield. The dibromide mixture was reductively coupled using 2% lithium amalgam in THF, giving **45** as a white crystalline product in 70% yield.

The ¹H NMR spectrum of **45** contained the characteristic N-methyl peak at δ 2.97 and two triplets which were coupled to each other ($J = 1.71$ Hz) at δ 2.84 and 4.60. These signals were assigned to the bicyclobutane

Scheme 1-3.



Scheme 1-3.



ring protons (H_A and H_B). The chemical shifts and small H-H coupling constants are similar to those of the related urazole⁴⁵ **46** and the analogous ketone²³ **32** (Table 1-2).

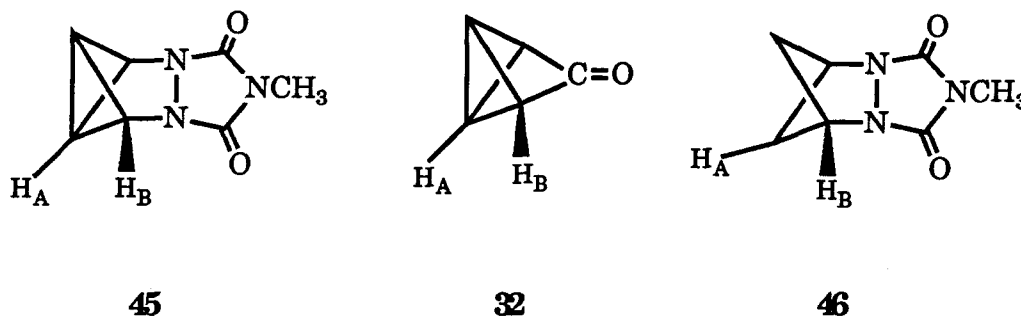


Table 1-2. ^1H NMR Data for **45**, **46**, and **32**

| | H_A^a | H_B^a | J_{H-H} (Hz) |
|-----------|---------|---------|----------------|
| 45 | 2.84 | 4.60 | 1.71 |
| 46 | 2.30 | 4.70 | 2.0 |
| 32 | 2.08 | 4.01 | 1.0 |

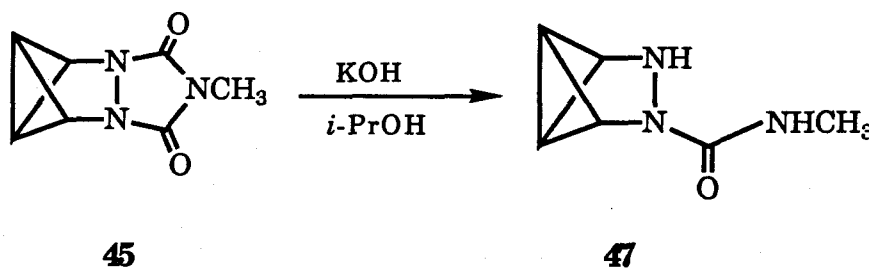
^a PPM relative to TMS (CDCl_3).

The ^{13}C chemical shifts of the A and B carbons in **45** occur at δ 7.51 and 52.35 while in **32** they occur at δ -1.0 and 36.6. The strained character of the bicyclobutane ring in **45** is reflected in the large ^{13}C - ^1H coupling constants ($J_{13\text{C}_A\text{H}_A} = 223.02$ Hz; $J_{13\text{C}_B\text{H}_B} = 195.00$ Hz). These large $J_{13\text{C-H}}$ coupling constants were also observed in **38**.⁹

The next step of the synthetic scheme is the formation of the azo compound. There are several methods of converting the urazole ring to the

azo group. Traditionally, hydrolysis of the urazole ring followed by oxidation with CuBr_2 has been used.⁴⁶ This method has the drawback of requiring relatively high temperatures. In light of the possible thermal instability of the azo product, low temperature oxidation of the semicarbazide of **45** was accomplished using nickel peroxide at -78°C . This procedure has proven to be remarkably valuable in the conversion of semicarbazides to thermally labile 1,2-diazenes.^{43,47}

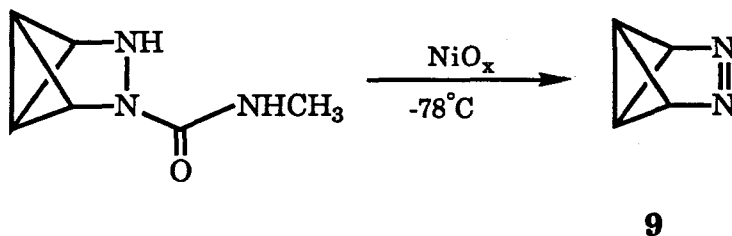
Hydrolysis of the urazole ring in **45** was accomplished with potassium hydroxide in isopropanol under anaerobic conditions. The resulting semicarbazide, **47**, exhibited the characteristic N-methyl doublet and inequivalence of the C_2 and C_5 ring protons in the ^1H NMR spectrum.



The labile semicarbazide did not lend itself to further purification. In the presence of atmospheric oxygen, the peaks attributed to **47** in the ^1H NMR spectrum decreased while a new set of absorbances consisting of a singlet (δ 3.01) and two asymmetric triplets (δ 7.46, 9.19) appeared. The new peaks correspond to the spectra for pyridazine and methyl isocyanate. Apparently, the semicarbazide undergoes air oxidation to give the aromatic pyridazine with methyl isocyanate as a byproduct. The decay path probably does not go through the 3,4-diazabenzvalene intermediate

since thermal decomposition would have yielded cyclobutadiene products (*vide infra*).

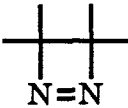

Oxidation of the semicarbazide to the diazene was accomplished using nickel peroxide⁴⁸ in a methylene chloride/dimethyl ether solution at -78°C. Cold filtration of the heterogenous mixture followed by distillation of the solvent at -78°C completed the synthesis of **9**.



The ¹H NMR spectrum of **9** in methylene chloride-*d*₂⁴⁹ exhibits two coupled triplets (*J* = 1.22 Hz) at δ 3.87 and δ 4.91. The absorption of δ 4.91 corresponds to the C₂ and C₅ positions and may be compared to that found for the similar proton in **48**⁴⁵ (δ 4.80). The C₁ and C₆ bridgehead protons show a similar shift to those of benzvalene⁹ (δ 3.53). The UV spectrum of 3,4-diazabenzvalene in diethyl ether is highly structured with an intense O, O band (λ_{max} = 310 nm) and two smaller peaks (304, 300 nm). The spectral shape seen is similar to that of **48** and is consistent with the rigid structure of **9**.⁴⁵ The λ_{max} is at shorter wavelength than that seen for **48** (331 nm) and most other cyclic diazenes (Table 1-3).⁵⁹

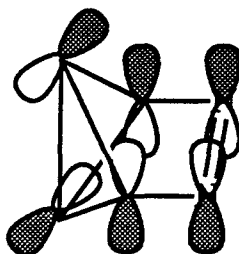
**48**

Table 1-3. UV Absorptions of Several Azoalkanes⁵⁹

| | λ_{max} (nm) |
|---|-----------------------------|
| 9 | 304 |
| 48^a | 331 |
|  | 347 |
|  | 341 |

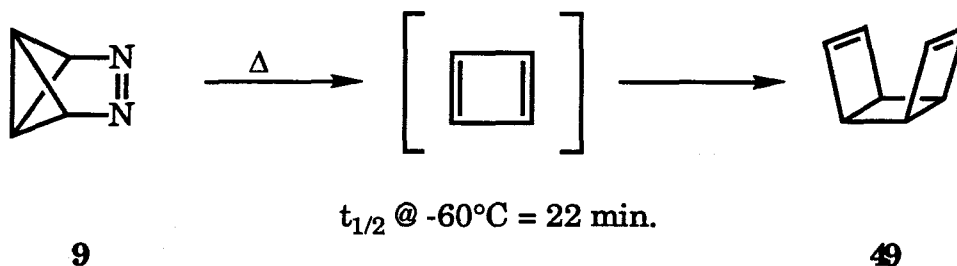
^a Ref. 45.

This observation can be attributed to a favorable interaction between the N=N π^* orbital and the a_2 orbital of the bicyclobutane group in **9**.⁹ This interaction raises the energy of the π^* orbital and hence the energy of the n- π^* absorption.



Thermal Reactivity

The diazene **9** is highly unstable with regard to thermal reactivity and is quite difficult to handle. 3,4-Diazabenzvalene thermally decays to produce syn-tricyclooctadiene **49**, presumably via cyclobutadiene.



The unimolecular reaction rate constant for thermal decay of 3,4-diazabenzvalene was evaluated using ^1H NMR spectroscopy.

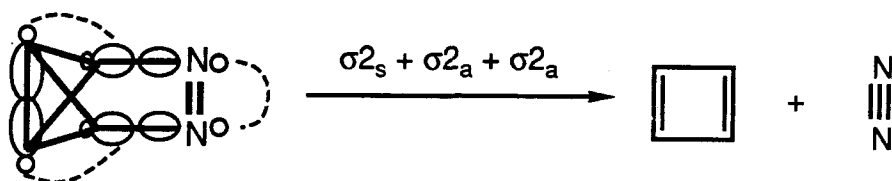
The rate constant for the decay is $5.24 \times 10^{-4} \text{ sec}^{-1}$, which corresponds to a reaction half-life of 22 minutes at -60°C .

For comparison, the closely related diazene **48** decomposes with $\log A = 15.5$, $E_a = 34.4 \text{ kcal/mol}$,⁵¹ giving it a similar half-life at a much higher temperature of 133°C . If decomposition of 3,4-diazabenzvalene occurs with an A value that is similar to the decomposition of **48**, then the activation energy barrier for thermal decomposition is calculated to be only 18 kcal/mol for **9**.

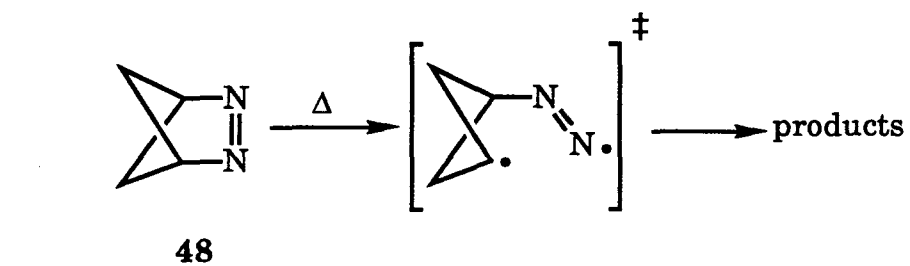
The high reactivity of **9** as compared to **48** is surprising when the driving force of strain energy release is considered. The thermal decomposition of **48** has been shown to proceed via one-bond cleavage, producing an intermediate diazenyl biradical.⁵¹ The estimated decrease in

strain energy for this process is 20 kcal/mol (Figure 1-4).⁵² If **9** decomposes by the same one-bond cleavage mechanism, then the difference in estimated strain energy between the diazenyl transition state and the reactant is only 14 kcal/mol. Thus, even though by strain energy relief evidence one may infer that the driving force for decomposition of **48** is greater than that of **9**, in reality **9** has a 16 kcal/mol lower activation energy towards decomposition than **48**.

An alternate explanation of the stability difference between **9** and **48** would be a change in mechanism. Diazene **9** can undergo a direct, concerted, $[\sigma_{2s} + \sigma_{2a} + \sigma_{2a}]$ conversion to cyclobutadiene plus N_2 .



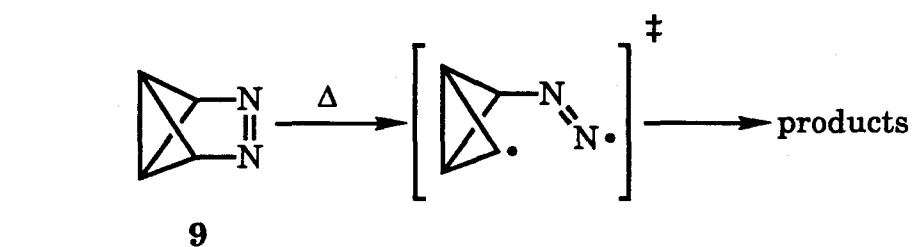
There is ample precedent⁵⁴ for dramatic rate accelerations of diazene decomposition upon introduction of a strained σ bond that can divert the reaction from a biradical path to a concerted six-electron process. For instance, **84** has a 10^{11} rate enhancement over **85** with regard to deazetation. This result has been interpreted in terms of a concerted 6-electron process involving participation of the strain σ bond in **84**. While the orientation of the strained bond in **9** is different than in **84**, the cyclic array shown seems quite feasible.



strain
energy
(kcal/mol)

47

27



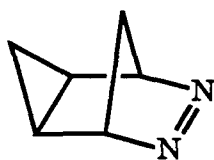
strain
energy
(kcal/mol)

77

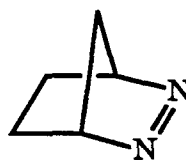
63

| | E_a | Strain Relief |
|-----------|-------------|---------------|
| 48 | 34 kcal/mol | 20 kcal/mol |
| 9 | 18 kcal/mol | 14 kcal/mol |

Figure 1-4. One-bond cleavage mechanism for decomposition of **9** and **48**.



84



85

It is interesting to compare the thermal decomposition of benzvalene⁹ and 3,4-diazabenzvalene (Figure 1-5). Both can rearrange to an aromatic product (benzene or pyridazine) in a reaction that is highly exothermic, but still possesses a substantial barrier. Only for diazene **9**, though, is the fragmentation path to cyclobutadiene exothermic. This is, of course, a consequence of the much greater thermodynamic stability of N₂ versus acetylene.

Photochemical Reactivity. The photochemical behavior of **9** has been studied using several solvents at varying temperatures (Scheme 1-4). Photolysis of 3,4-diazabenzvalene at -196°C followed by ¹H NMR at -150°C (propane-*d*₈) or at -100°C (diethyl ether-*d*₁₀) resulted in cyclobutadiene dimer. The diazene was only partially soluble in propane-*d*₈. Photolysis of **9** in a 1:3 mixture of CDCl₂F:CDClF₂⁵⁵ at -196°C followed by ¹H NMR at -150°C produce both cyclobutadiene dimer and pyridazine (*ca.* 1:1). The diazene was completely soluble in the deuterated freon solution.

In these ¹H NMR studies no direct evidence of tetrahedrane was found. The previously mentioned theoretical models have all concluded that tetrahedrane does lie in a potential energy well. If it is assumed that tetrahedrane is a photolysis product of **9**, and if log A = 15 for the thermal

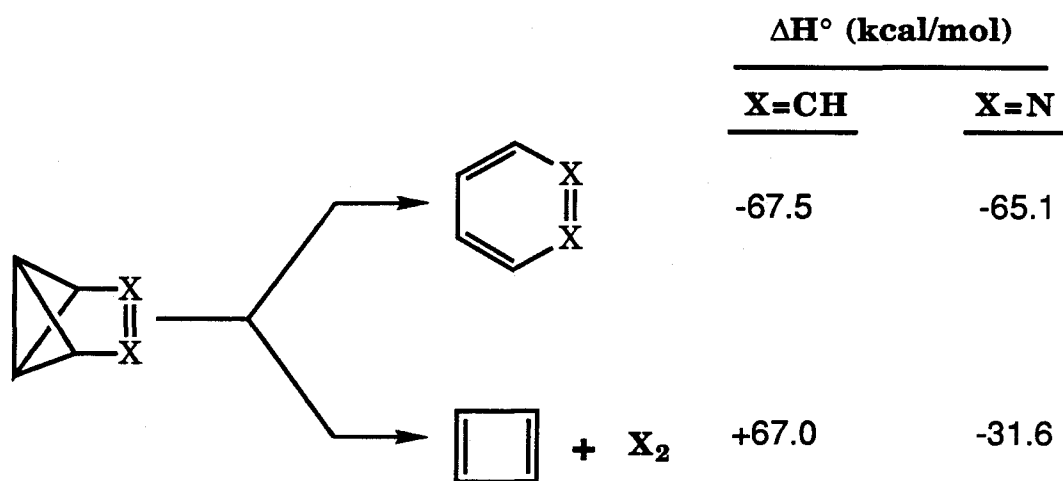
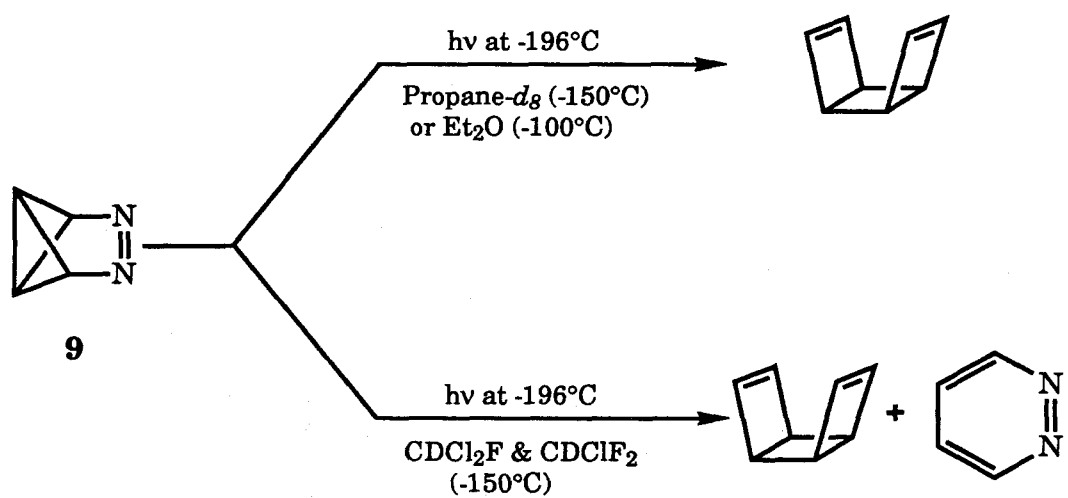


Figure 1-5. Thermochemistry of 3,4-diazabenzvalene versus benzvalene.

Scheme 1-4. ^1H NMR photolysis studies of **9**.

decomposition of tetrahydrane, then an upper limit 10 kcal/mol is imposed upon E_a for the decay path of tetrahydrane by the -150°C ^1H NMR experiments.

Matrix Isolation Studies.⁵⁷ Several attempts were made to conduct matrix isolation experiments with 3,4-diazabenzvalene without success. In order to perform the studies, it is first necessary to co-deposit the reactant with argon on an optically transparent window at 20 K. For non-gaseous substances, this is done by subliming the material onto the cooled surface. Once this is accomplished, the argon matrix containing the reactant can be photolyzed with a light source and analyzed by FT-IR spectroscopy. The high thermal reactivity of **9** required low temperature sublimation of the material onto the 20 K window. Unfortunately, it appeared that the vapor pressure of **9** was too small at the low temperatures required for its manipulation to allow sublimation to occur. Attempts were made to sublime the diazene at -78 , -60 , and -40°C with no resultant evidence of diazene present in the argon matrix by FT-IR spectroscopy. It is possible that the relatively long path which the sublimed molecules must travel before depositing onto the argon matrix may contribute to the failure of the deposition process. Also, it has been suggested that direct introduction of the matrix gas (argon) to the diazene followed by concurrent deposition may assist sublimation of the non-volatile diazene. In the current experiment the diazene and the matrix gas are introduced to the cooled window at two separate physical locations in the instrument.

Conclusion

We have synthesized the highly reactive diazene, 3,4-diazabenzvalene. This molecule has proven to be thermally quite labile, undergoing decomposition at -60°C to give cyclobutadiene with a half-life for the reaction of 22 min. In light of the relatively small release of strain energy upon cleavage of a C–N bond in the transition state for the one-bond diazenyl biradical decomposition mechanism, an alternate mechanism is proposed. A direct, concerted, $\sigma_{2s} + \sigma_{2a} + \sigma_{2a}$ process may account for the rapid rate of decomposition when compared to similar diazenes.

Upon photolysis at -196°C and thawing to -150°C , the diazene decomposes to give cyclobutadiene and pyridazine. Tetrahedrane was not observed under these conditions. Unfortunately, attempts to perform matrix isolation photolysis experiments on **9** at 10 K failed due to inability to deposit the labile diazene at low temperatures. Thus, it is not yet clear if 3,4-diazabenzvalene is a viable precursor to the much sought after, but never observed molecule, tetrahedrane.

Experimental

General

^1H NMR spectra were recorded on a Varian EM-390 spectrometer. Fourier transform NMR spectra (^1H and ^{13}C) were recorded on a JEOL FX-90Q or JEOL GX-400 spectrometer. Analytical gas chromatography was performed on a Hewlett-Packard 5840A chromatograph equipped with a J and W DB5-30W capillary column and a flame ionization detector. Elemental analysis and mass spectra were obtained by the California Institute of Technology Analytic Facility. Exact mass measurements were obtained by the University of Riverside Analytic Facility.

The matrix isolation experiments were performed on a system that was designed and assembled by A. P. Sylwester.⁵⁷

All solvents were reagent grade and used as purchased except where noted. Tetrahydrofuran was distilled from sodium-benzophenone ketyl just prior to use. Flash column chromatography was done using the method of Still⁵⁶ with 230-400 mesh silica.

Nickel peroxide (activated)

To a stirring solution of 13g of $\text{NiSO}_4 \cdot 6\text{H}_2\text{O}$ in 30 mL of H_2O was added dropwise a solution of 4.2g of NaOH (88%) in 35 mL of 5% sodium hypochlorite solution (Aldrich). A black precipitate resulted. The mixture was stirred for 30 min, after which the black solid was suctioned and washed with 3 x 30 mL of H_2O . The solid was air-dried on the filter for 18 hr. The solid was then dried through application of vacuum over P_2O_5 in a vacuum dessicator for 24 hr.

To 4g of this ground, dried black solid was added 40 mL of 5% sodium hypochlorite solution, with a resultant evolution of gas. The black slurry was stirred for 30 minutes, then filtered and washed thrice with 20 mL of water. The black filter cake was then dried under vacuum over P_2O_5 for 48 hr. The nickel peroxide was then used immediately for the oxidation of 47.

4-Methyl-*endo,endo*-8,9-di(hydroxymethyl)-2,4,6-triazatricyclo-[5.1.1.0^{2,6}]-nonane-3,5-dione (42)

The diol was prepared by the method of Dougherty and Snyder⁴³ from benzvalene.⁹ The diol was purified by recrystallization from THF prior to use. Yield: 8.4%.

4-Methyl-*endo,endo*-8,9-dioic-2,4,6-triazatricyclo[5.1.1.0^{2,6}]-nonane-3,5-dione (43)

A 250 mL three-necked round bottom flask containing potassium permanganate (2.41g, 15.28 mmol) dissolved in 50 mL of H_2O and 3.8 mL of 1.0 M HCl (3.8 mmol) and a stir bar was fitted with an N_2 gas inlet, reflux condenser, and a 25 mL addition funnel containing 42 (1.3g, 5.2 mmol) dissolved in 15 mL of H_2O . The slightly cloudy diol solution was added dropwise to the stirring purple permanganate solution over a period of 15 minutes at room temperature. The mixture was stirred under N_2 for 17 hours, gradually forming a dark brown precipitate of MnO_2 . When the reaction was complete, 0.5g of sodium bisulfite and 0.9g of sodium bicarbonate were added to the mixture to neutralize any remaining permanganate and turn the solution basic. This mixture was filtered through a fine glass frit, and the dark brown filter cake was washed several times with H_2O to remove entrapped diacid salts. The combined

clear filtrate was acidified to pH 2 with concentrated HCl. The acidic aqueous solution was washed with CH₂Cl₂ (3 x 20 mL). The aqueous solution was then continuously extracted with diethyl ether over a period of 10 days. Removal of diethyl ether afforded a white powder. Yield: 0.698g (55%). ¹H NMR (acetone-d₆) δ 2.81 (s, 3H), 3.45 (t, 2H, J = 1.90 Hz), 5.13 (t, 2H, J = 1.90 Hz): ¹³C NMR (acetone-d₆) δ 25.42, 50.32, 64.45, 158.34, 167.22.

4-Methyl-8,9-dibromo-2,4,6-triazatricyclo[5.1.1.0^{2,6}]-nonane-3,5-dione (44)

To a dry 25 mL three-necked round bottom flask containing a stir bar was added **43** (0.0909g, 0.3564 mmol), MgSO₄ (0.1206g) and HgO (0.1627g, 0.7532 mmol). After the flask was fitted with a reflux condenser and an Ar inlet, 5 mL of CH₂Cl₂ (distilled over P₂O₅) was added via syringe. The flask was then flushed with Ar for 10 min. The orange insoluble HgO settled to the bottom of the flask while the insoluble MgSO₄ and diacid were suspended in the solution. To the stirring mixture was added Br₂ (0.1914g, 1.197 mmol) via syringe in one shot. The stirring mixture was heated to reflux (ca. 40°C) while being irradiated with an incandescent light bulb (67 watts) placed close to the flask. After 30 min the Br₂ had disappeared and very little HgO was left. The reaction mixture was cooled and additional Br₂ (0.084g, 0.58 mmol) was syringed into the flask, along with additional HgO (0.1g, 0.46 mmol). Reflux and irradiation were continued for 40 additional min. The flask and contents were cooled to room temperature and the mixture was filtered through a fine frit. The filter cake was washed several times with CH₂Cl₂ and pentane. The pale yellow filtrate and washings were washed with 1.0 M HCl (6 x 15 mL) to remove HgBr₂. The organic solution was dried and removal of solvent yielded a yellow solid which was determined by ¹H NMR to contain the impure dibromide.

Purification was achieved by flash column chromatography using 50 mL of 64%, 100 mL of 58%, and 100 mL of 50% petroleum ether:ethyl acetate eluent. Yield: 50.9 mg (44%) of white powder. Three isomers of the dibromide in approximate ratios of 1:10:100 (*exo,exo:endo,exo:endo,endo*) were detected by ^1H NMR (CDCl_3) *endo,endo*; δ 3.05 (s, 3H), 4.23 (t, 2H, $J = 1.71$ Hz), 4.92 (t, 1H, $J = 1.71$ Hz); *exo,exo*; 3.10 (s, 3H), 4.15 (s, 2H), 4.79 (s, 2H). ^{13}C NMR (CDCl_3): *endo,endo*; δ 26.58, 39.87, 67.57, 158.11; *exo,endo*; 26.64, 47.49, 47.81, 68.76, 158.10; *exo,exo*; 26.64, 48.42, 67.75, 158.20. Mass spectrum: Three parent peaks corresponding to the bromide isotope effect in a dibromide are at 323, 325, and 327 m/e with ratios of 1.05:2.12:1.00.

4-Methyl-2,4,6-triazatetracyclo[6.1.0.0^{2,6}.0^{7,9}]-nonane-4,6-dione (45)

To a stirring solution of 189 mg (0.58 mmol) of 44 in 20 mL of THF was added 1.21 g (3.5 mmol) of 2% lithium amalgam. The mixture was stirred for 24 hr. under argon. The gray mixture was then filtered and the solvent evaporated. The crude material was purified using flash column chromatography techniques with 7:4 petroleum ether/ethyl acetate as the eluent (two flash columns were required for full purification). Gave 72.8 mg (0.44 mmol, 75%) of white crystals: ^1H NMR (CDCl_3) δ 2.84 (t, 2H, $J = 1.71$ Hz), 2.97 (s, 3H), 4.60 (t, 2H, $J = 1.71$ Hz); ^{13}C NMR (CDCl_3) δ 7.51 (dd, $^1J_{\text{CH}} = 223.02$ Hz, $^2J_{\text{CH}} = 3.67$ Hz), 25.97 (quartet), 52.35 (dtd, $^1J_{\text{CH}} = 195.14$ Hz, $^2J_{\text{CH}} = 3.67$ Hz, $^3J_{\text{CH}} = 10.27$ Hz), 161.86 (s); Exact mass calculated: 165.0538, found: 165.0539; Melting point 116.0-116.5°C.

Semicarbazide (48)

To a 10 mL round bottom flask containing 35 mg (0.212 mmol) of **45** and 107 mg (1.06 mmol) of 88% KOH (solid) was added 5 mL of degassed isopropanol. After stirring 60 min under argon, thin layer chromatography showed no remaining starting material. The stirring solution was carefully acidified with 1.0 M HCl to pH 1, during which a white solid formed at pH 8, then disappeared at pH 2. Gas evolution was observed upon initial addition of the 1.0 M HCl. The solution was diluted with 1.0 mL of H₂O and extracted with CH₂Cl₂ (6 extractions of 2.0 mL). The solvent from the combined organic extractions was evaporated using a strong flow of argon, and the product (a yellow oil with some solid) was placed under high vacuum for 30 min. The semicarbazide was immediately brought forward to the next reaction (oxidation to 3,4-diazabenzvalene). ¹H NMR (CDCl₃): δ 2.43 (bs, 2H), 2.77 (d, 3H, J = 6.5 Hz), 3.89 (t of d, 1H, J = 4.4, 1.3 Hz), 4.68 (t of d, 1H, J = 4.0, 1.5 Hz), 6.22 (bs).

3,4 Diazabenzvalene (9)

To an empty, degassed 2-neck, 10 mL pear-shaped flask fitted with a solid addition ampoule containing 787 mg of activated nickel peroxide was added the semicarbazide (0.212 mmol calculated) dissolved in 1 mL CH₂Cl₂. Using a flow of argon, all but *ca.* 60 µL of solvent was evaporated. The concentrated semicarbazide solution was cooled to -78°C under argon and 7 mL of dimethyl ether was condensed in the flask (the dimethyl ether was distilled over calcium hydride).

To the stirring, slightly cloudy semicarbazide solution was added 787 mg of activated nickel peroxide (from the solid addition ampoule) under argon at -78°C over a 15 min period. The reaction was monitored by TLC.

If, after 15 min, TLC showed semicarbazide still present, $\frac{1}{2}$ of the initial amount of nickel peroxide was added to the stirring, cooled mixture under argon.

When the semicarbazide was consumed, the cold slurry was transferred quickly via an 18 gauge Teflon cannula onto a cooled (-78°C) filtration frit and vacuum filtered into a cooled (-78°C), argon-flushed receiving flask. The solvent was removed at -78°C under high vacuum to yield a slightly yellow solid: ^1H NMR (CD_2Cl_2) δ 3.87 (t, 2H, $J = 1.22$ Hz), 4.91 (t, 2H, $J = 1.22$ Hz); UV (diethyl ether) $\lambda_{\text{max}} = 310$ nm (304, 300 nm).

^1H Photolysis/Thermolysis Experiments

A cooled (-78°C-100°C) 300-500 μL solution of 1-5 mg of **9** (made from 10-30 mg of **47**) in the appropriate NMR solvent was transferred to a cooled (-100°C) 5 mm-o.d. quartz NMR tube equipped with a high vacuum stopcock. The sample was degassed using three freeze (77 K)/pump/thaw (to -78°C) cycles, and then the NMR tube was sealed.

The frozen (77 K) sample was photolyzed using an Oriel 1000-W mercury-xenon arc lamp. Optical filters (Schott WG-280, KG-4, UG11-#2) were used to obtain narrow bands of light in the desired wavelength range (300-360 nm). The sample was then quickly placed in the pre-cooled probe of the ^1H NMR spectrometer and NMR spectra were taken at various time intervals at -60°C.

For the thermolysis kinetics experiments, the cooled, sealed 5 mm NMR tube containing 1-4 mg of **9** (made from 15-25 mg of **47**) was placed in the cooled probe of the ^1H NMR spectrometer and NMR spectra were taken at various time intervals at -60°C. The relative peak height of the triplet of

9 at δ 3.87 referenced to a mesitylene standard was used to determine the unimolecular rate constant for thermal decomposition.

References

1. For a review, See Greenberg, A.; Liebman, J.F. *Strained Organic Molecules*; Academic: New York, 1978.
2. Wheland, G.W. *Advanced Organic Chemistry*; 2nd ed.; Wiley: New York, 1960; pp. 474-514.
3. Wiberg, K.B.; Walker, F.J. *J. Am. Chem. Soc.* **1982**, *104*, 5239.
4. Schultz, H.P., *J. Org. Chem.* **1965**, *30*, 1361-1364.
5. Paquette, L.A.; Ternansky, R.J.; Balogh, D.W.; Kentgen, G. *J. Am. Chem. Soc.* **1983**, *105*, 5446-5450.
6. For general reviews of tetrahedrane: (a) Zefirov, N.S.; Kozmin, A.S.; Abramnikov, A.V., *Russ. Chem. Rev.* **1978**, *47*, 163-171. (b) Maier, G. *Angew. Chem. Int. Ed. Engl.* **1988**, *27*, 309-446.
7. Wiberg, K.B. *Angew. Chem. Int. Ed. Engl.* **1986**, *25*, 312-322.
8. (a) Engel, P.S. *Chem. Rev.* **1980**, *80*, 99-150. (b) Adam, W.; De Lucchi, O. *Angew. Chem. Int. Ed. Engl.* **1980**, *19*, 762-779.
9. For an excellent overview of the chemistry of benzvalene, see: Christl, M. *Angew. Chem. Int. Ed. Engl.* **1981**, *20*, 529-546.
10. (a) Buenker, R.J.; Peyerimhoff, S.D., *J. Am. Chem. Soc.* **1969**, *91*, 4342-6. (b) Baird, N.C., *Tetrahedron* **1970**, *26*, 2185-90. (c) Martensson, R., *Acta Chem. Scand.* **1971**, *25*, 1140-2. (d) Maksic, Z.B.; Kovacevic, K.; Mogus, A. *Theor. Chim. Acta* **1980**, *55*, 127-132.
11. Schulman, J.M.; Venanzi, T.J. *J. Am. Chem. Soc.* **1974**, *96*, 4739-46.
12. Hehre, W.J.; Pople, J.A. *J. Am. Chem. Soc.* **1975**, *97*, 6941-6955.
13. Kollmar, J., *J. Am. Chem. Soc.* **1980**, *102*, 2617-2621.

14. Disch, R.L.; Schulman, J.M.; Sabio, M.L., *J. Am. Chem. Soc.* **1985**, *107*, 1904-1906.
15. Hess, B.A.; Schaad, L.J., *J. Am. Chem. Soc.* **1985**, *107*, 865-866.
16. Schweig, A.; Thiel, W. *J. Am. Chem. Soc.* **1979**, *101*, 4742-4743.
17. Kollmar, H.; Carrion, F.; Dewar, M.J.S.; Bingham, R.C., *J. Am. Chem. Soc.* **1981**, *103*, 5292-5303.
18. Woodward, R.B.; Hoffmann, R. *Angew. Chem. Int. Ed. Engl.* **1969**, *8*, 781.
19. This is compared to an "unstrained" molecule of four methines which had a heat of formation of 0.8 kcal/mol using Franklin's tables.
20. Newton, M.D.; Schulman, J.M., *J. Am. Chem. Soc.* **1972**, *94*, 767.
21. Newton, M.D.; Schulman, J.M., *J. Am. Chem. Soc.* **1974**, *96*, 17.
22. Silverstein, Rm.M.; Bassler, G.C.; Morrill, T.C. *Spectrometric Identification of Organic Compounds*; 4th ed.; Wiley: New York, 1981, pp. 249-304.
23. Maier, G.; Hoppe, M.; Reisenauer, H.P., *Angew. Chem. Int. Ed. Engl.* **1978**, *22*, 990-991.
24. Clark, T. *A Handbook of Computational Chemistry*; Wiley: New York, 1985; pp. 233-316.
25. Beesly, R.M.; Thorpe, J.F. *J. Chem Soc.* **1920**, *117*, 591.
26. Larson, H.O.; Woodward, R.B. *Chem. Ind. (London)*, **1959**, 193.
27. Maier, G.; Pfriem, S.; Schafer, U.; Matusch, R. *Angew. Chem. Int. Ed. Engl.* **1978**, *17*, 520.
28. Irngartinger, H.; Goldmann, A.; Jahn, R.; Nixdorf, M.; Rodewald, H.; Maier, G.; Malsh, K.; Enrich, R. *Angew. Chem. Int. Ed. Engl.* **1984**, *23*, 993.

29. Loerzer, T.; Machinek, R.; Luttke, W.; Franz, L.H.; Malsh, K.; Maier, G. *Angew. Chem. Int. Ed. Engl.* **1983**, *22*, 878.
30. Masamune, S.; Kato, M. *J. Am. Chem. Soc.* **1965**, *87*, 4190.
31. Masamune, S.; Kato, M. *J. Am. Chem. Soc.* **1966**, *88*, 610.
32. White, E.H.; Winter, R.E.K.; Graeve, R.; Zirngibl, U.; Friend, E.W. *J. Am. Chem. Soc.* **1966**, *88*, 611.
33. White, E.H.; Winter, R.E.K.; Graeve, R.; Zirngibl, U.; Friend, E.W.; Maskill, H.; Mende, U.; Kreiling, G.; Reisenauer, H.P.; Maier, G. *Chem. Ber.* **1981**, *114*, 3906.
34. Shelvin, P.B.; Wolf, A.P. *J. Am. Chem. Soc.* **1970**, *92*, 405.
35. Chang, J.H.W.; Lautzenheiser, A.; Wolf, A.P. *Tetrahedron Lett.* **1966**, 6295.
36. Rodewald, L.B.; Lee, H. *J. Am. Chem. Soc.* **1973**, *95*, 623.
37. Maier, G.; Hoppe, M.; Reisenauer, H.P.; Kruger, C. *Angew. Chem. Int. Ed. Engl.* **1982**, *21*, 347.
38. Ona, H.; Uamaguchi, H.; Masamune, S. *J. Am. Chem. Soc.* **1970**, *92*, 7495.
39. Maier, G.; Reisenauer, H.P. *Chem. Ber.* **1981**, *114*, 3916.
40. Maier, G.; Reisenauer, H.P. *Chem. Ber.* **1981**, *114*, 3959.
41. Kobayashi, Y.; Nakano, T.; Shirahashi, K.; Takeda, A.; Kumadaki, I. *Tetrahedron Lett.* **1980**, *21*, 4615.
42. Staab, H.A.; Mack, H.; Wehinger, E. *Tetrahedron Lett.* **1968**, *12*, 1465.
43. Snyder, G.J.; Dougherty, D.A. *J. Am. Chem. Soc.* **1985**, *107*, 1774-1775.
44. Meyers, A.I.; Fleming, M.P. *J. Org. Chem.* **1979**, *44*, 3405-3406.
Wiberg, K.B.; Dailey, W.P.; Walker, F.H.; Waddel, S.T.; Crocker, L.S.; Newton, M. *J. Am. Chem. Soc.* **1985**, *107*, 7247-7257.

45. Chang, M.H.; Dougherty, D.A. *J. Org. Chem.* **1981**, *46*, 4092-4093.
46. Josel, R.; Schroder, G. *Liebigs Ann. Chem.* **1980**, 1428-1437.
47. Jain, R.; Sponsler, M.B.; Coms, F.D.; Dougherty, D.A. *J. Am. Chem. Soc.* **1988**, *110*, 1356.
48. Nakagawa, K.; Konaka, R.; Nakata, T. *J. Org. Chem.* **1962**, *27*, 1597-1601.
49. All ^1H NMR solutions contained varying amounts of unreacted and rearranged semicarbazide which could not be separated from **9**. However, the thermal behavior of **9** is unaffected by the impurities. Similarly, both the thermal and photochemical behavior of **9** is unchanged by the addition of 2,6-lutidine, indicating that acid catalysis is not involved.
50. Laidler, K.J.; Meiser, J.H. *Physical Chemistry*; Benjamin/Cummings Pub. Co., Inc.: Menlo Park, CA, 1982.
51. Chang, M.H.; Jain, R.; Dougherty, D.A. *J. Am. Chem. Soc.* **1984**, *106*, 4211-4217.
52. Strain energies were calculated as follows: 77 kcal/mol as an upper limit for **9** based on the observations of Kao⁵³ that polycyclic diazenes have strain energies that are slightly less than the analogous alkene (**38**, in this case); 47.3 kcal/mol for **48** calculated using the molecular mechanics model of Kao⁵³ and Wiberg's⁷ values for cyclobutane and bicyclobutane (26.5 and 63.9 kcal/mol, respectively).
53. Kao, J.; Huang, T. *J. Am. Chem. Soc.* **1979**, *101*, 5546-5557.
54. Berson, J.A.; Olin, S.S.; Petrillo, E.W.; Bickart, P. *Tetrahedron* **1974**, *30*, 1639-1649.
55. Squillacote, M.E.; Neth, J.M. *Mag. Res. Chem.* **1987**, *25*, 53-56.
56. Still, W.C.; Kahn, M.; Mitra, A. *J. Org. Chem.* **1978**, *43*, 2923.

57. Sylwester, A.P. Doctoral Dissertation, California Institute of Technology, Pasadena, CA 91125.
58. Maier, G.; Born, B. *Angew. Chem. Int. Ed. Engl.* **1989**, *28*, 1050-1052.
59. Mirbach, M.J.; Liu, K.; Mirbach, M.F. ; Cherry, W.R. ; Turro, N.J.; Engel, P.S. *J. Am. Chem. Soc.* **1978**, *100*, 5122-5127.

PART II

MAGNETIC PROPERTIES

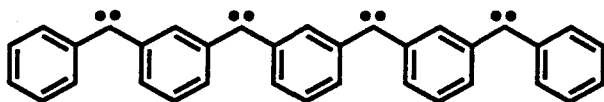
OF

POLARONIC POLYMERS

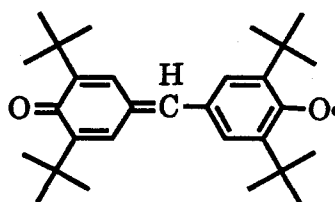
Chapter 2

Design of Molecular Materials

The design of molecular ferromagnetic materials is an area of increasing theoretical and experimental interest.¹ Until recently, the only materials that have exhibited ferromagnetic behavior have been inorganic systems that contain elements such as nickel or chromium in three-dimensional matrices. The discovery of ferromagnetic characteristics in crystalline charge transfer salts of decamethylferrocene and tetracyanoethylene by Miller and coworkers² has given impetus to the realization that a molecular-based ferromagnet is within experimental reach. Organic molecules such as elegant polycarbene (50) of Itoh and Iwamura³ have demonstrated intramolecular high spin behavior while Kinoshita's study of galvinoxyl (51) mixtures illustrated intermolecular organic ferromagnetic coupling between as many as six separate molecules.⁴ In addition, there have been several reports of ferromagnetic organic-based polymers.¹¹ These polymeric materials, however, have been poorly characterized in terms of their structure and magnetic behavior. The uncertainty of the composition and magnetic qualities of these polymers emphasizes the need for rationally designed, well-defined systems.



50



51

Since ferromagnetism is a macroscopic bulk function it requires magnetic interactions in three dimensions.^{5,31} Unlike the metallic ionic systems, such as Fe_2O_3 , whose spin centers are part of an infinite lattice, organic molecules and polymers are discrete microscopic entities. A

molecular-based ferromagnet must contain both molecules that have a magnetic moment and also a means for the moments to couple to one another in a parallel (high spin) configuration. Consequently, the pursuit of structures which have stable high-spin states and mechanisms to control intermolecular magnetic coupling is of prime importance in this scientific field. As such structures become large, eventually polymeric materials will be formed. There have been several theoretical models for the design of potentially ferromagnetic polymers.^{13,15,16,17,20} An advantage of polymers is that along the polymer backbone, exchange interactions (and hence high-spin preferences) among spins might be larger than those experienced by spins in a crystal lattice with minimal direct overlap. In addition, the favorable mechanical properties of polymers will have advantages over crystalline materials for certain applications. However, the control of interchain spin coupling will likely be at least as challenging in the polymer systems as it is for the crystalline structures.

There are several general approaches to the design of molecular ferromagnetic materials. Some of these models deal primarily with the construction of high spin structures, while others also address alternatives for intermolecular magnetic communication. A common denominator of these models (and of magnetic materials in general) is the requirement of unpaired electrons whose collective spin angular momenta gives rise to magnetic behavior.

The next section discusses several of these models for controlling magnetic interactions in molecular spin-containing materials. They are as follows:

- 1) Hund's Rule
- 2) McConnell Spin-Exchange Model
- 3) Charge Transfer Model
- 4) Topological Coupling Model
- 5) Polaronic Ferromagnetism Model

The present work approaches the design and synthesis of magnetic organic polymers from the viewpoint of the polaronic ferromagnetism model.

Hund's Rule

Virtually every college introductory general chemistry text at some point defines Hund's Rule in the context of the electronic structures of atoms. For instance,

"When electrons are added to orbitals of the same energy, one electron will enter each of the available orbitals before a second electron enters any one orbital. This follows Hund's rule, which states that in orbitals of identical energy electrons remain unpaired if possible."¹⁸

By this simple definition, one could approach the synthesis of high spin materials by designing molecules that contain a large number of degenerate p- or d-orbitals, each containing a single electron. Unfortunately, this approach will not suffice in molecular systems. The existence of initially degenerate or nearly degenerate non-bonding

molecular orbitals (NBMO's) is a necessary, but not sufficient criterion for the formation of high spin, ferromagnetic ground states.

Consider two initially degenerate p-type orbitals (ϕ_A, ϕ_B) each containing a single electron (Figure 2-1). At all separations r , the radical pair assumes a singlet ground state.²¹ The overlap of the system is described by

$$S_{AB} = \int \phi_A \phi_B d\tau, \quad (1)$$

where S_{AB} is the overlap integral. As the overlap between ϕ_A and ϕ_B becomes finite, the orbitals cease to have non-bonding character. One orbital becomes bonding and its energy is lowered, while the other becomes antibonding and its energy is raised, giving rise to a singlet preference. As r decreases and S_{AB} increases, a large HOMO-LUMO gap emerges. The orbitals have a strong bonding interaction, which is inherently low spin.

The preference of a low spin ground state does not change with increased separation of the orbitals. This is also seen in H_2 ³³ (Figure 2-2). As r increases, the singlet state rises in energy. However, the triplet state, though continually decreasing, is always above the singlet state except at infinite r . At this point, there is no interaction between the electrons (*i.e.*, a paramagnetic state).

High spin behavior (and magnetism in general) is a consequence of exchange interactions.¹⁹ Exchange is a quantum mechanical characteristic that has no classical counterpart. Exchange interactions favor parallel alignment of spins. For a two-electron system, the exchange integral is defined³² as

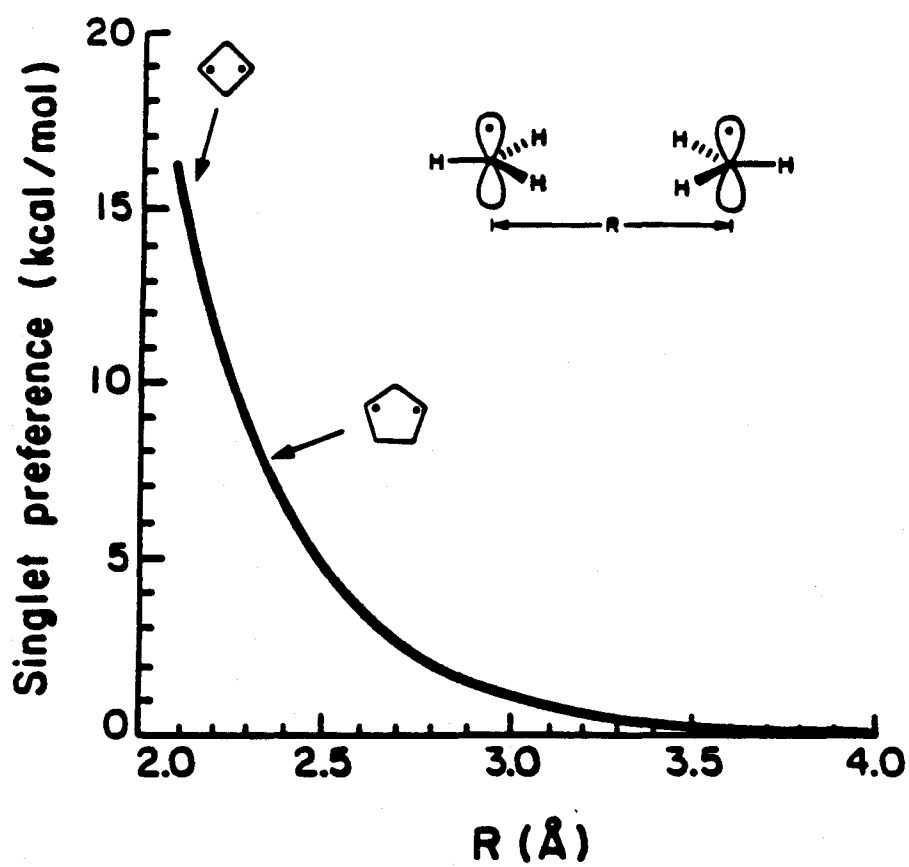


Figure 2-1. Singlet state preference for two p-type orbitals at distance R .

Singlet state preference for two p-type orbitals at distance R .

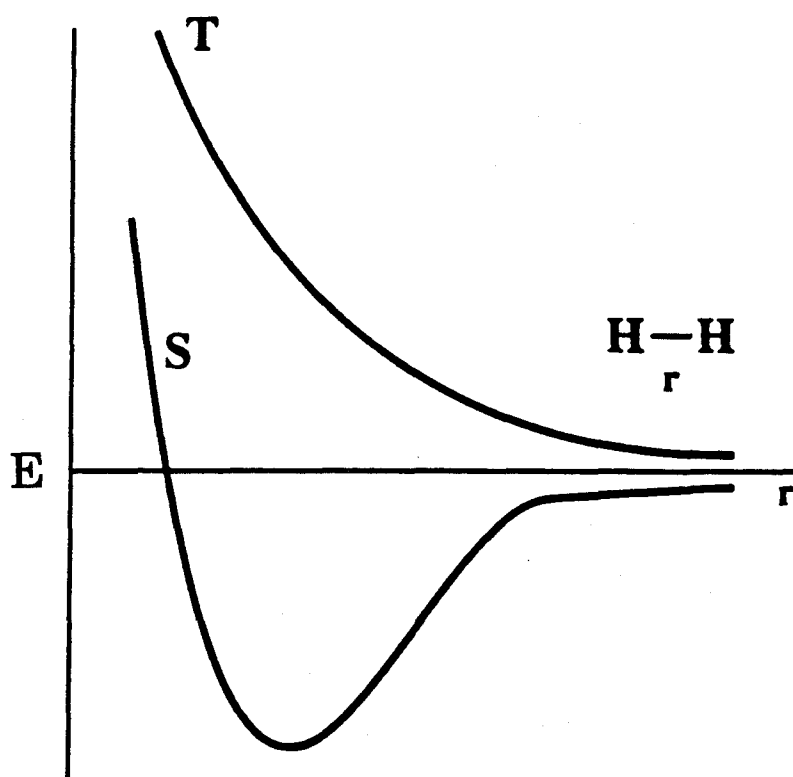


Figure 2-2. Potential energy diagram for H_2 .

$$K_{AB} = \int \phi_A(1) \phi_B(1) \frac{1}{r_{12}} \phi_A(2) \phi_B(2) d\tau_1 d\tau_2. \quad (2)$$

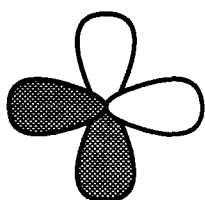
Note that, because of the form, the exchange integral is proportional to the overlap of the squares of the orbital wave functions.

$$K_{AB} \propto \int \phi_A^2 \cdot \phi_B^2 d\tau. \quad (3)$$

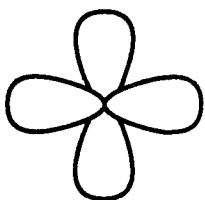
To create a high spin, two-electron system, there must be significant exchange interactions. One method of accomplishing this is by decreasing the distance between the p-orbitals. Unfortunately, this also increases S_{AB} , which leads to a situation where overlap will always be greater than the exchange interaction, hence the singlet state is always lower in energy than the triplet state (as in the cases shown in Figure 1 or 2).

To circumvent this dilemma for two p-type radicals, a situation must be created where $S_{AB} \equiv 0$ yet $K_{AB} \neq 0$. This is possible in systems that contain orthogonal orbitals. As shown in Figure 2-3, two orthogonal orbitals have zero overlap due to their nodal properties. Since K_{AB} scales with ϕ^2 , the signs of the lobes of the p-orbitals become equivalent when squared, and the nodal properties become immaterial as far as K_{AB} is concerned. There is substantial overlap between ϕ_A^2 and ϕ_B^2 , which lends to significant exchange interactions and subsequently a high spin ground state.

The cancelation of overlap between orthogonal orbitals is the basis of Hund's rule in atomic systems. In these systems, the orbitals are centered



$$S_{A,B} = \int \phi_A \phi_B d\tau = 0$$

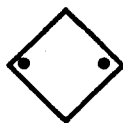


$$K_{A,B} \propto \int \phi_A^2 \cdot \phi_B^2 d\tau \neq 0$$

Figure 2-3. Overlap and exchange integrals for two orthogonal p-orbitals.

on a single nucleus. For the set of the three p-orbitals (p_x , p_y , p_z) or the set of five d-orbitals, the nodal properties are such that the net overlap S between orbitals within a set is zero. The exchange integrals between these orbitals are non-zero. Thus exchange, with the absence of overlap, allows one to predict that three unpaired electrons placed in the set of five 3d orbitals (*i.e.*, Cr^{3+}) will be high spin.

Consequently, Hund's rule is only directly applicable to atomic systems. In systems with separated NBMO's containing unpaired electrons, the overlap S must somehow be minimized and exchange must be significant to obtain high spin ground states. As in atomic systems, the creation of orthogonal NBMO's is one solution. In practice, this is difficult to accomplish. Another mechanism which effectively cancels the effects of overlap in p-type orbitals is through-bond coupling. This has been observed in 1,3-cyclobutanediyl (52), a triplet ground state biradical.²¹ The singlet-triplet gap created by the overlap of the radical centers is eliminated by interactions with the π CH_2 orbitals. However, this effect is limited to few examples.



McConnell Spin-Exchange Model

The problem of intermolecular ferromagnetic coupling was addressed by McConnell in 1963.⁶ For a system of two radicals, A and B, the Heisenburg Hamiltonian describes the magnetic interaction between spins:

$$\mathcal{H}^{AB} = - \sum_{ij} J_{ij}^{AB} S_i^A \cdot S_j^B \quad (4)$$

where S_i^A is the π -electron spin on atom i of molecule A, S_j^B is the π -electron spin on atom j of molecule B, and J_{ij} is the exchange interaction between atom i and j . Equation 4 can also be expressed in terms of the π -spin densities on atom i and j of molecules A and B (ρ_i^A and ρ_i^B , respectively);

$$\mathcal{H}^{AB} = - S^A \cdot S^B \sum_{ij} J_{ij} \rho_i^A \rho_j^B, \quad (5)$$

where S^A and S^B are the spin operators for A and B. For most organic radicals, J_{ij} is negative, or antiferromagnetic (due to the overlap versus exchange dilemma outlined earlier).^{4,34}

McConnell⁶ proposed that identical radicals with large positive and negative atomic π spin densities which stack such that atoms of positive spin density are exchange-coupled to atoms with negative spin density on neighboring molecules will have a high-spin ground state. By controlling the stacking of organic conjugated π radicals, it should be possible to construct a very high spin system.

Itoh and Iwamura have elegantly examined this approach in the study of a series of diphenylcarbenes.⁷ They have synthesized the pseudo-*ortho*-, -*para*-, and -*meta*-bis(phenylmethylenyl)[2.2]cyclophanes (52a, 52b, 52c). McConnell's model predicts that the pseudo-*meta* isomer should be antiferromagnetically ordered, while the pseudo-*para* and -*ortho* isomers should be ferromagnetically ordered. This can be seen by examining the π spin density in diphenylcarbene (Figure 2-4). The spin densities alternate in sign between neighboring atoms. If the same atomic π densities are transferred to the cyclophane in the pseudo-*meta* isomer, the interacting atoms on the neighboring benzene rings have similar π density signs. This is predicted to result in a low-spin (antiferromagnetic) spin state. The pseudo-*ortho* and -*para* isomers have opposing π densities on their respective interacting pairs of benzene rings. This is predicted to result in a ferromagnetic ground state. EPR spectroscopy and magnetic susceptibility measurements confirm this analysis.⁷

Technically, the aforementioned study did not address intermolecular coupling, since the diphenylcarbene pairs were part of a single molecule. McConnell's original theoretical treatment dealt only with interactions between pairs of radicals. The nature of intermolecular coupling between several radicals was addressed by another study using substituted diphenylcarbenes. Through the use of different substituents on the benzene ring, Iwamura⁸ was able to control the magnetic coupling between pairs of interacting diphenylcarbenes without tying them together with chemical bonds. The substituents forced the diphenylcarbenes to orient in an *ortho*-, *meta*-, *para*-, or *gem*- fashion with respect to each other, thus causing the π spin densities on the benzene rings to overlap differently. The multiplicity of the materials varied accordingly. A sample

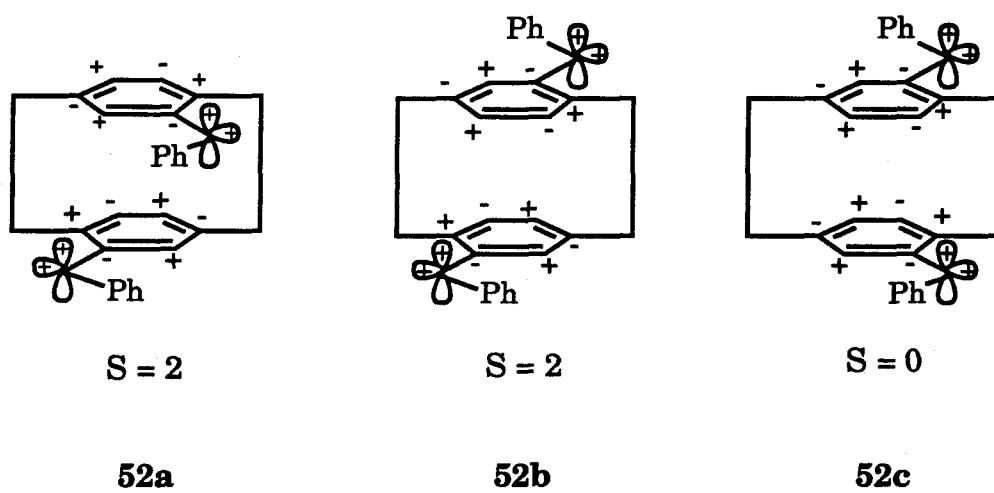
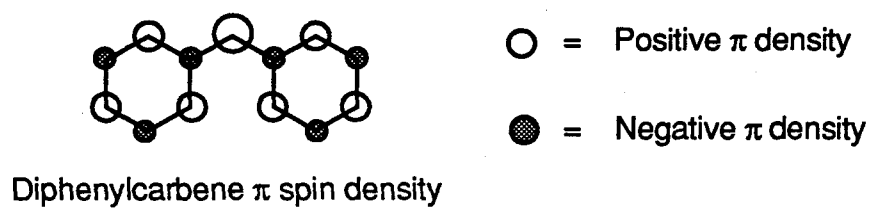


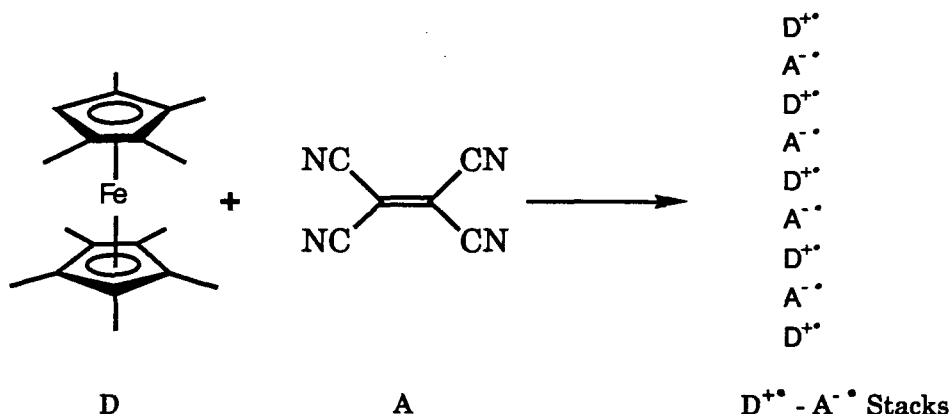
Figure 2-4. Spin densities of diphenylcarbene cyclophane isomers.

of bis(O-octyl) diphenylcarbene was found to behave similarly to an $S=8/2$ molecule, indicating that intermolecular spin alignment occurred over four molecules.⁹

These experimental results show that a certain degree of ferromagnetic ordering can be achieved through the McConnell model. There had been no evidence of bulk ferromagnetic ordering in any of the previous studies. The applicability to molecules other than diphenylcarbenes is unknown. This approach is limited by the ability to correctly pack and arrange the radical structures over large distances. This may be a significant obstacle in molecular systems, especially partially disordered polymers. The extension of the carbenes to larger systems is also limited by the high reactivity and low stability of such materials at higher temperatures.

Charge Transfer Model

This model, initially proposed by McConnell and later extended by Breslow^{12,22} and Miller,² is based on a charge transfer system of electron donors (D) and acceptors (A). If there is an excited state available (either $D^{++}A^{--}$ or D^0A^0) in which either the donor or acceptor (but not both) is a triplet, then this triplet excited state will mix with and stabilize the ferromagnetic charge transfer state relative to the antiferromagnetic state. Miller and coworkers have synthesized a charge transfer salt of decamethylferrocene and TCNE, and this may be an example of such behavior.



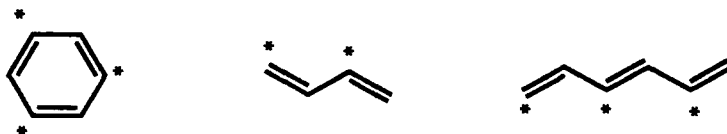
These molecules form alternating donor/acceptor stacks in the solid state which interact to form a ferromagnetically coupled material at low temperatures. This complex exhibits spontaneous magnetization and hysteresis below 5 K.

Other attempts by Miller to extend these unprecedented results using similar donors and acceptors have failed. Breslow and coworkers^{12,22} attempted to synthesize a series of benzene based triplet dications that could fit the charge transfer model. They found that upon crystallization the singlet state is preferred, which would destroy the stabilization of the ferromagnetic ground state. It appears that in these systems the crystal packing forces of molecules are the primary factors that determine the nature of the magnetic couplings. The control of these crystal packing forces is a significant problem that must be overcome before this model becomes feasible for a wider variety of materials.

Topological Coupling Model

There is a class of organic compounds that, by virtue of their topology, is predicted to have interesting magnetic properties. These structures are typically alternant hydrocarbons, *i.e.*, π conjugated

molecules whose atoms can be divided into two sets, star (*) and non-star, such that no two atoms of the same set are bonded to one another. Benzene, butadiene, and hexadiene are examples of even alternant hydrocarbons.



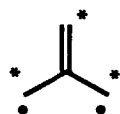
Ovchinnikov, extending previous theoretical work on π alternant systems, used valence bond theory to predict the multiplicities of alternant hydrocarbons.¹³ The spin state of such a molecule can be simply calculated using equation 6, where n^* = number of starred atoms and n^0 = number of non-starred atoms.

$$S = \frac{(n^* - n^0)}{2} \quad (6)$$

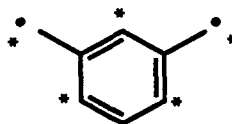
For example, trimethylenemethane (53) is predicted by this theory to have $S=1$. Likewise, *meta*-benzoquinodimethane (54) is predicted to have a triplet ground state. This has been experimentally corroborated by EPR spectroscopy.¹⁴ If the CH_2 groups are changed to a *para* configuration, then the multiplicity of the benzoquinodimethane becomes $S=0$ and the ground state becomes singlet.

This simple rule has proven to be useful in predicting the spin states of several alternant hydrocarbons. It is quite easy to design on paper larger molecules with high multiplicities. For instance, polymer 55 should have a spin state that is proportional to the number of monomers in

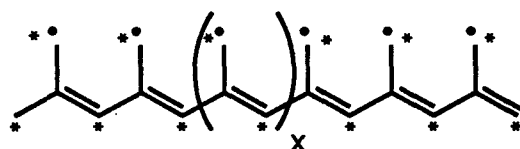
each chain. For every unit cell, there is an extra * atom, resulting in an overall spin state of $S = \frac{x}{2}$.



53

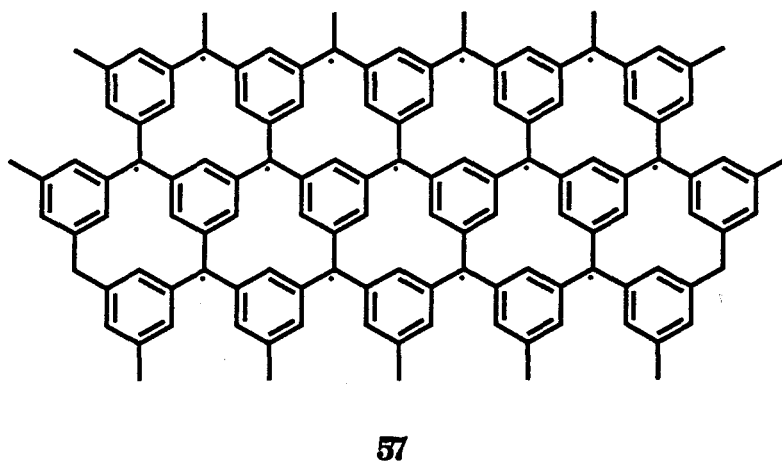
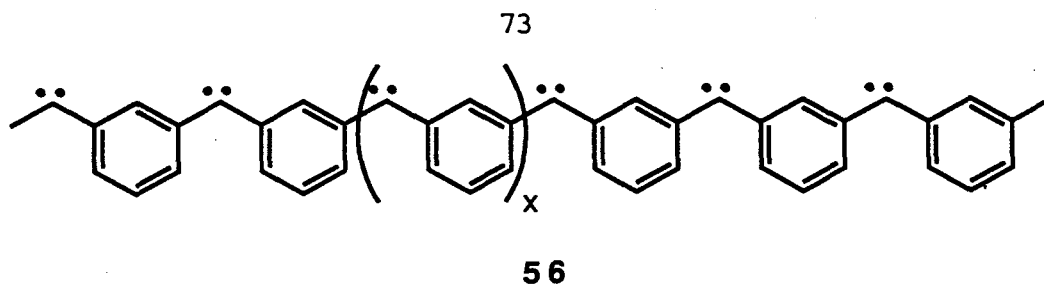


54

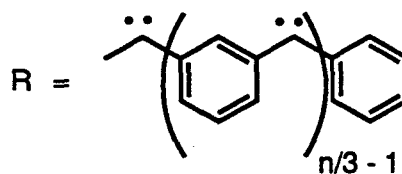
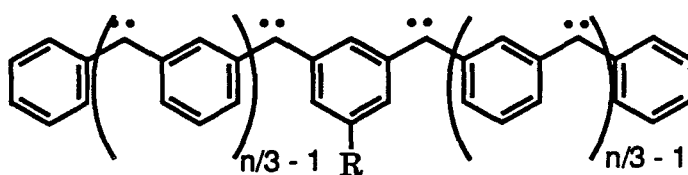
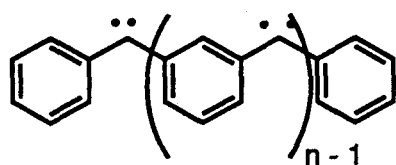


55

Related to the Ovchinnikov model are the theoretical work of Mataga¹⁵ and later experimental studies of Itoh and Iwamura.^{3,7} With the discovery of the ground state triplet behavior of diphenylcarbene, Mataga suggested that a structure composed of *meta*-connected diphenylcarbenes (**56**) would have a high-spin ground state. It was also proposed that a 1,3,5- connected network of trimethylenebenzene units (**57**) would be ferromagnetic. Ovchinnikov's theory does not directly apply to carbenes since only electrons in π orbitals are treated. Hence, equation 6 does not necessarily predict that the multiplicity of **56** should be proportional to the number of benzene rings.



The predictions of Mataga proved relevant as seen in the experimental studies of Itoh and Iwamura.^{3,7} They synthesized a series of diphenylcarbenes, each successively with a larger number of *meta*-connected diphenylcarbenes.



Polycarbenes **58** and **59**, generated by the photolysis of diazo precursors, have as their ground states the highest possible multiplicities.

An attempt to prepare a polymer similar to **57**, based on the polymerization of 1,3,5-triaminobenzene with iodine, was reported by Torrance and coworkers.¹⁶ They reported the tantalizing result of magnetic hysteresis, which is indicative of ferromagnetic ordering, in a single "great batch." Further attempts to reproduce this result failed.

This topological model appears to have great utility in the design and prediction of high spin alternant molecules. The *meta*-benzoquinodimethane topology is especially predisposed toward a high-spin ground state, even with extensive modification of the structure. However, this model has several potential barriers to its experimental application to molecular bulk ferromagnetism. For instance, there is no mechanism for intermolecular communication between high-spin fragments. This is crucial since ferromagnetism requires cooperative behavior in three dimensions. Generally, organic radicals tend to couple antiferromagnetically to each other.⁴ This effect can be seen in the tetracarbene (**50**) which has antiferromagnetic *intermolecular* interactions at high concentrations.^{3b} Bulk ferromagnetism may be achieved if the spin-containing molecules are large enough to form their own macroscopic ferromagnetic domains. Alternatively, it may be possible to link smaller segments together so that they can interact through space by means of the McConnell mechanism to form ferromagnetic domains.

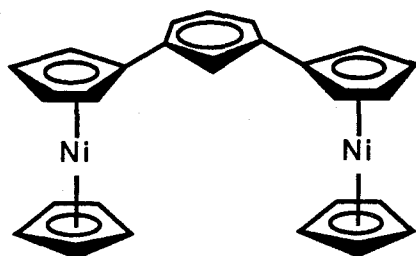
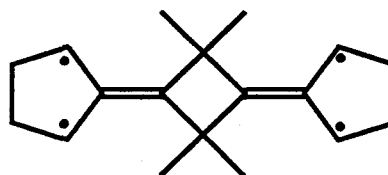
To date, the only examples of an extended high spin system using the topological model are the polycarbenes. These materials suffer from the drawbacks of instability and reactivity inherent to carbene centers. In general, there are non-trivial synthetic hurdles to overcome concerning

the construction of extended π -based radical topologies. The use of stabilized radicals such as galvinoxyl-based compounds may enhance the utility of this approach to macroscopic magnetic materials.

Polaronic Ferromagnetism

The most recent and untested approach to the design of molecular ferromagnets is the polaronic ferromagnetism model.^{17,35} One can conceptually break down the structure of a ferromagnetic polymer into two units: the monomers and coupling units (Figure 2-5). The monomer unit is simply any structure that contains a localized magnetic moment. This may be a radical or a higher spin state moiety. The coupling unit is a structure which can ferromagnetically couple the two spin containing monomers to which it is linked. In an alternating copolymer of these two units, the ferromagnetic coupling will be propagated down the chain, resulting in a high spin polymer chain whose multiplicity is proportional to the number of spin-containing monomer units. The separation of the polymer into spin-containing units and coupling units is somewhat arbitrary since the coupling units themselves may contain spin.

There has been much progress in the development of potential ferromagnetic spin-coupling units. The best documented case is "*meta* through a benzene." That is, two spin containing units that are linked to the 1,3- positions of a benzene ring are ferromagnetically coupled. This coupling is observed in the aforementioned polycarbene systems^{3,7} and simple monoradicals.^{14,23} Ferromagnetic coupling has also been observed in *meta*-benzene-linked bis-nickelocene²⁴ (**60**). Other potential ferromagnetic coupling units include localized 1,3-biradicals such as cyclobutanediyls,²⁵ cyclopentanediiyls,²⁶ and the delocalized biradical, trimethylenemethane. The ability of 1,3-cyclobutanediyl to ferromagnetically couple two magnetic spin centers (other than the parent biradical) was demonstrated by the synthesis of tetraradical **61**. This molecule is a ground state quintet.²⁷

**60****61**

There are a wide range of possible spin-containing units that may be used in this design. Potential spin units include carbon-based radicals, biradicals, and carbenes, or metallocene radical cations. For practical considerations it would be advantageous to have the spin centers be as thermally and environmentally stable as possible. Our interest in the conducting polymers area²⁸ lead us to consider polarons as a potentially

AN APPROACH TO FERROMAGNETIC POLYMERS



is any unit
with a permanent
magnetic moment.



is a ferromagnetic
coupling unit.

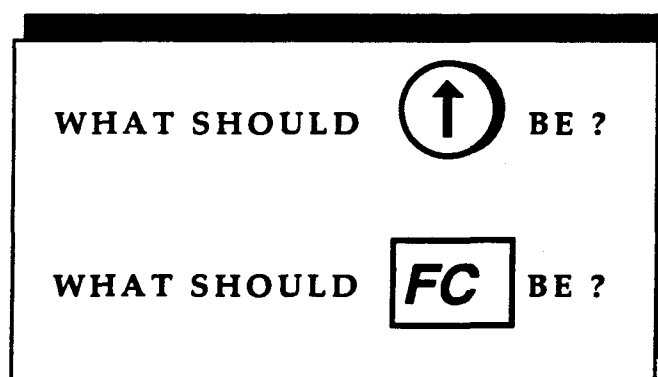
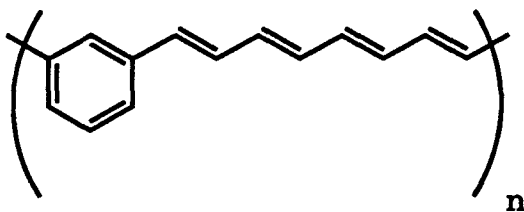


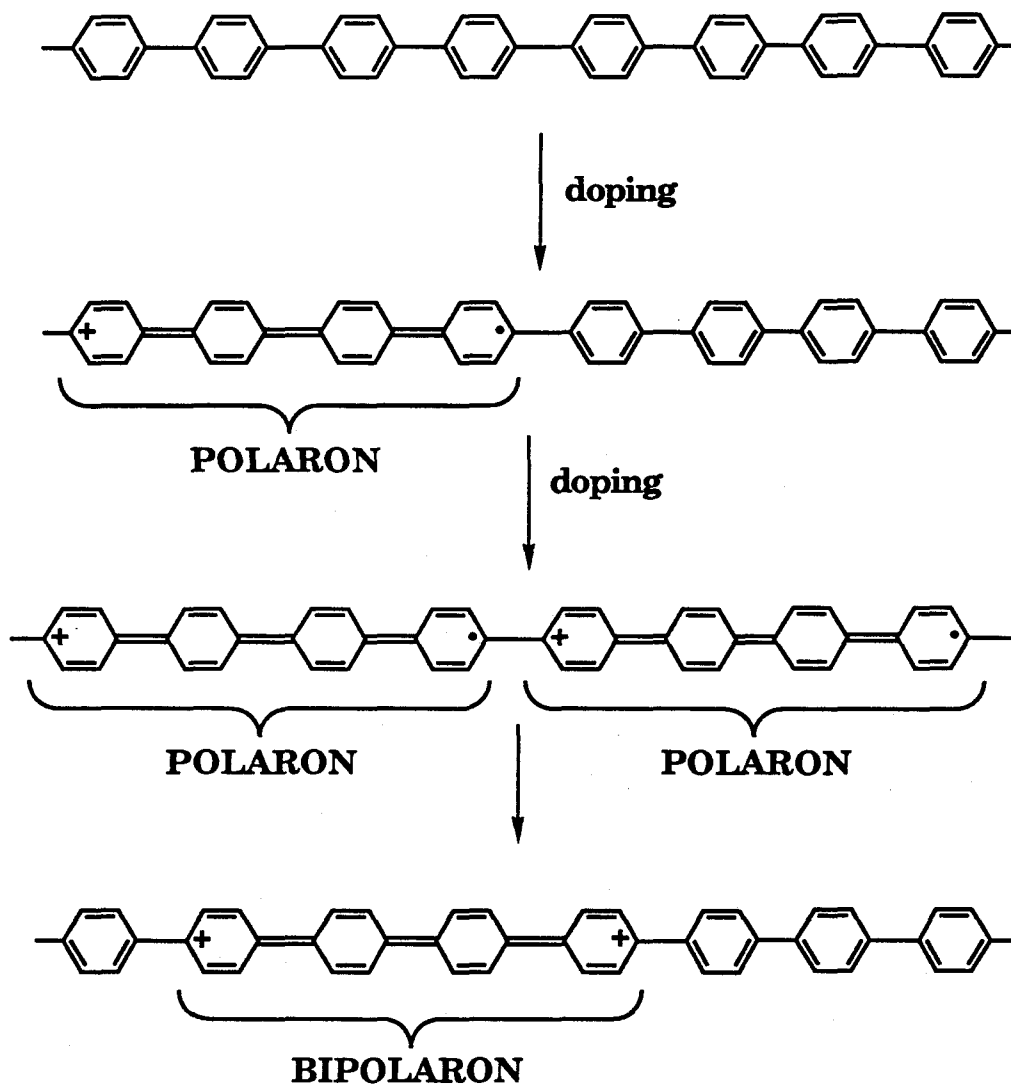
Figure 2-5. An approach to ferromagnetic polymers.

stable spin-containing unit. One can think of a polaron as a partially delocalized radical cation (or radical anion) that is formed upon removal (or addition) of an electron from a conjugated polymer chain^{29,30} (Scheme 2-1). This is typically accomplished by oxidation or reduction of the polymer through chemical or electrochemical means (this process is alternatively defined as "doping"). Further oxidation or combination of polarons results in formation of dications, or bipolarons. Fukutome has shown¹⁷ theoretically that polarons on short polyene chains linked by ferromagnetic coupling units such as *meta*-benzoquinodimethane or TMM results in a one-dimensional ferromagnetically-coupled polymer chain and coined the term "polaronic ferromagnetism" to describe such behavior. The highly thermal stability of spin centers such as polarons is an advantage that other models which utilize reactive carbene or radical spin centers do not have.

The present work is concerned with the design, synthesis, and magnetic characterization of polaron-containing polymers that exhibit high spin behavior. Based on considerations of synthetic feasibility, Fukutome's analysis, and ease of doping, substituted derivatives of poly(*meta*-phenyleneoctatetraene) (PMPOT, **63**) were synthesized.

**63**

Scheme 2-1. Polaron formation and annihilation to form bipolarons.



The polaronic polymers are formed from these precursors through oxidative doping of the polyene segments to yield the desired radical cations (polarons). Magnetic susceptibility and magnetization studies indicate that PMPOT derivatives containing low concentrations of polarons have stable spin states that are a result of ferromagnetic coupling between several polarons.

References

1. See Proceedings of the Symposium of Ferromagnetic and High Spin Molecular Based Materials, 197th National American Chemical Society Meeting in Dallas, Tx.; Miller J.S.; Dougherty, D.A., Eds. *Mol. Cryst. Liq. Cryst.* **1989**, *176*, 1-562.
2. Miller, J.S.; Epstein, A.J.; Reiff, W.M. *Chem. Rev.* **1988**, *88*, 201-220.
3. (a) Teki, Y.; Takui, T.; Itoh, K.; Iwamura, H.; Kobayashi, K. *J. Am. Chem. Soc.* **1986**, *108*, 2147-2156. (b) Sugawara, T.; Bandow, S.; Kimura, K.; Iwamura, H.; Itoh, K. *J. Am. Chem. Soc.* **1986**, *108*, 368-371.
4. Agawa, K.; Sugano, T.; Kinoshita, M. *J. Chem. Phys.* **1986**, *85*, 2211-2218.
5. For a review of the many types of magnetism, see Hurd, C.M. *Contemp. Phys.* **1982**, *23*, 469.
6. McConnell, H.M. *J. Chem. Phys.* **1963**, *39*, 1910.
7. Iwamura, H. *Pure & Appl. Chem.* **1986**, *58*, 187-196.
8. Sugawara, T.; Tukada, H.; Izuoka, A.; Murata, S.; Iwamura, H. *J. Am. Chem. Soc.* **1986**, *108*, 4272-4278.
9. Sugawara, T.; Murata, S.; Kimura, K.; Iwamura, H. *J. Am. Chem. Soc.* **1985**, *107*, 5293-5294.
10. (a) Caneschi, A.; Gatteschi, D.; Laugier, J.; Rey, P.; Sessoli, R.; Zanchini, C. *J. Am. Chem. Soc.* **1988**, *110*, 2795. (b) Kahn, O.; Pei, Y.; Verdaguer, M.; Renard, J.P.; Sletten, J. *J. Am. Chem. Soc.* **1988**, *110*, 782.

11. (a) Ota, M.; Otani, S.; Kobayashi, K.; Igarashi, M. *Mol. Cryst. Liq. Cryst.* **1989**, *176*, 99-108. (b) Medvedeva, T.V.; Ovchinnikov, A.A.; Spector, V.N. *Nature* **1987**, *326*, 370.
12. Breslow, R.; Jaun, B.; Kluttz, R.Q.; Xia, C.Z. *Tetrahedron* **1982**, *38*, 863.
13. Ovchinnikov, A.A. *Theoret. Chim. Acta (Berl.)* **1978**, *47*, 297-304.
14. *Diradicals*; W.T. Borden, Ed.; Wiley: New York, 1982.
15. Mataga, N. *Theoret. Chim. Acta (Berl.)* **1968**, *10*, 372-376.
16. Torrance, J.B.; Oostra, S.; Nazzari, A. *Synthetic Metals* **1987**, *19*, 709.
17. Fukutome, H.; Takahashi, A.; Ozaki, M. *Chem Phys. Lett.* **1987**, *133*, 34.
18. Laidler, K.J.; Meiser, J.H. *Physical Chemistry*; Benjamin/Cummings: Menlo Park, CA, 1982.
19. Mattis, D.C. *The Theory of Magnetism I. Statistics and Dynamics*; Springer-Verlag: Berlin, 1988.
20. Caneschi, A.; Gatteschi, D.; Sessoli, R. *Acc. Chem. Res.* **1989**, *22*, 392-398.
21. Goldberg, A.H.; Dougherty, D.A. *J. Am. Chem. Soc.* **1983**, *105*, 284-290.
22. Thomaidis, J.; Maslak, P.; Breslow, R. *J. Am. Chem. Soc.* **1988**, *110*, 3970. LePage, T.J.; Breslow, R. *J. Am. Chem. Soc.* **1987**, *109*, 6412.
23. Rule, M.; Matlin, A.R.; Hilinski, E.F.; Dougherty, D.A.; Berson, J.A. *J. Am. Chem. Soc.* **1979**, *101*, 5098. Senthilnathan, V.P.; Platz, M.S. *J. Am. Chem. Soc.* **1980**, *102*, 7637.
24. Manriquez, J.M.; Ward, M.D.; Calabrese, J.M.; Fagen, P.A.; Epstein, A.J.; Miller, J.S. *Mol. Cryst. Liq. Cryst.* **1989**, *176*, 527

25. Jain, R.; Sponsler, M.B.; Coms, F.D.; Dougherty, D.A. *J. Am. Chem. Soc.* **1988**, *110*, 1356. Sponsler, M.B.; Jain, R.; Coms, F.D.; Dougherty, D.A. *J. Am. Chem. Soc.* **1989**, *111*, 2240.
26. Coms, F.D.; Dougherty, D.A. *Tetrahedron Lett.* **1988**, *29*, 3753. Buchwalter, S.L.; Closs, G.L. *J. Am. Chem. Soc.* **1979**, *101*, 4688.
27. Novak, J.A.; Jain, R.; Dougherty, D.A. *J. Am. Chem. Soc.* **1989**, *111*, 7618.
28. Pranata, J.; Dougherty, D.A. *J. Am. Chem. Soc.* **1987**, *109*, 1621. Pranata, J.; Dougherty, D.A. *Synth. Metals* **1987**, *22*, 171. Pranata, J.; Grubbs, R.H.; Dougherty, D.A. *J. Am. Chem. Soc.* **1988**, *110*, 2973. Swager, T.M.; Dougherty, D.A.; Grubbs, R.H. *J. Am. Chem. Soc.* **1988**, *110*, 2973. Pranata, J.; Marudaragan, V.S.; Dougherty, D.A. *J. Am. Chem. Soc.* **1989**, *111*, 2026.
29. Epstein, A.J.; MacDiarmid, A.G. *J. Mol. Electron.* **1988**, *4*, 161-165. Bredas, J.L.; Street, G.B. *Acc. Chem. Res.* **1985**, *18*, 309.
30. *Handbook of Conducting Polymers*; Skotheim, T.A., Ed.; Marcel Dekker: New York, 1986; Vol. 2.
31. See Chapter 3.
32. Salem, L.; Rowland, C. *Angew. Chem. Int. Ed.* **1972**, *11*, 92-111.
33. Hanna, M.W. *Quantum Mechanics in Chemistry*, 2nd ed.; W.A. Benjamin: Menlo Park, CA., 1969.
34. J_{ij} is not to be confused with K or S. It is an energetic parameter that describes the strength and type of coupling between two centers. In this work, a positive J_{ij} implies ferromagnetic coupling, while a negative J_{ij} implies antiferromagnetic coupling. Unfortunately, this sign convention of J_{ij} is not universally followed by all

researchers in the field. Thus, when dealing with the Heisenburg Hamiltonian, one must be cautious when defining the sign of J_{ij} .

35. Dougherty, D.A. *Mol. Cryst. Liq. Cryst.* **1989**, *176*, 25-32.

Chapter 3

Magnetism

Introduction

All materials respond to an externally applied magnetic field. The behavior of a substance in a magnetic field can be used to classify that system, and in fact there are at least 14 different types of magnetic behavior known (Figure 3-1).² In general, though, the majority of substances fall under the classification of five general forms: diamagnetic, paramagnetic, antiferromagnetic, ferromagnetic, or ferrimagnetic materials. This chapter discusses the interactions of these five families with a magnetic field, with special focus on the study of isolated paramagnetic and coupled-paramagnetic systems.

Magnetic Definitions

If a material is placed in a magnetic field, H , then the density of lines of force in the sample, known as the magnetic induction, B , is given by H plus a contribution $4\pi M$ due to the sample itself:

$$B = H + 4\pi M \quad (1)$$

where M is the magnetic moment of the sample per unit volume. M , or magnetization, is representative of the inherent magnetic polarization of the material. The intensity of magnetization M induced in a body is proportional to the strength of the applied field, H :

$$M = \chi H \text{ or } \chi = \frac{M}{H} \quad (2)$$

where χ is the magnetic susceptibility of the sample. χ May be qualitatively

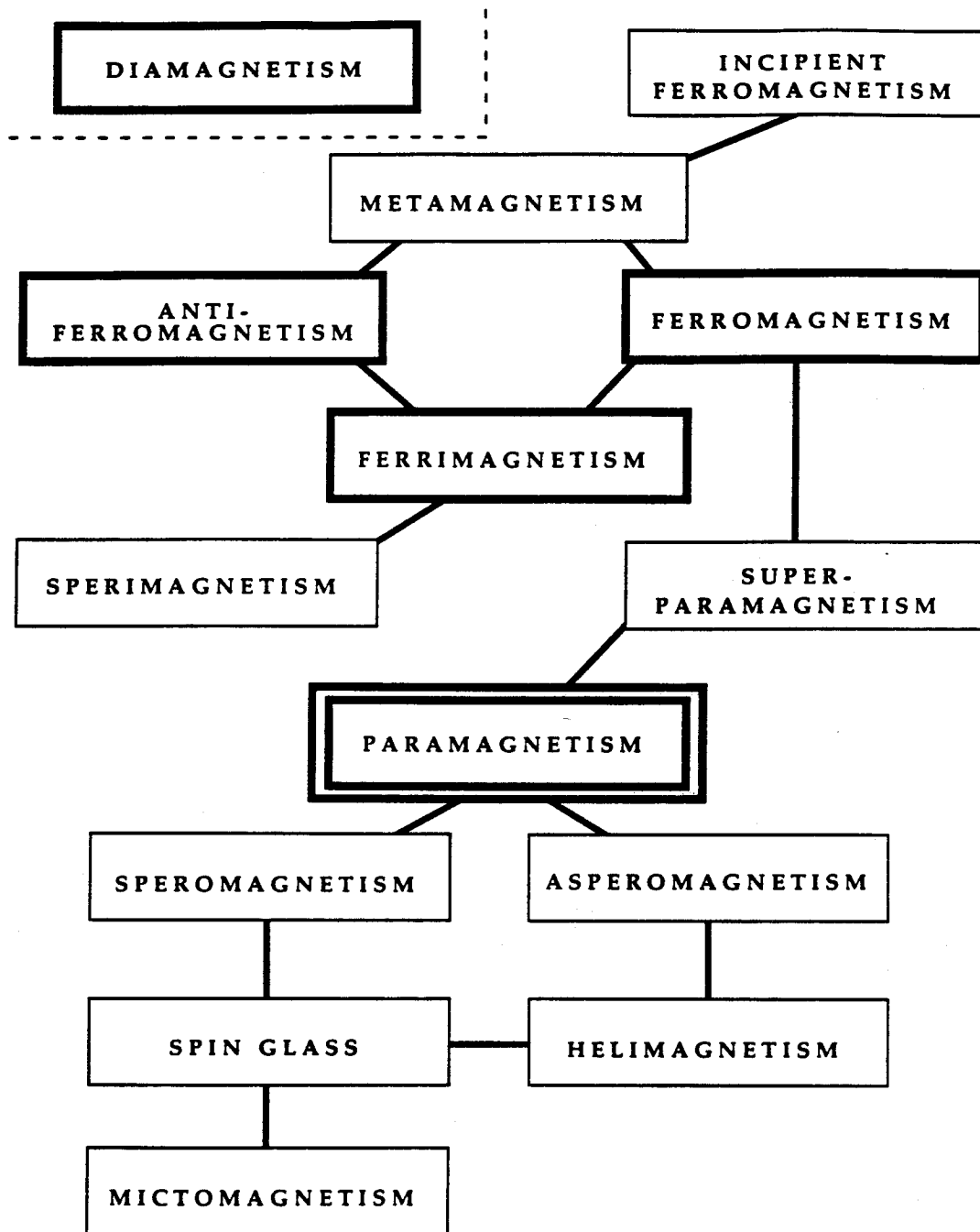


Figure 3-1. Types of magnetic behavior.

defined as the extent to which a material is susceptible to induced magnetization. In an isotropic material, the magnetic susceptibility of a material is the same in all directions. However, in anisotropic crystals and oriented films the susceptibility may differ depending on the orientation of the molecular axes.³

Magnetic susceptibility can be defined in terms of either volume, molar, or mass quantities. In the CGS rationalized system of units, the volume susceptibility is unitless, while the molar susceptibility χ_m is defined in units of emu/mole and the mass susceptibility χ_g is defined in units of emu/gram. The magnetization M of a body is in units of gauss, while the weight magnetization M_g is in units of emu gauss per gram. An emu, or electromagnetic unit, is also defined as a cm³. At this point, it must be stressed that one must be careful when dealing with the system of units of magnetic quantities such as susceptibility or magnetization. There has been a great deal of inconsistency among the systems of units employed by researchers in various fields and countries.⁴ The conversions between the systems of units are not always straightforward. All data reported here will be in the CGS rationalized system of units.

The term, "macroscopic" magnetization of a body implies that there exists a more fundamental term that microscopically describes the magnetic character of a system. This term, the magnetic moment, refers to the turning effect produced in a magnetic field. When a magnetic dipole is placed in a magnetic field, it experiences a turning force (torque) which is proportional to a specific characteristic named the magnetic moment. If a uniform magnetic field H acts on a magnetic dipole N-S of length ℓ and strength m' , the N and S poles of the dipole will experience forces equal to $+m'H$ and $-m'H$, respectively (Figure 3-2). That is, the field exerts a force on the dipole so that it will be

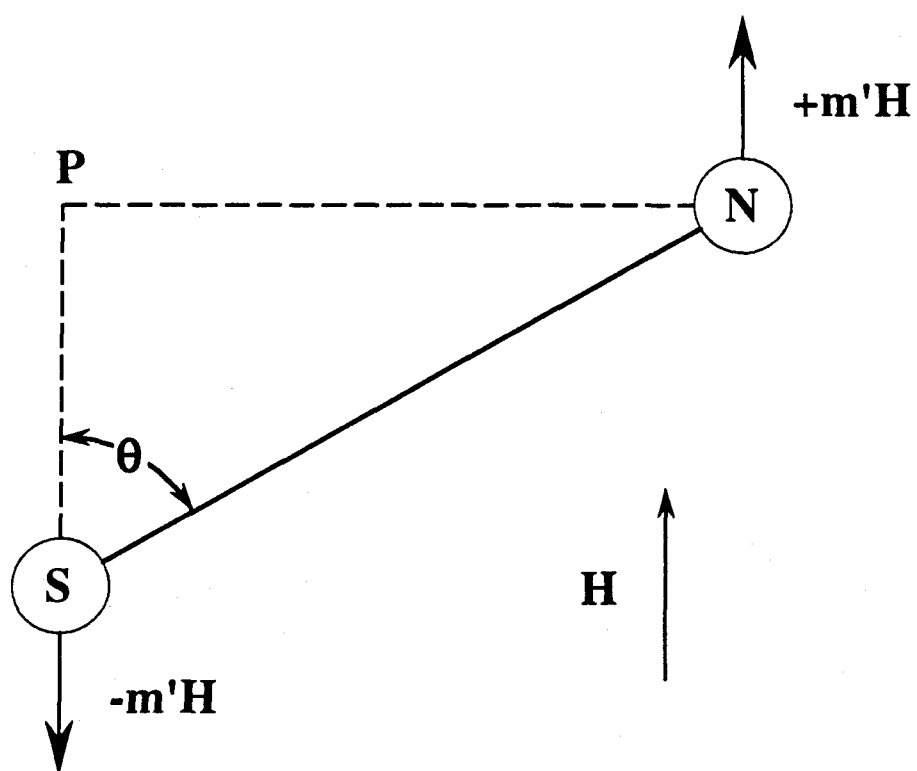


Figure 3-2. Forces on a magnetic dipole (N-S) placed in a field (H), showing the "moment" or turning effect (torque).

parallel to the direction of the magnetic field. These two equal and opposite forces are a "couple" whose turning moment M' is given by

$$\begin{aligned} M' &= \text{force} \times \text{distance (PN)} \\ &= m'H \times \ell \sin \theta \\ &= \mu H \sin \theta \end{aligned}$$

where θ is the angle between the magnetic dipole and the direction of H .

The quantity μ ($= m'\ell$) defines the magnetic moment and is a measure of the turning effect in a magnetic field. The study of the electrical and magnetic properties of fundamental particles has shown the existence of a fundamental unit of magnetic moment known as the Bohr magneton (μ_B). This is analogous to the fundamental charge of the electron and is defined as

$$\mu_B = eh/4\pi mc$$

where e and m are the charge and mass of the electron, h is Planck's constant, and c is the velocity of light. In the CGS system, $\mu_B = 9.274 \times 10^{-21}$ erg Oe⁻¹ (or emu Gauss).

Magnetic Substances

As previously mentioned, most materials fall under the categories of diamagnetic, paramagnetic, ferromagnetic, ferrimagnetic, or antiferromagnetic substances. The latter four families imply the existence of unpaired electrons in the molecules and henceforth will be generally referred to as magnetic. Diamagnetism, however, arises from the interaction of the paired electrons in the filled molecular orbitals with an externally applied

magnetic field. Since virtually all molecules of interest have paired electrons, diamagnetism is a property of all matter.

If a material is placed in a magnetic field, the field within the material is generally different than the outside of the body (see eq. 1). If the density of the lines of force of the magnetic field within the material is less than the density which would exist in vacuum (*i.e.*, a negative M) then the substance is diamagnetic (Figure 3-3a). Since this is equivalent to saying the material is producing a flux opposed to the applied field, the material will tend to move to regions of lower field strength or be repelled by the magnetic field. This effect can be measured in the Gouy experiment, in which a diamagnetic sample weighs less when an inhomogeneous field is applied than in the absence of such a field.

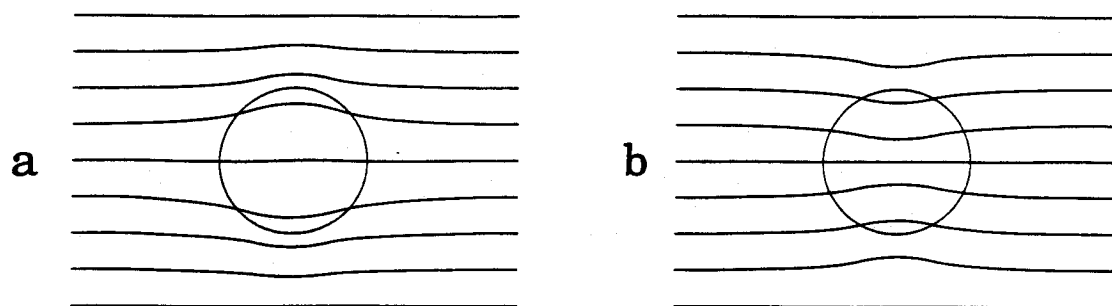


Figure 3-3. (a) Diamagnetic body in a magnetic field; (b) paramagnetic body in a magnetic field.

The magnetic susceptibility, χ , for a purely diamagnetic substance is typically very small and negative in sign. This is in contrast to materials which have paramagnetic or ferromagnetic interactions, in which the magnetic susceptibility due to the paramagnetic or ferromagnetic components is positive and substantially greater in magnitude. The diamagnetic susceptibilities of atoms in molecules are additive in nature. This allows one to easily predict an approximate value of the magnetic susceptibility resulting from diamagnetism in almost any molecule of choice.

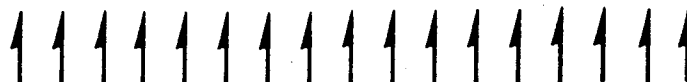
While diamagnetism arises from the interaction of paired electrons, the other forms of magnetic materials and behavior result from unpaired electrons. For example the macroscopic characteristics of a three-dimensional ferromagnetic solid, such as the existence of a magnetic field and magnetic moment, are a result of spin and orbital angular momenta of unpaired electrons. Qualitatively, the spin and orbital motion of the unpaired electron result in a magnetic moment similar to a microscopic bar magnet with two poles. The interactions (or lack of them) among the unpaired electrons in a system will determine the type of magnetic material and resultant behavior.

Paramagnetic substances, for instance, are characterized by random orientations of the magnetic moments resulting from spin angular momenta of unpaired electrons (Figure 3-4a). The moment may be a $S = 1/2$ or higher multiplicity radical. There is no interaction between neighboring spin centers. The application of an external magnetic field will tend to align the spin moments parallel to the direction of the magnetic field. At elevated temperatures, this effect will be opposed by thermal energy, which tends to destroy the parallel alignment of the radicals in the magnetic field. This is the basis of one of the first fundamental theories of paramagnetism known as the Curie law, which will be discussed later. Paramagnetic materials are also

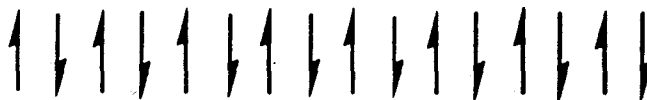
Paramagnetism: The radical spins are randomly oriented .
Zero overall magnetic moment.



Ferromagnetism: The radical spins are aligned in a parallel orientation throughout the material. An overall magnetic moment results.



Antiferromagnetism: The radical spins are opposed to each other. Zero overall magnetic moment.



Ferrimagnetism: The radicals are unequal and oppositely aligned. An overall magnetic moment results.

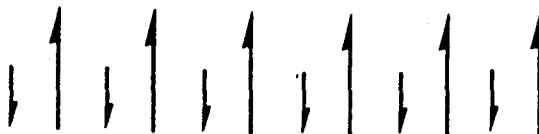


Figure 3-4. Electron spin alignment for (a) paramagnetic substance; (b) ferromagnetic substance; (c) antiferromagnetic substance; (d) ferrimagnetic substance.

characterized by a zero overall magnetic moment in the absence of an external magnetic field. This is a consequence of the random orientations of the isolated electron magnetic moments.

In contrast to the non-communicative nature of paramagnetic centers, ferromagnetism arises from the interactions among unpaired electrons. A ferromagnetic material is characterized by the parallel orientation of the magnetic moments of the unpaired electrons (Figure 3-4b). There exists some mechanism which couples the electrons such that they all are in equivalent spin states (that is, $M_s = \text{all } +\frac{1}{2} \text{ or all } -\frac{1}{2}$). The coupling of the electron spins results in the energetic stabilization of the high spin state (all spins parallel) as opposed to any other configuration. The parallel spins give rise to a permanent magnetic moment in the absence of an external magnetic field. This can be seen in any household bar magnet, which has a permanent moment due to the coupled electron spins on the atoms that constitute the material.

Virtually all ferromagnetic materials which are commercially used at the present time are composed of inorganic metals such as iron, cobalt, or chromium in crystalline or non-crystalline lattice networks.⁵ They have the physical characteristics of metals. There do not exist any discrete, covalent bonds between magnetic ions in these systems. Instead, there are infinite repetitions of unit cells of inorganic ions in three dimensions. The strength and thermal stability of the magnetism in ferromagnetic materials are directly related to the number of parallel spins and the magnitude of the energetic coupling between them.

A third class of magnetic materials, antiferromagnetism, also involves the participation of coupled unpaired electron spins. However, in contrast to ferromagnetism, antiferromagnetism arises from the antiparallel

configuration of the magnetic moments of each electron (Figure 3-4c). The coupling mechanism is such that the antiparallel configuration is of lower energy than either the parallel or random configurations.

It must be stressed that both ferro- and antiferromagnetism arise from interactions between electron spins or sets of spins. The coupling forces which produce the cooperative behaviors are often a mixture of both intra- and intermolecular interactions. Ferromagnetism is by definition a bulk, macroscopic quality. This implies that the interactions which couple the electron spins must occur in three dimensions. Inorganic ferromagnetic systems often have metal centers which are high spin due to Hund's rule (Cr^{3+} , for instance) and intermolecular coupling forces which align the metal centers throughout the material in all directions. It should be noted that without the coupling interaction between spin centers, the magnetic material would become paramagnetic in nature. In general, there are two necessary criteria for a material to be ferromagnetic:

1. Unpaired spins: These provide the microscopic magnetic moments which result in macroscopic magnetization.
2. Coupling interactions between spins: These provide the necessary mechanism to obtain three-dimensional ferromagnetic order.

In conventional ferromagnets, the coupling interactions are strong, which imparts high temperature stability to the magnetic material. Above a certain temperature T_c (known as the Curie point) a ferromagnetic material behaves as a paramagnet. At this temperature the thermal energy, which tends to randomize the directions of the electron spin magnetic moments, has

overcome the energy of coupling between magnetic moments. Iron, for instance, has a Curie temperature of 770°C.⁶

The vast majority of molecules that contain unpaired electrons, however, fall into a category that is actually a combination of paramagnetism and ferro- or antiferromagnetism. For the purpose of this discussion, a ferromagnetic material will be defined as a substance that undergoes spontaneous magnetization at a temperature T_s . That is, a ferromagnetic material has three dimensional coupling interactions which, below T_s , align the spin magnetic moments to give a macroscopic magnetization without the help of an external magnetic field. Related to this extensively coupled ferromagnetic system is the concept of paramagnetic materials that have short range weak intermolecular ferro- or antiferromagnetic interactions. Unlike the ferromagnets defined above, these ferromagnetically (or antiferromagnetically)-coupled paramagnets do not couple to each other throughout the entire material and hence do not have a macroscopic magnetization in the absence of a magnetic field. An external magnetic field is still required before this type of material exhibits a macroscopic magnetization (similar to isolated paramagnets). Most radical-containing molecules, even though they may not have a designed intermolecular coupling mechanism, do interact magnetically to give behavior that at lower temperatures is not purely isolated in nature. Organic radicals, for instance, typically have a weak antiferromagnetic coupling between several neighboring molecules which is manifested at low temperatures. At higher temperatures the coupling is small compared to the thermal energy, and such materials will behave like a paramagnetic system.

While the current explosion of research efforts aimed toward the synthesis of molecular magnetic materials has been expressed in terms of the goal of a molecular ferromagnet, the results of the early work in this area have

been more in the scope of *partially* ferromagnetically coupled systems.⁷ The spin centers are often weakly coupled in one dimension, or partially coupled in two or three dimensions. However, the extensive three-dimensional coupling of spins which is necessary in a ferromagnet is usually not achieved. Thus, these materials at low temperatures may exhibit partial ferromagnetic coupling (but no spontaneous magnetization) in an external magnetic field which disappears at higher temperatures. The magnitude of the ferromagnetic coupling between spin centers in these molecular systems is also quite small compared to conventional ferromagnets, which may account for the lack of extensive interactions throughout the material.

The third class of magnetically active materials is that of ferrimagnets. Ferrimagnetism is a consequence of antiferromagnetically coupled spin centers, A and B, in which the magnitude of the magnetic moments of A and B are unequal. This can be seen in Figure 3-4d in which A is represented by a large arrow and B is a small arrow. Even though in the linear chain A's and B's are aligned in an antiparallel configuration, since the multiplicity of A is larger than B there is an incomplete cancellation of magnetic moments and the chain has an overall magnetic moment. If this is extended to three dimensions, one forms a ferrimagnet which has many of the characteristics (such as spontaneous magnetization) of ferromagnets. Ferrimagnets have important uses as conventional magnetic materials. The first known magnetic material, magnetite, which was discovered by 800 B.C., is a ferrimagnet of composition $\text{FeO} \cdot \text{Fe}_2\text{O}_3$.

While there are a number of other types of magnetic behavior known, they are all derived from paramagnetism, ferromagnetism, and antiferromagnetism.

Magnetic Characterization

The characterization of magnetic materials typically involve magnetic susceptibility measurements, which examine the interaction of the magnetic substance with an externally applied magnetic field. Other equally important methods of defining magnetic phenomena³ include heat capacity measurements (which are an indication of the phase transitions of magnetic materials) and neutron diffraction studies. The latter two methods are especially useful for strongly coupled antiferromagnetic or ferromagnetic systems. For the purpose of this work, magnetic susceptibility methods will be examined, with the intent of applying a theoretical treatment of the interactions of unpaired electrons in an external magnetic field to real experimental phenomena in organic polymeric systems. This section will specifically deal with the temperature and external field dependence of magnetization (M) and susceptibility (χ) of ferromagnetically and antiferromagnetically coupled spin matrices.

As previously discussed, magnetic susceptibility is a function of the induced magnetization in the sample and the amount of field required to induce the moment ($\chi = M/H$). Purely diamagnetic materials (*i.e.*, no unpaired electrons) have χ values that are typically small and negative (Table 3-1). The sign of χ reflects the characteristic of diamagnetic materials to have a field density within the body smaller than that outside of the body. The diamagnetic susceptibility is constant with regard to variations in applied field or temperature.

The magnetic susceptibility from paramagnetism, on the other hand, is positive in sign (Table 3-1). A purely paramagnetic material has no field dependence on χ . It differs from diamagnetic susceptibility in that there is a temperature dependence of χ . A material which has ferromagnetic interactions

Table 3-1. Magnetic Susceptibilities

| | Typical χ value (emu/mol). | Temperature dependence? | Field dependence? |
|--------------------|------------------------------------|----------------------------|----------------------|
| Diamagnetism | -1×10^{-6} | No | No |
| Paramagnetism | $0 - 10^{-2}$ | Yes | No |
| Ferromagnetism | $10^{-2} - 10^6$ | Yes | Yes |
| Antiferromagnetism | $0 - 10^{-2}$ | Yes | Yes |

between spin units, on the other hand, has susceptibility values which are both temperature and magnetic field dependent. A ferromagnet has large positive values of χ which are usually, but not always, larger than in paramagnets. The strength and extent of magnetic coupling interactions between spins greatly affect the nature of the temperature and field effects on χ . Antiferromagnetically coupled materials usually have low values of χ with a corresponding temperature dependence.

When measuring the experimental magnetic susceptibility (χ_e) of a system with unpaired spins, the values observed are actually a combination of paramagnetic-derived susceptibility (χ_p), the negative diamagnetic-derived susceptibility (χ_{dia}) and in certain cases a temperature-independent, positive susceptibility, known as Pauli susceptibility (χ_{Pauli}):

$$\chi_e = \chi_p + \chi_{dia} + \chi_{Pauli} \quad (3)$$

This temperature independent susceptibility, χ_{Pauli} , is sometimes seen in singlet ground states. It is especially characteristic of metallic systems in which there are partially filled bands of electrons. Pauli susceptibility arises from a mixing of the ground state of a system with excited states that are not thermally populated. This behavior is governed by Fermi-Dirac statistics (instead of Boltzmann statistics, as in Curie behavior) and is therefore temperature independent.

Curie Law. In the late 19th century, Curie⁸ found that, for a number of paramagnetic substances, the magnetic susceptibility (χ_p) was inversely proportional to temperature. That is,

$$\chi_p = \frac{C}{T} \quad (4)$$

where C is the Curie constant. This empirical result was later modified to give the Curie-Weiss law

$$\chi_p = \frac{C}{T - \theta} \quad (5)$$

where θ is a constant known as the Weiss constant. The Weiss constant is indicative of *intermolecular* short range interactions between magnetic centers. *A positive value of θ is the result of ferromagnetic coupling, while a negative value of θ is the result of antiferromagnetic coupling.* Thus the Curie-

Weiss law allows one to evaluate the type of interactions, if any, that occur between spin centers.

Magnetic susceptibility, and hence the Curie and Curie-Weiss law, can be expressed in terms of volume, molar, or mass relationships. χ_p is defined as volume magnetic susceptibility and is unitless. Equations 4 and 5 also can be used to describe the temperature-dependent behavior of the molar susceptibility (χ_m , in units of emu/mol) with a Curie constant C' and Weiss constant θ' . Similarly, the mass susceptibility (χ_g , in units of emu/gram) of a paramagnetic material has a corresponding Curie constant C'' and Weiss constant θ'' . A paramagnetic material will follow the Curie or Curie-Weiss law with its magnetic susceptibility expressed in molar, mass, or volume forms. The magnitude and units of the Curie and Weiss constant will depend on the reference units used.

The Curie-Weiss law is often experimentally evaluated using the inverse susceptibility, χ_p^{-1} , such that

$$\frac{1}{\chi_p} = T \left(\frac{1}{C} \right) - \frac{\theta}{C} \quad (6)$$

When χ_p^{-1} is plotted versus T , with χ_p^{-1} as the ordinate, then at higher temperatures the fit will be linear in nature. The slope of the line will be the inverse Curie constant. If the material is truly paramagnetic, that is, if there are no intermolecular magnetic interactions, then the plot throughout the entire temperature range will be linear and the x-intercept will be zero (Figure 3-5a). However, if there are intermolecular ferromagnetic couplings, a positive θ will be observed and a deviation from a linear fit will be seen at low temperatures (Figure 3-5b). The difference in behavior of the Curie plot at low

Curie-Weiss Law

$$\chi = C/(T - \theta)$$

θ = Weiss constant (x-intercept of high T data)

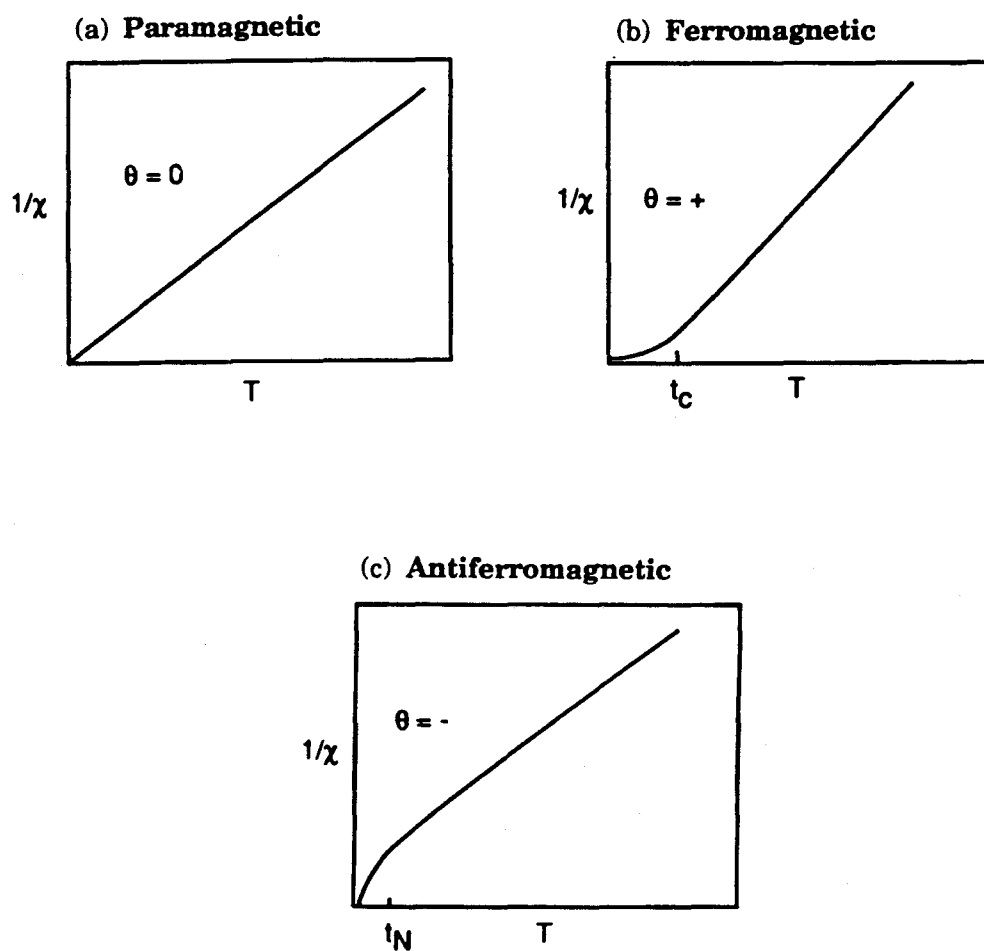


Figure 3-5. Curie-Weiss law behavior for (a) paramagnetic materials; (b) ferromagnetic couplings; (c) antiferromagnetic couplings.

and high temperatures is rationalized in terms of the effect of temperature on ferromagnetic coupling. At temperatures well above the onset of curvature (roughly the Curie point, T_c), the strength of intermolecular ferromagnetic coupling is small compared to the thermal energy present. The materials behave in this temperature range paramagnetically with a linear fit to a χ_p^{-1} versus T plot. If the high temperature portion of the plot is extended to the x intercept, the Weiss constant will be obtained (at $\chi_p^{-1} = 0$, $\theta = T$). As the temperature is decreased, the magnitude of the intermolecular ferromagnetic coupling becomes comparable to the thermal energy, and a deviation from linearity is observed in the χ_p^{-1} vs T plot. For a ferromagnetically-coupled material, the curvature is such that the slope of the line decreases with decreasing T . This corresponds to an increase of C (since $C = 1/\text{slope}$) compared to the C obtained from the linear, high temperature portion of the fit. As will be later shown quantitatively, the Curie constant is proportional to the multiplicity of the molecules present in the material. Thus the increase of C reflects the increase of the high spin coupling between magnetic centers at low temperatures.

Antiferromagnetically coupled molecules which have negative θ constants display qualitatively similar behavior to ferromagnetically coupled materials (Figure 3-5c). At higher temperatures a χ_p^{-1} versus T plot will give a linear fit. The x -intercept of the high temperature data, though, will be negative, corresponding to a negative Weiss constant (θ). The curvature at low temperatures will now be in a direction so as to give an increasing slope as the temperature is decreased. This results in a smaller C as temperature is lowered and hence a smaller overall multiplicity. This is in qualitative agreement with the effects of antiferromagnetic coupling, which tend to decrease the magnetic moment and multiplicity of spin containing systems.

As equation 3 notes, the measured experimental susceptibility of a material with unpaired electrons can be decomposed into separate terms for the paramagnetic (χ_p), diamagnetic (χ_{dia}), and Pauli (χ_{Pauli}) contributions to the overall measured susceptibility (χ_e):

$$\chi_e = \chi_p + \chi_{dia} + \chi_{Pauli} .$$

Since the Curie law applies only to paramagnetic susceptibility (χ_p), in order to evaluate magnetic susceptibility one must separate the paramagnetic portion of the overall susceptibility from the diamagnetic and Pauli contributions. Noting that $\chi_p = C/(T-\theta)$, if this is substituted into equation 3 one obtains

$$\chi_e = [C/(T-\theta)] + \chi_{dia} + \chi_{Pauli} .$$

At high temperatures and if θ is small, this reduces to

$$\chi_e = (C/T) + \chi_{dia} + \chi_{Pauli} .$$

Recalling that χ_{dia} and χ_{Pauli} are temperature independent, let $\chi_T = \chi_{dia} + \chi_{Pauli}$, where χ_T is a constant with regard to variation in temperature. Therefore,

$$\chi_e = (C/T) + \chi_T .$$

Plotting χ_e versus T^{-1} will give a straight line at high temperatures with a y-intercept corresponding to χ_T . This can then be subtracted from the overall susceptibility to give χ_p . In most materials which are non-metallic or poor conductors, the Pauli susceptibility is zero and hence the y-intercept will simply be the diamagnetic susceptibility of the material.

The above procedure is often neglected when dealing with ferromagnetic materials or paramagnets which have large paramagnetic susceptibilities. In these systems, the diamagnetic contribution to the overall susceptibility is quite small compared to χ_p , so it is often ignored. In magnetically dilute materials, with low magnitudes of χ_p , it is extremely important that the temperature independent contribution be subtracted from the overall susceptibility to give an accurate χ_p . Since χ_p is inherently small in these systems, a moderate error in its determination (by neglecting χ_{dia}) can lead to serious errors in the Curie plot.

Effective Magnetic Moment. A sometimes more convenient method of expressing the amount of magnetization of a system is the effective magnetic moment, μ_{eff} , of a molecule. To a first approximation (neglecting orbital angular momentum), μ_{eff} is directly related to the number of unpaired electrons in the molecule of interest.

$$\mu_{eff} = g \left[S(S+1) \right]^{1/2} \mu_B \quad (7)$$

where S is the spin quantum number, μ_B is the Bohr magneton, and g is the Landé constant. Recalling that μ_B is a fundamental unit of magnetic moment for an electron, μ_{eff} is usually referred to in units of Bohr magnetons. Table 3-2

shows the calculated effective moments for a series of high spin molecules (assuming $g = 2$).

Table 3-2. Effective Magnetic Moment (μ_{eff})

| S | 1/2 | 2/2 | 3/2 | 4/2 | 5/2 | 6/2 | 7/2 | 8/2 |
|----------------------------|------|------|------|------|------|------|------|------|
| $\mu_{\text{eff}} (\mu_B)$ | 1.73 | 2.83 | 3.87 | 4.89 | 5.91 | 6.93 | 7.94 | 8.94 |

In certain cases (mainly molecules with partially filled d orbitals) the orbital angular momentum may contribute significantly to the effective magnetic moment and give μ_{eff} values substantially higher than the spin-only values.

The effective moment is related to the molar paramagnet susceptibility, χ_m , as shown:

$$\chi_m = \frac{N\mu_{\text{eff}}^2}{3kT} \quad (8)$$

where N is Avogadro's number, k is the Boltzmann constant, and T is

temperature. Since $\chi_m = C'/T$,

$$\mu_{eff} = \left(\frac{3 kC}{N} \right)^{1/2} \quad (9)$$

or

$$\mu_{eff} = 2.824 (C')^{1/2} \quad (10)$$

or

$$\mu_{eff} = 2.824 (\chi_m T)^{1/2} \quad (11)$$

If χ_m is in units of emu/mol and T is in Kelvin, then μ_{eff} above is in units of Bohr magnetons. This can then be compared to the calculated values of μ_{eff} in Table 2 to find the spin state of the system.

A plot of $(\chi_m T)^{1/2}$ or $(\chi_m T)$ versus T for a given system determines the effect of temperature on μ_{eff} . If there are no interactions between neighboring spins, then $(\chi_m T)^{1/2}$ and thus μ_{eff} will be constant throughout the temperature range (Figure 3-6). If a spin experiences a ferromagnetic exchange field due to the neighboring spins (*i.e.*, a positive θ), then at low temperatures roughly corresponding to θ the measured susceptibilities will be greater than that predicted for isolated spins. The μ_{eff} will then increase at these low temperatures as the ferromagnetic interactions overcome the thermal energy present. In the case of an antiferromagnetic exchange interaction between neighboring spins (negative θ), μ_{eff} will decrease at temperatures roughly corresponding to $-\theta$.

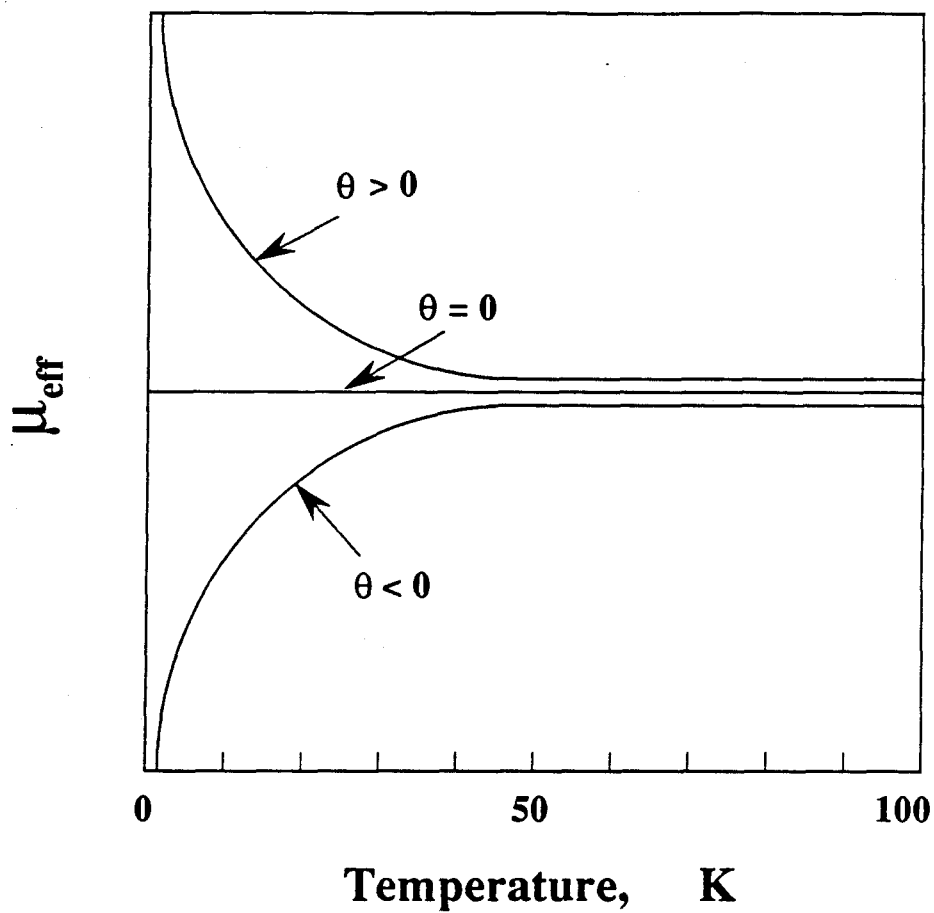


Figure 3-6. Temperature dependence of μ_{eff} for paramagnetic, antiferromagnetically-, and ferromagnetically-coupled materials.

The use of μ_{eff} instead of χ_m is helpful when dealing with magnetic systems that have small ferromagnetic or antiferromagnetic interactions between neighboring spins. A plot of χ_m^{-1} versus T for a material with a small ferromagnetic Weiss constant may have only very subtle deviations from linearity, which makes it difficult to graphically observe the onset of ferromagnetic interactions. This can be seen in Figure 3-7, in which Miller *et al.* reported the Curie behavior of several metallocene salts that interact ferromagnetically and antiferromagnetically.⁹

However, when μ_{eff} is plotted (versus T), the differences between antiferromagnetically and ferromagnetically coupled materials becomes much more apparent. It is immediately observed in Figure 3-8 that $[\text{Fe}(\text{C}_5\text{Me}_5)_2]^+ (\text{TCNE})^-$ has a substantial degree of ferromagnetic interactions at low temperatures (in fact, it is a ferromagnet below 4.2 K). This characteristic is not as apparent in the Curie plot of Figure 3-7.

Curie Behavior -- A Closer Look. The Curie law of magnetic susceptibility originally was found in the 19th century through empirical observations of several magnetic compounds. This relationship between magnetic moment and temperature was understood at the time in the context of classical physics. The later development of quantum theory had a profound impact on the study of magnetism. Weiss' use of a "molecular field" in the interactions between magnetic molecules to explain deviations from the Curie law signaled the beginning of a new era, one in which magnetism could be viewed as a cooperative phenomenon. This has led to the use of statistical mechanical methods to explain the many facets of magnetism. This section examines the characteristics of the temperature-dependent behavior of magnetic materials from a quantum mechanical viewpoint.

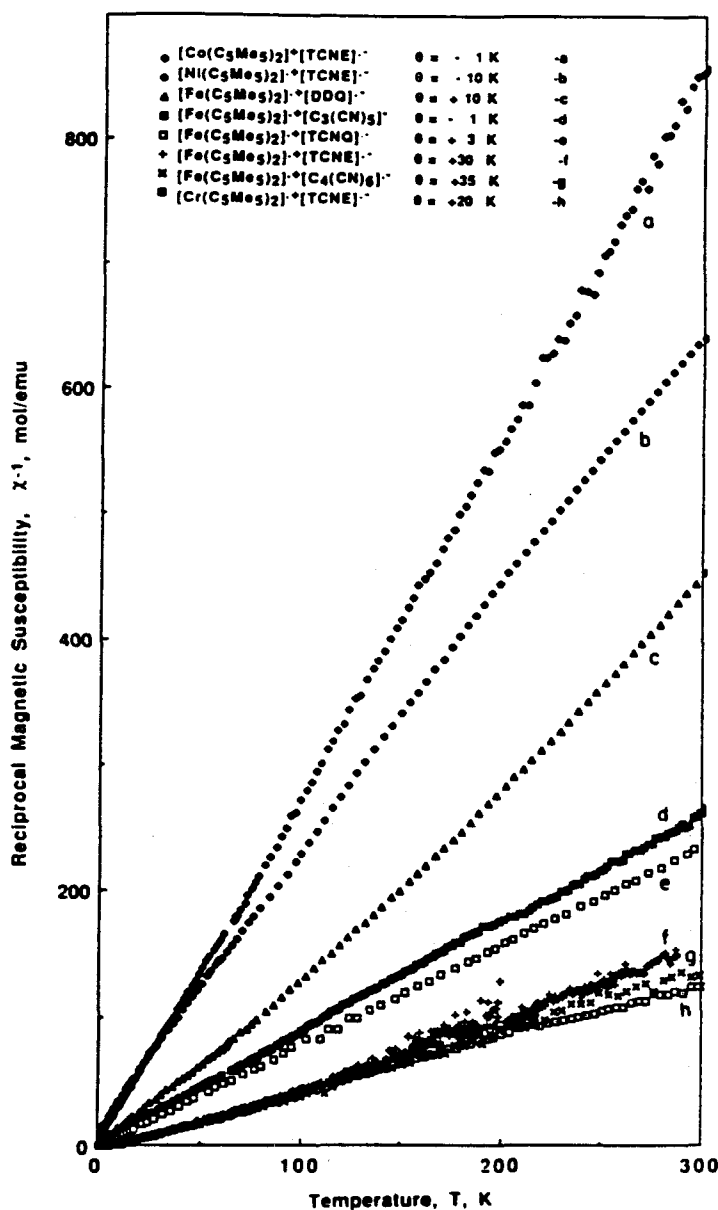


Figure 3-7. Reciprocal magnetic susceptibility (χ^{-1}) as a function of temperature for [Fe^{III}(C₅Me₅)₂]⁺[A]⁻ [A = TCNQ, TCNE, DDQ, C₄(CN)₆, C₃(CN)₅] and [M^{III}(C₅Me₅)₂]⁺[TCNE]⁻ (M = Co, Cr, Ni). The points are experimental results of Miller.⁹

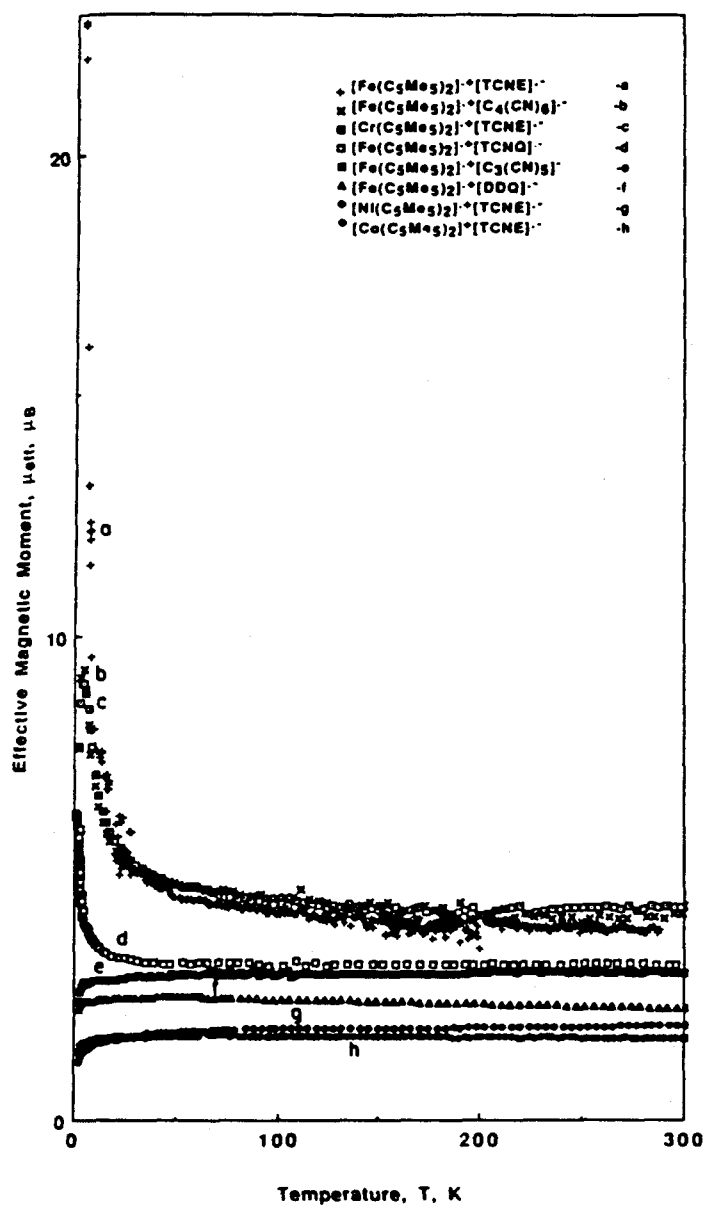


Figure 3-8. Effective moment (μ_{eff}) as a function of temperature for $[\text{Fe}^{\text{III}}(\text{C}_5\text{Me}_5)_2]^+[\text{A}]^-$ [$\text{A} = \text{TCNQ}, \text{TCNE}, \text{DDQ}, \text{C}_4(\text{CN})_6, \text{C}_3(\text{CN})_5$] and $[\text{M}^{\text{III}}(\text{C}_5\text{Me}_5)_2]^+[\text{TCNE}]^-$ ($\text{M} = \text{Co}, \text{Cr}, \text{Ni}$). The points are experimental results of Miller.⁹

In the absence of an external magnetic field, and ignoring dipole-dipole interactions (*i.e.*, zero field splitting), the magnetic quantum states of a molecule with $S = J$ are degenerate. For instance, the ground state of an isolated ion with $S = 5/2$ has six states with $m_s = \pm 1/2, \pm 3/2, \pm 5/2$ which are of equal energy in the absence of a field. Application of a magnetic field H splits the degeneracy to give six states with differing energy levels (Figure 3-9). The energy of each level is

$$E_{m_s} = m_s g \mu_B H \quad (12)$$

where m_s is the magnetic quantum number, μ_B is the Bohr magneton, and g is the Landé constant.

If it is assumed that the magnetic ions in the $S = 5/2$ system are only weakly interacting, distinguishable, and isotropic, then one may apply Boltzmann statistics to determine the relative population of each energy level at a given temperature. Since each state corresponds to a different orientation of the magnetic moment of the molecule with respect to the external magnetic field, different populations of the energy levels will result in different magnetizations.

This can be seen more simply in a system with $S = 1/2$ particles. There are two magnetic states, $m_s = +1/2$ and $m_s = -1/2$, for such a system and they are degenerate in zero applied field. Similar to the $S = 5/2$ example, once a magnetic field (H) is applied, the states are no longer degenerate and split into two levels, $m_s = \pm 1/2$ (Figure 3-10). The energies of the two states are $(1/2)g\mu_B H$ for and $(-1/2)g\mu_B H$. The separation between states is $g\mu_B H$.

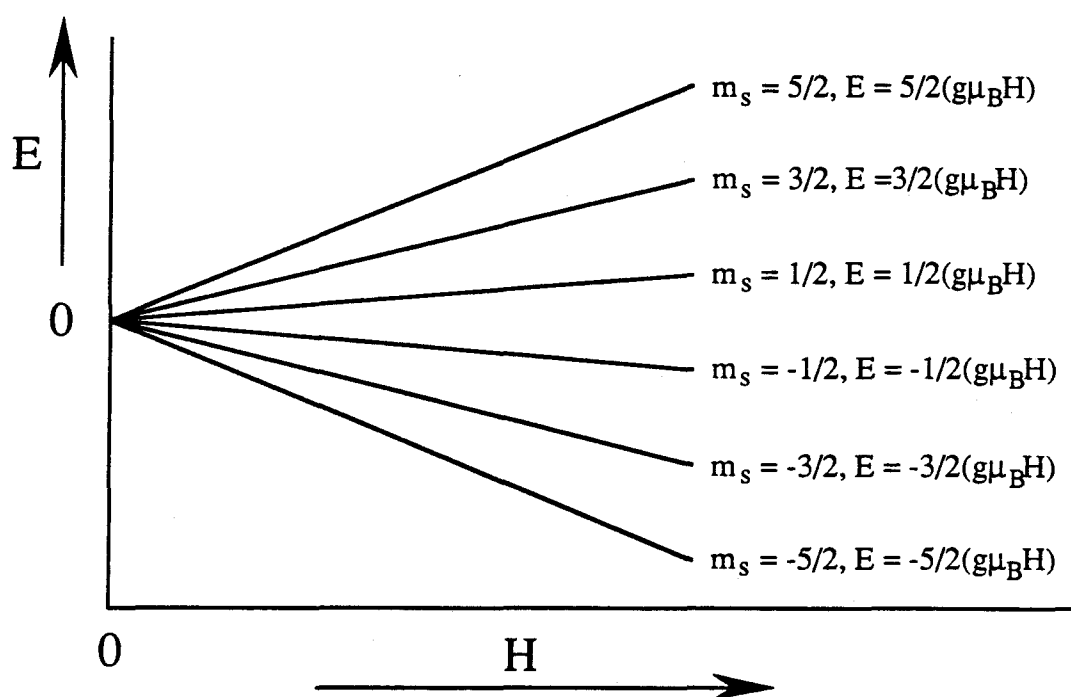


Figure 3-9. Energy levels of a $S = \frac{5}{2}$ system in the presence of a magnetic field.

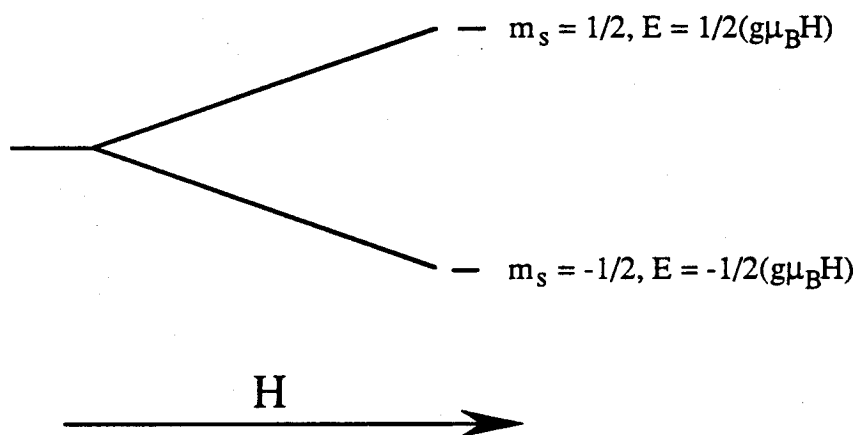


Figure 3-10. Energy levels of a $S = \frac{1}{2}$ system in the presence of a magnetic field.

The relative populations of the energy levels can be found using Boltzmann statistics. Recall that if n_i is the number of particles in the i th energy level and if

$$\sum_i n_i = N$$

where N is the total number of particles in the entire system then for $N = 1$ mole of molecules,

$$P_i = \frac{n_i}{N} = \frac{e^{-\epsilon_i/kT}}{\sum_i e^{-\epsilon_i/kT}} \quad (13)$$

in which P_i is simply the fraction of molecules in a specified state of energy ϵ_i .

If the energy of a single ion in energy level i is $\epsilon_i = m_s g \mu_B H$, and the magnetic moment of an ion in the energy level i is given as $\mu_i = -m_s g \mu_B$, then the total molar macroscopic magnetic moment M is given by the sum of the moments μ_i corresponding to all possible levels (two in this case, $m_s = \pm 1/2$) weighted according to their respective Boltzmann factors P_i :

$$M = N \sum_i \mu_i P_i, \quad (14)$$

Substituting equation 13 yields

$$M = N \frac{\sum_{m_s = -1/2}^{1/2} (-m_s g \mu_B) e^{(-m_s g \mu_B H/kT)}}{\sum_{m_s = -1/2}^{1/2} e^{(-m_s g \mu_B H/kT)}} \quad (15)$$

$$= \frac{Ng \mu_B}{2} \left[\frac{e^{g \mu_B H/kT} - e^{-g \mu_B H/kT}}{e^{g \mu_B H/kT} + e^{-g \mu_B H/kT}} \right]$$

$$= \frac{Ng \mu_B}{2} \tanh \left(\frac{g \mu_B H}{2kT} \right) \quad (16)$$

where \tanh is the hyperbolic tangent:

$$\tanh y = \frac{e^y - e^{-y}}{e^y + e^{-y}} .$$

One of the properties of the hyperbolic tangent is that, for Y much less than 1, $\tanh y = y$. Therefore, if $g \mu_B H/2kT$ is much less than one (*i.e.*, at moderate fields and temperatures), then

$$\tanh\left(\frac{g\mu_B H}{2kT}\right) \approx \left(\frac{g\mu_B H}{2kT}\right)$$

and

$$M = \frac{N g^2 \mu_B^2 H}{4kT} \quad (17)$$

Since molar magnetic susceptibility is defined as $\chi_m = M/H$,

$$\chi_m = \frac{M}{H} = \frac{N g^2 \mu_B^2}{4kT} \quad (18)$$

Or, since χ_m is also equal to C'/T in which C' is the molar Curie constant,

$$\chi_m = \frac{C'}{T} \quad \text{where } C' = \frac{N g^2 \mu_B^2}{4kT} \quad (19)$$

This is the specialized form of the Curie law for $S = 1/2$. Recalling that $\mu_{\text{eff}} = g[S(S+1)]^{1/2}\mu_B$, for a $S = 1/2$ system,

$$\mu_B^2 = \frac{4\mu_{\text{eff}}^2}{3g^2}$$

If $g = 2$, then equation 19 now simplifies to the general form of the Curie law, which was previously defined in equation 8,

$$\chi_m = \frac{N\mu_{eff}^2}{3kT} \quad (8)$$

It must be stressed that the Curie law for $S = 1/2$ molecules is valid only when $g\mu_B H/2kT \ll 1$. This means that the ratio H/T must be less than 1.49 Tesla/K. It is also of interest to examine the magnetization behavior at high magnetic fields and low temperatures; that is if $g\mu_B H/2kT \gg 1$ (i.e., if $H/T \gg 1.49$ Tesla/K). It is known that $\tanh y$ converges to 1 as y becomes much larger than 1. Thus, equation 16 becomes

$$M_{Sat} = \frac{Ng\mu_B}{2},$$

where the molar magnetization achieves a saturated value and becomes independent of the temperature and field. This is the maximum value of M and corresponds to the complete alignment of the unpaired electrons with the external magnetic field. The more general version of the equation is

$$M_{Sat} = Ng\mu_B S. \quad (20)$$

Thus, at high fields and low temperatures, the molar magnetization (and susceptibility) do not scale linearly with temperature, as the classical Curie law would imply. The rate of change of χ with temperature decreases as the conditions for saturation, or complete alignment of all electrons with the applied field are approached. In terms of Figure 3-10, this condition corresponds to complete, or nearly complete population of the lowest energy level. As previously mentioned, the lowest energy level has the largest

magnetic moment parallel with the field; hence the maximum macroscopic magnetization M is achieved. It is interesting to note that the population of the lowest level becomes large when kT is smaller than $g\mu_B H$. When kT is equivalent to $g\mu_B H$, the ratio of the population of the $m_s = +1/2$ and the $m_s = -1/2$ levels is 0.37, indicating that the lower level is appreciably overpopulated relative to the upper level.

Brillouin Treatment. It is of considerable importance to the experimentalist that the spin state of a system be identifiable from experimental data. Often times Curie plots are used, which as outlined earlier, can be evaluated in terms of μ_{eff} and thus S . However, for quantitative determination of S by these methods, accurate values of the molar susceptibility must be obtained. While for systems that contain a well-defined number of unpaired spins this may seem a trivial problem, systems that have an imprecise number of spins also have imprecise values of the molar susceptibility. This makes it virtually impossible to quantitatively evaluate μ_{eff} and S in these systems using molar susceptibility data. In polymeric systems that depend on chemical reactions to produce spins, this poses a substantial limitation to the use of Curie plots, since the yields of such spin-producing reactions are not obtainable to the accuracy required for Curie analysis.

There is another, more fundamental measurement of magnetic behavior which has certain advantages compared to the Curie law when dealing with the characterization of magnetic spin states. Magnetization M , to which χ_m is related, can be evaluated in such a way so that the quantity of molar concentration of spins in a sample is irrelevant. This section examines the theoretical treatment of magnetization as it relates to spin state, external magnetic field and temperature.

Consider a single magnetic ion or molecule with an arbitrary spin-quantum number such that $J = S$ (i.e., no orbital angular momentum contribution to J). Assume that the ion is isotropic with respect to its interaction with a magnetic field, and the ion has very weak interactions with neighboring ions. This isolated system can then be treated using Boltzmann statistics similar to the spin 1/2 system examined earlier. For an ion with $J = S$, there are $2S + 1$ degenerate states which in the presence of an external magnetic field split into $2S + 1$ levels corresponding to $m_s = +J, J-1, \dots, -J$ (again, dipole-dipole interactions are ignored). The energy of each state is $E_{m_s} = m_s g \mu_B H$, with an energy difference between levels of $g \mu_B H$. Each level or state corresponds to a different orientation of the ions magnetic moment with respect to the applied field, H . The relative populations of each state determine the overall magnetization of the substance. The macroscopic magnetization is largest when a single (the lowest) level is populated.

The net magnetic moment of a single atom (μ) is the sum of all possible magnetic moments corresponding to each energy level (where $\mu_{m_s} = -m_s g \mu_B$) weighted by the Boltzmann factor P_{m_s} :

$$\mu = \sum_{m_s} \mu_{m_s} P_{m_s} ,$$

where

$$P = \frac{e^{\frac{-m_s g \mu_B H}{kT}}}{\sum_{m_s} e^{\frac{-m_s g \mu_B H}{kT}}}$$

Thus,

$$\mu = \frac{\sum_{m_s=-J}^J (-m_s g \mu_B) e^{\left(\frac{-m_s g \mu_B H}{kT}\right)}}{\sum_{m_s=-J}^J e^{\left(\frac{-m_s g \mu_B H}{kT}\right)}}$$

This expression can be simplified to give

$$\mu = g \mu_B \left[\frac{(J + \frac{1}{2}) \cosh(J + \frac{1}{2})x}{\sinh(J + \frac{1}{2})x} - \frac{\frac{1}{2} \cosh \frac{x}{2}}{\sinh \frac{x}{2}} \right]$$

where $x = g \mu_B H / kT$. This can be further simplified to give

$$\mu = g \mu_B J B_J(x),$$

where the Brillouin function $B_J(x)$ is defined as

$$B_J(x) = \frac{1}{J} \left[\left(J + \frac{1}{2} \right) \coth \left[\left(J + \frac{1}{2} \right) x \right] - \frac{1}{2} \coth \frac{x}{2} \right]. \quad (21)$$

For a system of 1 mole of noninteracting ions (N), the net molar magnetization **M** is

$$M = N\mu = Ng\mu_B JB_J(x) . \quad (22)$$

Thus, for a given J , the magnetization of a substance will vary according to changes in applied field and temperature. A plot of the Brillouin function for several values of J is seen in Figure 3-11.

There are two cases of limiting behavior of the Brillouin function which will now be examined.

a) High fields and low temperatures ($x \gg 1$).

At large values of x , the Brillouin function approaches 1. Since $x = g\mu_B H_z/kT$, and for a given J , the quantities g , μ_B , k , and J are constant, this condition corresponds to large values of H_z and small values of T , or $H_z/T \gg 0.7$ Tesla/K. Thus, in large magnetic fields and at low temperatures the Brillouin function approaches unity and the overall magnetization M becomes

$$M = Ng\mu_B JB_J(x) = Ng\mu_B J ,$$

which was previously defined in equation 20. In other words, the macroscopic magnetization M becomes saturated under these conditions and becomes constant relative to further changes in field or temperature.

Now, if the saturated magnetism M_{Sat} is known, then one may define the normalized magnetization as being the ratio of the magnetization $M_{H,T}$ at any field or temperature to the saturation magnetization M_{Sat} , such that

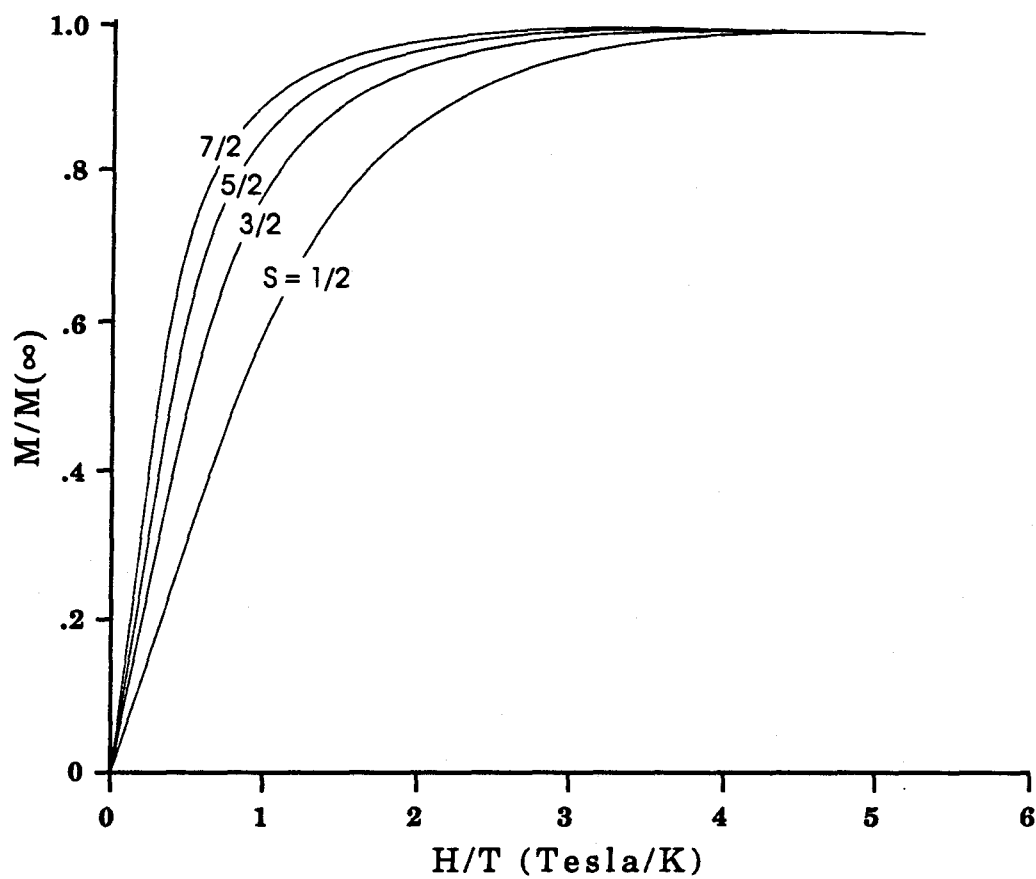


Figure 3-11. The Brillouin equation as a function of H/T .

$$\frac{M_{H,T}}{M_{Sat}} = \frac{Ng\mu_B J B_J(x)}{Ng\mu_B J} = B_J(x) . \quad (22)$$

Therefore, the normalized magnetization is simply the Brillouin function. If the spin state of the substance is unknown, one may fit the experimental normalized magnetization data to the Brillouin function to find J .

A useful characteristic of the normalized magnetization and hence the Brillouin function is that they are unitless quantities. Therefore, the experimentalist who is interested in using a Brillouin plot to determine the spin state S of a substance is not confined to using molar magnetization measurements (*i.e.*, M in units of emuG/mol). As long as the saturation magnetization M_{sat} and $M_{H,T}$ are in similar units, then the Brillouin treatment is valid. Thus, one may use the weight magnetization M_g (emuG/gram) of a sample to evaluate its spin state. This is highly advantageous in systems, like organic polymers, in which the molar concentrations of spin are unknown, since all that is needed is the mass of the sample and the magnetization corresponding to that amount of sample.¹⁰

Figure 3-12 shows plots of magnetization versus H/T for Cr^{3+} ($S = 3/2$), Fe^{3+} ($S = 5/2$), and Gd^{3+} ($S = 7/2$) and the corresponding Brillouin functions for their respective J values.¹¹ A normalized magnetization plot was not used since the molar magnetization values were known. The fit to the theoretical Brillouin function is excellent.

b) Moderate fields and temperatures ($x \ll 1$).

The $\coth x$ can be approximated for small x as shown

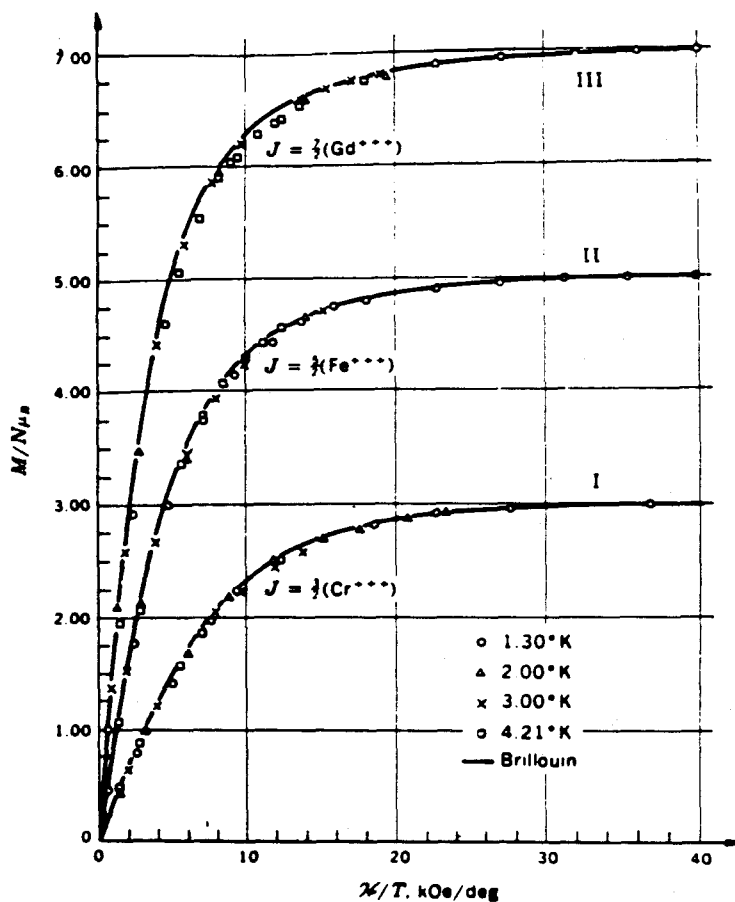


Figure 3-12. Plot of magnetization per magnetic ion against H/T for (I) chromium potassium alum ($J = \frac{3}{2}$); (II) iron ammonium alum ($J = \frac{5}{2}$); and (III) gadolinium sulfate ($J = \frac{7}{2}$); The points are experimental results and the solid curves are graphs of the Brillouin equation.

$$\coth x = \frac{1}{x} + \frac{x}{3} .$$

If $x \ll 1$ and since $x = g\mu_B H/kT$, then

$$H/T < < \frac{k}{g\mu_B} = \frac{1.38 \times 10^{-23} J/K}{2 \times 9.27 \times 10^{-24} J/Tesla}$$

$$\approx 0.7 \text{ Tesla/K} .$$

Therefore, at $H/T < < 0.7 \text{ Tesla/K}$, the Brillouin function can be approximated by

$$B_J(x) = \left(\frac{1}{J}\right) \left\{ \left(J + \frac{1}{2}\right) \left[\left(\left(J + \frac{1}{2}\right)x\right)^{-1} + \left(\frac{1}{3}\right)\left(J + \frac{1}{2}\right)x \right] - \frac{1}{2} \left[\frac{2}{x} + \frac{x}{6} \right] \right\}$$

$$= \frac{1}{J} \left\{ \frac{1}{3} \left(J + \frac{1}{2}\right)^2 x - \frac{1}{12} x \right\}$$

$$= \left(\frac{x}{3J}\right) \left(J^2 + J + \frac{1}{4} - \frac{1}{4}\right)$$

$$= (J + 1) \frac{x}{3} .$$

Converting this into the molar magnetization gives

$$M = Ng^2 \mu_B^2 J(J+1) (g \mu_B H) \left(\frac{1}{3kT} \right)$$

$$= Ng^2 \mu_B^2 J(J+1) \left(\frac{1}{3kT} \right) H.$$

Conversion of M into units of χ_m (where $\chi_m = M/H$) yields

$$\chi = \frac{Ng^2 \mu_B^2 J(J+1)}{3kT},$$

which is simply the Curie law for a molecule with spin state J (see equation 8, where $\mu_{\text{eff}} = g[J(J+1)]^{1/2}$).

This result at small values of H/T has important repercussions concerning the use of Curie law. Classically, the Curie law is assumed to be valid at all temperatures and magnetic fields. However, in the quantum mechanical treatment of Curie behavior with Boltzmann statistics, the linearity associated with a χ^{-1} versus $1/T$ plot will only be observed when the magnetic field and temperature are such that $H/T < 0.7$ Tesla/K (as shown in the $S = 1/2$ system). When the field is large and/or the temperature is very low such that $H/T > 0.7$ Tesla/K, the magnetization begins to saturate and thus the rate of change of magnetization as temperature is decreased does not stay constant. Therefore, the susceptibility does not vary according to $\chi_p = C/T$. This effect can be seen upon examination of the Brillouin function for $S = 1/2$ (Figure 3-11). Between $H/T = 0$ and $H/T \approx 0.4$, the function is essentially linear, and Curie behavior results (H being held constant as T is varied). Above this point, curvature becomes apparent and the Curie law is no longer

applicable. The curvature and eventual saturation of the moment are due to the increased population of the lowest energy state ($m_s = -1/2$) of the magnetic levels relative to the population of the other levels. At very high fields and low temperatures, the $m_s = -1/2$ level (which corresponds to the largest moment with respect to the applied field) is almost totally populated with very little population of the upper energy levels. The Boltzmann energy kT is smaller than the difference in energy levels ($g\mu_B H$). Saturation of the macroscopic moment is observed and no further change of magnetization with a decrease of temperature is seen, which contradicts the Curie law.

The aforementioned quantum mechanical treatment of the Curie law and Brillouin function involves two significant assumptions about the nature of the magnetic species involved:

- 1) The molecules are isolated from neighboring molecules.
- 2) Molecules are isotropic with respect to magnetic field interactions.

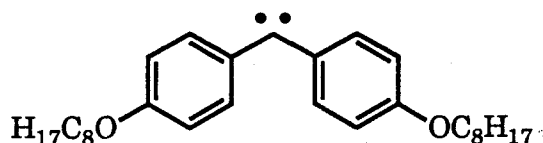
This first assumption is reminiscent of the ideal gas law, $PV = nRT$. When the pressure of a gas becomes too high or molecular interactions occur, deviations from the ideal gas law occur. Similarly, the Curie law begins to break down when magnetic interactions occur among neighboring spins. As previously discussed, the Curie-Weiss law can reflect these couplings through the Weiss constant. The effective magnetic moment (μ_{eff}) can also be used to evaluate the nature of intermolecular magnetic interactions. For spin centers with a small number of neighboring interactions (like dimers and trimers) the Bleaney-Bowers equation has proven useful in evaluating quantitatively the nature and energy of couplings between radical centers in a number of

transition metal compounds. The Curie-Weiss law has no provision for measuring the energy of magnetic coupling.

The Brillouin treatment of magnetic behavior, at first glance, appears even more limited than the Curie-Weiss law in this respect. As derived, it applies solely to isolated systems of $S = 1/2, 2/2, \dots$ etc. However, in the real world there are usually interactions between molecules, especially as their concentration becomes relatively high. The Brillouin treatment has proven to be surprisingly useful even when intermolecular interactions occur.¹⁰ For instance, if one is interested in the type of coupling between magnetic molecules, a normalized magnetization plot at two different concentrations would be very illuminating. At low concentrations of magnetic species with individual spin state S , intermolecular couplings will be at a minimum and one would observe a spin state S from the corresponding best fit of the Brillouin function to the data. At higher concentrations, if the magnitude of the magnetic coupling is not significantly smaller than kT , then the intermolecular couplings (if any are present) will be manifested by a change in the J required to fit the Brillouin function to the normalized magnetization data. Since it is experimentally feasible to do the magnetization measurements as low as 2.0 K, this corresponds to an approximate lower limit of $kT = 2.76 \times 10^{-23}$ J or 1.39 cm^{-1} for the magnitude of magnetic coupling between neighboring magnetic centers that can be observed.

The usefulness of the Brillouin function for determining the nature of magnetic interactions *between* organic magnetic molecules was seen in a study by Itoh and coworkers on substituted diphenylcarbenes.¹⁰ Crystals of *p,p'*-dimethoxydiphenylmethylenes generated from the diazo precursor gave a normalized magnetization plot corresponding to a Brillouin function with $S =$

3.8/2. Since isolated diphenylcarbenes can give a maximum value of $S = 2/2$, the crystalline form had two triplet dimethoxy substituted diphenylcarbenes interacting ferromagnetically to give a $S = 3.8/2$ complex.¹⁰ EPR spectroscopy also showed the existence of a quintet, which temperature dependent EPR signal intensity studies indicated was the ground state. More extensive intermolecular ferromagnetic coupling was seen in a bis(O-octyl) substituted diphenylcarbene crystal,¹² which gave a normalized magnetization plot that fit a Brillouin function with $S = 8/2$. This demonstrated that high spin coupling was occurring between four magnetic centers, each individually containing spin $S = 2/2$, to form a complex with a nonet ground state.



Thus, by examining the change of J between the ideal isolated spin state and the actual experimental system, one may use the Brillouin function to interpret the nature of coupling between neighboring spins in materials such as crystals or amorphous polymers. While this does not shed any light of the quantitative energetics of the couplings, a qualitative picture may be obtained by measuring the normalized magnetization plots at different temperatures. Typically, the Brillouin plot is experimentally created by varying the applied magnetic field at a constant temperature to obtain magnetization measurements for a range of H/T between 0.0 and 2.5 Tesla/K

at 2.0K and 0-5 Tesla. If, for instance, S of the fitted Brillouin function decreases for a given sample as the temperature is raised, then the ferromagnetic coupling between spins is decreasing. If thermal energy is the primary factor causing the loss of ferromagnetic coupling due to population of an uncoupled, low spin state, one may approximate the amount of energy required to disrupt the coupling as kT . Realistically, the Brillouin plots may be determined only up to *ca.* 6K, since the range of H/T decreases to only between 0.0-0.8 Tesla/K (for a 5 Tesla system). It is possible to estimate the magnitudes of ferromagnetic (or antiferromagnetic) coupling with this method only in systems that have fairly weak coupling energies.

A second assumption of the Brillouin (and Curie law) treatment of magnetic materials, that is, the magnetic moments of the spin systems are isotropic with respect to their interactions with the applied magnetic field, is almost certainly a vast oversimplification of real molecules. Only in atomic systems such as Cr^{3+} is this probably true. In systems such as organic π radicals, there are almost certainly limits to the orientation of the magnetic moment due to the non-symmetric geometry of the p-orbitals and the molecule itself. This would result in anisotropic magnetic behavior. This can be observed in crystalline systems in which the measured magnetic susceptibility differs depending on the orientation of the crystal axis with respect to the applied magnetic field.³ Structures such as ordered polymer chains, whose magnetic interactions are primarily one or two-dimensional in nature, may also have a highly anisotropic interaction with the external field. Disordered amorphous substances, though, would have little macroscopic anisotropy since there would be no single orientation of the molecular axis for all of the molecules. However, the absolute value of the saturation magnetization in these systems may be lower than the theoretical maximum.

While the anisotropic nature of organic molecules may cast doubt on the use of the preceding theories to characterize magnetic behavior in organic materials, in reality the theories hold up quite well. In the aforementioned diphenylcarbene work, the magnetization studies correlated well with EPR spectroscopy. In the tetracarbene **50**, the Brillouin function fit the normalized magnetization curve with $S = 8/2$, exactly what one would expect from EPR results. This has been observed in other molecules as well. Thus, it appears that the anisotropic nature of the geometry of organic molecules such as diphenylcarbenes does not significantly affect their magnetization behavior as it relates to the Brillouin function.

References

1. General references for this chapter: (a) Hurd, C.M. *Contemp. Phys.* **1982**, *23*, 469-493. (b) Gerlock, M. *Magnetism and Ligand-Field Analysis*; Cambridge University: New York, 1983. (c) Carlin, R.L. *Magnetochemistry*; Springer-Verlag: New York, 1986. (d) McCaig, M.; Clegg, A.G. *Permanent Magnets in Theory and Practice*, 2nd ed.; Wiley: New York, 1987. (e) Van Vleck, J.H. *The Theory of Electric and Magnetic Susceptibilities*; Clarendon: Oxford, 1932. (f) Mattis, D.C. *The Theory of Magnetism I: Statics and Dynamics*; Solid-State Sciences 17; Springer-Verlag: New York, 1988. (g) Mabbs, F.E.; Machin, D.J. *Magnetism and Transition Metal Complexes*; Chapman and Hall: London, 1973. (h) Earnshaw, A. *Introduction to Magnetochemistry*; Academic: New York, 1968. (i) Carlin, R.L.; van Duyneveldt, A.J. *Magnetic Properties of Transition Metal Compounds*; Springer-Verlag: New York, 1977.
2. Hurd, C.M. *Contemp. Phys.* **1982**, *23*, 469-493.
3. Carlin, R.L. *Magnetochemistry*; Springer-Verlag: New York, 1986.
4. Quickenden, T.I.; Marshall, R.C. *Journal of Chemical Education* **1972**, *49*, 114-116.
5. McCaig, M.; Clegg, A.G. *Permanent Magnets in Theory and Practice*, 2nd ed.; Wiley: New York, 1987.
6. Reimann, A.L. *Physics: Volume II: Electricity, Magnetism and Optics*; Barnes & Noble: New York, 1971.
7. See Proceedings of the Symposium on Ferromagnetic and High Spin Molecular Based Materials, 197th National American Chemical

- Society Meeting in Dallas, TX.; Miller, J.S.; Dougherty, D.A., Eds.; *Mol. Cryst. Liq. Cryst.* **1989**, 176.
8. (a) Curie, P. *Ann. de Chim. et Phys.* **1895**, 5, 289. (b) Langevin, P. *J. de Physique* **1905**, 4, 678.
 9. Miller, J.S.; Epstein, A.J.; Reiff, W.M. *Chem. Rev.* **1988**, 88, 201-220.
 10. (a) Sugawara, T.; Tukada, H.; Izuoka, A.; Murata, S.; Iwamura, H. *J. Am. Chem. Soc.* **1986**, 108, 4272-4278. (b) Iwamura, H. *Pure Appl. Chem.* **1987**, 59, 1595-1604.
 11. Henry, W.E. *Phys. Rev.* **1952**, 88, 559-562.
 12. Sugawara, T.; Murata, S.; Kimura, K.; Iwamura, H. *J. Am. Chem. Soc.* **1985**, 107, 5293-5294.
 13. Sugawara, T.; Bandow, S.; Kimura, K.; Iwamura, H. Itoh, K. *J. Am. Chem. Soc.* **1986**, 108, 368-371.

Chapter 4

Magnetic Properties

of

Doped Poly(*meta*-phenyleneoctatetraene) Derivatives

This chapter details the experimental studies of polaronic organic polymers. The synthesis and magnetic qualities of the polaronic poly(*meta*-phenyleneoctatetraene) (PMPOT) derivatives will be discussed, as well as several model polymers.

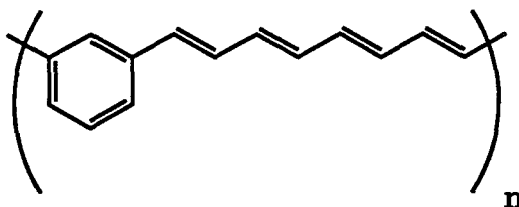
General Considerations

The present work approaches the synthesis of molecular magnetic materials from the viewpoint of the polaronic ferromagnetism model. The choice of *m*-xylylene as a high spin coupler is based on previous experimental evidence that indicates the ability of a *m*-xylylene structure to ferromagnetically couple different types of spin centers, such as carbon- or oxygen-based radicals,^{1,2} carbenes,³ and nickelocenes.⁴ *M*-xylylene also has been estimated to have a relatively large singlet-triplet gap (7.8 kcal/mol).¹ In addition, the *m*-xylylene unit can be easily incorporated in a polymer backbone.

The formation of polarons upon oxidation of conjugated hydrocarbon chains is well documented in the literature.^{6,7,8} The appearance of these spin 1/2 entities at room temperature indicates a remarkable thermal stability that is not present in most other carbon-based radical or carbene systems. The current interest in conducting polymers has given rise to numerous methods for the formation of polarons.^{5,8}

In light of these factors, along with considerations of synthetic feasibility and the materials-related advantages of organic polymers, we approach the design of magnetic materials from the concept of the

polaronic ferromagnetism model using the poly(*meta*-phenyleneoctatetraene) structure.



The neutral precursor polymers were exposed to either gas phase arsenic pentafluoride or gas or solution phase iodine to form the polaron-containing polymers (Scheme 4-1). This polaron-forming oxidation will be referred to as "doping", analogous to the doping in conducting polymer systems.^{5,8} Both film and powder materials were used as precursors.

At the outset of this work, there were several critical questions concerning the viability of PMPOT derivatives as potential ferromagnetically-coupled materials. They were:

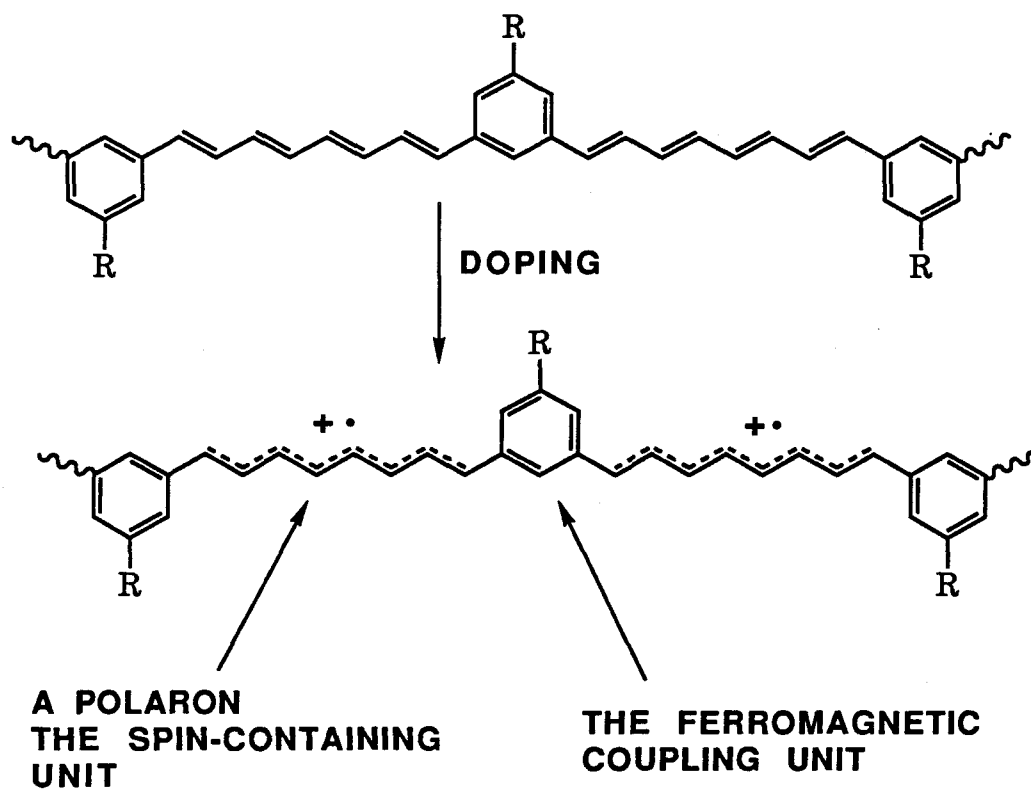
- 1) Can such structures be readily synthesized?
- 2) Can a high density of polarons be produced?
- 3) Is one-dimensional coupling ferromagnetic?
- 4) Can three-dimensional order be obtained?

These questions were addressed through the synthesis and characterization of several PMPOT derivatives in conjunction with the study of the magnetic properties of their doped counterparts.

The concentrations of polarons are small (less than 5 spins per 100 repeat units) in these systems, which required the use of very sensitive

Scheme 4-1.

Polaronic Polymer Design



means of detecting magnetization. While EPR spectroscopy has the requisite sensitivity to detect the formation of very small numbers of radicals, it is limited in terms of differentiation between different types of magnetic behavior (ferro- or antiferromagnetic couplings, for instance). In biradicals⁹ and higher spin systems¹⁰ that have been previously studied using EPR techniques, the magnetically active molecules are typically identical to each other and are of the same multiplicity. Since there is only one magnetic species present, the transitions between different magnetic energy levels will be well defined and give rise to a single EPR spectrum. This is especially true for single crystal EPR experiments, in which all of the molecules are aligned along a single axis or plane. However, if there are numerous different centers and magnetic couplings, then instead of a single set of transitions, a number of superimposed lines will appear.¹¹ If the magnetic centers differ significantly, then the absorption spectrum will become broader and be very difficult to assign. In the disordered polymeric materials in the present work, the magnetic centers are probably in a number of chemically non-equivalent sites due in part to the inhomogenous nature of the doping reaction.¹² In addition, there are different magnetic interactions between the spin centers (both ferro- and antiferromagnetic). These factors create a substantial obstacle to unambiguous characterization of spin states and coupling interactions using EPR spectroscopy.

EPR spectroscopy has been used to quantify the spin concentration in doped conducting polymers.^{5,13} Caution must be exercised in accepting these results as an accurate determination of the number of spins in a material due to the use of inappropriate spin standards. A radical standard such as diphenylpicrylhydrazyl (DPPH) must be employed to

determine the number of spins in an unknown material to find the spin concentration. The problem lies in the fact that the intensity of a single radical spin such as DPPH may differ from a single unknown radical due to differing relaxation times.¹¹ This will give erroneous results for the spin concentration of the unknown sample. In this work, EPR spin counts are used in conjunction with saturation magnetization measurements to estimate spin concentrations.

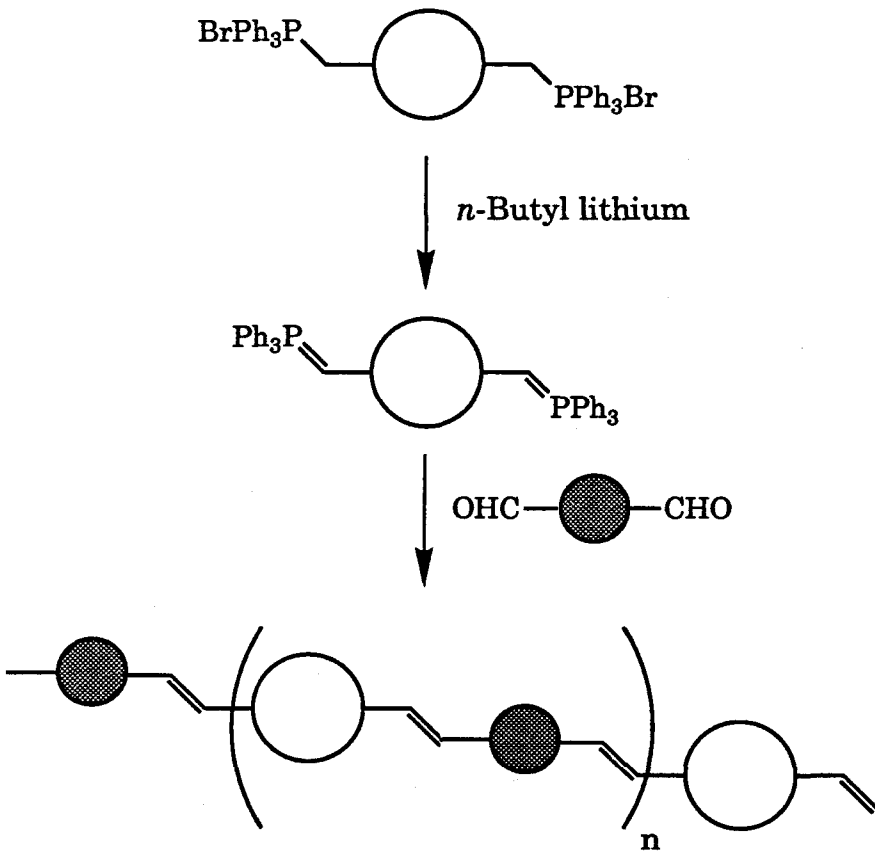
The magnetic characterization is performed primarily through the use of a superconducting quantum interference device (SQUID) magnetometer. This method is highly sensitive (to 10^{-12} emu/gram)¹⁴ and is quite amenable to polymer samples. While certain magnetic measurements are done at low temperatures (1.95 K), the magnetically active samples are initially prepared at room temperature.

Synthesis and Characterization

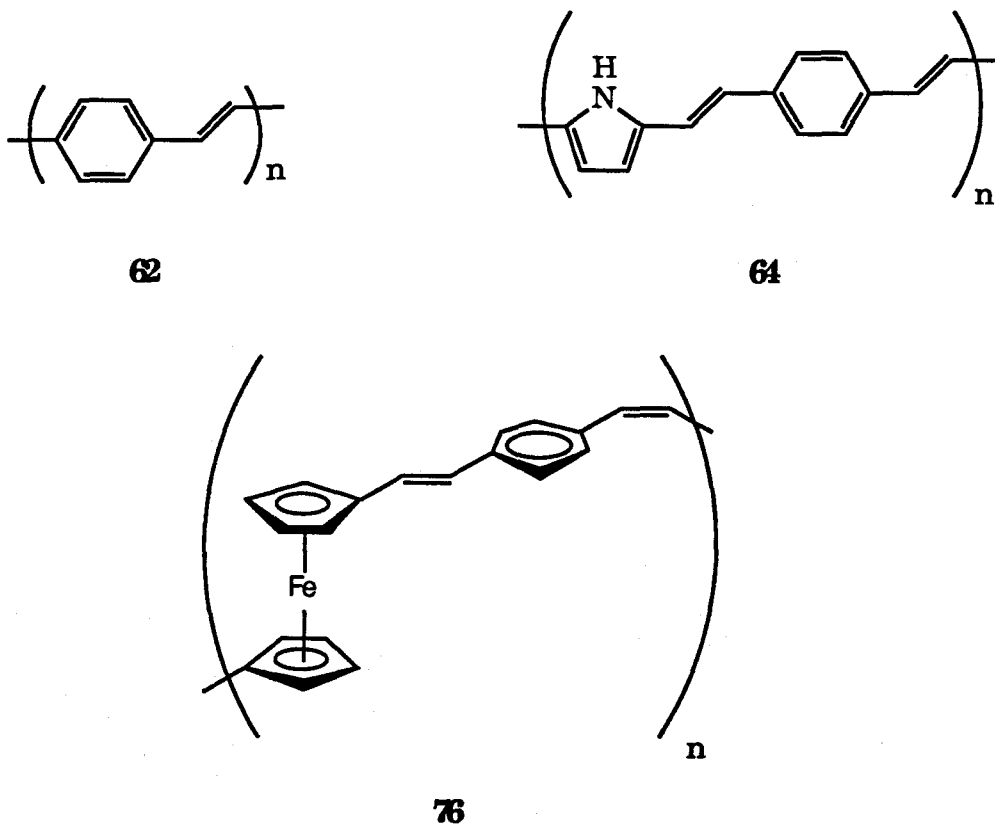
The polaron-containing polymers discussed in this work are formed from their neutral, fully conjugated precursors. Oxidative doping of the polyene segment of the precursor polymer results in the formation of a polaron.^{5,7} The precursor polymers are synthesized using the Wittig polymerization, which utilizes bis-phosphorus ylides and bis-aldehydes as starting materials (Scheme 4-2).

The Wittig polymerization has been used to synthesize a variety of conducting polymers.^{5,13,15} Since it is a double bond forming reaction with relatively mild conditions and easily separable products, this procedure has certain advantages which make it a useful polymerization route. Conjugated polymers which were synthesized via the Wittig reaction include poly-(*p a r a* -phenylenevinylene) (62),^{1 3}

Scheme 4-2.



poly(ferrocenylenevinylene) (76),¹⁶ and poly(N-methylpyrrole-2,5-diylvinylene-1,4-phenylenevinylene) (64).¹⁷ Upon treatment with an oxidant such as AsF₅ or I₂, these intrinsically insulating polymers show substantial increases in their conductivities.



The Wittig reaction as a polymerization method falls under the classification of a condensation or step-growth type polymerization.¹⁸ Certain characteristics of this type of polymerization have an impact on the properties of the final product. One important consideration is the degree of polymerization, DP. This is equivalent to the average number of monomer units in each polymer chain. In a step-growth polymerization,

$$DP = \frac{1}{(1-P)},$$

where P is the yield of the reaction involved.¹⁸ High yields are required to form polymer chains with a large number of repeat units. The yield for the Wittig reaction can typically be between 70-95%.¹⁹ This corresponds to a theoretical degree of polymerization between 3 and 20. Since the DP is dependent on the efficiency of the reaction, it is advantageous to use starting materials of the highest possible purity.

Another important consideration is the kinetics of polymerization as they relate to molecular weight. For a step-growth polymerization, the number average molecular weight (MW_N) of the product increases very slowly until the majority of the starting material has been reacted.¹⁸ The highest molecular weight polymer does not appear until the last part of the reaction in which the monomer has been almost completely consumed (Figure 4-1). Thus, for maximum chain lengths, it is important that the reaction goes to completion.

There are obstacles to the synthesis of polymer chains with a large number of repeat units that are inherent to the types of precursor polymers synthesized in this work. Polymers that contain only conjugated units or phenyl rings in the backbone structure are quite rigid when compared to saturated systems.⁸ The rigidity of these structures adversely affects their solubility properties and in certain cases the polymerization kinetics.⁸ This can be observed in the extreme case of poly(*para*-phenylene) (**65**). This rigid-rod polymer is intractable and insoluble in organic solvents.^{5,8} Due to the inherent insolubility of poly(*para*-phenylene), the product tends to precipitate before completion of the polymerization reaction. Consequently,

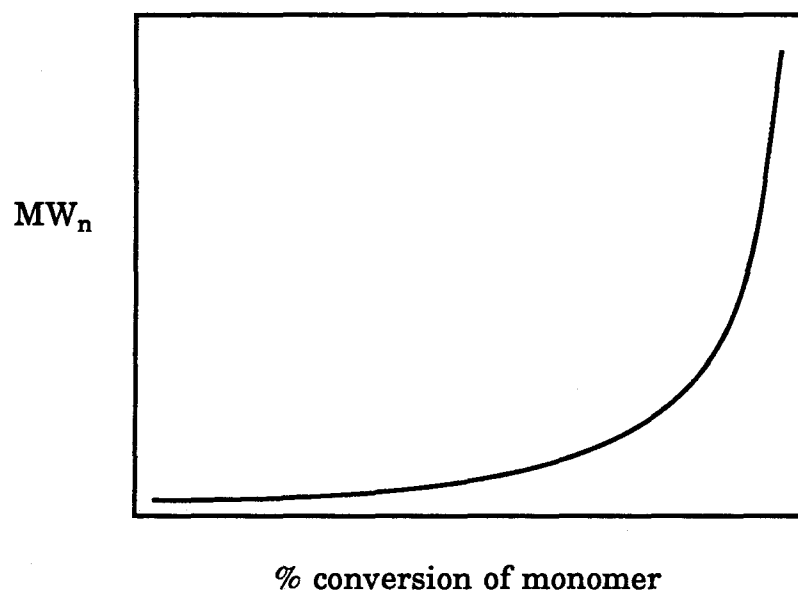
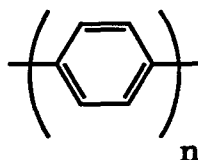


Figure 4-1. Polymer molecular weight (MW_n) as a function of monomer concentration in a step-growth polymerization.

the number of repeat units in each chain is small (less than 15) for many of the methods used to synthesize poly(*para*-phenylene).



65

Polymers of the type **62** and **76** are not as rigid as the phenylene network described above. They are, though, rigid enough to be intractable and insoluble almost to the same degree as poly(*para*-phenylene).^{5,13,15}

Chien and coworkers,¹³ using the Wittig polymerization in ethanol, synthesized **62** and studied its electrical properties. Elemental analysis data indicated that the material, an intractable and insoluble yellow powder, had a degree of polymerization of only 4-9 repeat units. We repeated this reaction and found that elemental analysis gave a degree of polymerization of 12. There is a large error associated with this result. This is due to relatively imprecise elemental analysis results which gave significantly different C, H, O contents between identical samples. Evidently, the product precipitates before the reaction is complete, producing oligimers instead of long chains.

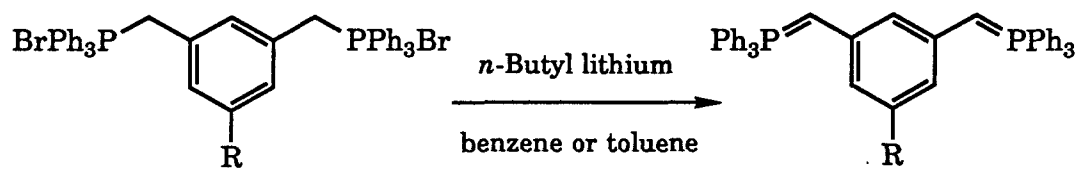
While in electrically active polymers, long chains with a significant number of repeat units may not be a necessary component in highly conductive materials, it is crucial for the successful determination of the validity of the polaronic ferromagnetism model that the polymer chains be long enough to support at least several polarons. Inherent in the design of the ferromagnetically coupled systems in this work is the mechanism of

intrachain high spin coupling of unpaired spins.²⁰ In the mechanism of electrical conduction in doped organic polymers, it is necessary that efficient interchain pathways exist for electrons to migrate between short oligimers, even though there may not be a preconceived "designed" mechanism (such as a structural linkage between oligimers) present.^{5,8} The intermolecular conduction pathway is often simply described as electron "hopping" between spatially close sites.^{5,8} For instance, AsF₅-doped PPPV is conductive even though the polymer chains are actually short oligimers.¹³

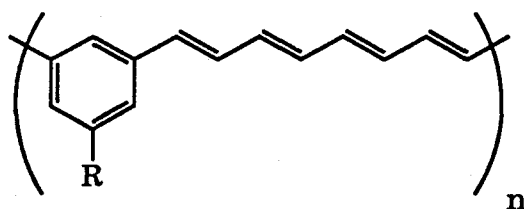
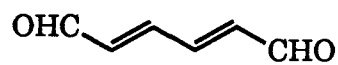
However, it is highly improbable that simple spatial interchain communication between oligimers containing single polarons could result in a ferromagnetically coupled system. In general, it is known that radicals in close spatial proximity to one another will usually interact antiferromagnetically in the absence of any specific structural connectivity.²¹ Ferromagnetic ordering must come from a non-random interaction of spins.²² Therefore, it is an important prerequisite for the application of the polaronic ferromagnetism model that the chains be long enough so that several polarons are able to reside along a single chain. It is highly desirable to obtain polymers with as large as possible DP.

PMPOT. Initially, poly(*meta*-phenyleneoctatetraene) (PMPOT, **63**), was synthesized from the known muconic aldehyde (**64**)²³ and *meta*-bis-phosphonium salt (**69**) using the Wittig polymerization in benzene (Scheme 4-3). The phosphonium salt was formed from a reaction of dibromoxylylene and triphenylphosphine in dimethylformamide. The C=C bonds of the polymers formed in the Wittig reaction are actually a mixture of *cis*- and *trans*-isomers, not purely *trans* as shown in Scheme 4-3.¹⁹

Scheme 4-3.

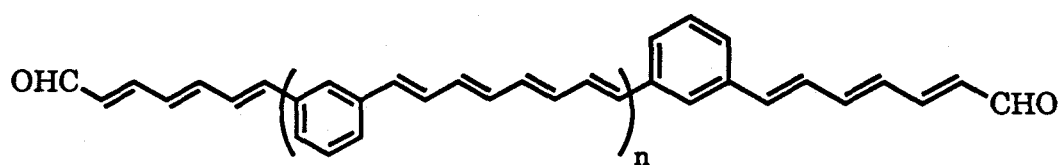


- 69** R=H
70 R=*t*-Butyl
71 R=OC₆H₁₃
72 R=OC₁₈H₃₇



- 63** R=H
65 R=*t*-Butyl
66 R=OC₆H₁₃
67 R=OC₁₈H₃₇

After purification using Soxhlet extraction techniques, a bright yellow, intractable, insoluble powder was isolated. Due to the physical nature of this polymer, conventional methods of molecular weight determination such as gel permeation chromatography (GPC) or osmometry were not possible. Instead, the molecular weight was estimated using endgroup analysis, which had been used by Chien²² to estimate the molecular weight of PPPV. Assuming that the terminal groups on the polymer chain are muconic aldehyde groups, then each polymer chain should have two oxygen atoms (see 63A). As the number of repeat units increases, the ratio of C (or H) to O will decrease accordingly. One can then match the ratio of C, H, and O content from the experimental elemental analysis to the polymer with the correct number of repeat units. This method is most accurate for small chains, where the C, H, O content difference between polymers with differing repeat units is significant. The differences of C, H, and O content becomes insignificant for polymers with high molecular weights.



63A

As can be seen in Table 4-1, the elemental analysis for PMPOT indicates that only low molecular weight oligimers were formed. The degree of polymerization is only 2. It would appear that PMPOT, like

Table 4-1. Elemental Analysis and DP of Conjugated Polymers.

| | Found | | | | | Calculated ^a | | | | |
|-----------------------|-------|-------|------|-------|------|---|----|-------|------|------|
| | C | H | O | Br | P | Structure | DP | C | H | O |
| PPPV ^{b,d} | 90.43 | 5.70 | 2.16 | 0.013 | 0.19 | C ₁₀₄ H ₇₈ O ₂ | 12 | 91.9 | 5.73 | 2.35 |
| PPPV ^{b,d} | 90.46 | 5.82 | 1.73 | 0.08 | 0.02 | | | | | |
| PPPV ^c | 90.6 | 5.74 | 3.4 | | | C ₇₂ H ₅₄ O ₂ | 8 | 90.95 | 5.70 | 3.04 |
| PMPOT | 85.68 | 6.11 | 7.98 | 0.074 | 0.22 | C ₄₈ H ₄₂ O ₂ | 2 | 86.8 | 6.38 | 6.8 |
| PPPOT | 92.79 | 5.82 | 1.91 | 0.05 | 0.25 | C ₁₁₈ H ₁₀₂ O ₂ | 7 | 91.37 | 6.57 | 2.06 |
| PMPOT- <i>t</i> Bu | 86.84 | 8.16 | 8.0 | 0.072 | 0.56 | C ₆₀ H ₆₆ O ₂ | 2 | 88.03 | 8.06 | 3.9 |
| PMPOT-6 | 81.93 | 8.04 | 6.61 | 1.02 | 0.04 | C ₁₆₆ H ₁₉₈ O ₁₀ | 8 | 84.77 | 8.41 | 6.8 |
| PMPOT-18 ^e | 84.24 | 10.72 | 4.22 | 0.18 | 0.27 | | | | | |

^a Assuming aldehyde endcaps. ^b This work. ^c Reported by Chien²². ^d Duplicate analysis of the same sample. ^e Poor fit to any calculated DP and structure.

PPPV, precipitated prior to formation of long polymer chains. This is supported by the fact that solid was observed immediately after the onset of addition of muconic aldehyde to the bis-ylide intermediate. Elemental analysis results are also shown for phosphorus and bromine. Their low values along with the high oxygen content provide evidence that the muconic aldehyde (as opposed to the phosphorus ylide) is the endcap.

The low degree of polymerization was a very discouraging result, since it prevented the examination of the true polymeric properties of these *meta*-linked materials. The problem of low solubility in conjugated polymers has plagued the field since its inception.^{5,8} For many materials, such as polyacetylene, the insoluble nature of the product of the polymerization does not preclude the formation of extensive polymer chains.⁵ In PMPOT though, it seemed highly probable that the tendency for the material to precipitate during the polymerization was a factor that at least contributed to the inability of the reaction to give intermediate or high molecular weight polymers. Examination of the literature showed that, in general, homogenous polymerization reactions such as the Wittig polymerization resulted in low molecular weight products.⁵ The assumption that the extended polyene segment of PMPOT as compared to PPPV would allow greater flexibility of the chain and higher degrees of polymerization proved to be invalid.

The insolubility of the materials synthesized by the Wittig method also has a negative effect on our ability to characterize the polymers. The endgroup method using elemental analysis data is the only molecular weight determination available to these intractable systems. This method has the significant drawback of only being accurate in low molecular weight systems, and is also suspect due to the inherent lack of precision in

the elemental analysis results. Similar samples sometimes had wide variations in C, H, and O content (see PPPV in Table 4-1). These variations, especially in the oxygen content, cast substantial doubt on the accuracy of this method.

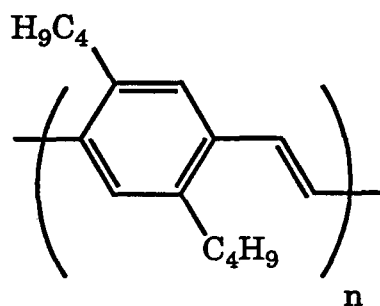
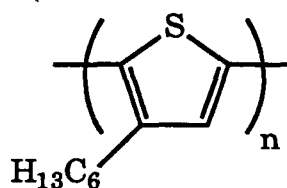
Therefore, two problems concerning the precursor polymers arose from the analysis of PMPOT and PPPV materials:

- 1) Low molecular weight products
- 2) Inability to adequately characterize materials.

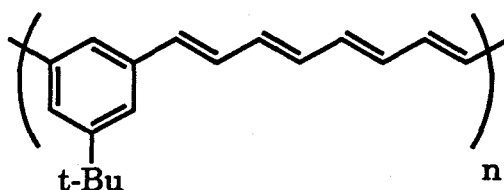
These barriers led us to consider tactics to increase the solubility of the polymer chains while keeping the fundamental conjugated structure of the backbone intact.

In the conducting polymer field, alkyl chains have been used successfully to increase the solubility of conjugated polymers.^{25,26} These groups are flexible and have many more degrees of freedom than the conjugated backbone. They increase solubility of the conjugated system by disrupting the crystal packing forces between polymer chains. There is also a substantial increase of entropy when going from the solid to a dissolved state for the flexible alkyl groups. In contrast, the stiff conjugated chains show small entropy change upon solvation since they are unable to increase their degrees of freedom upon solubilization.

This technique has been used in systems such as the PPPV derivative **73**²⁵ and polythiophene **74**.²⁶ Compound **73** can be cast into a thin film from a solution in 1,2,4-trichlorobenzene.²⁵

**73****74**

In an attempt to disrupt the crystal packing forces between phenyl rings which may have contributed to the intractability of the material, a *t*-butyl-substituted polymer (**65**) was synthesized according to Scheme 4-3. However, elemental analysis of polymer **65** showed a low degree of polymerization of only 2 (Table 4-1).

**65**

A series of O-alkyl-substituted PMPOT derivatives were synthesized in the hopes of obtaining, at the very least, longer chains and, at most, soluble materials. The method of polymerization was the Wittig reaction (Scheme 4-3).

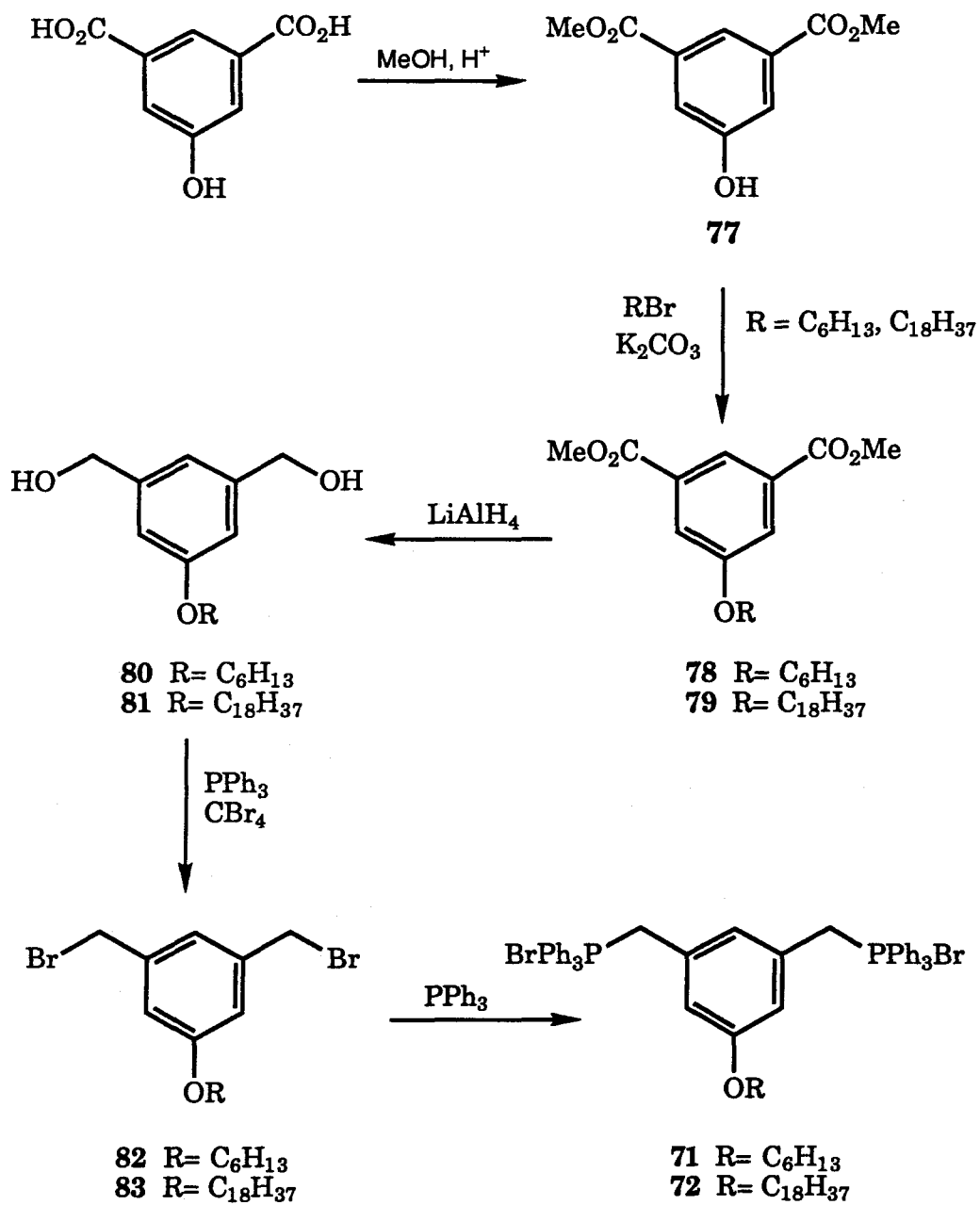
PMPOT-6. Initially, due to the success of O-hexyl units in solubilizing PPPV, the O-hexyl-substituted polymer PMPOT-6 (**66**) was synthesized. A general route to the synthesis of the substituted bis-phosphonium salt **71** is

seen in Scheme 4-4. Transesterification of 5-hydroxyisophthalic acid was followed by alkylation with 1-bromohexane. The methyl esters were then reduced to yield the bis-hydroxy compound with lithium aluminum hydride. The dibromo compound was prepared with carbon tetrabromide and triphenylphosphine.²⁹ The bis-phosphonium salt **71** was formed through treatment of the dibromide compound with triphenylphosphine in dimethylformamide.¹⁵ Repeated recrystallizations in methanol/diethyl ether were performed to ensure high purity.

The polymerization was done in refluxing benzene, with the bis-ylide **12** generated *in situ* by reaction of **71** with a *n*-butyl lithium, followed by addition of muconic aldehyde to give PMPOT-6 (Scheme 4-3).

The work-up of the reaction is outlined in Figure 4-2. The crude product was a mixture of solid and liquid phases. The two phases were purified by removal of reaction byproducts such as triphenylphosphine oxide and lithium salts as well as unreacted starting material through extraction with methanol. This was accomplished by precipitation of the organic polymer using methanol (Fraction A) for the reaction liquid and by methanol Soxhlet extraction for the solid product phase. Further Soxhlet extraction of the solid phase removed a portion of organic material (Fraction B), with a large amount of insoluble solid remaining (Fraction C). If the lack of solubility of the polymer is directly related to the molecular weight of the chains, then the most soluble material, which is the fraction from the liquid product phase, should have the lowest molecular weight (Fraction A). One would expect that Fraction B, which is the benzene-soluble Soxhlet liquid, should be a higher molecular weight material since it required a long Soxhlet extraction period to obtain

Scheme 4-4.



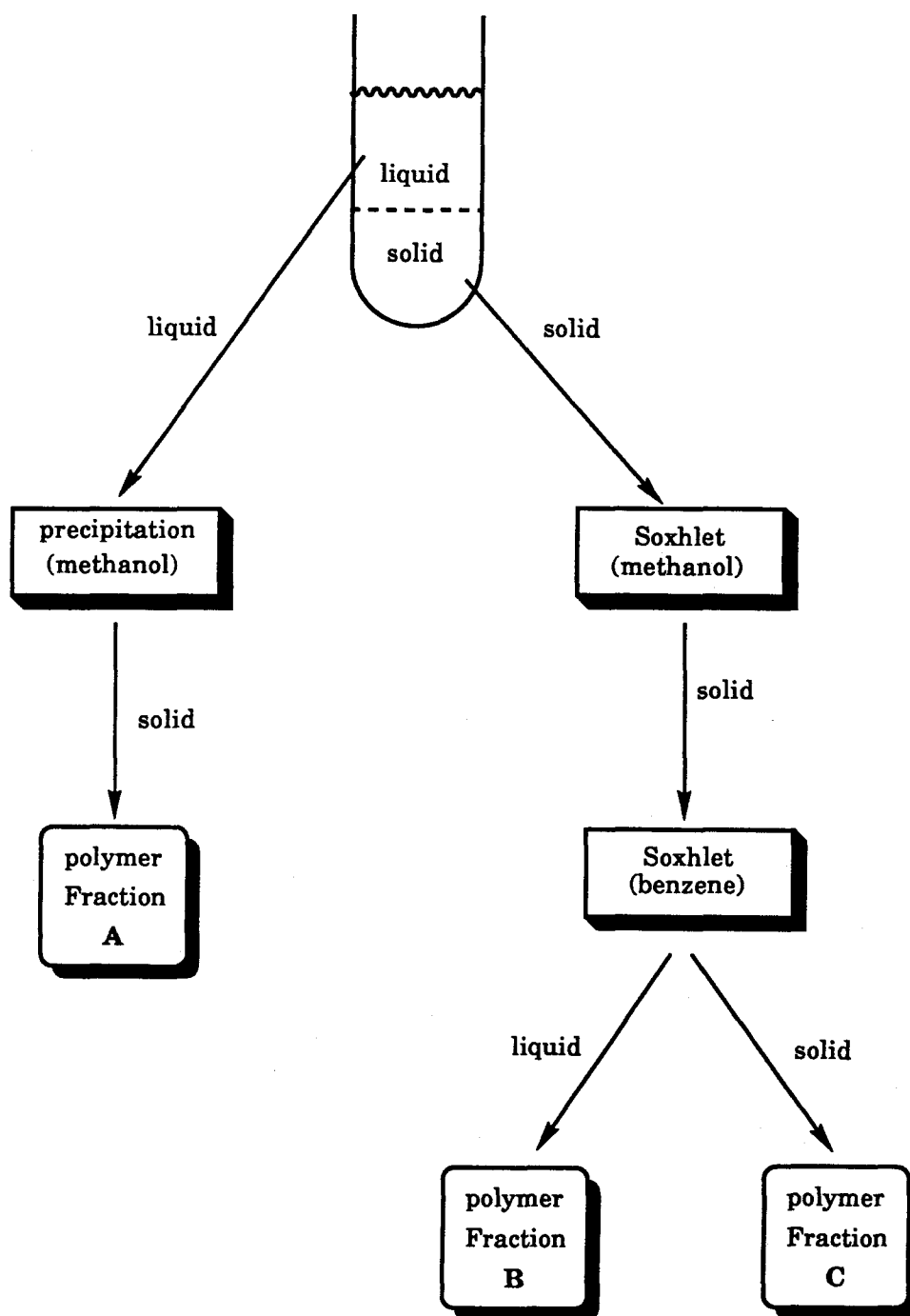


Figure 4-2. PMPOT-6 polymerization work-up.

polymeric material. The insoluble, intractable solid (Fraction C) should be of even higher molecular weight than the other two fractions.

The soluble nature of Fraction A and B allowed the determination of molecular weight by gel permeation chromatography (GPC)²⁷ as opposed to the more inaccurate method of endgroup analysis. Figure 4-3 shows the GPC traces for the two fractions (polystyrene standard). Note that the number average molecular weight (MW_N) for Fraction A (Fig. 4-3a) is 1589, with the largest peak corresponding to a molecular weight of 1407. Fraction B (Fig. 4-3b) has a MW_N equal to 1837 with a peak maximum at molecular weight of 1795. The difference in molecular weight of the maximum peaks in Fraction A and B is approximately 270. This number is very close to the molecular weight difference between chains that differ in degree of polymerization by one repeat unit (280).

Table 4-2 details the DP for the three fractions of PMPOT-6 and their respective molecular weights. The number average molecular weight for Fraction A and B correspond to numbers of repeat units of six and seven, respectively. The insoluble nature of Fraction C prevented molecular weight determination by GPC techniques. Instead, endgroup analysis assuming muconic aldehyde endcaps was used. Elemental analysis gave C, H, and O content corresponding to a material with, on the average, eight repeat units per chain. The molecular weight is higher than the other two more soluble fractions. It would appear that a trend of decreasing solubility with increasing chain length is followed in this system. All magnetic measurements were performed on material from Fraction C.

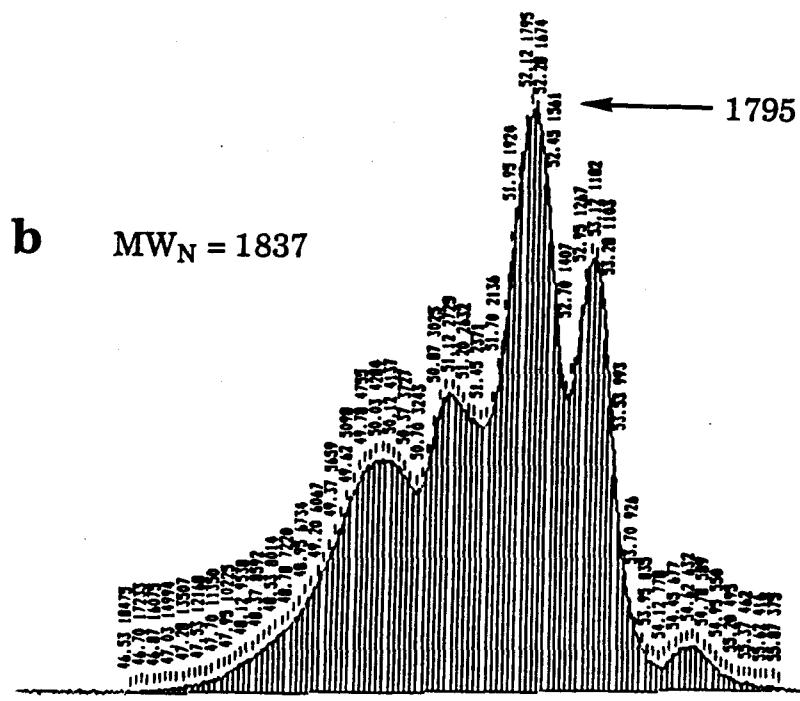
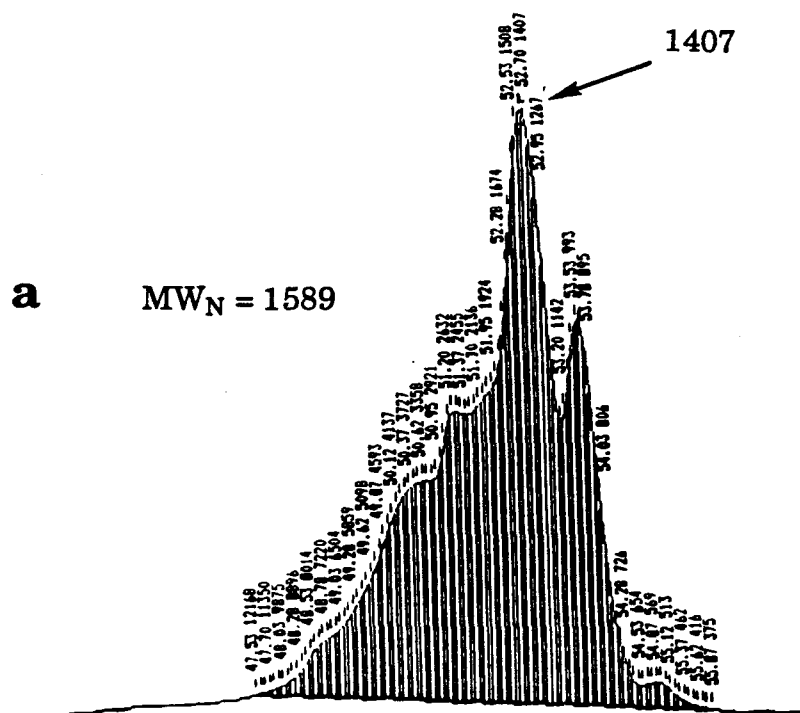


Figure 4-3. GPC analysis of soluble Fraction A (a) and Fraction B (b).

Table 4-2. MW_N and DP of PMPOT-6 Fractions

| | MW _N | DP |
|-------------------------|-----------------|----|
| Fraction A ^a | 1589 | 6 |
| Fraction B ^a | 1837 | 7 |
| Fraction C ^b | 2349 | 8 |

^a From GPC. ^b From elemental analysis data.

An IR spectrum of PMPOT-6 (KBr pellet) is shown in Figure 4-4. The absorbances at 2854 cm⁻¹ and 2925 cm⁻¹ are due to the CH stretches from the alkyl chain while the smaller peak at 3015 cm⁻¹ is due to the olefinic and aryl CH stretches. The large peak at 1582 cm⁻¹ and smaller peak at 1436 are due to the C=C stretches of the olefins and phenyl ring. The C=C-H out-of-plane bending absorption can be seen at 996 cm⁻¹, along with the CH out-of-plane bending absorptions for a 1,3,5-substituted phenyl ring superimposed on this peak and at 681 cm⁻¹. The CO stretch is not unambiguously assignable and may be attributed to either the pair of peaks at 1051.4 and 1287 cm⁻¹ or the single peak at 1163 cm⁻¹. The small size of the absorbance at 1707 cm⁻¹ indicates that there is a relatively small number of C=O groups present in the material. This is in contrast to PPPV, which has a substantial C=O absorbance at 1697 cm⁻¹.²⁴ A UV spectrum of PMPOT-6 (Fraction C) exhibited a broad absorption centered at

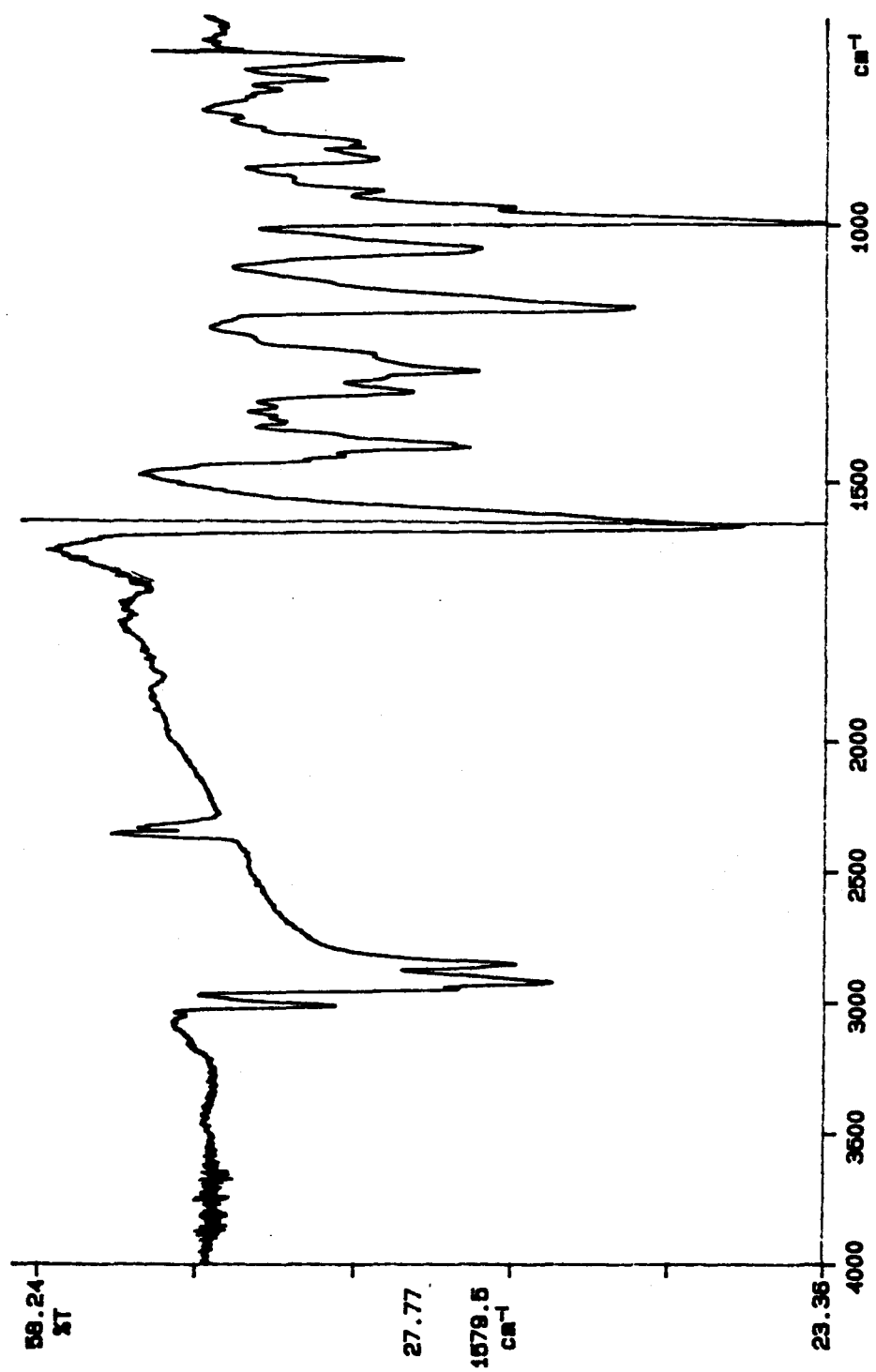
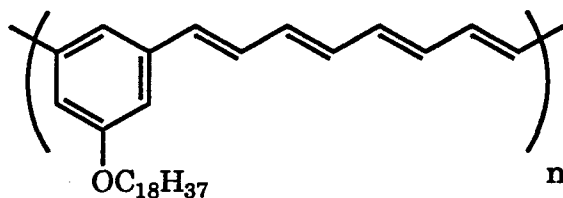


Figure 4-4. IR spectrum of PMPOT-6.

approximately 400 nm. The polymer was dispersed in a KBr pellet, which results in a poor signal-to-noise ratio due to poor pellet quality.

PMPOT-18. With the intent of further increasing the solubility and molecular weight of poly(*meta*-phenyleneoctatetraene), the O-octadecyl-substituted polymer PMPOT-18 (**67**) was synthesized according to Scheme 4-3. The substituted bis-phosphonium salt was formed using the reaction route outlined in Scheme 4-4. The alkylation was performed using octadecyl bromide.



67

Polymerization in toluene at 100°C gave an opaque, yellow, heterogenous mixture. Purification by methanol Soxhlet extraction to remove polar byproducts gave a yellow solid. This solid is completely soluble in organic solvents such as toluene or chloroform. Thin transparent yellow films (0.05 mm thick) can be cast onto a Teflon or glass plate from a concentrated chloroform solution. These films are freestanding and pliable. They are not elastomeric. The films can be easily cut into a variety of shapes with scissors.

The high solubility of PMPOT-18 allowed ready characterization by GPC. The number average molecular weight of PMPOT was found to be 9717. This corresponds to an average degree of polymerization of 22. The weight average molecular weight is 445521, which corresponds to a degree

of polymerization of 994. The range of molecular weights is large, with a polydispersity of 45. Thus, there is a significant amount of polymer with high molecular weight.

The GPC analysis shows that there has been a significant increase in polymer chain length upon addition of an O-octadecyl group to the PMPOT structure. The improvement from a 2-mer (for PMPOT) to a 22-mer (for PMPOT-18) allows the *polymeric* magnetic properties of doped PMPOT structure to be confidently examined. The relatively large number of repeat units allows multiple polarons to reside on a single polymer chain. For comparison, Table 4-3 lists molecular weights and degrees of polymerization of PMPOT-derived and other polymers.

Table 4-3. MW_N and DP of PMPOT Derivatives

| | MW_N | DP |
|---------------------------------|--------|----|
| PMPOT-18 ^a | 9717 | 22 |
| PMPOT-6 ^{a,b} | 1589 | 6 |
| PMPOT-6 ^{a,c} | 1837 | 7 |
| PMPOT ^d | | 2 |
| PMPOT- <i>t</i> Bu ^d | | 2 |

^a From GPC analysis. ^b Fraction A. ^c Fraction C.

^d From elemental analysis.

Elemental analysis was performed on PMPOT-18. Assuming the endgroups are from muconic aldehyde, the H data best fit to a material with a DP greater than 50. However, the C and O content fit a material with DP less than 10. Also, the O content has a range of 0.3% between duplicate analysis of the same sample. This translates to a large range of possible molecular weights based on O content. In view of these results, we do not believe that the endgroup method of molecular weight analysis provides an accurate means of molecular weight determination for this material due to inaccurate and imprecise elemental analysis results. This is especially true in structures (such as PMOT-6 or -18) that contain O in addition to the O found in the endcaps. This is due to the fact that differences in C, H, and O content between O-containing polymers with differing degrees of polymerizations are even smaller than in all-hydrocarbon systems such as PMPOT or PPPV. Unfortunately, we are limited to this crude method as our only means of estimating molecular weight in intractable materials.

An IR spectrum (Figure 4-5) of the PMPOT-18 film shows absorptions, as expected, at 2852, 2922, and 3018 cm^{-1} due to C-H stretches in the alkyl chain and vinylic and aryl backbone. It also exhibits peaks at 1586 and 1465 cm^{-1} from C=C stretches. The C=C-H out-of-plane bending is present at 998 cm^{-1} . The C=C-H out-of-plane bending absorptions due to a 1,3,5-substituted phenyl ring are observed at 680 and 973 cm^{-1} . An extremely small peak is observed at 1718 cm^{-1} . This is due to a C=O stretch and can be attributed to the muconic aldehyde endcaps. The lack of any significant absorption between 1600 and 1800 cm^{-1} due to C=O absorption indicates that air oxidation of the conjugated chain had not taken place. The small peaks present in this region are not well resolved and cannot be

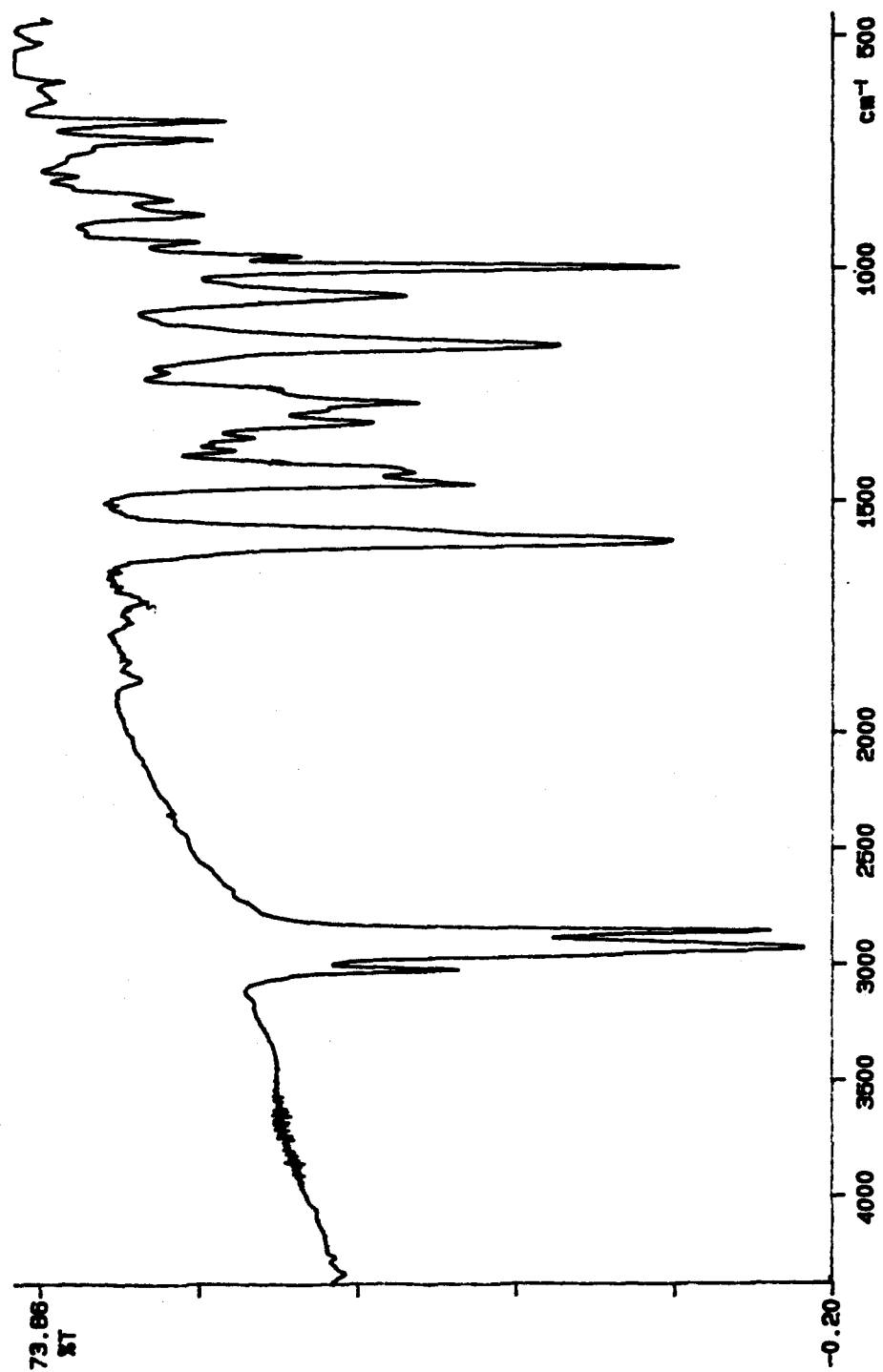


Figure 4-5. IR spectrum of PMPOT-18.

assigned to the overtone absorptions from a 1,3,5-substituted benzene group.

The similarity between the IR spectra of PMPOT-6 and PMPOT-18 should be noted. The only substantial difference between the two polymers is the increased intensity of the absorbances at 2800-3000 cm^{-1} in PMPOT-18. This is due to the increased number of aliphatic C-H modes in a C_{18} chain compared to a C_6 chain.

The ^1H NMR spectrum of PMPOT-18 is shown in Figure 4-6. The broad nature of the peaks is due to slow tumbling of polymer chains and is typically observed in solutions of organic polymers. The broadness of the peaks may also be due to the different *cis/trans* mixtures of C=C bonds formed in the polymer from the Wittig reaction. The triplet from the terminal CH_3 group is barely resolved at 0.85 ppm. The peak at 3.9 ppm is due to the O- CH_2 protons and the peaks between 0.8 and 1.8 ppm are due to the remainder of the octadecyl protons. The two broad peaks between 6.3 and 7.1 ppm are due to the phenyl and octatetraene protons. The peak integrals are in agreement with the proposed structure of PMPOT-18. Attention should be drawn to the complete lack of other signals in the spectrum. The absence of absorptions between 5.0 and 5.5 ppm showed that there is complete elimination of the phosphonium groups from the polymer. There also are no peaks between 9.0 and 15.0 ppm, indicating that there is not a large concentration of aldehyde protons. The proton NMR spectrum also indicates that the polymer is free from H-containing impurities such as triphenylphosphine oxide.

The UV spectrum of PMPOT-18 in CHCl_3 shows a broad peak at $\lambda_{\text{max}} = 400$ nm, with a superimposed, slightly smaller absorption at 422 nm and a shoulder on the λ_{max} peak at *ca.* 382 nm. In comparison,

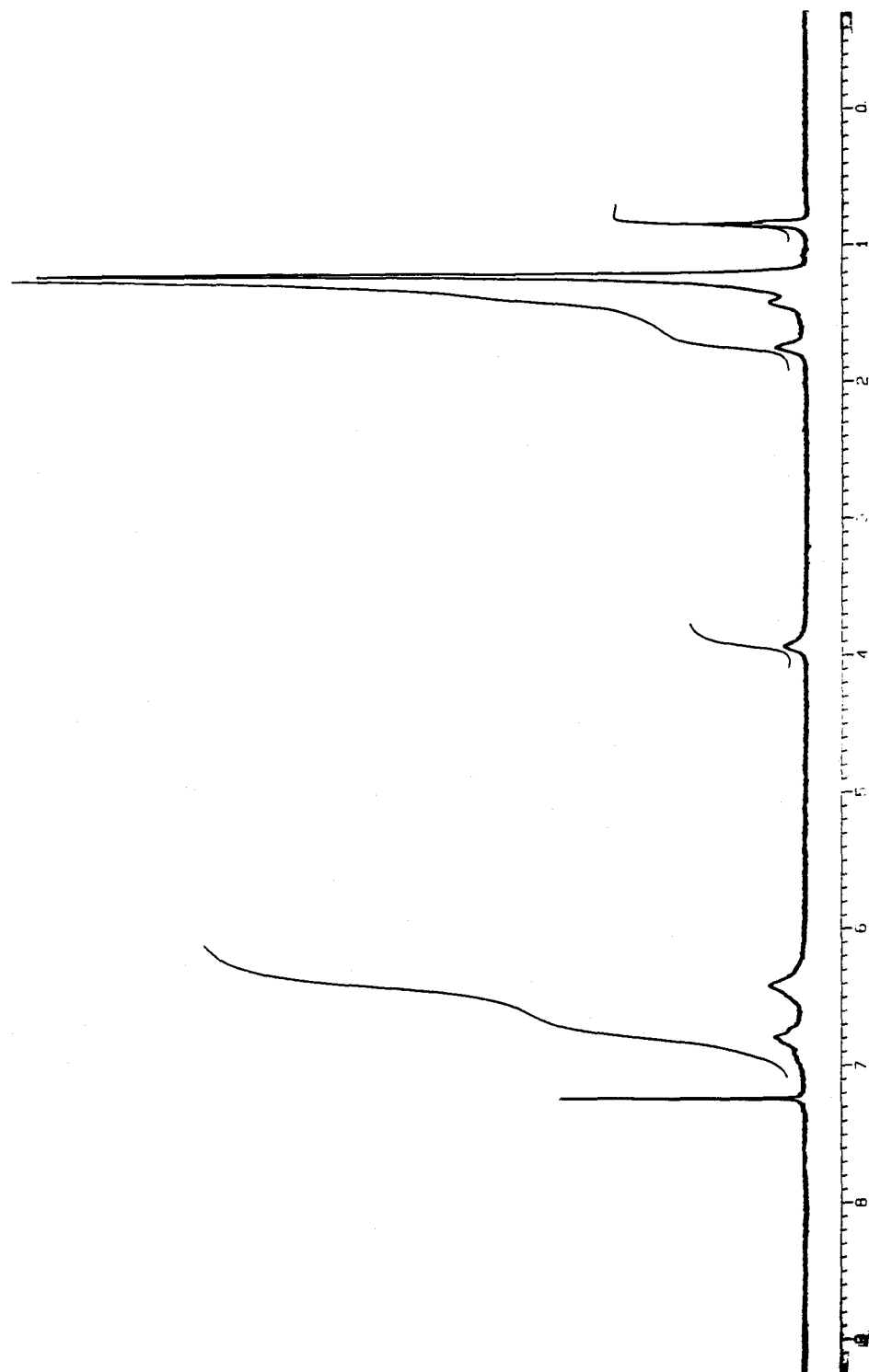
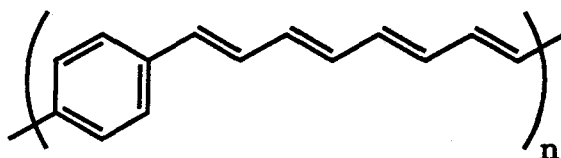


Figure 4-6. ^1H spectrum of PMPOT-18 (CDCl_3).

diphenyloctatetraene has a $\lambda_{\max} = 377$ nm, with superimposed absorptions at 360 and 403 nm.⁴³

Other Polymers. In addition to the polymers with substantial degrees of polymerization (PMPOT-6 and PMPOT-18), several other polymers which were used in magnetic doping studies were synthesized. These include PMPOT-*t*-Bu, PPPV, and PMPOT, which were discussed previously .

Poly(*para*-phenyleneoctatetraene) (PPPOT, **75**), an insoluble, intractable red solid, was also synthesized using the Wittig reaction. The molecular weights of this polymer were roughly estimated by endgroup analysis (Table 4-1).



75

Each of these materials has low degrees of polymerization and low molecular weights. These oligimers were used as comparison for the magnetic doping behavior of PMPOT-18 and PMPOT-6.

Spin Concentration

The spin concentrations for the doped PMPOT polymers were evaluated using *in situ* EPR experiments. The polymer was exposed to the gaseous oxidant (I₂ or AsF₅) in the cavity of an EPR spectrometer while spectra were recorded. Double integration of the first derivative EPR

spectrum gave the relative peak areas. The spin concentrations were then estimated using a DPPH standard (solid and solution).

PMPOT-6. When exposed to gas phase I_2 , the powder sample of PMPOT-6 shows an immediate increase in the intensity of the EPR signal. There was an extremely small signal before the dopant was introduced. This is due to radical defects formed by light or air oxidation.^{5,8} If the molecular weight of the repeat unit is known, then the concentration of spins per 100 repeat units can be found using equation 1.

Figure 4-7 shows the spin concentration for a sample of PMPOT-6 powder which was exposed to iodine in atmospheric pressure N_2 . There is a slow rise of polaron concentration up to 3500 - 4500 min, after which the polaron concentration decreases slightly. Note that the number of spins per monomer is very small - at most, there is less than 0.2 spins per 100 monomer units present.

A decay of polarons after exposure to concentrated I_2 vapor was observed, and is shown graphically in Figure 4-8. A sample of PMPOT-6 powder was exposed to I_2 in a static vacuum. The pressure of I_2 is much higher than in the atmospheric pressure N_2/I_2 experiment. Initially, the sample was exposed for seven min, after which I_2 access was closed. The maximum spin concentration (0.011 spin/monomer) was observed in the first measurement, which was immediately after the I_2 access was closed (7.5 min.). The spin concentration then rapidly decayed to *ca.* 0.002 spin/monomer. After the spin concentration reached a steady state, the I_2 access was re-opened and left open for the duration of the experiment. The spin concentration rose rapidly to reach another maximum at 0.006, subsequently decaying to 0.004 after 200 min of continuous exposure to I_2 .

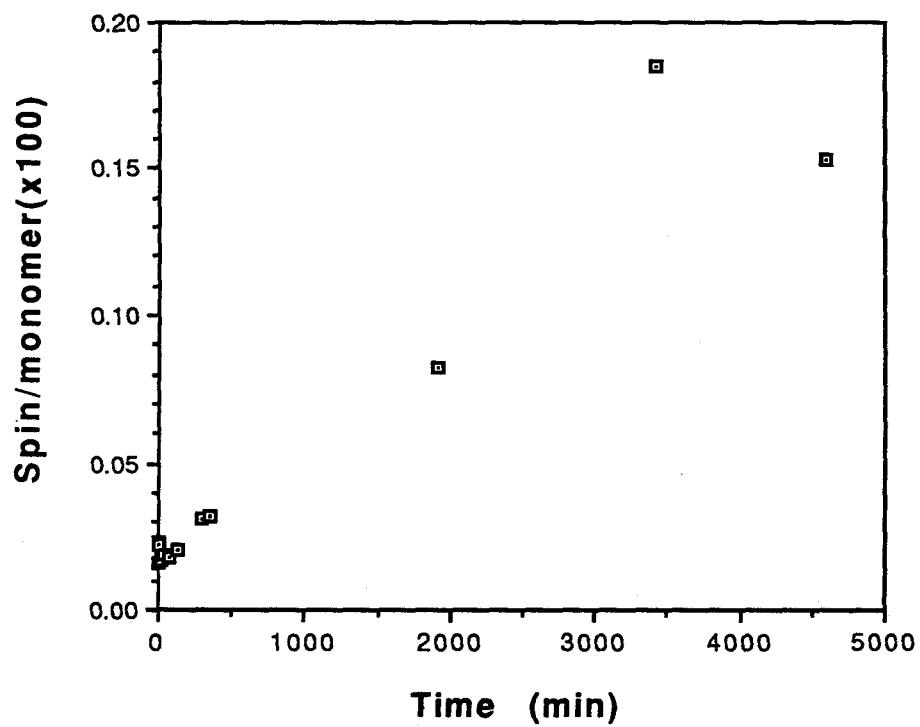


Figure 4-7. Spin concentration of I₂-doped PMPOT-6 as a function of dopant exposure time.

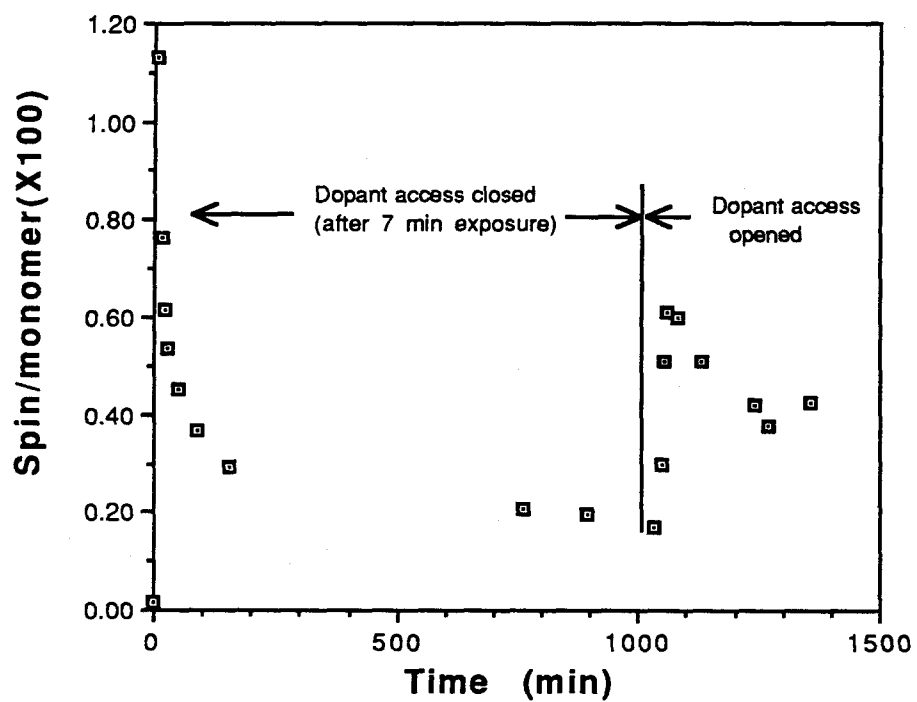


Figure 4-8. Spin concentration of vacuum I₂-doped PMPOT-6 as a function of dopant exposure time.

It appears that the maximum polaron concentration from exposure of PMPOT-6 to iodine is unstable. The polarons decay to reach a relatively steady value of 0.2 - 0.4 spins per 100 monomers after saturation with I_2 .

The preceding experiment details the ability of PMPOT-6 to support a small concentration of spins, although only after an initial decay from a higher concentration. In an attempt to increase the polaron concentrations above those reported for iodine, arsenic pentafluoride was used to oxidatively dope PMPOT-6. Figure 4-9 details the spin concentration of PMPOT-6 as a function of continuous exposure to 300 torr of AsF_5 . The first 100 minutes of doping was done at a reduced pressure of 0.4 torr followed by 600 min at 60 torr, with the remainder of the experiment at the full pressure. In contrast to the iodine doping, exposure to AsF_5 did not produce a decay of polaron concentration after exposure to dopant. The concentration rises to a maximum of 0.030-0.035 and remains fairly steady with no significant decrease as in the iodine experiment. The maximum spin concentration is significantly larger than in the iodine doped sample. Apparently the higher concentrations of spins present in AsF_5 doped PMPOT-6 are more stable relative to the low spin concentrations of I_2 doped PMPOT-6 with regards to recombination or further oxidation by the dopant. This is a surprising result, since intuitively one would expect radicals in close proximity and high concentrations to react more readily and decay faster than radicals at lower concentrations.

PMPOT-18. The *in situ* doping behavior of thin films of PMPOT-18 is qualitatively similar to PMPOT-6. Figure 4-10 details the time dependent behavior of vacuum I_2 doping of PMPOT-18 film. There is an initial rise of

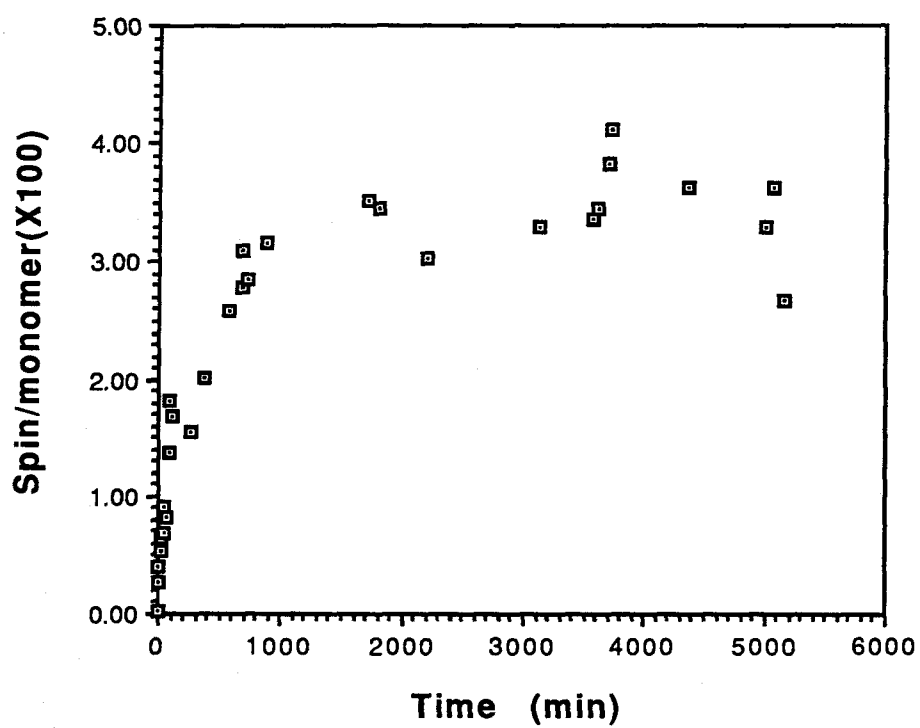


Figure 4-9. Spin concentration of AsF_5 -doped PMPOT-6 as a function of dopant exposure time.

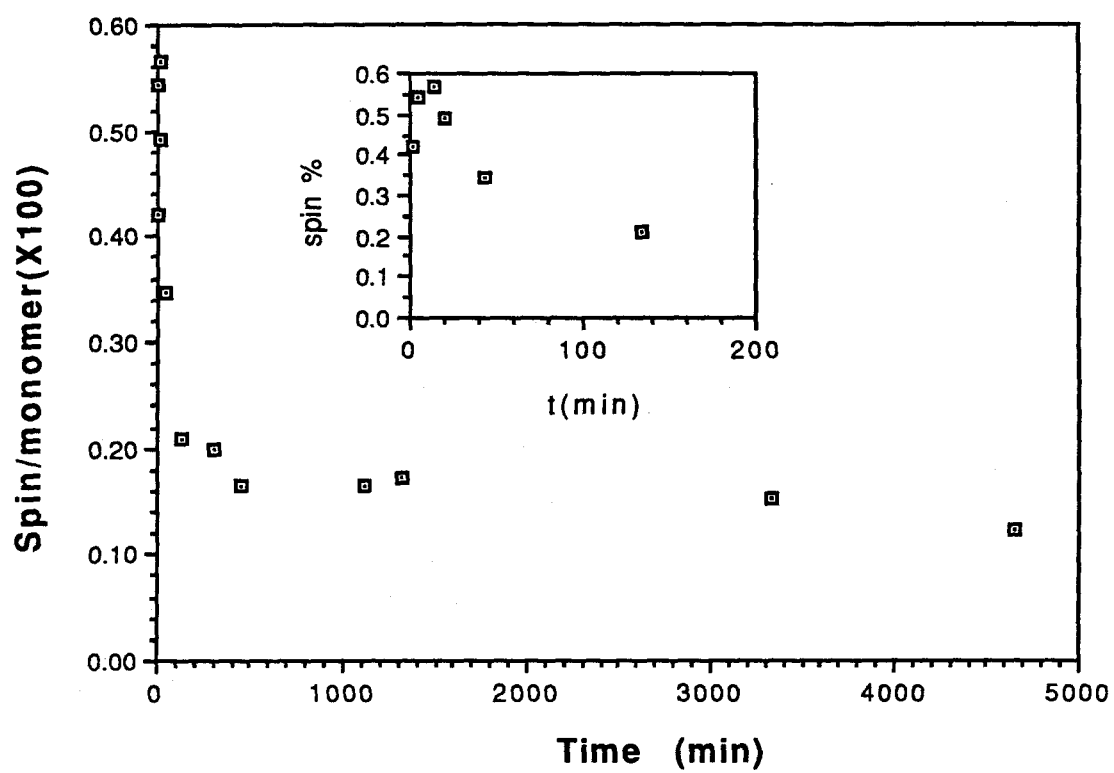


Figure 4-10. Spin concentration of vacuum I₂-doped PMPOT-18 as a function of dopant exposure time.

the spin concentration which reaches a maximum at 0.57 spins per 100 monomer units after 13 min exposure to AsF_5 . Similar to PMPOT-6, the polarons rapidly decay to reach a steady concentration of 0.2 spins per 100 monomers after 100 min of iodine exposure. The spin concentration does not decrease substantially beyond this value after 4500 min.

The AsF_5 doping behavior is significantly different, both qualitatively and quantitatively. Exposure of a thin film of PMPOT-18 to 0.3 torr of AsF_5 followed by 70 and 400 torr exposure results in a continuous increase of polaron concentration to a constant concentration (3.5 spins/100 monomers) after 2000 min exposure time (Figure 4-11). Unlike in the iodine experiment, there is no substantial decay of spin concentration in the sample 4000 min after initial exposure to AsF_5 . This behavior is intriguing since the concentration of polarons is much larger in the AsF_5 -doped PMPOT-18 than in the I_2 -exposed material (3.5 versus 0.5 spins per 100 monomers).

One possible explanation for the stability of the radicals at high spin concentrations is cross-linking of the polymer.⁸ AsF_5 is a strong oxidant that is known to cause significant degradation of the physical properties of conducting polymers. The brittleness and decrease in processability of AsF_5 -doped conducting polymers has been attributed to the formation of saturated bonds, or cross-links, between polymer chains.⁸ In the PMPOT derivatives, the extensive cross-linking may trap the spin centers and prevent recombination or oxidation of the polarons by AsF_5 .

In the I_2 -doped material, the oxidant is much weaker than AsF_5 .⁵ Hence the extent of cross-linking is probably less than the AsF_5 -treated material, and the fewer radicals present in I_2 -doped material are more accessible to further oxidation from the gaseous iodine and/or

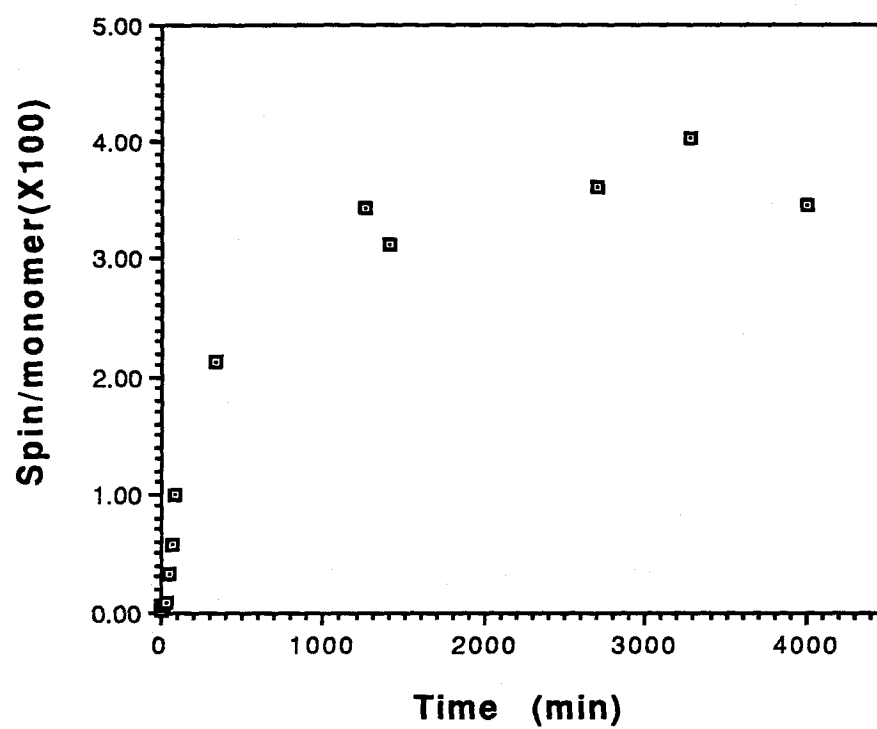


Figure 4-11. Spin concentration of vacuum AsF_5 -doped PMPOT-18 as a function of dopant exposure time.

recombination. This would explain the decay of spin concentration observed in the I₂-doped polymers.

Doped PMPOT Spin States

This section details the experimental results from the magnetization and magnetic susceptibility measurements of doped PMPOT derivatives and other model polymers. The primary focus is on the magnetic coupling of polarons in the PMPOT-6 powders and PMPOT-18 thin films.

PMPOT-6. As previously discussed, the magnetically active polaron containing form of PMPOT-6 is formed via oxidative doping of the precursor polymer with AsF₅ or I₂ (Scheme 4-1). These doped polymers are then placed in a sample holder (in this case, a small aluminum bucket) and the magnetic measurements at applied fields between 1 and 50 kGauss and temperatures between 1.95 and 300 K are taken using the SQUID magnetometer. It is of interest at this point to examine the data manipulation that is necessary to characterize these and other magnetic materials using the Curie and Brillouin analysis.²⁸

The magnetic susceptibility (and magnetization) which is measured χ_{exp} is actually a combination of paramagnetic and temperature independent terms that must be separated before Brillouin or Curie analysis. That is,

$$\chi_e = \chi_g + \chi_{\text{Pauli}} + \chi_{\text{dia}} ,$$

where χ_g is the mass paramagnetic susceptibility (in emu/gram). As previously noted,²⁸ since $\chi_g = C''/T$, a plot of T^{-1} versus χ_e at moderate to

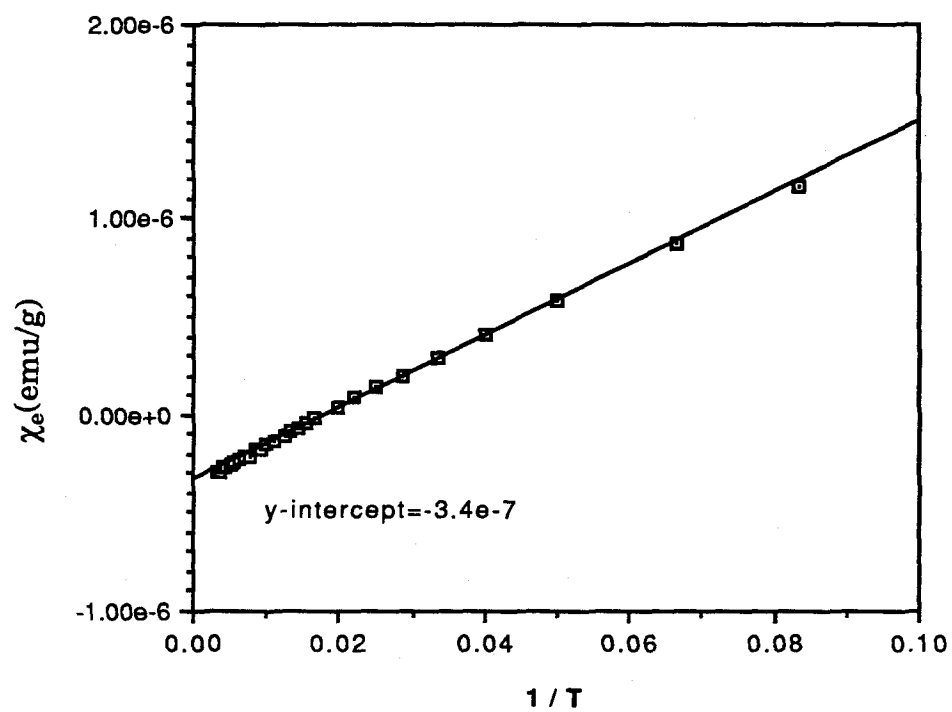


Figure 4-12. Plot of χ_e versus $1/T$ for AsF_5 -doped PMPOT-6.

high temperatures and in moderate magnetic fields will give a linear fit with a y-intercept equal to the temperature independent susceptibility terms. Figure 4-12 shows such a plot for a sample of gas phase AsF₅-doped PMPOT-6. The y-intercept shows a temperature independent component of the overall susceptibility of -3.4×10^{-7} emu/gram. The Pauli contribution to susceptibility is assumed to be negligible, so this number is equal to the diamagnetic susceptibility. The paramagnetic susceptibility χ_g can then be calculated.

The Curie behavior can be examined by plotting χ_g^{-1} at variable temperatures (Figure 4-13). Between 0 and *ca.* 150 K, the fit of χ_g^{-1} versus T is linear, with some curvature at temperatures above 150 K. The data is more scattered at the higher temperatures. This scattering is sometimes seen in these plots and is due to the small concentration of radicals in the sample. At higher temperatures, the paramagnetic susceptibility can decrease to the point where the baseline noise becomes equivalent to the sample signal.

The uncertainty of the concentration of the polarons prohibits evaluation of the spin state of the material using the Curie law since only the mass susceptibility χ_g (and not the molar susceptibility χ_m) is known. However, one can obtain a qualitative understanding of the magnetic couplings in the system using χ_g data. Recalling the Curie-Weiss law, the x-intercept of the linear χ_g^{-1} versus T fit will give the Weiss constant, θ'' , which is indicative of intermolecular magnetic interactions. Antiferromagnetic couplings give negative θ'' values, and ferromagnetic couplings give positive θ'' values. Examination of Figure 4-13 shows two regions with different Curie-Weiss behavior: a linear low temperature region between 0 and 120 K that has an x-intercept and θ'' of -1 K (see

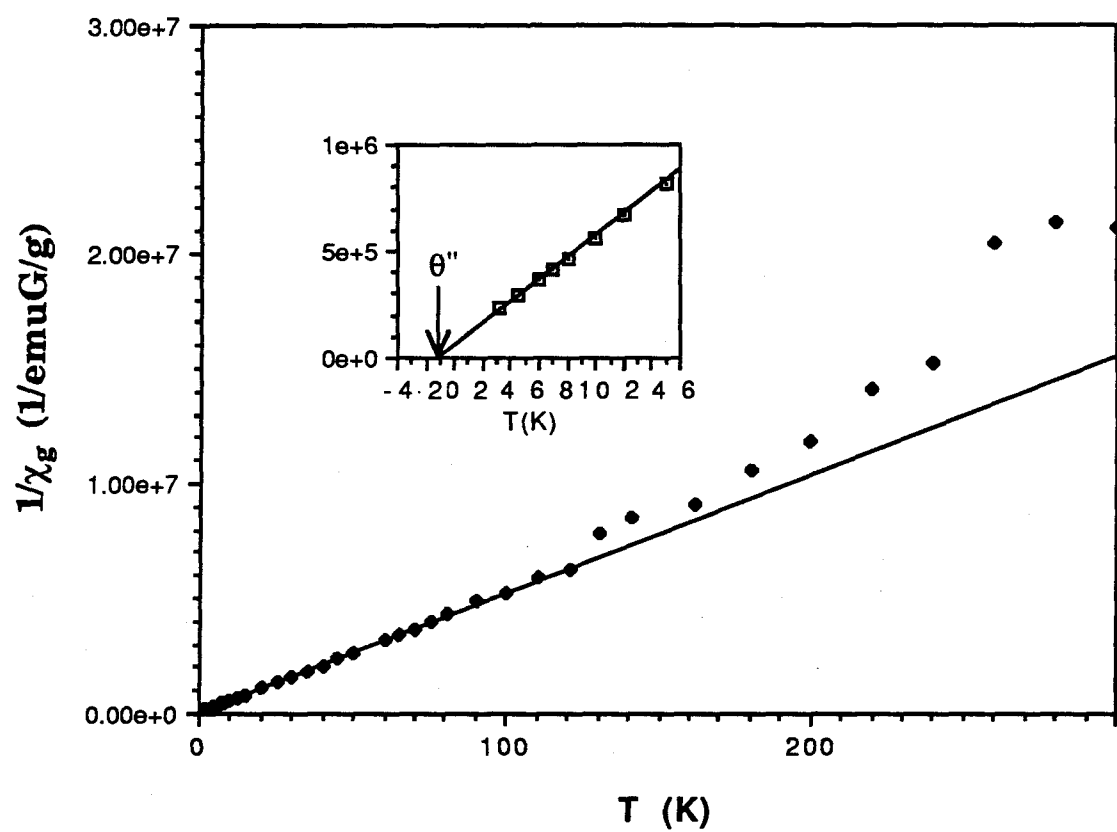


Figure 4-13. Plot of χ_g^{-1} versus T for AsF_5 -doped PMPOT-6.

inset) and a high temperature region above 150 K that has significant curvature. The line in Figure 4-13 represents the fit to the linear low temperature data. The low temperature region is characterized by a small antiferromagnetic coupling. The high curvature in the temperature region is due to non-Curie-like behavior in which the coupling between magnetic centers is not constant in this temperature range.

These magnetic transitions can be seen more graphically in a plot of relative effective magnetic moment (μ'_{eff}) versus temperature (Figure 4-14). Since the mass susceptibility must be used, the units for μ'_{eff} are arbitrary in nature and μ'_{eff} can be defined as $(\chi_g T)^{1/2}$. As the temperature is decreased, the magnetic moment increases slightly and reaches a plateau at approximately 100 K. The increase of moment is reflective of increased ferromagnetic coupling in this temperature range. Note that the region of this change of coupling corresponds to the temperature range in which non-Curie-Weiss behavior was observed in Figure 4-13. As the temperature is further lowered, the moment decreases abruptly below 15 K, indicating the onset of antiferromagnetic interactions. There are two qualitatively different magnetic transitions occurring in this material. One type is a weak antiferromagnetic coupling that is apparent only below 5-10 K. The other type is a stronger coupling which is ferromagnetic and is present to at least 100 K, if not higher, as will be discussed later.

The spin state of these materials is found by measuring the magnetization M of the material at variable magnetic fields and constant temperature. If the saturation magnetization M_{Sat} is known, then one can fit the magnetization data at various values of H/T to the Brillouin function to find the spin state S . Unlike the Curie and Curie-Weiss equations, the

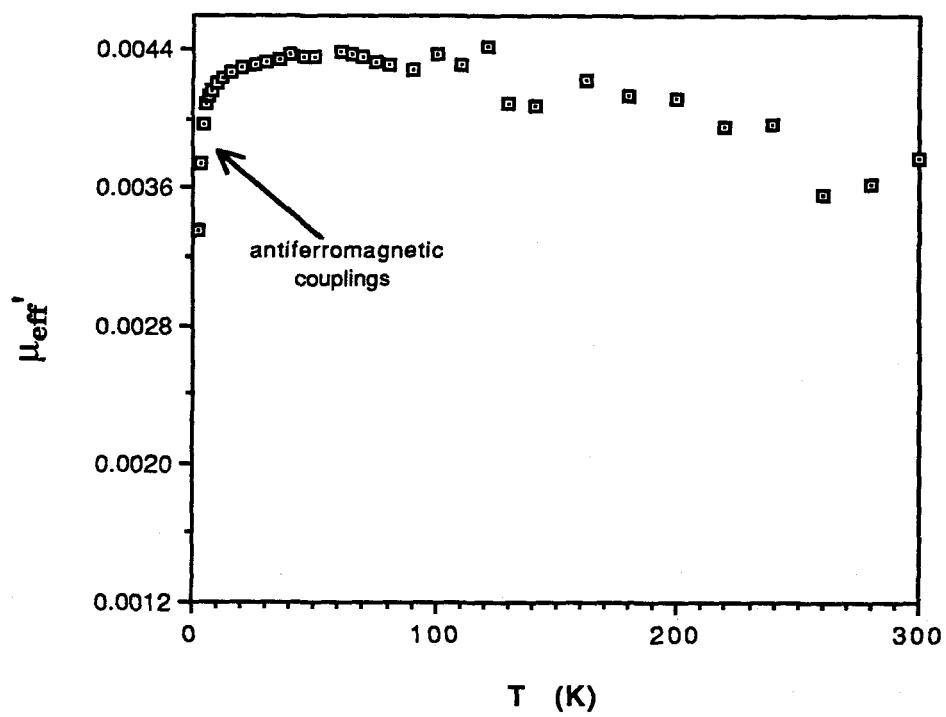


Figure 4-14. Relative effective magnetic moment of AsF₅-doped PMPOT-6 as a function of temperature.

molar quantities of the magnetic centers are not necessary as long as M and M_{Sat} are in the same units (in this case, emuGauss/gram). Ideally, one would like to perform the magnetization measurements at temperatures sufficiently low so that thermal population of excited states with differing multiplicities is not possible. Therefore, the initial magnetization measurements were done at 1.95 K. Figure 4-15 shows the magnetization of AsF₅-doped PMPOT-6 in external magnetic fields between 1 and 50 kGauss.

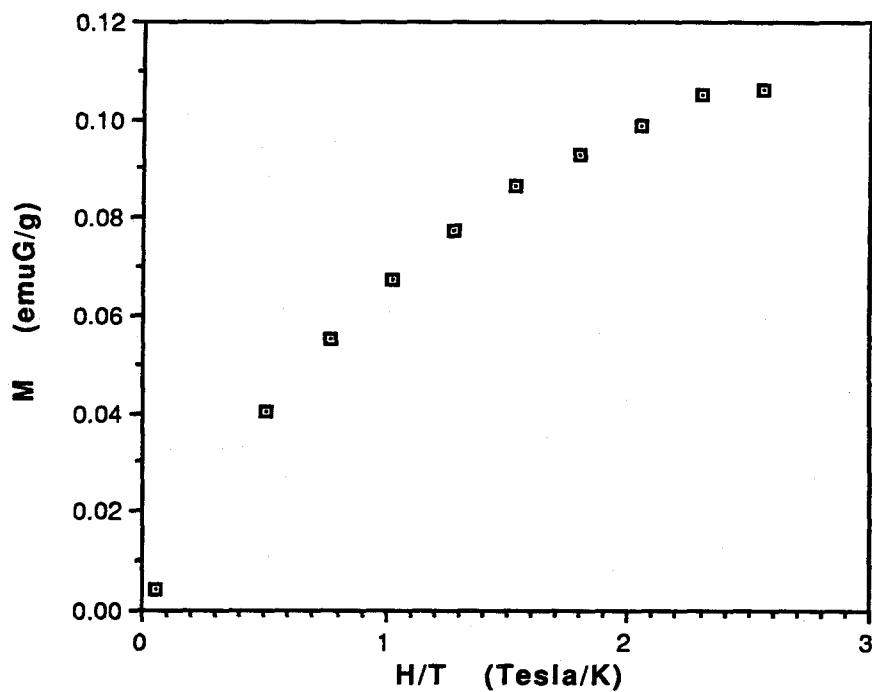


Figure 4-15. Magnetization behavior of AsF₅-doped PMPOT-18 at 1.95 K.

Similar to the magnetic susceptibility, the diamagnetic magnetization must be subtracted from the observed magnetization to find the magnetization due to the paramagnetic polarons. The diamagnetic magnetization M_{dia} is equal to $H\chi_{\text{dia}}$ (note that while χ_{dia} is constant with respect to field changes, M_{dia} is not). The diamagnetic-corrected magnetization curve rises rapidly, then nears a plateau as the polarons become nearly completely aligned parallel to the applied field.

An approximate M_{Sat} is estimated from Figure 4-15 and then the true M_{Sat} is found by varying M_{Sat} until the best fit of the normalized magnetization M/M_{Sat} to the Brillouin function with arbitrary S is found. Once this is done, the S for which the Brillouin function best fits the normalized magnetization is the normalized spin state of the material. Figure 16a shows the normalized magnetization of AsF_5 -doped PMPOT-6 as it compares to the Brillouin function for $S = 1/2, 2/2 \dots 8/2$. Figure 16b shows the exact fit of the Brillouin function to the experimental data, which corresponds in this case to a spin state of $S = 0.5$.

At first glance, the method of estimating M_{Sat} in systems which do not saturate in the experimental range of H/T may seem imprecise since both M_{Sat} and S must be varied in order to fit the magnetization data to the Brillouin function. However, it turns out that the fit of the normalized magnetization data to the Brillouin function is very sensitive to the correct M_{Sat} value. Small differences in the value estimated for M_{Sat} will result in normalized magnetization curves which will have poor fits to the Brillouin function no matter which value S is chosen. Therefore, only a close estimation of the correct M_{Sat} will give a normalized magnetization curve that will fit the Brillouin function regardless of the true value of S . This is especially the case for materials with S larger than 1.0.

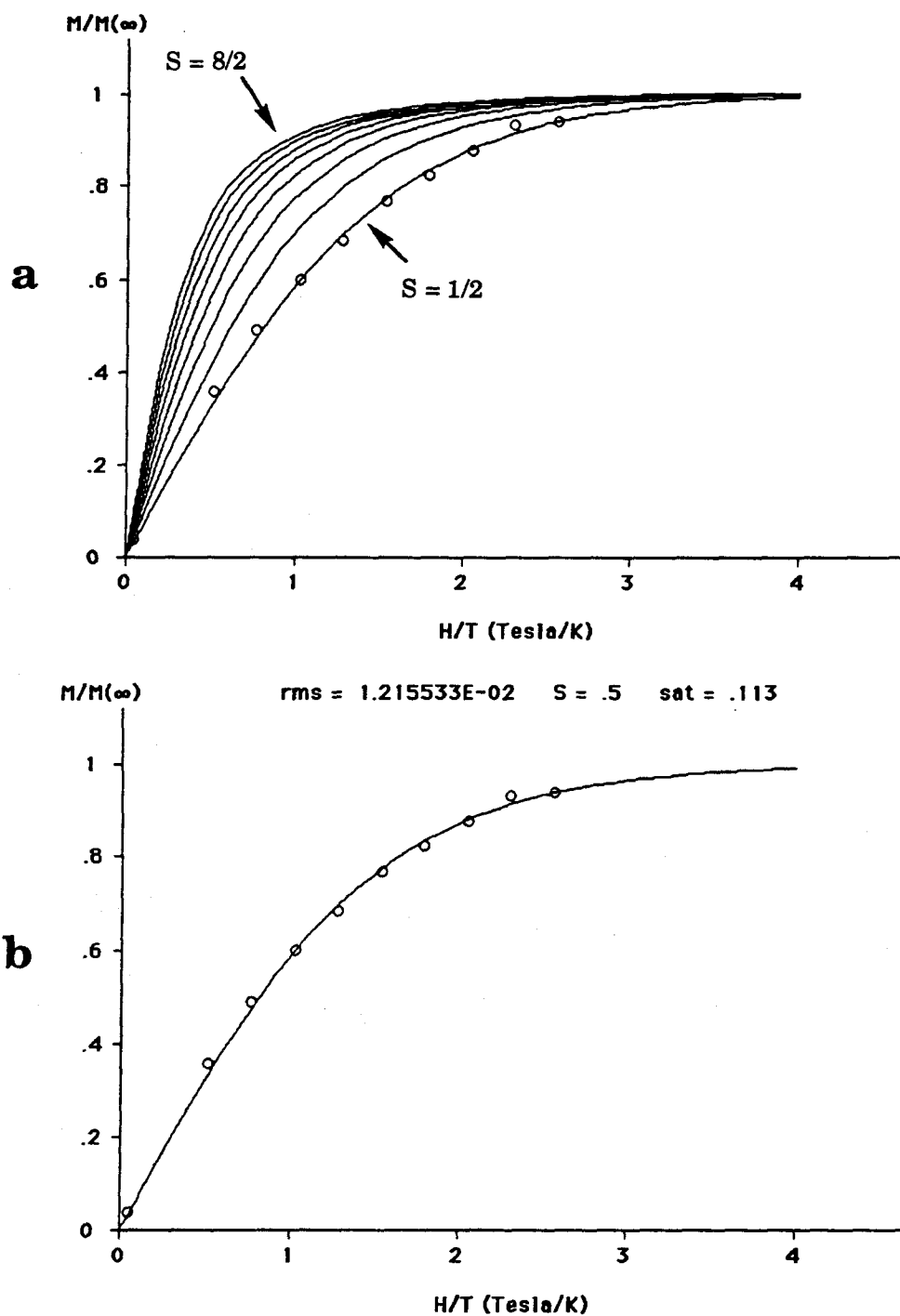


Figure 4-16. Normalized magnetization behavior (M/M_{Sat} , where $M_{\text{Sat}} = M_{\infty}$) of AsF_5 -doped PMPOT-6 as a function of H/T with (a) Brillouin functions for $S = \frac{1}{2}, \frac{2}{2}, \dots, \frac{8}{2}$, and (b) the best fit to a single Brillouin Function ($S = 0.5$). Magnetization measurements were done at 1.95 K.

The magnetic characteristics of PMPOT-6 which had been doped with I_2 were also examined. Figure 4-17 and 4-18 are the normalized magnetization plots for PMPOT-6 which had been oxidized with gas phase and solution phase (CCl_4) I_2 , respectively. Shown are the normalized plots with Brillouin functions of different spin states (a) and the Brillouin function with the spin state that gives the best fit (b). The normalized spin state for the gas phase I_2 -doped sample is $S = 1.3$, while the solution phase doped sample fitting to an $S = 1.2$ system.

The spin state of a material with non-interacting polarons (*i.e.*, purely paramagnetic) is $S = 0.5$. Any deviation from this standard polaronic spin state is the result of magnetic interactions between polarons. The spin state of 1.2 and 1.3 found for the I_2 -doped material is indicative of net ferromagnetic couplings between polarons such that between two ($S = 1.0$) and three ($S = 1.5$) polarons are high-spin coupled to form a high spin ground state of $S = 1.3$ for the material at this temperature. It should be emphasized that the $S = 1.3$ magnetic spin state may be due to a combination of ferromagnetic and antiferromagnetic interactions. The behavior of the effective magnetic moment for the AsF_5 -doped material implied that there were significant antiferromagnetic interactions occurring at the low temperatures at which the magnetization measurements were taken. The magnetic properties of oxidized PMPOT-6 are summarized in Table 4-4.

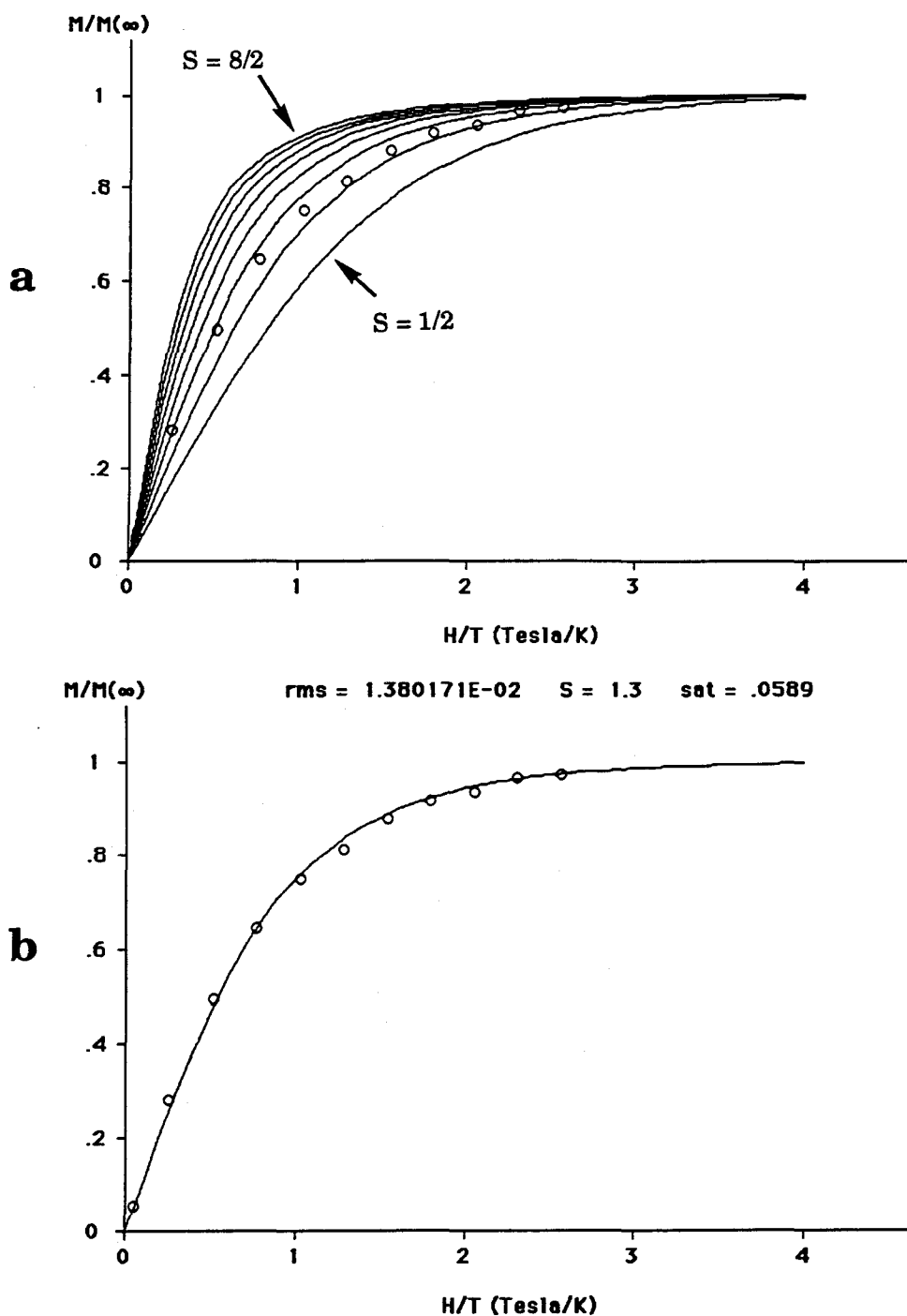


Figure 4-17. Normalized magnetization behavior (M/M_{Sat} , where $M_{\text{Sat}} = M_{\infty}$) of I_2 -doped PMPOT-6 as a function of H/T with (a) Brillouin functions for $S = \frac{1}{2}, \frac{2}{2}, \dots, \frac{8}{2}$, and (b) the best fit to a single Brillouin Function ($S = 1.3$). Magnetization measurements were done at 1.95 K.

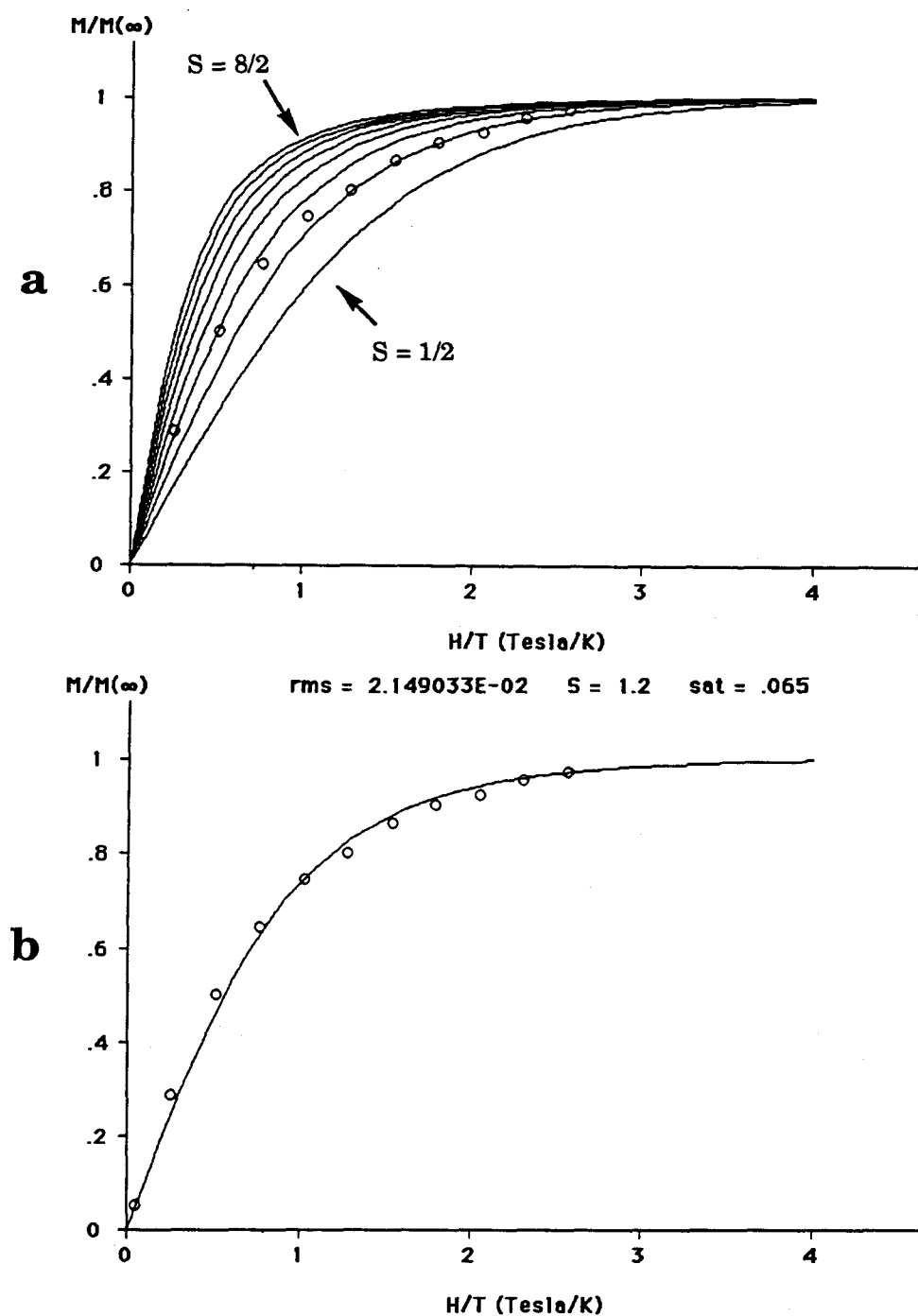


Figure 4-18. Normalized magnetization behavior (M/M_{Sat} , where $M_{\text{Sat}} = M_{\infty}$) of I_2 -doped PMPOT-6 (solution-phase) as a function of H/T with (a) Brillouin functions for $S = \frac{1}{2}, \frac{2}{2}, \dots, \frac{8}{2}$, and (b) the best fit to a single Brillouin Function ($S = 1.2$). Magnetization measurements were done at 1.95 K.

Table 4-4. Doped PMPOT-6 Spin States

| | S | $M_{\text{Sat}}^{\text{a}}$ |
|--------------------------------------|-----|-----------------------------|
| PMPOT-6(AsF_5) | 0.5 | 0.113 |
| PMPOT-6(I_2) ^b | 1.3 | 0.0589 |
| PMPOT-6(I_2) ^c | 1.2 | 0.065 |

^a EmuGauss/gram. ^b Gas phase. ^c Solution phase (in CCl_4).

PMPOT-18. The magnetic behavior of oxidized PMPOT-18 was studied using the technique previously outlined for PMPOT-6. The oxidants used to form the polaronic polymer were gas-phase and solution-phase I_2 and gas-phase AsF_5 . The precursor polymer was in the form of a thin film prior to doping.

The normalized magnetization behavior at 1.95 K of PMPOT-18 doped with iodine is shown in Figure 4-19 (gas-phase) and 4-20 (solution-phase). The magnetization behaviors of gas-phase and solution-phase I_2 -doped PMPOT-18 is quite similar, with spin states of $S = 1.4$ for the gas-phase material and $S = 1.3$ for the solution-phase (CCl_4) material. Unlike the insoluble PMPOT-6 material, PMPOT-18 films were soluble in the dopant solvent. The PMPOT-18 appeared to undergo precipitation as the oxidation proceeded. There is an overall ferromagnetic interaction

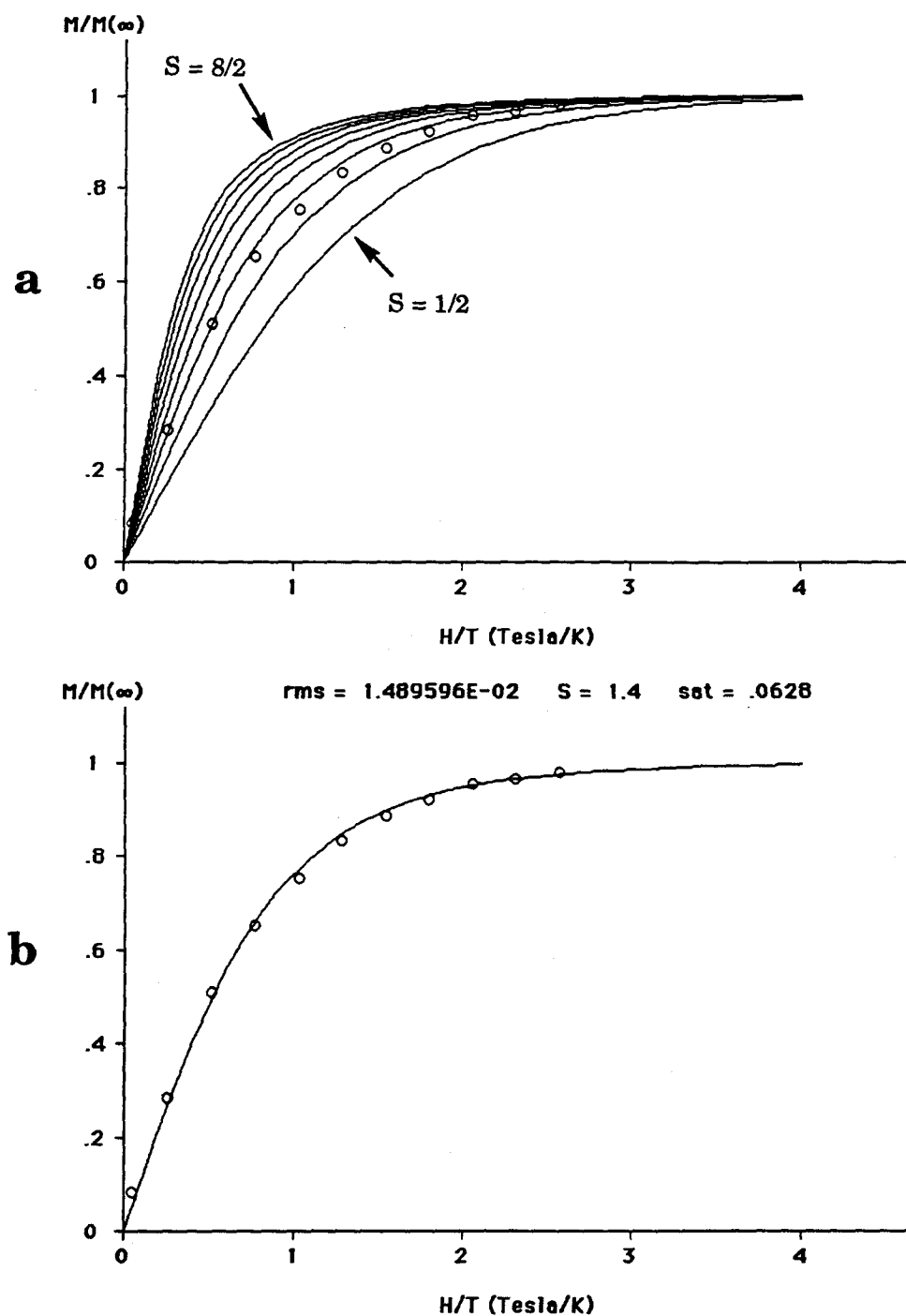


Figure 4-19. Normalized magnetization behavior (M/M_{Sat} , where $M_{\text{Sat}} = M_{\infty}$) of I_2 -doped PMPOT-18 (gas-phase) as a function of H/T with (a) Brillouin functions for $S = \frac{1}{2}, \frac{2}{2}, \dots, \frac{8}{2}$, and (b) the best fit to a single Brillouin Function ($S = 1.4$). Magnetization measurements were done at 1.95 K.

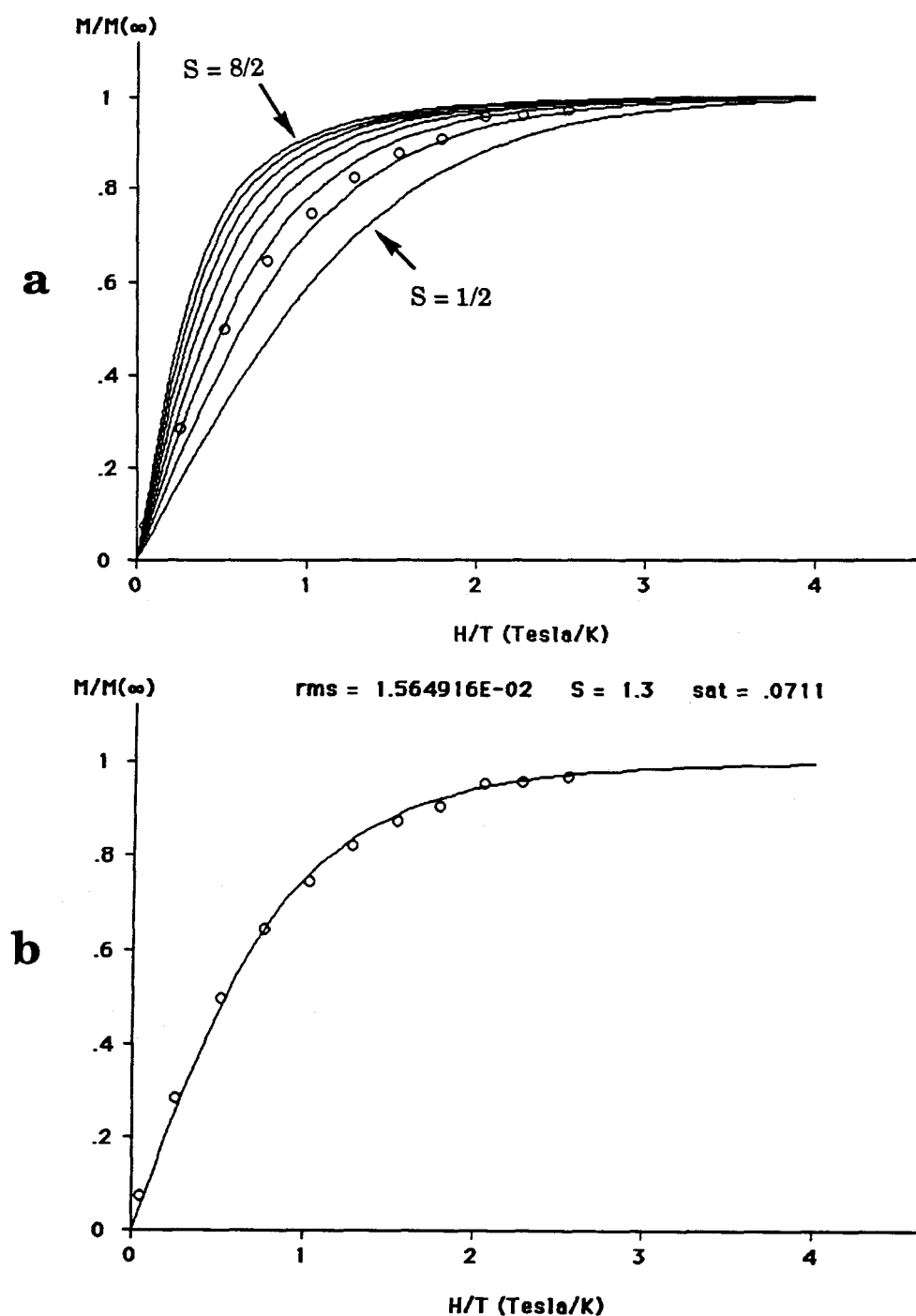


Figure 4-20. Normalized magnetization behavior (M/M_{Sat} , where $M_{\text{Sat}} = M_{\infty}$) of I_2 -doped PMPOT-18 (solution-phase) as a function of H/T with (a) Brillouin functions for $S = \frac{1}{2}, \frac{2}{2}, \dots, \frac{8}{2}$, and (b) the best fit to a single Brillouin Function ($S = 1.3$). Magnetization measurements were done at 1.95 K.

between the $S = 1/2$ polarons in the I_2 -doped material which averages to almost three polarons coupling ferromagnetically at 1.95 K.

The relative effective magnetic moment (μ_{eff}) was also examined at 25 kGauss at temperatures between 6.0 and 300 K (Figure 4-21). At temperatures below 50 K, there is a decrease in μ_{eff} due to antiferromagnetic interactions. As the temperature decreases from 300 K to 130 K, there is a slight increase in μ_{eff} due to an increase of ferromagnetic interactions. Thus, it appears that there are two different magnetic transitions in this material as the temperature is decreased from 300 K to 6 K.

The monomer to polaron ratio Ω of these doped materials can be estimated from the estimated saturation magnetization of the sample:

$$M_{\text{Sat}} = N_s S \mu_B$$

where N_s is the number of spins and μ_B is the Bohr magneton (9.274×10^{-21} emuGauss) and $g=2$ (the Lande' constant). The monomer to polaron ratio is simply

$$\Omega = \frac{N_{\text{monomer}}}{N_s} \quad (1)$$

where N_{monomer} is the number of repeat units in the sample. This is easily calculated from the mass of PMPOT-18 in the sample and the known molecular weight of the repeat unit (448.35 g/mole). For the magnetization plot in Figure 4-19, the sample size was 7.7 mg. of which 6.9 mg. was

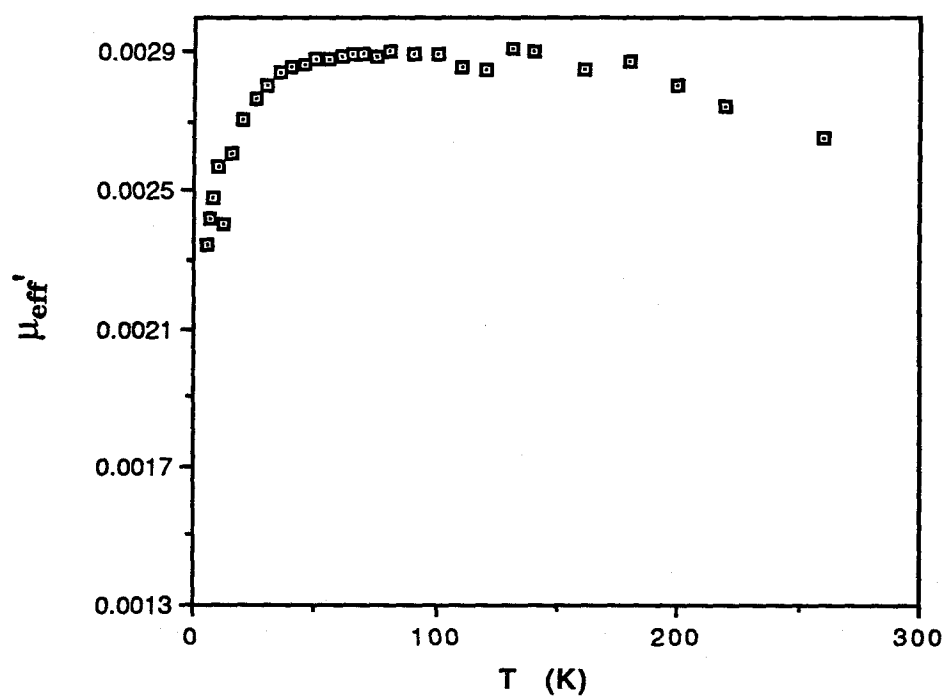


Figure 4-21. Relative effective magnetic moment (μ'_{eff}) of I_2 -doped PMPOT-18 as a function of temperature.

PMPOT-18 (the remainder of the mass of the sample is I^{3-}). The number of $S = 1/2$ spins corresponding to a M_{Sat} of 0.0628 emuGauss/gram are

$$N_s = \frac{M_{Sat}}{\mu_B}$$

$$= \frac{(0.0077 \text{ g})(0.0628 \text{ emuG/g})}{9.274 \times 10^{-21} \text{ emuG}}$$

$$N_s = 5.214 \times 10^{16} \text{ spins.}$$

If 6.9 mg. of the sample was actually PMPOT-18, then

$$\Omega = \frac{N_{monomer}}{N}$$

$$= \frac{9.2677 \times 10^{18} \text{ monomer}}{5.214 \times 10^{16} \text{ spin}}$$

$$= 178 \text{ monomers/spin.}$$

The spin concentration is simple defined as $1/\Omega$, or 0.0056 spins per monomer.

The spin concentration of I_2 -doped PMPOT-18 is quite small, with only about six polarons for every 1000 PMPOT-18 repeat units. The sample is magnetically quite dilute when compared to other molecular paramagnets that contain at least one spin per monomer or ferromagnets that can have several spins per atom in some cases.

The normalized magnetization behavior of a sample of PMPOT-18 that was heavily doped with AsF_5 at a pressure of 400 torr is shown in Figure 4-22. The ratio of arsenic to oxygen is 5.5:1 (this is the ratio of

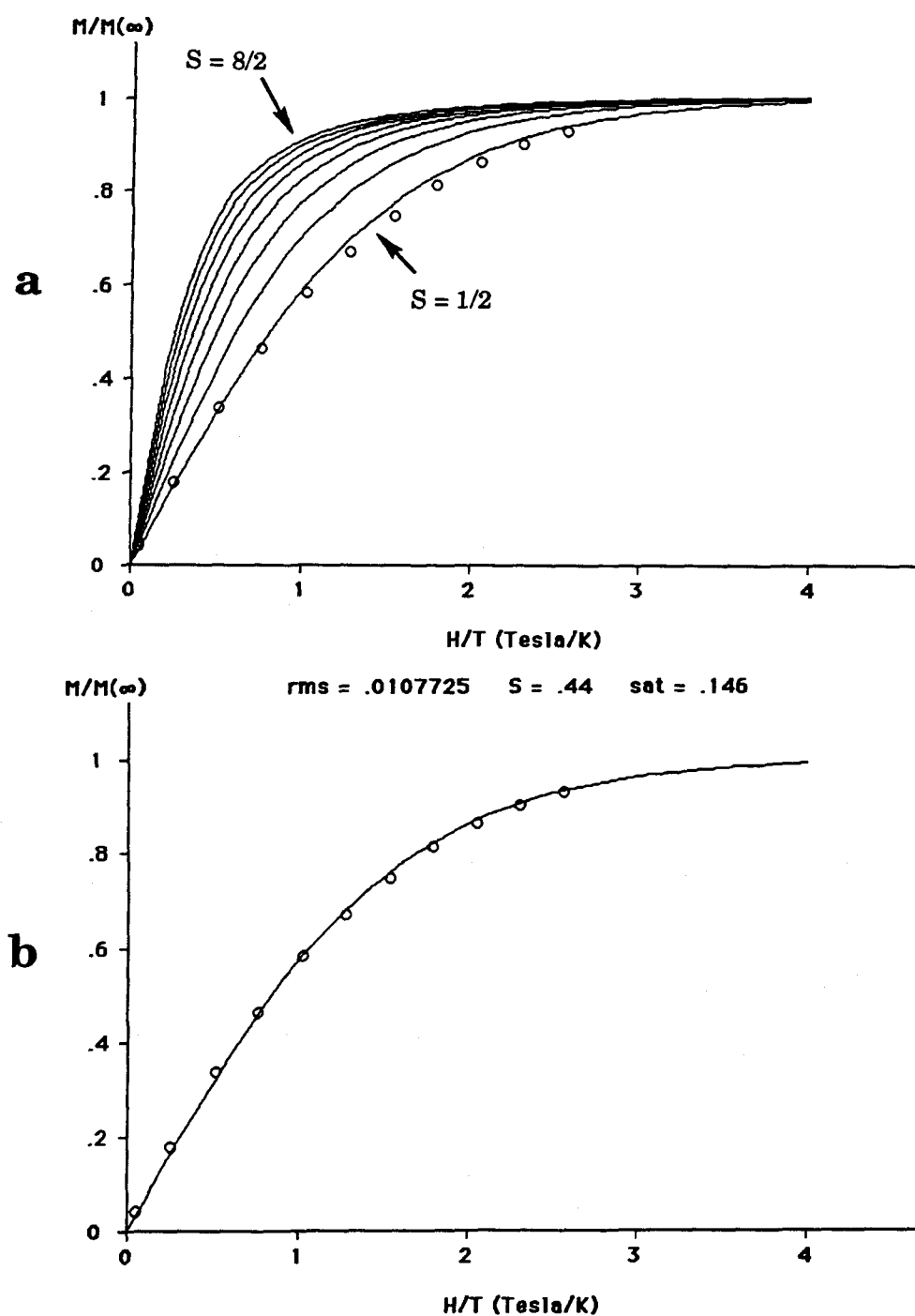


Figure 4-22. Normalized magnetization behavior (M/M_{Sat} , where $M_{\text{Sat}} = M_{\infty}$) of AsF_5 -doped PMPOT-18 as a function of H/T with (a) Brillouin functions for $S = \frac{1}{2}, \frac{2}{2}, \dots, \frac{8}{2}$, and (b) the best fit to a single Brillouin Function ($S = 0.44$). Magnetization measurements were done at 1.95 K.

dopant to monomer, since there is one oxygen atom per PMPOT-18 repeat unit). The spin state of the material at 1.95 K is $S = 0.44$. This value is slightly less than the spin state of isolated polarons ($S = 0.5$). The spin concentration for heavily doped PMPOT-18 is substantially larger than that for I_2 -doped PMPOT-18 (0.039 *vs.* 0.0056 spin/repeat unit). At this temperature, the antiferromagnetic interactions are slightly dominant.

The small polaron concentrations associated with the iodine-doped PMPOT-18 samples are a consequence of the weaker oxidizing capability of I_2 as compared to AsF_5 . As observed in the *in situ* EPR doping experiments, long exposure to AsF_5 results in a significantly larger polaron concentrations than saturation doping with I_2 . In an attempt to examine the relationship between spin concentration and spin state, a sample of PMPOT-18 film was oxidized with AsF_5 at low pressures and short exposure time to form a lightly doped polaronic material. Physically, this material was still flexible and similar to the I_2 -doped PMPOT-18, with none of the extreme brittleness that is usually present after prolonged exposure to AsF_5 .

The magnetization behavior in external fields between 1 and 50 kGauss at 1.95 K of this sample is shown in Figure 4-23. The sample is very near complete saturation of the polaronic moments at 50 kGauss. This allows a more accurate estimation of M_{Sat} than was possible in the other polaronic materials that were still approaching their saturation values at 50 kGauss.

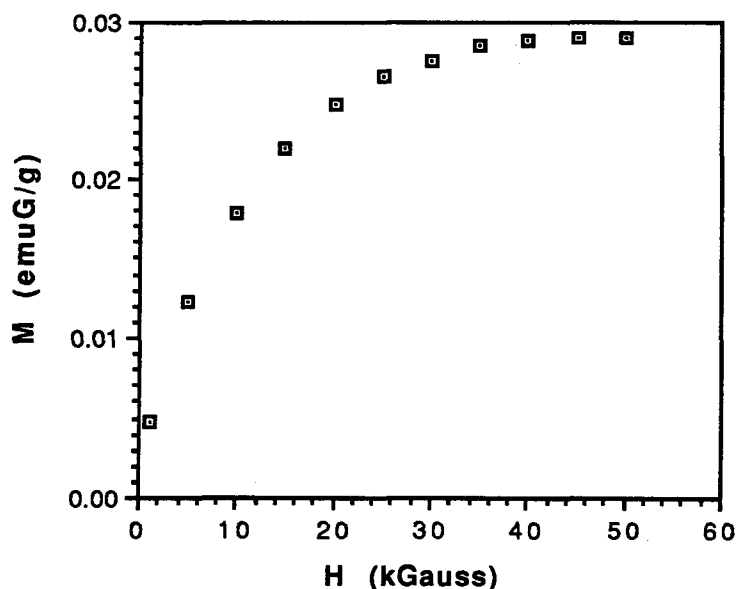


Figure 4-23. Magnetization of lightly AsF_5 -doped PMPOT-18 as a function of field ($T = 1.95$ K).

The normalized magnetization behavior is seen in Figure 4-24 with the closest Brillouin fit with $S = 2.2$ detailed in Figure 4-24b (assuming a M_{Sat} of 0.0295 emuGauss/gram). The saturation magnetization is much smaller than the heavily doped-PMPOT-18 and also smaller than the iodine doped PMPOT-18 samples, yet this material has the highest spin state of any of our doped materials to date at 1.95 K.

The sample that was lightly doped with AsF_5 to give a $S = 2.2$ Brillouin fit was then exposed to 500 torr of AsF_5 for 20 hours, effectively saturating the material with AsF_5 . The polymer became extremely brittle after this long of an exposure to AsF_5 . Figure 4-25 details the normalized magnetization behavior at 1.95 K of the heavily doped PMPOT-18. The data fits a Brillouin function with $S = 0.5$. The PMPOT-18 sample has a

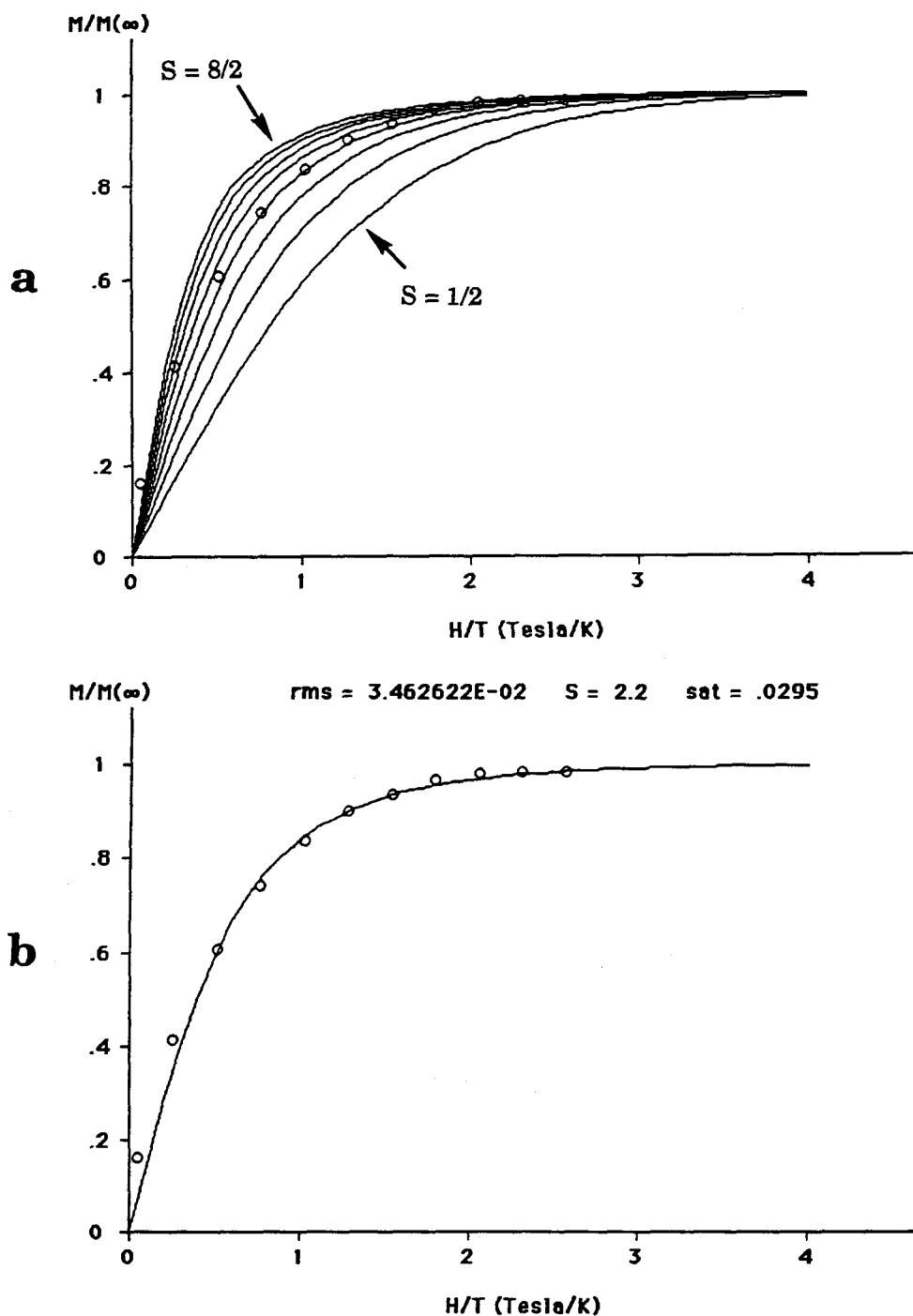


Figure 4-24. Normalized magnetization behavior (M/M_{Sat} , where $M_{\text{Sat}} = M_{\infty}$) of lightly AsF_5 -doped PMOT-18 as a function of H/T with (a) Brillouin functions for $S = \frac{1}{2}, \frac{2}{2}, \dots, \frac{8}{2}$, and (b) the best fit to a single Brillouin Function ($S = 2.2$). Magnetization measurements were done at 1.95 K.

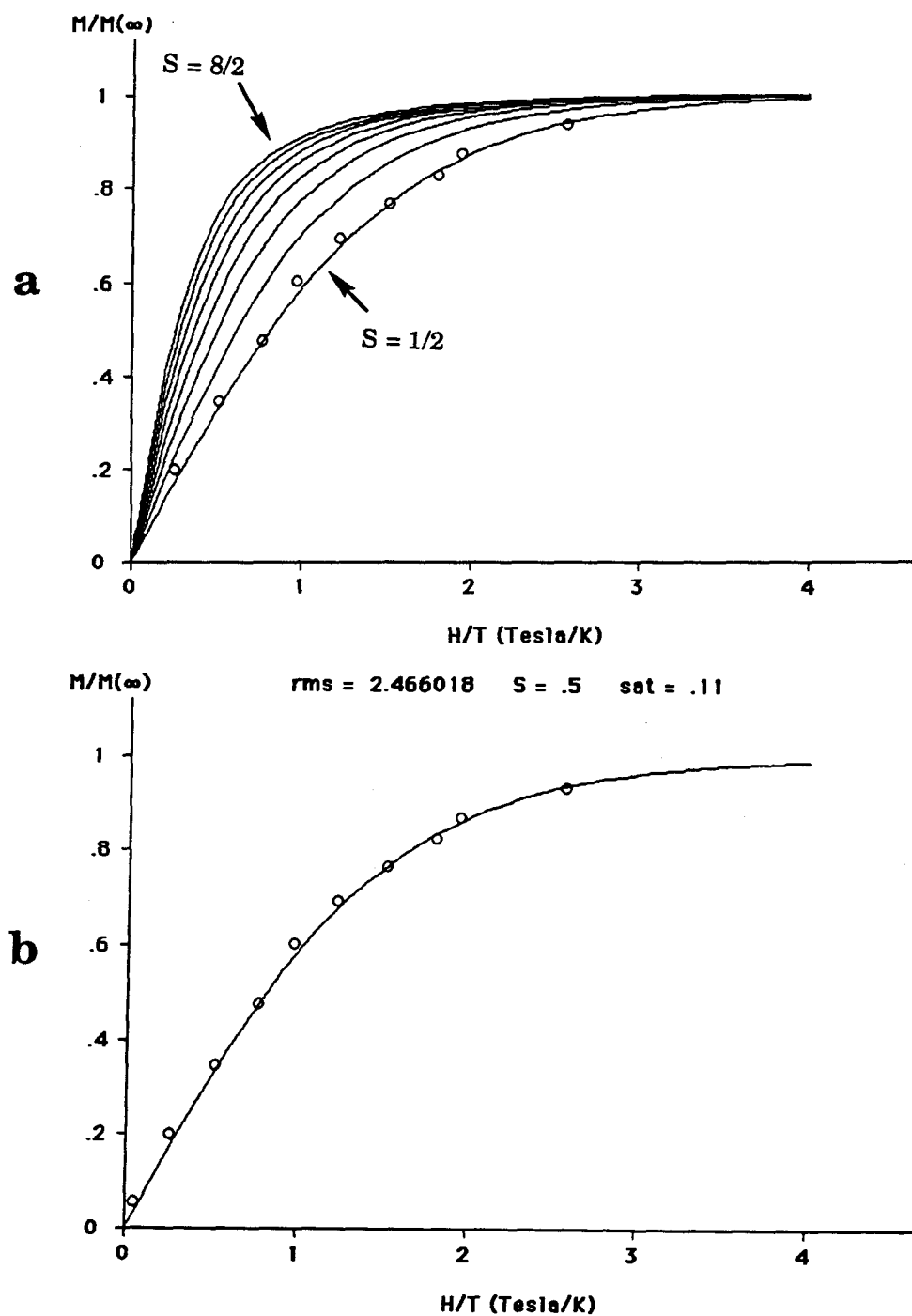


Figure 4-25. Normalized magnetization behavior (M/M_{Sat} , where $M_{\text{Sat}} = M_{\infty}$) of heavily AsF_5 -doped PMPOT-18 (from Figure 4-24) as a function of H/T with (a) Brillouin functions for $S = \frac{1}{2}, \frac{2}{2}, \dots, \frac{8}{2}$, and (b) the best fit to a single Brillouin Function ($S = 0.5$). Magnetization measurements were done at 1.95 K.

substantially larger saturation moment than before, with $M_{Sat} = 0.11$ emuGauss/gram. The normalized magnetization behavior of this heavily doped sample, which had been initially lightly doped with AsF_5 , is almost the same as the PMPOT-18 sample which was initially heavily doped (Figure 4-22). It would appear that the lightly doped PMPOT-18 material has the smallest polaron concentrations, yet also has the highest overall spin state. Treatment of PMPOT-18 with AsF_5 or I_2 gives qualitatively similar magnetic materials for equal polaron concentrations.

The inverse magnetic susceptibility data of AsF_5 -treated PMPOT-18 with $S = 2.2$ at 25 kGauss between temperatures of 6 and 300 K is plotted in Figure 4-26. The graph can be separated into two regions with qualitatively different behavior. The region below 150 K is characterized by a linear fit. The x-intercept of the fit in this region is -6 K. This is the Weiss constant for the low temperature χ_g^{-1} data. The second region of data above 150 K has significant curvature. This implies a transition in the magnetic interactions as compared to the linear low temperature region. In the linear range of the plot, the couplings are constant at low temperature. In the curved portion of the plot, the couplings are changing with temperature. The negative Weiss constant ($\theta = -6$ K) of the low temperature data indicates antiferromagnetic interactions.

The difference in magnetic interactions at low and high temperatures is apparent in the relative effective magnetic moment behavior μ'_{eff} of the lightly doped AsF_5 material, shown in Figure 4-27. This resembles the μ'_{eff} behavior of AsF_5 -doped PMPOT-6 (Figure 4-14), which at 1.95 K had a spin state of only $S = 0.5$, and the (μ'_{eff}) behavior of I_2 doped PMPOT-18 (Figure 4-21), which at 1.95 K had a spin state of $S = 1.4$. In Figure 4-27, the μ'_{eff} rises in the temperature range of 300 K to 200 K as

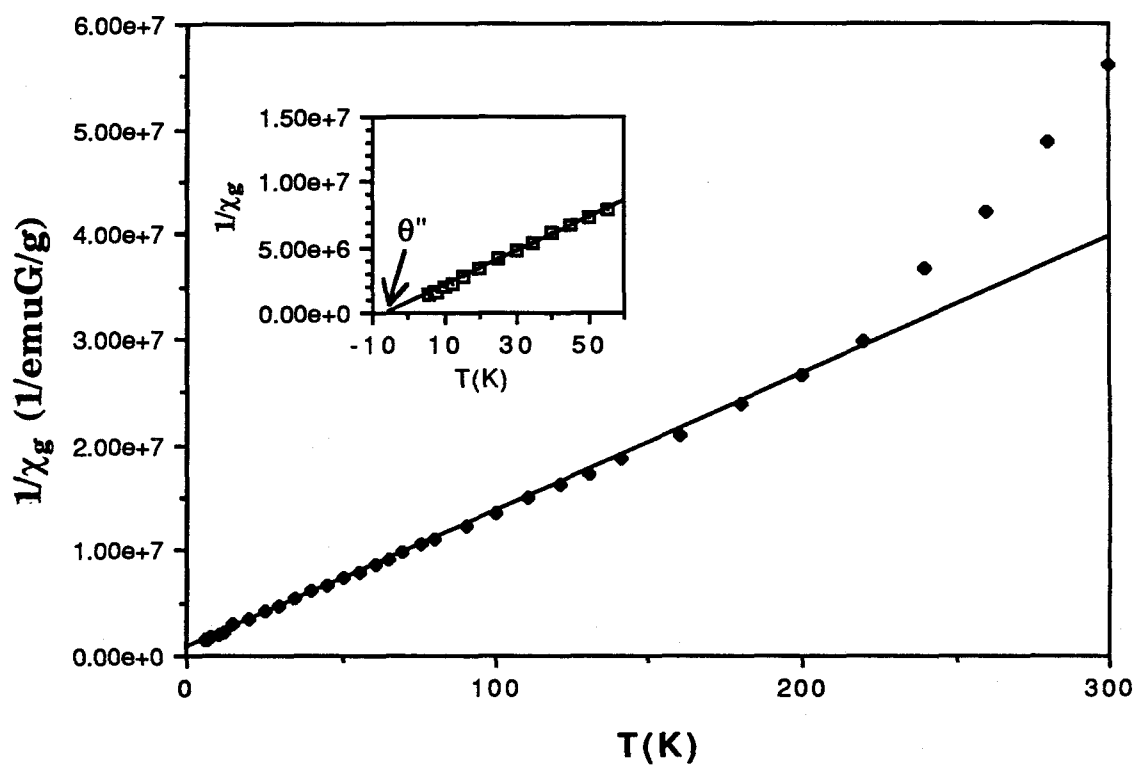


Figure 4-26. Curie-Weiss plot for lightly AsF_5 -doped PMPOT-18. The Weiss constant (θ'') is -6 K.

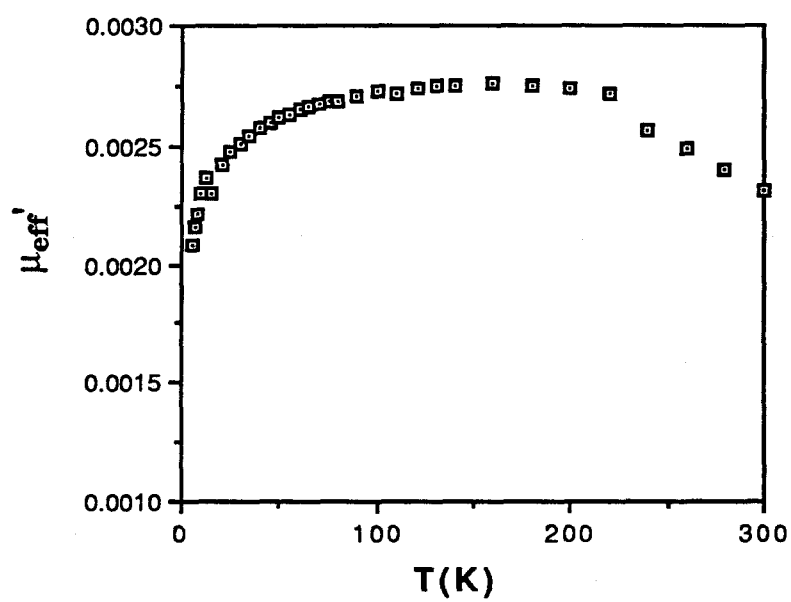


Figure 4-27. Relative effective magnetic moment (μ_{eff}') of lightly AsF_5 -doped PMPOT-18 as a function of temperature.

ferromagnetic coupling is increasing. The moment is then constant to 60 K, then decreases as the temperature nears 6.0 K. This decrease is the result of antiferromagnetic interactions which are observed to be relatively weak since their onset occurs only at very low temperatures.

The spin state of an AsF₅-lightly doped sample of PMPOT-18 film was also determined at two different temperatures. Figure 4-28 shows the normalized magnetization for AsF₅-doped PMPOT-18 at 2 K and 4 K. The $S = 2.2$ Brillouin function best fits the 2 K data. If the spin state of the material was invariant between 2 and 4 K, then the data points for the 4 K measurements should lie on the same curve as the 2 K data. As the plot shows, the 4 K normalized magnetization points lie, in general, to the left of, and above the 2 K data set and in a region of higher multiplicity. In fact, if the saturation magnetization is identical for the two sets of magnetization measurements, then the 4 K data set best fits a Brillouin function with $S = 2.6$. The spin state of the material changes to a higher order as the temperature is increased from 2 to 4 K. This agrees well with the conduct of μ'_{eff} as the temperature was increased in the lowest temperature region (Figure 4-27).

Magnetization References

The magnetization behavior of several other polaronic phenylene-based polymers were investigated. These materials were synthesized by gas phase oxidation of the neutral conjugated precursors with I₂ and AsF₅. The precursor and doped polymers are in powder form.

Figure 4-29 illustrates the normalized magnetization behavior for poly(*para*-phenylenevinylene) (PPPV) which was treated with 620 torr of AsF₅ for 24 hours. A saturation magnetization of $M_{\text{Sat}} = 0.4$

LIGHTLY DOPED PMPOT-18

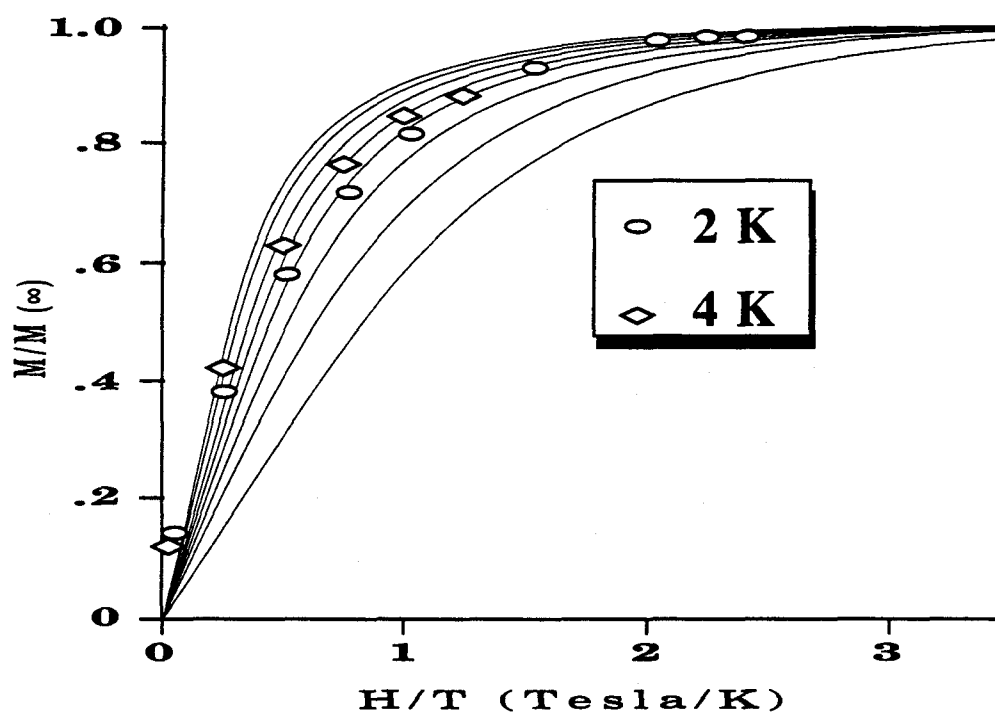


Figure 4-28. Normalized magnetization behavior of lightly AsF_5 -doped PMPOT-18 sample at 2 K and 4 K. $M_{\text{Sat}} = M_{\infty}$.

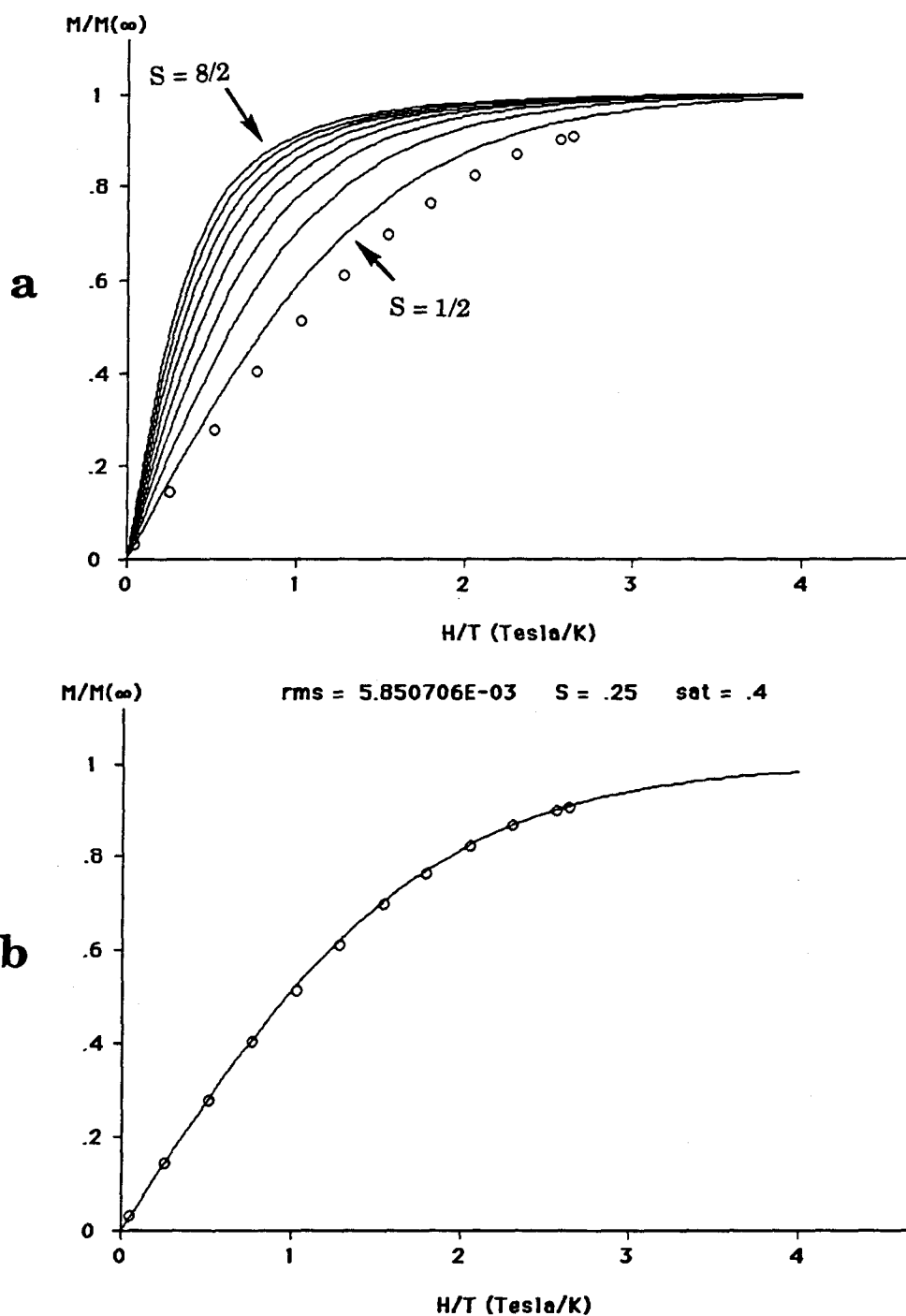


Figure 4-29. Normalized magnetization behavior (M/M_{Sat} , where $M_{Sat} = M_{\infty}$) of AsF_5 -doped PPPV as a function of H/T with (a) Brillouin functions for $S = \frac{1}{2}, \frac{2}{2}, \dots, \frac{8}{2}$, and (b) the best fit to a single Brillouin Function ($S = 0.25$). Magnetization measurements were done at 1.95 K.

emuGauss/gram gives a calculated Ω of 42 repeat units per spin. The data at 1.95 K gives a good fit to a Brillouin function with $S = 0.25$. The spin state for PPPV is significantly less than the $S = 0.5$ value for isolated radicals. The small value of the spin state is due to a large number of antiferromagnetic interactions between the radicals in the material.

The short conjugation length of the olefin group which links the phenylene unit does not readily allow oxidation to form polarons in PPPV. Very strong oxidants such as AsF_5 must be used to oxidize the polymer chain. Unfortunately, I_2 is too weak of an oxidant to form significant numbers of radical cations. The related polymer, poly(*para*-phenyleneoctatetraene) (PPPOT), is oxidized much more readily and allows the use of I_2 as a polaron-generating oxidant. Figure 4-30 details the normalized magnetization behavior for iodine-doped PPPOT. This material has a larger Ω (118 monomer/spin) than PPPV. The normalized magnetization data fit a Brillouin function with $S = 0.4$ at 1.95 K. Antiferromagnetic couplings cause the spin state to be less than the isolated polaron value of $S = 0.5$.

Discussion

At this juncture, it is worthwhile to review the primary areas of inquiry concerning the viability of PMPOT derivatives as polaronic ferromagnetic materials. As mentioned earlier, the critical questions are:

- (1) Can such structures be readily synthesized?
- (2) Can a high density of polarons be produced?
- (3) Is one-dimensional coupling ferromagnetic?
- (4) Can three-dimensional order be obtained?

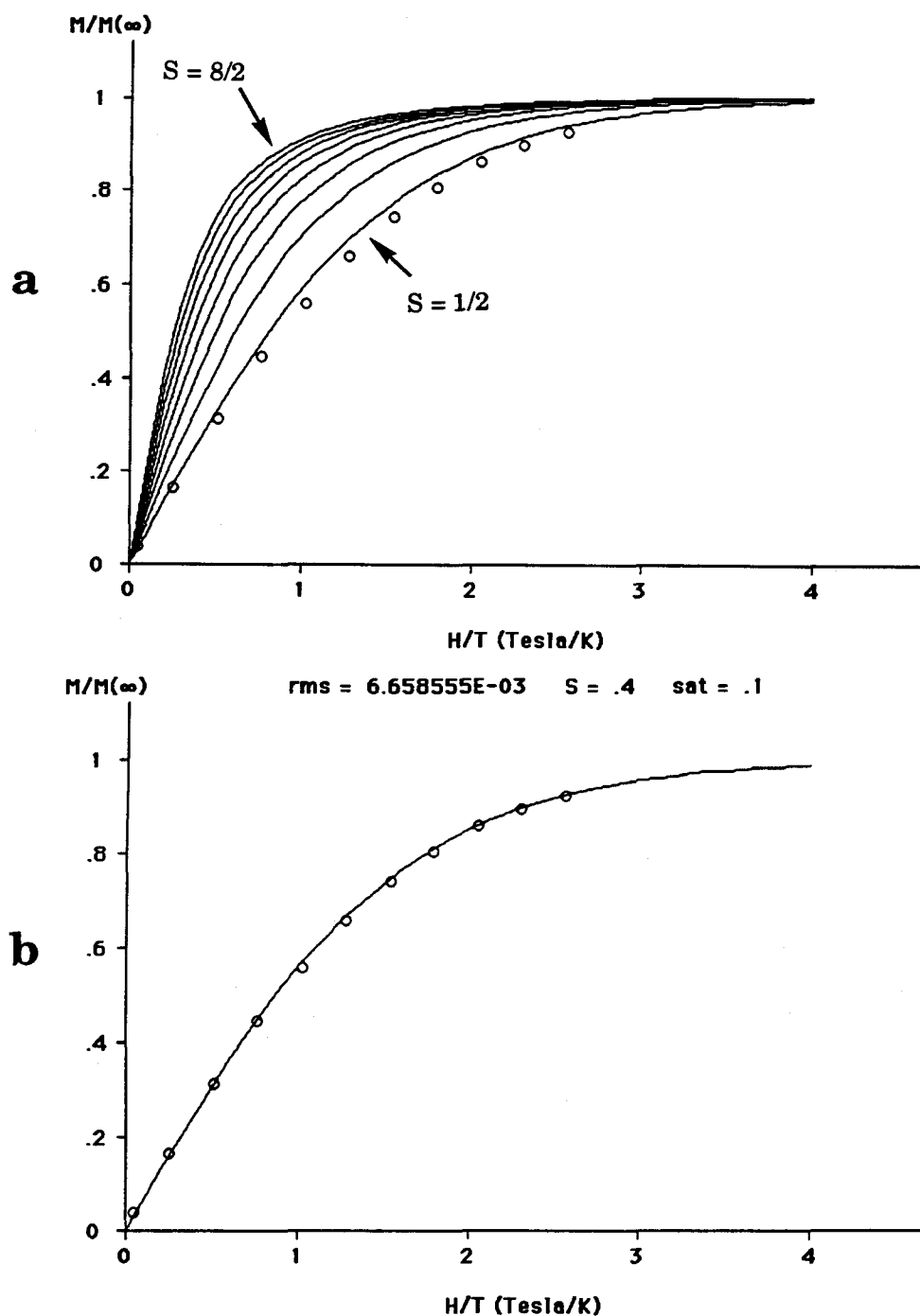


Figure 4-30. Normalized magnetization behavior (M/M_{Sat} , where $M_{\text{Sat}} = M_{\infty}$) of I_2 -doped PPPOT as a function of H/T with (a) Brillouin functions for $S = \frac{1}{2}, \frac{2}{2}, \dots, \frac{8}{2}$, and (b) the best fit to a single Brillouin Function ($S = 0.4$). Magnetization measurements were done at 1.95 K.

PMPOT Structure. The chain length of non-oxidized PMPOT is quite dependent on the solubility of the polymer. The precursor polymer is insoluble and intractable in the parent form, but becomes soluble with the introduction of O-octadecyl groups to the phenyl rings. The increased solubility of the product allows the the polymerization reaction to occur efficiently. The average degree of polymerization increases from 2 to 22 upon substitution of PMPOT with an O-C₁₈ group. Since PMPOT-18 is completely soluble in the reaction solvent (toluene), the chain lengths are no longer limited by solubility, rather by the efficiency of the Wittig reaction. While the unsubstituted PMPOT has a degree of polymerization which is too small to allow a significant number of polarons to reside on a single chain, the average degree of polymerization of PMPOT-18 is large enough to support multiple polarons. It should also be noted that although the average degree of polymerization is 22, there were significant amounts of material by GPC analysis in the molecular weight region corresponding to 200-300 repeat units per polymer chain.

It may, in fact, be possible to separate the material into fractions of different molecular weight, much the same way that PMPOT-6 separates into a low molecular weight soluble phase and a higher molecular weight insoluble phase. Precipitation of the higher molecular weight material while keeping the lower molecular weight fraction soluble is a feasible technique assuming that the appropriate recrystallization solvents can be found. This would allow separate magnetic characterization of short and long polaron-containing polymer chains. A comparison of the spin states of high and low molecular weight doped PMPOT-18 would determine whether long chains in high-spin materials are necessary. The current

magnetic studies use only material which contains the complete range of molecular weights of PMPOT-18 observed in the GPC characterization.

The elimination of insolubility as a barrier to production of long chain polymers may open up new possibilities for the synthesis of polymers with an even larger number of repeat units per chain. Since only the efficiency of the polymerization reaction now determines the size of the polymer chain, other more efficient carbon-carbon double bond forming reactions may be applied to the synthesis of PMPOT derivatives to yield higher molecular weight materials.

Even though the precursor material is fairly well characterized, and in the case of PMPOT-18 appears to be of high molecular weight with little defects by ^1H NMR analysis, the true structure of the polaron-containing polymers is not unambiguously known. Due to the intractable nature of the doped material, the characterization methods which were available to the soluble precursor are not amenable to the doped material. The polaron-containing material almost certainly contains cross-links and saturated centers in the backbone of the chain, which would disrupt the conjugation of the polymer. AsF_5 and I_2 -treated conducting polymers, as a rule, lose much of their processibility due to extensive cross-linking caused by the dopants.⁶ The scheme of precise oxidation of the polymer segment of PMPOT to form well defined polarons on pristine chains of PMPOT is almost certainly an idealized oversimplification of the true structure of doped PMPOT.

Polaron Densities. The ability of the PMPOT structure support to high densities of *stable* polarons is not yet clearly defined. It is certainly the case that treatment of PMPOT derivatives with AsF_5 or I_2 form radicals in

quantities that are measurable by EPR and SQUID techniques. Unfortunately, the number of spins is quite small when compared to the number of possible sites on each polymer in which a polaron can reside. The design of the polaronic ferromagnetic model is such that, at most, there can be one polaron on each polyene unit, or one polaron per monomer unit on each chain. By this standard, the highest spin state material only has an average of one spin per 222 repeat units.

It would be informative to examine the spin concentrations of other polymers to determine if the spin concentrations in these magnetic materials are orthodox. Table 4-5 lists the spin to monomer ratio for a variety of conjugated polymers which have been chemically or electrochemically oxidized. The results from the *in situ* EPR experiments with PMPOT-6 and PMPOT-18 are also included. Polymers 62 and 86 have degrees of polymerization ranging between three and ten. The method of oxidation for these polymers is exposure to gas-phase AsF_5 . These AsF_5 -treated materials have spin concentrations which are comparable to the equilibrium concentration of spins in AsF_5 -treated PMPOT-18 and PMPOT-18. It may be that these values are the upper limit to the amount of spins that can be created by this method of doping. The amount of AsF_5 in the PMPOT derivatives is substantially larger than the number of monomer units present. Further addition of dopant does not increase the spin concentration, as seen in the EPR experiments. Gas-phase doping of conducting polymers is thought to be inhomogeneous in nature due to the inability of the gas to penetrate the surface of the material. The PMPOT-18 films and the phenylene-based polymer powders may also not allow full permeation of the dopant throughout the material.^{5,8,30} The alkyl sidegroups would hinder this process further, since they are unreactive

Table 4-5. Spin Concentrations of Doped Polymers

| | $\frac{\text{spin}}{\text{gram}}$ | $\frac{\text{spin}}{\text{monomer}}$ |
|--|-----------------------------------|--------------------------------------|
| <p>62^{a,d}</p> | 1.0×10^{20} | 0.03 |
| <p>86^{a,d}</p> | 1.0×10^{20} | 0.04 |
| <p>87^{b,e}</p> | | 0.08 |
| <p>88^{b,e}</p> | | 0.08 |
| <p>89^{b,f}</p> | | 0.08 |
| PMPOT-6(I ₂) ^c | | 0.01 |
| PMPOT-6(AsF ₅) ^c | | 0.04 |
| PMPOT-18(I ₂) ^c | | 0.006 |
| PMPOT-18(AsF ₅) ^c | | 0.035 |

^a AsF₅ Doped. ^b Electrochemically doped. ^c EPR *in situ* results.

^d Ref.13. ^e Ref. 31,32. ^f Ref. 33.

towards doping and may shield the polyene chain from dopant contact. Therefore, it is not necessarily a surprise that the gas-phase doping with AsF₅ or I₂ gives polaron concentrations which are much smaller than the maximum possible values (1 spin per repeat unit). The use of thinner PMPOT-18 films may allow better dopant access to the polyene segment and higher resultant spin concentrations.³⁰

The spin concentrations of polypyrrole (87),³¹ polyaniline (88),³² and polymethylthiophene (89)³³ in Table 4-5 are significantly larger than the AsF₅-treated polymers. The electrochemical method of oxidation used in these materials is apparently a more efficient method of generating radical spins than the gas-phase AsF₅ procedure. Electrochemical oxidation may be especially suitable for doping of PMPOT-18 due to the soluble nature of the precursor polymer. Very thin films of PMPOT-18 can be deposited on the appropriate electrode, a process which is impossible to accomplish with the other intractable, insoluble polymers. The use of electrochemical methods with PMPOT-18 may thus be a route to higher polaron densities.

The ability to form large polaron densities in PMPOT derivatives is also limited by the reactivity of the polarons themselves. The design of this system is such that polarons separated by the *meta*-benzene group on a single chain cannot combine and annihilate to form a bipolaron. This can be seen in a similar system outlined in Figure 4-31, in which a *meta*-benzene group is separating polarons on two phenylene chains. In poly(*para*-phenylene) and the other polymers listed in Table 4-5 (with the exception of poly(*meta*-phenylene), the polarons are able to combine and annihilate along the polymer chains (see Chapter 2, Scheme 2-1). Another alternate route to polaron loss is simple oxidation to give a bipolaron. This route is possible in the PMPOT derivatives as well as the other polymers

**BIPOLARON FORMATION
SUPPRESSED WITH "META" COUPLING**

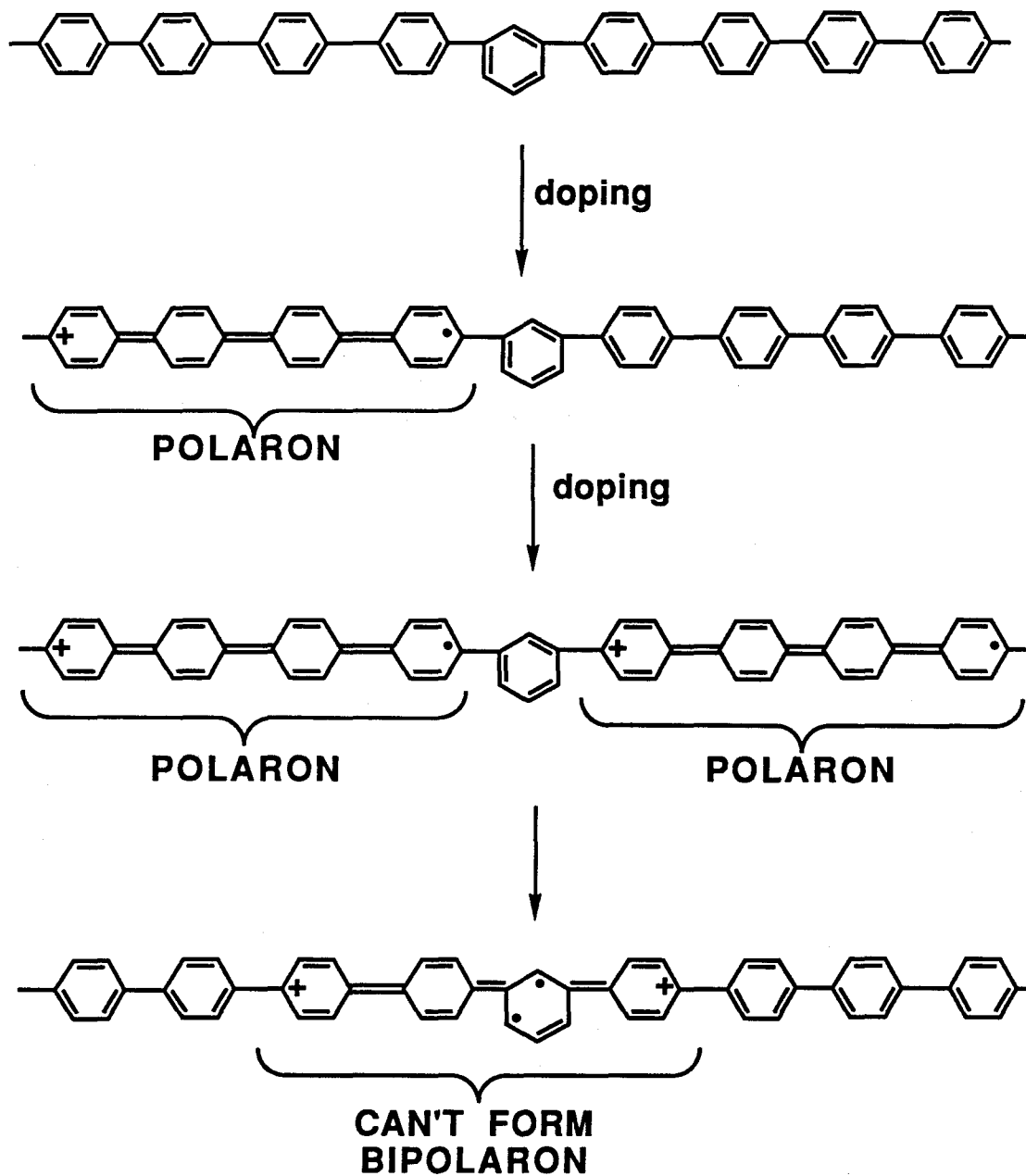


Figure 4-31 Bipolaron formation suppression in *meta*-benzene-linked systems.

discussed. It also is possible that polarons on different chains yet in close proximity to each other could combine to form two cations and a cross-link between the chains. The decay of polarons upon increased oxidation has been observed in polyaniline, polypyrrole, and polydithiophene.^{31,32,34} In fact, the spin concentrations listed in Table 4-5 for these three polymers are their maximum values. The general behavior of the spin concentration as the doping level increases is seen in Figure 4-32. The spin concentration of these three polymers rises at low doping levels, reaching a zenith and rapidly falling at higher doping levels. This is due to the formation of bipolaron species at the expense of the polarons formed in the early stages, either through disproportionation or further oxidation.

PMPOT-6 and PMPOT-18, however, show mixed results concerning the stability of the polarons. The AsF₅-doped material exhibits no sharp maximum and subsequent decrease of polarons, which implies that the spins formed are relatively stable species (there is a decrease in the spin concentration as seen in the magnetization studies of PMPOT samples taken at different times, but this is on the order of days, not minutes as observed in the aforementioned electrochemical studies). However, the I₂-treated PMPOT derivatives clearly show a decrease of spin concentration similar to Figure 4-32, signifying a decay of polarons. This is unexpected in light of the behavior of AsF₅-doping of PMPOT. The difference between I₂ versus AsF₅ may, though, be due to the stronger oxidizing capability of AsF₅. Doping with AsF₅ causes defects to form in the polymer structure, which could conceivably trap existing polarons and prevent their disproportionation or oxidation. The brittle nature of the AsF₅-doped material is an effect of the extensive crosslinks formed in the doping

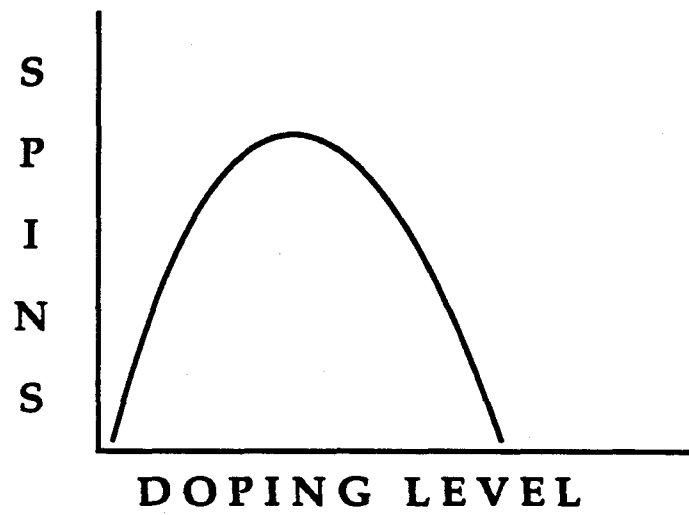


Figure 4-32. Spin concentration in 87, 88, and 89 as a function of doping level.

reaction. I_2 , being a weaker oxidant, may not cause such extensive degradation of the structure.

If one assumes that disproportionation of polarons along the polymer chain is not a mechanism available to the *meta*-coupled materials, then the disappearance of spins observed in I_2 -doped PMPOT derivatives must be due to *interchain* polaron recombination or further oxidation by the dopant. These two routes, in addition to the inherent inhomogeneity of the doping method, may explain the low maximum concentrations of polarons observed in the PMPOT system.

Another strategy to limit intermolecular reactions of existing polarons would be to use a counterion which effectively pins the radical cation to the polyene chain, shielding the polaron from other polarons on adjacent chains and from further oxidation by the dopant. This strategy may be tested quite easily using the electrochemical oxidation method. Large counterions would have the best chance of eliminating polaron decay. Alternatively, different chemical dopants may be used besides AsF_5 or I_2 , preferably oxidants which are as large as possible.

It should be stressed at this point that in the AsF_5 -doped PMPOT materials, and even in the I_2 -doped derivatives, a relatively stable (albeit low) concentration of polarons is observed. Although the AsF_5 -doped polymers, 62 and 86, in Table 4-5 show a stable radical population, this may be due more to the fact that these materials are oligimers with few repeat units. While in the PMPOT derivatives it cannot be stated absolutely that intrachain annihilation is **not** occurring due to the structural design (*i.e.*, *meta*-coupling) of the polymer, it seems much more likely that the low spin concentrations are due to inhomogeneous doping, intermolecular polaron reactions, or further oxidation by the dopant.

Is one-dimensional coupling ferromagnetic? Before addressing the questions of interchain and intrachain magnetic interactions in doped PMPOT derivatives, it is worthwhile to examine the general spin states of these materials. The Brillouin function does not differentiate between the spin state of a molecule and the magnetic couplings between molecules, but rather gives the spin state of the system as a whole. If the couplings (ferro- or antiferromagnetic) between magnetic centers are sufficiently strong such that at the temperature of the magnetization measurements, there is little thermal population of higher energy states corresponding to uncoupled magnetic centers, then the spin state from the Brillouin function will reflect magnetic couplings. If the spin state of the isolated magnetic centers is known, then one can qualitatively gauge the nature and extent of the magnetic couplings between the centers.

Table 4-6 lists the magnetic spin states of the doped PMPOT derivatives as well as the model polymers PPPOT and PPPV. The maximum multiplicity obtained at 2 K for any of the materials studied is the lightly doped AsF₅-treated PMPOT-18 ($S = 2.2$). Every other PMPOT derivative with a relatively low spin concentration has a spin state of at least $S = 1$. The spin state of an isolated polaron should be $S = 0.5$, similar to a single radical spin. Consequently, *there must be a net ferromagnetic interaction between polarons in these PMPOT systems*. No spontaneous magnetization at zero applied field was ever observed, indicating that the extent of the ferromagnetic couplings are not three-dimensional throughout the entire material. The material is not a ferromagnet, but rather a *ferromagnetically-coupled paramagnetic system*.²⁸ This is substantiated by the Curie-like behavior of the magnetic susceptibility of

Table 4-6. Spin States and Spin Concentrations of PMPOT-18 Derivatives

| | | $\frac{\text{spin}^e}{\text{monomer}}$ | $\frac{\text{monomer}}{\text{spin}}$ | $\frac{\text{dopant}^f}{\text{monomer}}$ | S |
|---|--|--|--------------------------------------|--|------|
| A | PMPOT-6(AsF ₅) ^{a,c} | 0.043 | 23 | 2.41 | 0.5 |
| B | PMPOT-6(AsF ₅) ^{a,c} | 0.015 | 66 | 2.41 | 0.5 |
| C | PMPOT-6(I ₂) ^{a,c} | 0.006 | 166 | 2.29 | 1.3 |
| D | PMPOT-6(I ₂) ^{a,d} | | | 2-3 | 1.2 |
| E | PMPOT-18(I ₂) ^{b,c} | 0.0056 | 178 | 0.39 | 1.4 |
| F | PMPOT-18(I ₂) ^{b,d} | | | | 1.3 |
| G | PMPOT-18(AsF ₅) ^{b,c} | 0.039 | 25 | 5.5 | 0.44 |
| H | PMPOT-18(AsF ₅) ^{b,c} | 0.0045 | 222 | 0.12 | 2.2 |
| I | PMPOT-18(AsF ₅) ^{b,c} | 0.0335 | 29 | 4.81 | 0.5 |
| J | PPOT(I ₂) ^{a,c} | 0.0085 | 118 | 2.32 | 0.4 |
| K | PPPV(AsF ₅) ^{a,c} | 0.0235 | 42 | 1.19 | 0.25 |

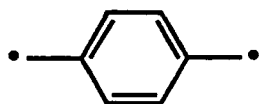
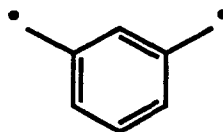
^a Powder. ^b Film. ^c Gas phase doping. ^d Solution phase(CCl₄) doping.

^e Calculated from M_{Sat}. ^f Calculated from mass uptake of dopant. The ratio is calculated for AsF₆⁻ in the case of AsF₅-doped material and I for I₂-doped material.

the doped polymers. The highest spin state system ($S = 2.1$) of doped PMPOT-18 correlates to a net high spin interaction between four polarons, or a net quintet state.

The use of the spin state for isolated polarons as the guideline for antiferromagnetic or ferromagnetic behavior in PMPOT derivatives is misleading to a certain extent. Most materials containing radicals in close proximity have magnetic interactions between the spin centers and hence would not exhibit spin states corresponding to the isolated scenario.¹⁹ The high spin behavior of the doped PMPOT materials hypothetically could be inherent to the nature of the doping process, or it may just be that polarons, in general, interact ferromagnetically. This would not be an unprecedented result, for even though most radicals interact antiferromagnetically, there are systems whose radicals interact ferromagnetically when in close proximity (such as galvinoxyl).¹⁹ It would be more appropriate to determine the magnetic capability of the polaronic ferromagnet design by comparing the spin state of the doped PMPOT derivatives with polaron-containing polymers which would *not* be predicted to have ferromagnetic interactions.

PPPV and PPPOT are polymers that have *para*-phenylene groups connected by polyene segments. Polarons formed by oxidative doping on the conjugated polyene chains will be antiferromagnetically coupled by the *para*-phenylene groups, a concept that is analogous to the proposed ferromagnetic capabilities of *meta*-xylylene. The isolated biradical *para*-xylylene is low spin (i.e., a ground state singlet), as opposed to the ground state triplet behavior of *meta*-xylylene.¹

*para*-xylylene*meta*-xylylene

The spin states of these *para*-linked materials are substantially different than the PMPOT materials. The spin state of AsF₅-doped PPPV is substantially lower than the spin state of PMPOT-18 with spin concentrations either larger or smaller than the PPPV material. The extremely low value of the spin state for PPPV ($S = 0.25$) implies the existence of antiferromagnetic interactions between polarons. The spin state of I₂-doped PPPV was not available due to the inability of I₂ to oxidize the polymer structure. I₂-doped PPPOT exhibited low spin concentrations which were comparable to the spin concentrations of the PMPOT derivatives with high spin states, yet had a spin state of only $S = 0.4$. Again, the low value of S indicates the presence of net antiferromagnetic interactions in the doped PPPOT. This is an especially significant result since PPPOT and PMPOT differ only in the phenyl coupling design. Therefore, the high spin states of the lightly doped PMPOT derivatives are unique when compared to other polaronic polymers, presumably due to the *meta*-coupled structure of the conjugated chains. However, one note of caution must be interjected here concerning the comparison of PPPV and PPPOT with the PMPOT derivatives. The degree of polymerization of PPPV and PPPOT are quite small, between four and nine. The antiferromagnetic coupling exhibited by these materials may be more a result of intermolecular polaron interactions, rather than the interactions of polarons along a single, shared chain. It cannot be absolutely stated

that *only* the *meta*-phenylene (and not the *para*-) polaronic polymers are capable of high spin behavior since the *para*-coupled polymers are actually oligimeric in nature and hence, may not have the intrachain interactions available to the PMPOT derivatives. *What is known is that the lightly doped PMPOT derivatives exhibit ferromagnetic interactions between polarons*, presumably due to the *meta*-connectivity of the structure, whereas polarons in similar concentrations in conjugated systems prefer to interact antiferromagnetically.

The antiferromagnetic interactions of polarons in doped PPPV and PPPOT is not without significant precedent. Most radicals interact antiferromagnetically in close proximity at low temperatures (galvinoxyl radical, which was mentioned earlier as a ferromagnetically interacting radical, is actually an anomaly).¹⁹ This is true in higher spin state molecules as well as spin 1/2 species. For example, $\text{Cr}^{3+}(\text{alum})$ has a large separation between chromium centers. The magnetization behavior fits a Brillouin function with $S = 1.5$, the expected value for isolated Cr^{3+} (see Chapter 3, Figure 3-12).³⁵ In contrast, the normalized magnetization of chromium(III)acetylacetonate ($\text{Cr}(\text{acac})_3$) fits to a Brillouin function with $S = 0.87$ at 2 K (Figure 4-33).³⁶ This difference in S is due to intermolecular antiferromagnetic interactions. The appearance of these magnetic interactions can be seen in the effective magnetic moment (μ_{eff}) variation with decreasing temperature. In Figure 4-34, the effective magnetic moment is constant at $3.76 \mu_B$, which is near the calculated value for isolated Cr^{3+} , from 300 K down to 50 K. At temperatures lower than 50 K, the μ_{eff} decreases rapidly, a consequence of weak antiferromagnetic interactions between the molecules which thermal energy disrupts above

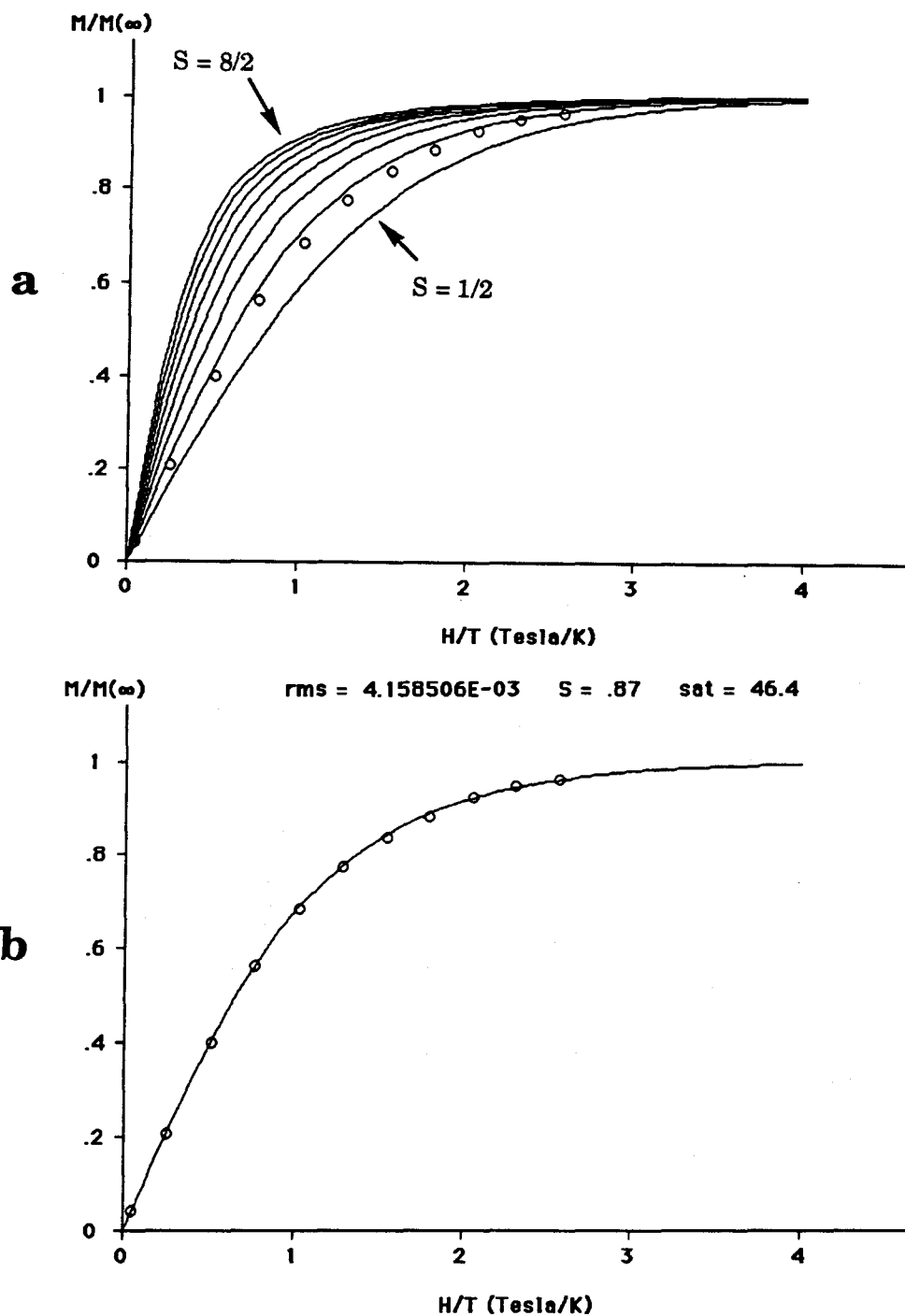


Figure 4-33. Normalized magnetization behavior (M/M_{Sat} , where $M_{\text{Sat}} = M_{\infty}$) of $\text{Cr}(\text{acac})_3$ as a function of H/T with (a) Brillouin functions for $S = \frac{1}{2}, \frac{2}{2}, \dots, \frac{8}{2}$, and (b) the best fit to a single Brillouin Function ($S = 0.87$). Magnetization measurements were done at 1.95 K.

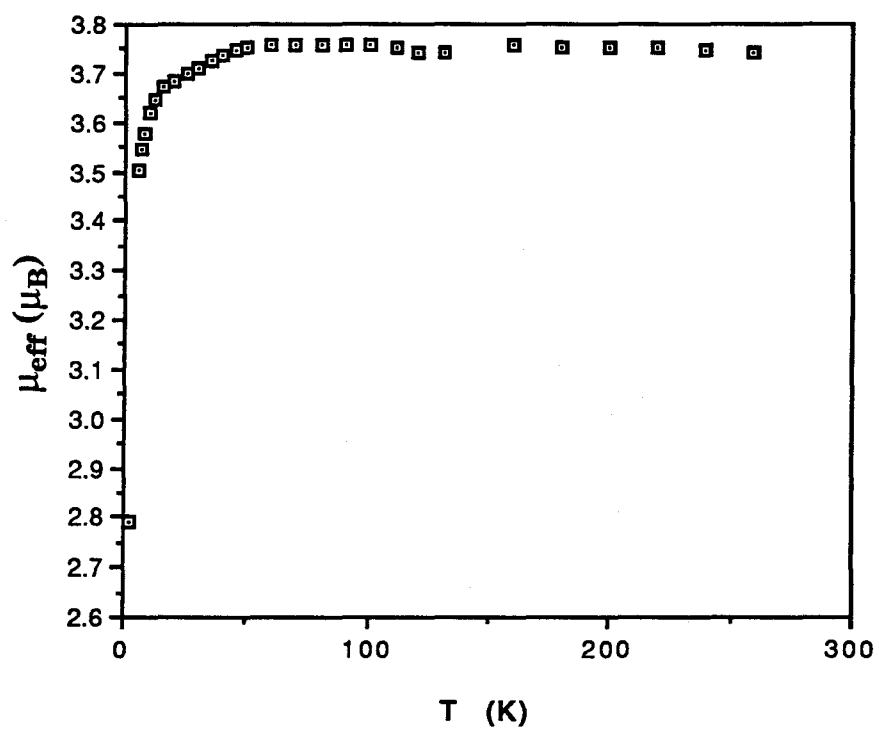


Figure 4-34. Effective magnetic moment of $\text{Cr}(\text{acac})_3$ as a function of temperature.

50 K (recall that thermal energy destroys both antiferromagnetic and ferromagnetic ordering).

The high-spin PMPOT derivatives have relative μ_{eff} behaviors which are reminiscent of the $\text{Cr}(\text{acac})_3$ system. The qualitative difference between the two systems is that in the PMPOT derivatives, the maximum μ_{eff} does not stay constant in the high temperature region, but instead decreases slightly. This is due to a decrease in the ferromagnetic couplings between polarons from thermal energy.

The decrease of μ_{eff} for doped PMPOT-18 at very low temperatures implies that an increase of temperature in this range will lessen the antiferromagnetic interactions and result in a material with a higher spin state. This is demonstrated by the 4 K magnetization measurements of doped PMPOT-18, which give a fit to a Brillouin function with $S = 2.6$ as opposed to the 2 K measurements which fit a Brillouin function with $S = 2.1$. The implication of this temperature dependence of the μ_{eff} and the Brillouin function is that the spin states measured at low temperatures are not representative of the maximum amount of ferromagnetic coupling in the doped PMPOT derivatives. With these results, a model is proposed which explains the magnetic behavior of PMPOT-18. This model is shown pictorially in Figure 4-35.

The polarons formed by the doping process interact ferromagnetically with a positive exchange interaction J_1 and form clusters of spins. These clusters interact with each other in an antiferromagnetic fashion, with an associated negative exchange interaction J_2 . The absolute magnitude of J_1 , is greater than J_2 . This is manifested by the increase of μ_{eff} as temperature rises in the low temperature region due to the destruction of antiferromagnetic ordering by

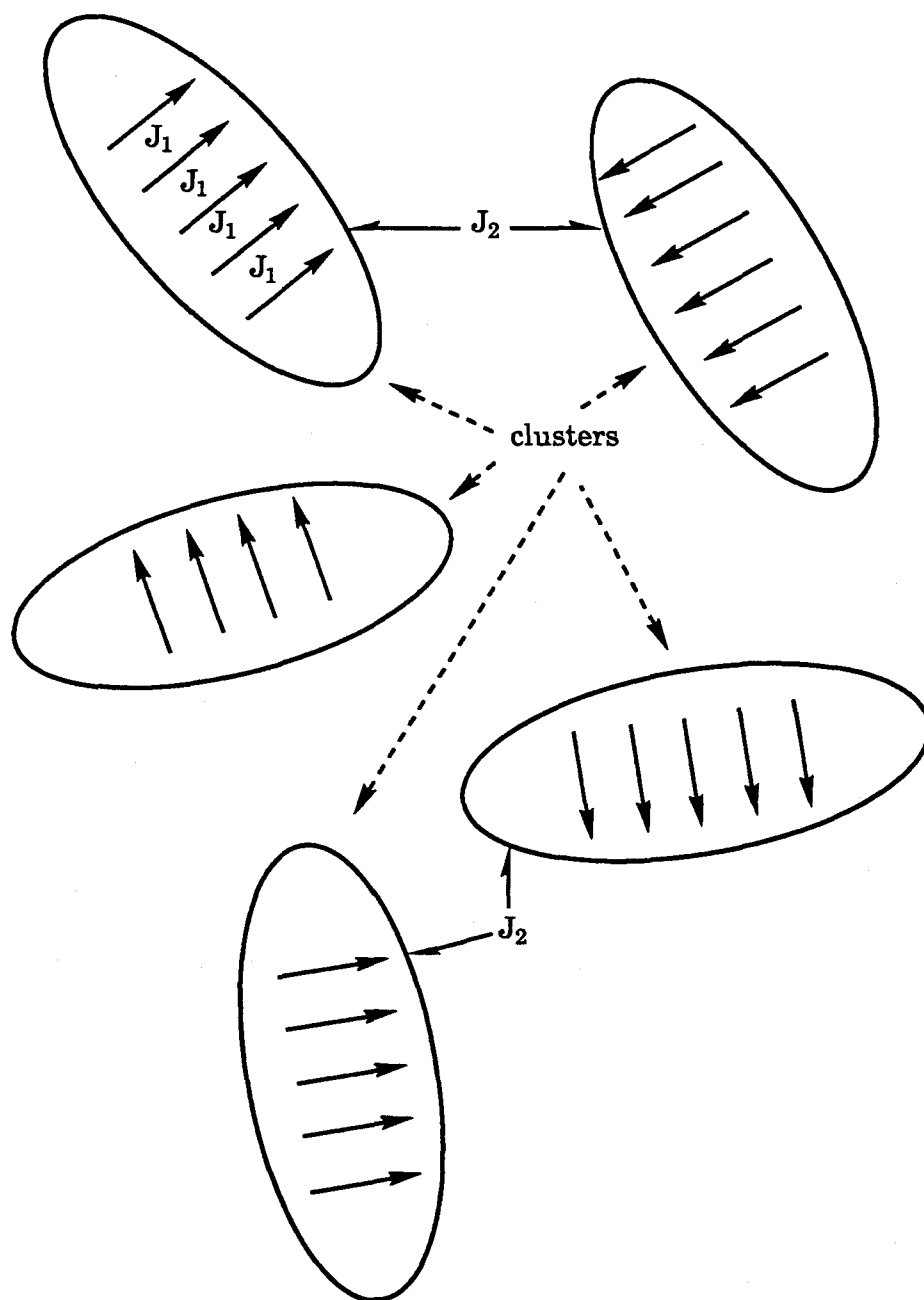
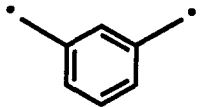




Figure 4-35. Cluster model for polaronic PMPOT derivatives. The arrows represent polarons. J_1 is the ferromagnetic exchange interaction (positive) between polarons within a cluster and J_2 is the antiferromagnetic exchange interaction (negative) between clusters.

thermal energy, followed by decrease of μ_{eff} at high temperatures due to the destruction of ferromagnetic ordering. The higher temperatures at which the ferromagnetic ordering is destroyed relative to antiferromagnetic ordering indicates that the ferromagnetic coupling is stronger than the antiferromagnetic coupling.

That the ferromagnetic couplings are relatively strong is not surprising when one considers the relative energies of the high and low spin state of the parent biradical of the high-spin linker used in the design, 1,3-benzoquinodimethane (54). The energy separating the low spin state from the high spin state of the biradical has been estimated to be 7.8 kcal/mol.¹ From the Boltzmann equation, significant population of the low spin state of 54 will occur at $T_B = \epsilon/k$ where ϵ is the energy difference between states and k is the Boltzmann constant. This temperature roughly corresponds to the point at which thermal energy has overcome ferromagnetic coupling between the radicals. For 1,3-benzoquinodimethane, T_B is 3935 K! The singlet-triplet gaps for cyclobutanediyl 52³⁸ and trimethylenemethane 53¹ and their corresponding T_B 's are listed in Table 4-7. As seen in Table 4-7, the energy gap between ferro- and antiferromagnetically coupled states in these biradicals gives quite high T_B 's. If one assumes the singlet-triplet energy gap for two polarons separated by a *meta*-phenylene group is of the same order of magnitude as the singlet-triplet energy gap for 1,3-benzoquinodimethane, then the existence of high temperature (greater than 100 K) ferromagnetic interactions as observed in the behavior of μ_{eff} is certainly possible, if not probable. Implicit in this analysis is the conclusion that the mechanism which couples the polarons in this design does not require a large energy gap between the high spin and low spin states.

Table 4-7. Biradical Singlet-Triplet Gaps

| | E_{s-t}^a | T_B (K) |
|---|------------------|-----------|
|  | 7.8 ^b | 3925 |
|  | 1.7 ^c | 855 |
|  | 15 ^b | 7549 |

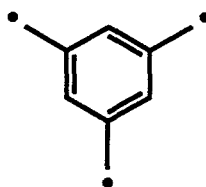
^a Kcal/mol. ^b Ref. 1. ^c Ref. 38.

The lowering of the spin state of PMPOT-18 when going from a lightly doped material with a small spin concentration to a heavily doped sample with a larger spin concentration can be explained in terms of the aforementioned cluster model. The magnetic interactions that determine the spin state of a system are inversely proportional to the distance separating the spins.³⁹ At low concentration of polarons, the clusters are spread apart, hence the antiferromagnetic interactions between high spin clusters are small and the net spin state is relatively high. At higher doping levels and spin concentrations, the clusters are closer to each other. This strengthens the antiferromagnetic interaction between clusters, and a lower net spin state results. As seen in Table 4-6, there is a crude

correlation between the spin state of PMPOT derivatives and the spin concentration.

This cluster model, at first glance, creates a dilemma concerning the low spin concentrations. One of the goals of this work is to create large concentrations of polarons. If the cluster model is valid, then simply increasing the number of spins will also increase the intercluster antiferromagnetic interactions, giving lower than optimum spin states.

Assuming that the ferromagnetic coupling of spins within a cluster is due primarily to intrachain interactions between polarons, then the antiferromagnetic couplings between clusters is a consequence of interchain polaronic interactions. The through-space antiferromagnetic interactions of polarons between separate chains may be counteracted by the use of a group which could ferromagnetically couple polarons on separate chains. One potential ferromagnetic chain coupler is the 1,3,5-trimethylenebenzene group, which is predicted to have a high spin ground state.⁴⁰



A copolymerization using a small amount of the 1,3,5-tris-phosphonium salt with the bis-phosphonium salt used in the PMPOT synthesis would give a conjugated polymer network composed of PMPOT chains connected by 1,3,5-trimethylenebenzene groups (Figure 4-36). Oxidation of the material would yield polarons that are ferromagnetically coupled between

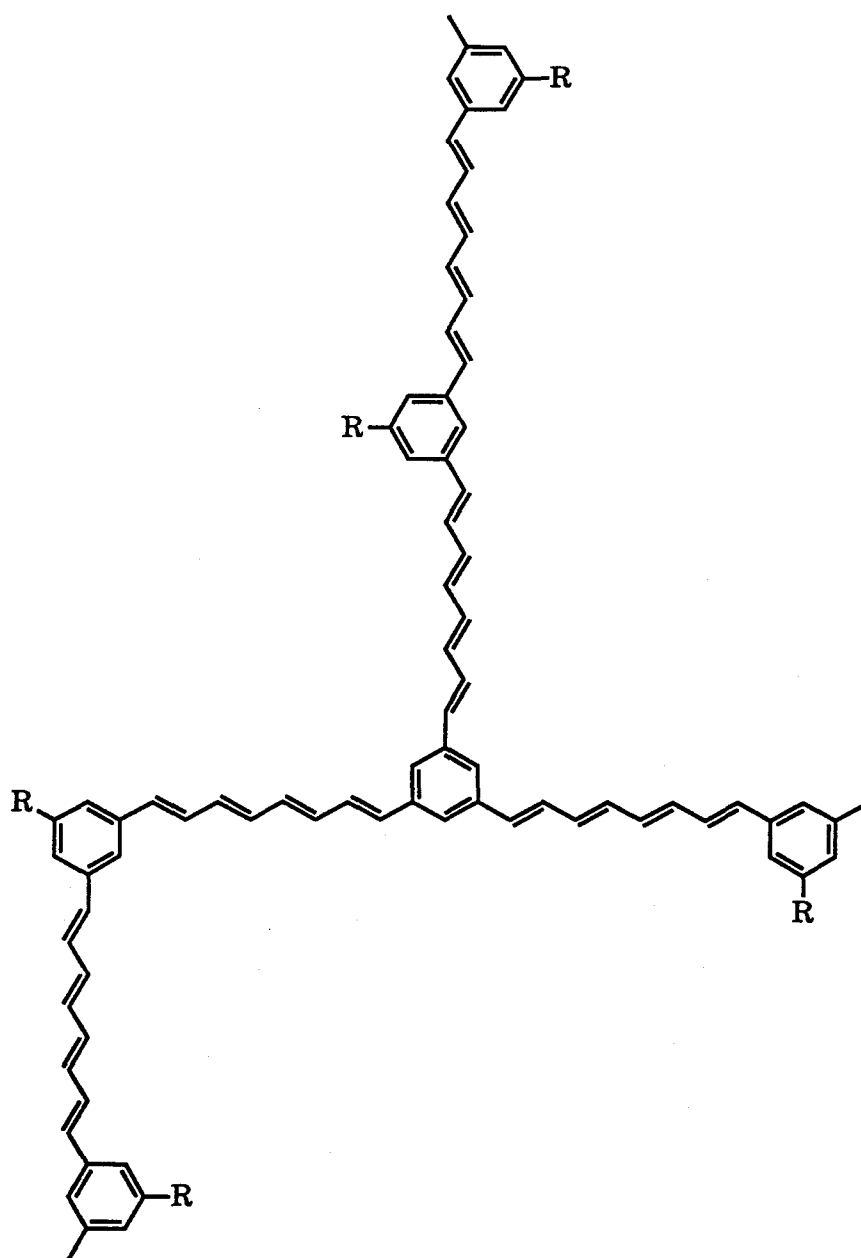


Figure 4-36. 1,3,5-Trimethylenebenzene-linked PMPOT network.

chains as well as along chains. This would allow high spin concentration as well as high spin state materials.

It should be noted at this point that there is an alternative explanation of the spin state as it relates to spin concentration. The correlation of a decrease of spin state along with an increase in spin concentration was observed only for the material which had been treated with a relatively high pressure of AsF_5 . This undoubtedly causes saturated cross-links and defects to form.⁸ If a large number of saturated defects were to appear on the polymer chains, the high spin coupling mechanism would become inoperative due to the destruction of the π topology. This would also lead to a decrease in spin state. Radicals that are trapped by extensive defect formation would give a spin state of approximately $S = 0.5$, and perhaps even lower due to through-space antiferromagnetic interactions.

Ferromagnetism - PMPOT and impurities. As previously mentioned, no characteristics of ferromagnets such as spontaneous magnetization were ever observed from the oxidized PMPOT derivatives. It is not believed at this point that these materials are true ferromagnets. It is important, though, to address the problem of ferromagnetic impurities such as iron which exist in the material at the time of the magnetization measurements. The effect of ferromagnetic impurities is of great concern due to the controversy that surrounds other previous claims of polymeric organic ferromagnets.⁴¹ We have obtained elemental analysis of Fe content of the doped polymers whose spin states were discussed earlier. Their Fe content ranges from 54 to 598 ppm. *There is no correlation between the Fe content of the doped PMPOT derivatives and their spin states obtained using the Brillouin fitting procedure.* Independent

analysis⁴⁸ using variable field magnetic susceptibility measurements⁴⁹ of the PMPOT-18 sample that first lightly, then heavily doped with AsF₅ (Figure 4-24, 4-25) gave only 16.3 ppm Fe content. This value corresponds to a saturation magnetization due to Fe in the material of 0.003 emuGauss/gram. This is only 10% of the total M_{Sat} of the lightly doped PMPOT-18 sample (Figure 4-24) and 3% of the total M_{Sat} observed upon heavier doping with AsF₅ (Figure 4-25). The majority of the observed magnetization in these samples is due to polarons.

The elemental analysis results are suspect due to the extremely small amount of each sample analyzed (10-25 mg). For samples with 5-100 ppm Fe content, a sample amount on the order of grams is recommended.⁵⁰ The small sample size leads to a large error for low Fe concentration measurements.

We believe the variable field magnetic susceptibility analysis is a more accurate method of determination of ferromagnetic impurities. This is due to the high sensitivity of magnetometers such as the Faraday balance or SQUID.¹⁴ For sample amounts of 10-25 mg, these are accurate to below 10 ppm for Fe impurities.

As it turns out, the relatively low spin state that we observe in the PMPOT derivatives eliminates the possibility of ferromagnetic impurities accounting for the magnetic behavior observed. A ferromagnetic impurity, by definition, will have a magnetization measurement that is constant as the external magnetic field is decreased at low temperatures.⁴² The magnetization curves found for the doped materials cannot be from impurities such as iron since iron alone would show a horizontal line, not a paramagnetic curve (Figure 4-37).⁴² A ferromagnetic impurity will raise

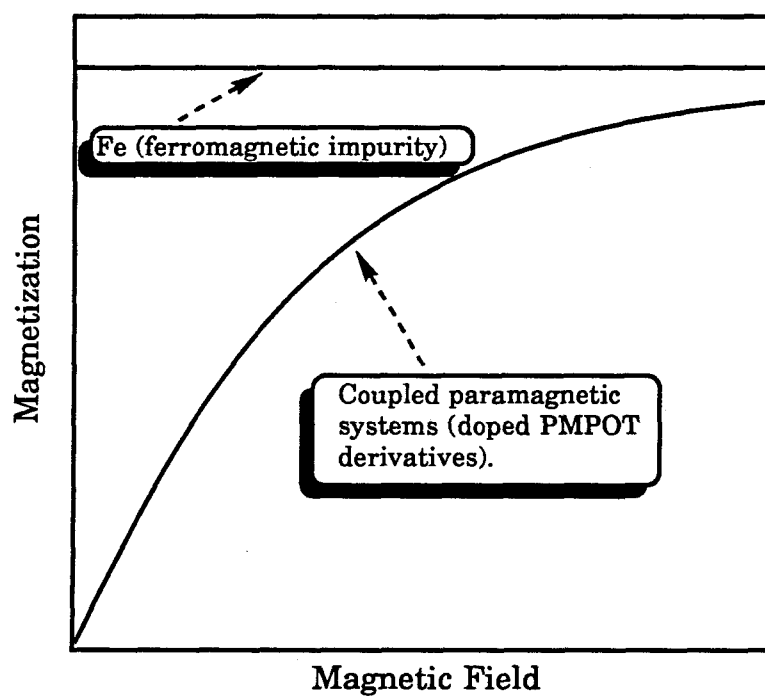


Figure 4-37. Magnetization behaviors of a ferromagnetic impurity and coupled paramagnetic systems.

the magnetization values at each field by a constant amount, but will not change the shape of the magnetization curve.

Conclusion

The results of this work indicate that the polaron-containing poly(*meta*-phenyleneoctatetraene) derivatives are a new class of high spin materials. Upon exposure of the polymers to oxidants such as arsenic pentafluoride or iodine, small concentrations of room temperature-stable polarons were formed. We have examined the magnetization behavior of these oxidized materials and have found novel magnetic behavior that is not observed in other oxidized conjugated polymers. When fit to the Brillouin function, the lightly doped polymers exhibit magnetization curves at 1.95 K that correspond to high spin states of $S = 1.2-2.2$. Temperature-dependent magnetic susceptibility measurements indicate that these high spin states are a result of both antiferromagnetic and ferromagnetic interactions.

We have substantially altered the properties of these undoped polymers by adding flexible O-alkyl groups to the polymer structure. The presence of an O-octadecyl group on the polymer chain creates a completely soluble material which can be cast into thin films. The increased solubility results in a substantial increase in the degree of polymerization as compared to the unsubstituted parent.

A model is proposed to explain the presence of both antiferromagnetic and ferromagnetic interactions in the doped materials. Doping creates clusters of polarons that are ferromagnetically coupled to each other. There is also a weaker antiferromagnetic interaction between clusters of polarons that is apparent at temperatures below *ca.* 50 K. This

model rationalizes the relationship between polaron concentration and spin state and is consistent with the decrease in spin state observed at high AsF_5 doping levels.

Experimental

General. Fourier transform NMR spectra (^1H and ^{13}C) were recorded on a Varian XL-200, JEOL FX-90Q, or JEOL GX-400 spectrometer. Gas chromatography/mass spectrometry was performed on a Hewlett-Packard 5840 GC/MS. Elemental analysis was obtained by Galbraith Laboratories. Ultraviolet spectra were obtained using a Hewlett-Packard 8451A diode array spectrophotometer.

All solvents were reagent grade or better. Column chromatography was performed by the method of Still employing 230-400 mesh silica gel.⁵¹ PPPB was synthesized by the method of McDonald.^{15,16}

Polymer Synthesis and Manipulation

All polymerizations were performed using air-sensitive techniques on a custom-built, 7-port Schlenk-type vacuum line. The vacuum line consisted of an inert gas manifold that was connected to a tower of 4Å molecular sieves and a tower of activated BASF Cu catalyst, and a vacuum manifold connected to a two-stage oil diffusion pump. Prior to the polymerizations, the polymer precursors were loaded in the reaction vessel (Schlenk tube) in the drybox. At no point in the synthesis or work-up did the polymer come into contact with atmospheric oxygen or water. The polymers were stored in a Vacuum Atmosphere dual-port drybox.

All solvents used in the polymerizations and subsequent work-ups were distilled from sodium/benzophenone ketyl or calcium hydride and degassed using at least three freeze/pump/thaw cycles.

Polymer contact with metallic surfaces was kept to a minimum. Whenever possible, plastic or Teflon-coated instruments were used. At no point was steel ball-milling ever used.

5-Hydroxy-dimethyl isophthalate (77). To a solution of 5.24 g (0.0287 mol) of hydroxyisophthalic acid in 300 mL of methanol was added 1 mL of concentrated sulfuric acid. The solution was heated to reflux for 12 hr under argon. The solvent was evaporated to give a white solid. The solid was dissolved in diethyl ether and washed with water. The organic solution was dried over MgSO_4 and the solvent evaporated to give 5.34 g (0.0254 mol, 88%) of white solid: ^1H NMR (acetone- d_4) δ 2.83 (bs, 1H), 3.89 (s, 6H), 7.67 (d, 2H, $J = 1.46$ Hz), 8.09 (t, 1H, $J = 1.46$ Hz).

5-Butoxy-dimethyl isophthalate (78). In a 1ℓ three-neck round bottom flask fitted with a mechanical stirrer and reflux condensor was added 29.84 g (0.142 mol) of **77** dissolved in 500 mL of acetonitrile and 119 mL (0.852 mol) of bromohexane. To the stirring solution was added 117g (0.85 mol) of potassium carbonate. The heterogeneous mixture was refluxed for 18 hr under argon. The mixture was then filtered and the solvent was removed from the filtrate to give a yellow solid. The solid was dissolved in diethyl ether and washed with water. The organic solution was dried with Na_2SO_4 and the solvent evaporated to give a yellow solid. The crude product was then recrystallized in petroleum ether to yield 29.4 g (0.09 mol, 70%) of white powder: ^1H NMR (CDCl_3) δ 0.86, 1.34, 1.85 (m, 11H), 3.88 (s, 6H), 3.98 (t, 2H), 7.68 (d, 2H), 8.19 (t, 1H); ^{13}C NMR (CDCl_3) δ 13.9, 22.5, 25.5, 29.0, 31.4, 52.2, 68.5, 119.6, 122.62, 131.5, 159.08, 166.03.

5-Butoxy-1,3-benzenedimethanol (80). To a dry 1ℓ, three-neck round bottom flask fitted with a condensor, addition funnel, and mechanical stirrer was added 500 mL of tetrahydrofuran (THF). To this was slowly added 10.45 g (0.275 mol) of lithium aluminum hydride under argon. To the stirring THF mixture was slowly added 34.6 g (0.145 mol) of **78** dissolved in 150 mL of THF. After addition of **78** was complete, the stirring mixture was heated to reflux for 2 hr under argon. The dark grey reaction mixture was allowed to cool to room temperature. The excess hydride was deactivated using the N,N,3N method. That is, 10.4 mL of H₂O was added *very carefully*, followed by careful addition of 10.4 mL of 15% aqueous NaOH solution, followed by careful addition of 30 mL of H₂O. Approximately 100 g of Na₂SO₄ was added to the grey mixture and the mixture was stirred for 18 hr. The resultant yellow mixture was filtered and the filtrate was dried over Na₂SO₄. The organic solvent was evaporated to give a white solid. The crude product was dissolved in diethyl ether and washed with water. The organic solution was washed with saturated NaCl solution, then dried with Na₂SO₄. The solvent was evaporated to give 24.47 g (0.103 mol, 71%) of white solid: ¹H NMR (acetone-d₆) δ 0.89 (at, 2H, J = 7.08 Hz), 1.18-1.32 (m), 3.96 (t, 2H, J = 6.5 Hz), 4.15 (t, 2H, J = 5.9 Hz), 4.56 (d, 2H, J = 5.9 Hz), 6.80 (s, 2H), 6.88 (s, 1H).

5-Butoxy-α,α'-dibromo-m-xylene (82). In a 2ℓ flask was dissolved 13.662 g (0.0573 mol) of **80** in 1ℓ CH₃CN and 95.18 g (0.387 mol) of CBr₄. To the stirring, slightly cloudy solution was slowly added 75.2 g (0.287 mol) of triphenylphosphine over a 15 min period. The flask grew warm, and a white precipitate appeared. The reaction progress was followed by TLC. The reaction was stirred for 12 hr under argon.

The reaction mixture was then gravity-filtered, and the solvent evaporated from the filtrate. The resulting brown oil was purified using flash-column chromatography techniques, using an eluent of 10:1 petroleum ether:ethyl acetate. Two flash columns were required for successful purification. Yield was 11.98g (0.0327 mol, 57%) of clear oil: ^1H NMR (CDCl_3) δ 0.95 (t, 3H), 1.60 (m, 8H), 3.97 (t, 2H), 4.39 (s, 4H), 6.93 (s, 2H), 6.96 (s, 1H); ^{13}C NMR (CDCl_3) δ 14.15, 22.67, 25.72, 29.23, 31.64 (alkyl chain), 33.06, (CH_2Br), 68.227 (OCH_2), 115.21, 121.64, 139.51, 159.53.

5-Butoxy-m-xylylenebis (triphenylphosphonium bromide) (71). To a solution of 5.9 g (0.0162 mol) of 82 in 150 mL dimethylformamide was added 21 g (0.081 mol) of triphenylphosphine. The stirring solution was heated to 120°C for 10 hr under Ar. The reaction was then allowed to cool to room temperature and the solvent was evaporated, yielding a yellow oil. The oil was placed under high vacuum for 24 hr. The oil was then dissolved in CHCl_3 and a white crude product was then precipitated by introduction of diethyl ether. The solid was recrystallized twice from CHCl_3 /diethyl ether. Alternatively, methanol/diethyl ether may be used. The slightly hygroscopic salt was dried in a vacuum drying pistol over refluxing chlorobenzene for 24 hr. Total yield was 8.6g (0.0097 mol, 60%) of white powder: ^1H NMR (CDCl_3) δ 0.88 (t, 3H, $J = 7.08, 7.33$ Hz), 1.25 (m, 8H), 3.34 (t, $J = 6.34$ Hz), 5.14 (d, $J = 14.65$ Hz), 6.51 (bs, 2H), 7.04 (bs, 1H), 7.72 (m, 30H); ^{31}P NMR (CDCl_3) δ 23.22 (s); Elemental analysis: Calculated ($\text{C}_{50}\text{H}_{50}\text{P}_2\text{Br}_2\text{O}$) C, 67.58; H, 5.67; O, 1.80; Br, 17.98; P, 6.97; Found C, 67.81; H, 5.65; O, 1.05; Br, 15.33; P, 7.03.

PMPOT-6 (66). To a septum-capped Schlenk tube containing 2.12 g (2.38 mol) of 71 under argon was added 15 mL of benzene via syringe. To the stirring

heterogeneous mixture was added 1.67 mL (4.76 mmol) of 2.85 M n-butyllithium solution (in hexanes) via syringe over a 10 minute period. A red, opaque mixture resulted. After 10 minutes, the stirring bis-ylide solution was heated to 60°C. To the stirring red mixture was slowly added 0.2625 g (2.38 mol) of muconic aldehyde dissolved in 10 mL of benzene at 60°C via 20 gauge Teflon cannula. The addition took place over a 20 minute period. The septum on the schlenk tube was replaced with a condensor, and the dark yellow mixture was heated to reflux under argon for 30 hours.

The mixture (now yellow-brown) was cooled to room temperature. The liquid from the reaction Schlenk tube was cannula-filtered into a centrifuge tube. To this liquid fraction (A) was added methanol, which resulted in precipitation of organic solid (A). The solid (A) was reprecipitated with methanol in benzene. The solid was then washed with methanol, collected, and placed under high vacuum to remove traces of solvent.

The solid from the Schlenk reaction tube was placed under vacuum, then transferred to a Soxhlet tube. The solid was purified via Soxhlet extraction with methanol (24 hr) and benzene (24 hr). The resulting solid (B) was placed under high vacuum for 24 hr. Total weight of solid (B) after extraction was 0.41 g of yellow-brown polymer. For solid (B): UV (KBr pellet) $\lambda_{\text{max}} = 410$ nm (broad), IR (KBr pellet, cm^{-1}) 681, 996, 1054, 1163, 1436, 1582, 2854, 2925, 3015. Liquid Fraction A; GPC (toluene, polystyrene standard) $M_n = 2229$, $P = 1.40$. Liquid Fraction B; GPC (toluene, polystyrene standard) $M_n = 1837$, $M_w = 2619$; $P = 1.43$; Elemental analysis (Fraction C): Calculated ($\text{C}_{166}\text{H}_{198}\text{O}_{18}$) C, 84.77; H, 8.41; O, 6.8. Found C, 81.93; H, 8.04; O, 1.02; Br, 1.02; P, 0.04.

PMPOT (63). To a Schlenk tube containing 1.64 g (2.08 mmol) of *m*-xylylenebis(triphenylphosphonium bromide) and 12 mL of benzene was added 1.57 mL (4.169 mmol) of 2.66 M *n*-butyl lithium (in hexanes) while stirring under argon. The red mixture was stirred for 2 hr. To the stirring red bis-ylide was added 0.2293 g (2.08 mmol) of muconic aldehyde over a 20 min period. The yellow mixture was heated to reflux for 24 hr. The solvent was then removed via application of vacuum and the resulting yellow solid was placed under vacuum for 12 hr. The solid was purified using Soxhlet extraction techniques with methanol (24 hr) and benzene (24 hr). Yield: 400 mg of yellow solid; Elemental analysis: Calculated ($C_{48}H_{42}O_2$) C, 86.8; H, 6.38; O, 6.8. Found C, 85.68; H, 6.11; O, 7.98; Br, 0.074; P, 0.22.

***m*-Xylylenebis(triphenylphosphonium bromide) (69).** To a solution of 15.42 g (0.0584 mol) of dibromo-*m*-xylene in 150 mL dimethylformamide was added 32.17 g (0.122 mol) of triphenylphosphine. The solution was heated to reflux for 4 hr, under argon after which the reaction solution was allowed to cool to room temperature. The solvent was evaporated to give an oily solid. The product was purified through multiple recrystallizations in acetonitrile. Excess solvent was removed using a vacuum drying pistol over refluxing toluene for 48 hr. Yielded 23.4 g (0.297 mol, 51%) of white solid. 1H NMR ($CDCl_3$) δ 5.12 (d, 4H, $J = 14.65$ Hz), 6.77 (t, 1H, $J = 7.81$ Hz), 6.89 (d, 2H), 7.42 (s, 1H), 7.59 (m, 30H); Elemental analysis: Calculated ($C_{62}H_{24}P_2Br_2O$) C, 70.45; H, 7.06; O, 1.51; P, 5.86; Br, 15.12. Found C, 70.79; H, 7.06; O, 0.90; Br, 15.16; P, 5.97.

PPPOT (75). To a Schlenk tube containing 1.59 g (2.01 mmol) of *p*-xylylenebis(tri-phenylphosphonium bromide) and 12 mL of benzene was added

1.52 mL (4.03 mmol) of n-butyl lithium with stirring over a 5 min period under argon. To the stirring dark mixture was slowly added 0.2217 g (2.01 mmol) of muconic aldehyde dissolved in 10 mL of benzene via cannula over a 20 min period. The dark red mixture was heated to reflux for 24 hr. The mixture was then allowed to cool, and the solvent was removed by the application of vacuum. The resulting red solid was purified using Soxhlet extraction with methanol (24 hr) and benzene (24 hr). Yielded: 300 mg of dark red powder; Elemental analysis: Calculated ($C_{118}H_{102}O_2$) C, 91.37; H, 6.57; O, 2.06. Found C, 92.79; H, 5.82; O, 1.91; Br, 0.05; P, 0.25.

Muconic aldehyde. This method is a modified version of the Kossmehl synthesis.^{23a} In a 250 mL round bottom flask was added 1.408 g (0.0201 mol) of glyoxal trimeric dihydrate, and 80 mL of dimethylformamide. The mixture was heated to 80°C under argon and stirred for 8 hr. The dark brown mixture was allowed to cool to room temperature and the solvent was evaporated to give a dark brown solid. This crude product was dissolved in 200 mL of benzene and gravity-filtered. The filtrate was passed through a short column (2 in) of silica with 800 mL of benzene. The solvent was evaporated, and the resulting brown solid was further purified by two successive flash chromatography columns using a 7:3:2 petroleum ether/benzene/ethyl acetate eluent system. The second column was done using an air-sensitive chromatography column, with collection of the product fractions under inert atmospheric conditions. The solvent was evaporated under vacuum in the absence of light to give the final product. The muconic aldehyde was brought into the dry box and used immediately. Alternatively, after the second flash column without the use of an air-sensitive flash chromatography column, the product was recrystallized from $CHCl_3$ /pentane under inert atmosphere. The

liquid was cannulated away from the solid and high vacuum applied (with the absence of light). This yielded 490 mg (4.45 mmol, 22%) of light yellow crystals: ^1H NMR (CDCl_3) δ 6.57 (m, 2H), 7.30 (m, 2H), 9.73 (3, 2H, $J = 7.54$ Hz); (C_6D_6) δ 5.76 (m, 2H), 5.96 (m, 2H), 9.11 (d, 2H, $J = 7.70$ Hz); ^{13}C NMR (CDCl_3) δ 137.96, 146.28, 192.29.

5-Octadecyloxy-dimethyl isophthalate (79). In a 2ℓ round bottom flask fitted with a mechanical stirrer were weighted 20 g (0.095 mol) of **77** and 131.6 g (0.95 mol) of potassium carbonate along with 1ℓ of acetonitrile. To the stirring mixture was added 158.7 g (0.46 mol) of 1-bromooctadecane. The stirring mixture was heated to reflux for 24 hr under argon. The reaction progress was monitored by TLC. The mixture was then gravity-filtered and the solvent was evaporated to give a yellow solid. The crude product was then recrystallized from petroleum ether to yield 31 g (0.067 mol, 70%) of white solid: ^1H NMR (CDCl_3) δ 0.85 (at, 3H, $J = 6.59, 7.08$ Hz), 1.23 (bs, 30H), 1.78 (m, 2H), 3.91 (s, 6H), 4.00 (t, 2H, $J = 6.59$ Hz), 7.71 (d, 2H, $J = 1.22$ Hz), 8.24 (t, 1H, $J = 1.22$ Hz).

5-Octadecyloxy-1,3-benzenedimethanol (81). To a stirring mixture of 4.93 g (0.13 mol) of LiAlH_4 in 800 mL tetrahydrofuran was slowly added 30 g (0.0648 mol) of **79** in 250 mL tetrahydrofuran. The mixture was heated to reflux under argon for 4 hr. The reaction was cooled to room temperature, and the excess hydride deactivated by careful addition of 5 mL H_2O , followed by 5 mL of 10% aqueous NaOH solution, followed by 15 mL of H_2O . To the stirring grey mixture was added 100 g of Na_2SO_4 . After stirring overnight in air, the yellow slurry was filtered and the solvent evaporated to give a light yellow solid. The solid was dissolved in diethyl ether and washed with H_2O . The

organic solution was dried over Na_2SO_4 and the solvent was evaporated to give 21.8 g (0.054 mol, 83%) of light yellow product: ^1H NMR (CDCl_3) δ 0.85 (at, 3H, $J = 6.59, 7.07$ Hz), 1.23 (bs, 32H), 1.62 (t, 2H, $J = 65.1$ Hz), 3.95 (t, 2H, $J = 6.59$ Hz), 4.65 (d, 4H, $J = 6.10$ Hz), 6.82 (s, 2H), 6.91 (s, 1H).

5-Octadecyl- α, α' -dibromo-*m*-xylene (83). To a solution of 10 g (0.0248 mol) of 81 in 1.2 L diethyl ether was added 41.2 g (0.124 mol) of carbon tetrabromide. The solution was heated slightly to dissolve the diol. To the stirring solution was then added 32.6 g (0.124 mol) of triphenylphosphine in small portions. After 8 hr, starting material was still present by TLC. Another two equivalents of carbon tetrabromide followed by two equivalents of triphenylphosphine were added to the stirring solution. The white-yellow mixture was stirred then for 10 hr. The mixture was filtered and the solvent was evaporated to give a white solid. The crude product was purified using flash chromatography techniques with 10:2 petroleum ether/ethyl acetate as eluent to give 5.1 g (0.0096 mol, 38%) of white solid: ^1H NMR (CDCl_3) δ 0.75 (at, 3H, $J = 6.59, 7.08$ Hz), 1.133 (bs, 32H), 3.83 (t, 2H, $J = 6.59$ Hz), 4.31 (s, 4H), 6.73 (s, 2H), 6.86 (s, 1H); ^{13}C NMR (CDCl_3) δ 14.09, 22.67, 26.01, 29.18, 29.36, 39.55, 29.59, 29.66, 29.69, 31.92, 32.86.

5-Octadecyl-*m*-xylylenebis(triphenylphosphonium bromide) (72). To a stirring solution of 2.0 g (3.76 mmol) of 83 in 50 mL of dimethylformamide was added 3.45 g (15 mmol) of triphenylphosphine. The solution was heated to 90°C under argon for 10 hr. The solvent was then evaporated to give a yellow oil. Upon application of high vacuum, an oily solid resulted. The crude product was initially recrystallized with CHCl_3 /diethyl ether, followed by recrystallization (twice) in methanol/diethyl ether to give 2.0 g (1.89 mmol,

50%) of white salt: ^1H NMR (CDCl_3) δ 3.84 (t, 3H, $J = 6.6$ Hz), 1.22 (bs, 30H), 1.40 (m, 2H), 3.30 (t, 2H, $J = 6.1$ Hz), 5.14 (d, 4H, $J = 14.64$ Hz), 6.35 (s, 2H), 6.86 (s, 1H), 7.7 (m, 30H); ^{31}P NMR (CDCl_3) δ 23.22 (s). Elemental analysis: Calculated ($\text{C}_{62}\text{H}_{74}\text{P}_2\text{Br}_2\text{O}$). Calculated C, 70.45; H, 7.06; O, 1.51; P, 5.86; Br, 15.12. Found C, 70.79; H, 7.06; O, 0.90; P, 5.97; Br, 15.16.

PMPOT-18 (67). To a stirring mixture of 1.6723 (1.538 mmol) of **72** in 10 mL of toluene contained in a Schlenk tube was slowly added 1.11 mL (3.167 mmol) of 2.8 M *n*-butyl lithium (in hexanes) under argon. The red opaque mixture was stirred for 15 min at room temperature then heated to 100°C. To the stirring red bis-ylide mixture was added 0.1743 g (1.583 mmol) of muconic aldehyde dissolved in 10 mL of toluene at 100°C via Teflon cannula. The addition took place over a 5 min period. When the addition of muconic aldehyde was complete, the mixture (yellow) was stirred at 100°C for 30 min, then refluxed for 72 hr under argon. The yellow mixture was allowed to cool to room temperature, and the solvent was removed by application of high vacuum. The remaining solid was purified using Soxhlet extraction techniques with methanol (3 day extraction). Solvent was removed by application of high vacuum. Yielded 660 mg of yellow solid which was soluble in toluene, chloroform, and dichlorobenzene: ^1H NMR (CDCl_3) δ 0.85 (bm, 3H), 1.28 (bs, 30H), 3.9 (bs, 2H), 6.4, 6.8 (bs, 11H); IR (thin film, cm^{-1}) 680, 972, 998, 1465, 1568, 2852, 2922, 3018; unassignable peaks at 720, 1058, 1165, 1289; small peak at 1718, 1884; UV (CHCl_3) $\lambda_{\text{max}} = 400$ nm (424 nm); GPC (o-dichlorobenzene, polystyrene standard) $\text{MW}_n = 9717$, $\text{MW}_w = 445521$, $P = 34$; Elemental analysis: C, 84.24; H, 10.72; O, 4.22; P, 0.27; Br, 0.18.

EPR *in situ* doping experiments

A Varian E-line Century Series X-band spectrometer was used to obtain EPR spectra at room temperature. A known mass of polymer was placed in a 5 mm quartz tube that was connected to a glass bulb containing the dopant (solid I₂ or gaseous AsF₅). The apparatus was evacuated prior to exposure of the polymer to the dopant. Spin concentrations were calculated using diphenylpicrylhydrazyl solid and solution as a spin count reference.

Magnetic susceptibility measurements

The sample was placed in a sample holder (aluminum for powders and films, plastic (polyethylene) for films only) which held 10-30 mg of material. The sample was degassed using 10 vacuum/He purge cycles in the antichamber of the SQUID before introduction to the probe. The magnetic susceptibility and magnetization of the sample was measured using the University of Southern California SHE SQUID magnetometer at a constant magnetic field at temperatures between 6 and 300 K using a computer-driven data accumulation program. The magnetic susceptibility from the aluminum sample holder was calibrated and subtracted from the measured susceptibility to obtain the sample magnetic susceptibility (χ_e) (the aluminum holder contains paramagnetic impurities that contribute to the measured susceptibility). The plastic holder was completely diamagnetic and hence did not need a separate calibration.

The χ_e was plotted versus T at temperatures above 25-50 K, with the y-intercept of the linear plot corresponding to the diamagnetic susceptibility (χ_{dia}). This was subtracted from χ_e to obtain χ_g (mass paramagnetic susceptibility in emu/gram). A plot of χ_g^{-1} versus T was used to investigate the

Curie-Weiss characteristics, while a plot of $(\chi_g T)^{1/2}$ versus T was used to investigate the relative effective moment (μ'_{eff}) at different temperatures.

Low temperature magnetization measurements

The magnetization values of the sample for the Brillouin fits were obtained manually at the desired fields and temperatures. Typically the sample would be initially cooled to ca. 4.15 K in a 50 kGauss field using the high temperature mode of the SQUID. The sample would then be cooled to 1.95 K using the low temperature mode of the SQUID magnetometer. The sample was allowed to equilibrate at the desired temperature for 10 min. When the SQUID control drift was negligible (after 5-180 min), the magnetization of the sample was measured. The magnetic field was then manually changed to the next lowest measurement point, and the above process repeated. An equilibration time of 15 min - 2 hr was required to allow the magnetic field to stabilize after changing fields. Magnetization measurements were only taken when the SQUID control drift was small. Similar to the magnetic susceptibility measurements, the aluminum sample holder was calibrated and subtracted from the measured magnetization values. A separate calibration was not done on the plastic sample holder.

The magnetization of a sample was typically measured at 50, 45, 40, 35, 30, 25, 20, 15, 10, 5, and 1 kGauss, always starting with the 50 kGauss measurement. This insures that any ferromagnetic impurities present will be saturated throughout the magnetic field range and hence will not affect the shape of the magnetization curve of the sample. For each Brillouin fit, the magnetization measurements were done at a constant temperature (1.95 K or 4-5 K).

The diamagnetic contribution to the sample magnetization ($\mu_{\text{dia}} = \chi_{\text{dia}} H$) was subtracted from the measured magnetization (M_e) to obtain the mass paramagnetic magnetization (M_g). This was plotted versus H/T and fit to the Brillouin function using an estimated M_{Sat} . The value of M_{Sat} was varied until the best fit to the Brillouin function with arbitrary S was found. The S for this fit corresponds to the spin state of the material. For samples with high multiplicities, the M_{Sat} could be measured directly from a plot of M_g versus H at constant T .

Doping of SQUID samples

In the case of I_2 -doping, the polymer powder or film was weighted into a tared glass vial and placed in a doping chamber. The glass bulb containing I_2 (solid) was attached to the chamber and the apparatus was evacuated. The polymer was then exposed to I_2 for 50 min, followed by application of vacuum for 8-24 hr to remove excess dopant. The tared vials were then weighed to measure dopant uptake.

In the case of AsF_5 doping, the polymers were weighed into a tared vial and placed in a doping chamber. The doping chamber was attached to the AsF_5 manifold and initially evacuated. The materials were then exposed to various pressures of AsF_5 . The AsF_5 pressure was regulated by condensing the AsF_5 gas in a cold finger which was also attached to the doping manifold. Pressures of 0.2-0.4 torr were obtained using a ℓN_2 /pentane bath. Pressures of 6-80 torr were obtained using a dry ice/acetone bath. When doping was complete, the excess dopant was removed by application of vacuum for 24 hr. The vial containing doped polymer was then weighed to find the weight uptake of dopant.

References

1. *Diradicals*; W.T. Borden, Ed.; Wiley: New York, 1982.
2. Rule, M.; Matlin, A.R.; Hilinski, E.F.; Dougherty, D.A.; Berson, J.A. *J. Am. Chem. Soc.* **1979**, *101*, 5098. Senthilnathan, V.P.; Platz, M.S. *J. Am. Chem. Soc.* **1980**, *102*, 7637.
3. (a) Teki, Y.; Takui, T.; Itoh, K.; Iwamura, H.; Kobayashi, K. *J. Am. Chem. Soc.* **1986**, *108*, 2147-2156. (b) Sugawara, T.; Bandow, S.; Kimura, K.; Iwamura, H.; Itoh, K. *J. Am. Chem. Soc.* **1986**, *108*, 368-371.
4. Manriquez, J.M.; Ward, M.D.; Calabrese, J.M.; Fagen, P.A.; Epstein, A.J.; Miller, J.S. *Mol. Cryst. Liq. Cryst.* **1989**, *176*, 527.
5. *Handbook of Conducting Polymers*; Skotheim, T.A., Ed.; Marcel Dekker: New York, 1986.
6. See reference 5; list authors and page.
7. Epstein, A.J.; MacDiarmid, A.G. *J. Mol. Electron.* **1988**, *4*, 161-165. Bredas, J.L.; Street, G.B. *Acc. Chem. Res.* **1985**, *18*, 309.
8. *Encyclopedia of Polymer Science and Engineering*; Mark, H.F.; Kroschwitz, J.I., Eds.; Wiley: New York, 1986; Vol. 5, p 463.
9. (a) Dougherty, D.A. In *Kinetics and Spectroscopy of Carbenes and Biradicals*; Platz, M.S., Ed.; Plenum: New York, 1990. (b) Jain, R.; Sponsler, M.B.; Combs, F.D.; Dougherty, D.A. *J. Am. Chem. Soc.* **1988**, *110*, 1356-1366. (c) Jain, R.; Snyder, G.J.; Dougherty, D.A. *J. Am. Chem. Soc.* **1984**, *106*, 7294-7295.
10. Teki, Y.; Takui, T.; Itoh, K.; Iwamura, H.; Kobayashi, K. *J. Am. Chem. Soc.* **1986**, *108*, 2147-2156.

11. Wertz, J.E.; Bolton, J.R. *Electron Spin Resonance: Elementary Theory and Practical Applications*; Chapman and Hall: New York, 1986.
12. *Handbook of Conducting Polymers*; Skotheim, T.A., Ed.; Marcel Dekker: New York, 1986, p 45. Epstein, A.J.; Rommelmann, H.; Druy, M.A.; Heeger, A.J.; MacDiarmid, A.G. *Solid State Communications* **1981**, *38*, 683-687.
13. Gourley, K.D.; Lillya, C.P.; Reynolds, J.R.; Chien, J.C.W. *Macromolecules* **1984**, *17*, 1025-1033.
14. Gerloch, M. *Magnetism and Ligand-Field Analysis*; Cambridge University: New York, 1983.
15. McDonald, R.N.; Campbell, T.W. *J. Am. Chem. Soc.* **1960**, *82*, 4669-4671.
16. Gooding, R.; Lillya, C.P.; Chien, C.W. *J. Chem Soc., Chem. Commun.* **1983**, 151-153.
17. Jen, K.-Y.; Cava, M.P.; Huang, W.-S.; MacDiarmid, A.G. *J. Chem. Soc., Chem. Commun.* **1983**, 1502-1503.
18. Hiemenz, P.C. *Polymer Chemistry: The Basic Concepts*; Marcel Dekker: New York, 1984, p 273.
19. *Organophosphorus Reagents in Organic Synthesis*; Cadogan, J.I.G., Ed.; Academic Press: New York, 1979.
20. Dougherty, D.A. *Mol. Cryst. Liq. Cryst.* **1989**, *176*, 25-32.
21. Agawa, K.; Sugano, T.; Kinoshita, M. *J. Chem. Phys.* **1986**, *85*, 2211-2218.
22. Mattis, D.C. *The Theory of Magnetism I. Statistics and Dynamics*; Springer-Verlag: Berlin, 1988.

23. (a) Davies, S.G.; Whitham, G.H. *J. Chem. Soc., Perkin Trans, 1* **1977**, 1346-1347. (b) Koßmehl, G.; Bohn, B. *Chem. Ber.* **1974**, *107*, 710-711.
24. Wnek, G.E.; Chien, J.C.W.; Karasz, F.E.; Lillya, C.P. *Polymer* **1979**, *20*, 1441-1443.
25. Askari, S.H.; Rughooputh, S.D.; Wudl, F. *Synthetic Metals* **1989**, *29*, E129-E134.
26. Winokur, M.J.; Spiegel, D.; Kim, Y.; Hotta, S.; Heeger, A.J. *Synthetic Metals* **1989**, *28*, C419-C426.
27. Swager, T.M. Ph.D. Thesis, California Institute of Technology, 1988.
28. See Chapter 3.
29. Hooz, J.; Gilani, S.S.H. *Can. J. Chem.* **1968**, *46*, 86-87.
30. Epstein, A.J.; Rommelmann, H.; Druy, M.A.; Heeger, A.J.; MacDiarmid, A.G. *Solid State Communications* **1981**, *38*, 683-687.
31. Scott, J.C.; Pfluger, P.; Kroundbi, M.T.; Street, G.B. *Phys. Rev. B* **1983**, *28*, 2140-2145.
32. Devreux, F. Genoud, F.; Nechtschein, M.; Villeret, B. In *Electronic Properties of Conjugated Polymers*; Kuzmany, H.; Mehring, M.; Roth, S., Eds.; Springer-Verlag: New York, 1987; pp 270-276.
33. Scharli, M.; Kiess, H.; Harbeke, G.; Berlinger, W.; Blazey, K.W.; Muller, K.A. In *Electronic Properties of Conjugated Polymers*; Kuzmany, H.; Mehring, M.; Roth, S., Eds.; Springer-Verlag: New York, 1987; pp 277-280.
34. Scott, J.C.; Bredas, J.L.; Kaufman, J.H.; Pfluger, P.; Street, G.B.; Yakushi, K. *Mol. Cryst. Liq. Cryst.* **1985**, *118*, 163. Kaufman, J.H.; Colaneri, N.; Scott, J.C.; Kanazawa, K.K.; Street, G.B. *Mol. Cryst. Liq. Cryst.* **1985**, *118*, 171. Kispert, L.D.; Joseph, J.; Miller, G.G.; Baughman, R.H. *Mol. Cryst. Liq. Cryst.* **1985**, *118*, 313. Kaufman,

- J.H.; Colaneri, N.; Scott, J.C.; Street, G.B. *Phys. Rev. Lett.* **1984**, *53*, 1005. Scott, J.C.; Bredas, J.L.; Yakushi, K.; Pfluger, P.; Street, G.B. *Synthetic Metals* **1984**, *9*, 165.
35. Henry, W.E. *Phys. Rev.* **1952**, *88*, 559-562.
 36. This work.
 37. μ_{eff} (for $S = 3/2$ system) = 3.87 Bohr Magnetons.
 38. Goldberg, A.H.; Dougherty, D.A. *J. Am. Chem. Soc.* **1983**, *105*, 284-290.
 39. See Chapter 2.
 40. (a) Mataga, N. *Theoret. Chim. Acta (Berl.)* **1968**, *10*, 372-376. (b) Ovchinnikov, A.A. *Theor. Chim. Acta* **1978**, *47*, 297-304.
 41. See Proceedings of the Symposium of Ferromagnetic and High Spin Molecular Based Materials, 197th National American Chemical Society Meeting in Dallas, TX.; Miller J.S.; Dougherty, D.A., Eds. *Mol. Cryst. Liq. Cryst.* **1989**, *176*, 1-562.
 42. Miller, J.S.; Epstein, A.J.; Reiff, W.M. *Chem. Rev.* **1988**, *88*, 201-220.
 43. Compton, C.; Bergmann, W. *J. Org. Chem.* **1947**, *12*, 363-368.
 44. The EPR spectrum observed upon exposure of PMPOT-6 or PMPOT-18 to AsF_5 consists of a broad peak at $g = 2.003$ with a linewidth of 6-10 gauss. The g -value is similar to that observed in other AsF_5 -doped conducting polymers.^{13,45} The line shape is isotropic and Gaussian, with a trend toward a Lorentzian lineshape⁴⁶ after *ca.* 60 min. dopant exposure time. Exposure of the polymers to I_2 results in a broad peak at $g = 2.0040$ - 2.0045 . This is consistent with previous EPR results on I_2 -doped systems.⁴⁷ The large g -value is the result of spin-orbit interactions of the polaron with iodine.⁴⁷ The lineshape is

broad (ca. 4-10 gauss) and non-isotropic (Dysonian¹³) after long I₂ exposure time.

45. (a) Kispert, L.D.; Joseph, J.; Miller, G.G.; Baughman, R.H. *Mol. Cryst. Liq. Cryst.* **1985**, *118*, 313-318. (b) Peo, M.; Roth, S.; Dransfeld, K.; Tieke, B.; Hocker, J.; Gross, H.; Grupp, A.; Sixl, H. *Solid State Communications* **1980**, *35*, 119-122. (c) DeVries, K.; Roylance, D. In *Encyclopedia of Polymer Science and Engineering*; Mark, H.F.; Kroschwitz, J.I., Eds.; Wiley: New York, 1986; Vol. 5, p 718.
46. Wertz, J.E.; Bolton, J.R. *Electron Spin Resonance: Elementary Theory and Practical Applications*; Chapman and Hall: New York, 1986.
47. Brown, I.M.; Wilbur, J.M. *Macromolecules* **1988**, *21*, 1859-1863.
48. By Joel Miller; E.I. duPont de Nemours and Co., Central Research and Development, Experimental Station, P.O. Box 80328, Wilmington, DE, 19880-0328.
49. A plot of χ_g (after diamagnetic correction) versus $1/H$ at a constant temperature (295 K) gives a line whose slope is equal to the magnetization due to ferromagnetic impurities. The concentration of Fe can then be calculated since $M_{FeSat} = 222$ emuG/gram (if Fe is assumed to be the only ferromagnetic impurity).
50. Galbraith Laboratories, Inc., P.O. Box 51616, Knoxville, TN, 37950-1610 (Private communication).